12-2010

Kinetic, Mechanistic, and Structural Investigation of Features Controlling Stereoselectivity of (R)- and (S)-Hydroxypropyl CoM Dehydrogenases from Xanthobacter autrophicus Strain Py2

Dariusz Adam Sliwa
Utah State University

KINETIC, MECHANISTIC, AND STRUCTURAL INVESTIGATION OF FEATURES CONTROLLING STEREOSELECTIVITY OF *(R)*- AND *(S)*-HYDROXYPROPYL COM DEHYDROGENASES FROM *XANTHOBACTER AUTOTROPHICUS* STRAIN PY2

by

Dariusz Adam Sliwa

A dissertation submitted in partial fulfillment
of the requirements for the degree

of

DOCTOR OF PHILOSOPHY

in

Biochemistry

Approved:

_____	_____
Scott A. Ensign, Ph.D. Major Professor	Lance C. Seefeldt, Ph.D. Committee Member
_____	_____
Sean J. Johnson, Ph.D. Committee Member	John L. Hubbard, Ph.D. Committee Member
_____	_____
Jeff R. Broadbent, Ph.D. Committee Member	Byron R. Burnham, Ph.D. Dean of Graduate Studies

UTAH STATE UNIVERSITY
Logan, Utah

2010

ABSTRACT

Kinetic, Mechanistic, and Structural Investigation of Features Controlling Stereoselectivity of (*R)*- and *(S)*-Hydroxypropyl CoM Dehydrogenases from *Xanthobacter autrophicus* Strain Py2

by

Dariusz Adam Sliwa, Doctor of Philosophy

Utah State University, 2010

Major Professor: Dr. Scott A. Ensign
Department: Chemistry and Biochemistry

Enantiopure alcohols are valuable intermediates in fine organic synthesis, in particular for preparation of biologically active compounds. The necessity of preparing single enantiomer drugs in an optically pure form has triggered much research, especially in the pharmaceutical industry. The biocatalytical production of chiral alcohols by alcohol dehydrogenase enzymes is characterized by the asymmetric reduction of the corresponding ketones, usually with high degree of stereoselectivity. The commercial value of the enzymes as stereoselective biocatalysts has been a significant driving force in understanding features that control their mechanism of catalysis and stereoselectivity. This work focuses on two enantiocomplementary dehydrogenase enzymes ((*R*)- and 2-(*S*)-hydroxypropyl-CoM (HPC) dehydrogenases (DH)) of the epoxide carboxylation pathway in *Xanthobacter autotrophicus* strain Py2. The main goal of this dissertation is to kinetically, mechanistically and structurally characterize *S*-HPCDH and through the comparison studies with *R*-HPCDH reveal the basis for high degree of stereoselectivity exhibited by both enzymes. Analysis of the molecular structure of *R*-HPCDH and the homology model of *S*-HPCDH suggests a mechanism of substrate specificity in which the binding of the

substrate sulfonate moiety at distinct sites on each stereoselective enzyme directs the orientation of the appropriate substrate enantiomer for the hydride abstraction. The positively charged residues responsible for binding the CoM moiety of the substrate were identified in *R*-HPCDH (Arg152 and Arg196), and in *S*-HPCDH (Arg211 and Lys214). Site-directed mutagenesis confirmed their importance in binding and orienting physiological substrates, but not the substrates lacking the CoM moiety. Extensive kinetic and mechanistic characterization of *S*-HPCDH reveals its key catalytic features similar to those of *R*-HPCDH, but also points out a few important differences. Furthermore, the role of the methionine residues flanking the substrate in the active site of both dehydrogenases was investigated. Substitution of these residues to alanine resulted in enzymes with significantly altered catalytic parameters and suggested their importance in binding and catalysis. Additionally, the X-ray crystal structures of the Met187Ala and Met192Ala mutants of *R*-HPCDH have revealed their role as "gate keepers," protecting the active site from the surrounding solvent. Kinetic analysis of Met187Leu and Met192Leu mutants implied a structural, rather than catalytic function of the methionines. It is proposed that steric clashes of the terminal methyl group of the HPC substrates with the nicotinamide ring of NAD^+ are a major determinant of the enantioselectivity in *S*-HPCDH. This research provides the first side-by-side characterization of a pair of short-chain dehydrogenase/reductase (SDR) enzymes expressed simultaneously to act on two enantiomers of the same alcohol produced in a metabolic pathway. The *R*-HPCDH and *S*-HPCDH enzymes are distinguished from all other known members of the SDR family in using the novel sulfonate functional group of coenzyme M as a handle for chiral discrimination. These results provide a standard for examining the molecular basis of stereoselectivity in other such enzyme pairs.

(206 pages)

ACKNOWLEDGMENTS

There are a lot of people who I owe a great deal of gratitude for their contribution to my success. Their kind help and support during the course of my Ph.D. work made this journey an enriching, meaningful and life-shaping experience. Without them any of these would not be possible and because of them all of these have sense and great value to me. For that I will always be grateful.

First of all, I would like to thank my advisor, Prof. Scott Ensign, for the opportunity to work in his laboratory and for his financial support. He has always encouraged me to become an independent researcher and gave me freedom to take my projects in a direction that interested me. I am very grateful for his academic guidance, for help in improving my writing skills and for the water-skiing trips in the sub-zero temperatures, which almost made my heart stop beating.

I also owe thanks to my supervisory committee: Prof. Lance C. Seefeldt, Prof. John L. Hubbard, Dr. Sean J. Johnson and Prof. Jeff R. Broadbent. I appreciate their time, patience, openness for questions and helpful discussions. Special thanks to Prof. John L. Hubbard for believing in me, for his continues encouragement and advice, for teaching me the “applied aspects of biochemistry” and for a great sense of humor.

I want to express my sincere gratitude to all of the former and present students of the Ensign lab that I have been fortunate to work with. In particular, I have to thank Dr. Jeff Boyd for getting me started in the biochemistry lab. Also, I would like to acknowledge Missy Kofoed, Ameya Mashruwala, Brandon Russel, Ashwini Wagh and Chris Potter for being great lab mates and friends. I extend my thanks to Danyal Karamatullah for his help, support and inspiring discussions on science, photography and life. Ameya and Danyal, thank you for your company during the long nights and weekends, while working in the lab side by side.

I must recognize my wonderful friends Jordan, Ellie, Shannon, Odessia, Malgorzata and Piotr for making me feel home far away from home. Undoubtedly without their help, encouragement and support in times of hardship I would not be where I am today. Special thanks to Dr. Jordan Ramilowski who has been on the path with me through collage and grad school. He's been a great friend, roommate and a skiing partner. We've celebrated together the high points and commiserated the low points over the last six years in Logan. I extend my thanks to my *departmental family*, especially to Kasia R. and Kasia G., Slava, Jeremy, Brenda, Ryan and Russ.

I will always be grateful for the love and support given to me by Mayra Iglesias. Your patience, understanding, hard work and optimism helped me more than the words can express.

I'd like to give very special thanks to my family (my Mum, Ania and Krzys) for trusting in me and investing in me. They have been very supportive and always believed in me. Without your love and encouragement this would have never been finished. I apologize to my niece and nephews for not being a very good uncle, I promise to make up for it when back in Europe.

Lastly, I would like to acknowledge Utah State University for giving me a great opportunity to persue my doctoral degree.

Dariusz A. Sliwa

To my mum Maria Sliwa I dedicate this dissertation.

CONTENTS

LIST OF TABLES

LIST OF FIGURES

LIST OF ABBREVIATIONS

AMO	alkene monooxygenase
Ala	alanine, (A)
Arg	arginine, (R)
Asn	asparagine, (N)
CoM	coenzyme M, (2-mercaptoethanesulfonate)
CD	circular dichroism
Cys	cysteine, (C)
BES	bromoethanesulfonate
EaCoMT	epoxyalkane:coenzyme M transferase
EDTA	ethylenediaminetetraacetic acid
ee	enantiomeric excess
E	enantioselectivity
FAD	oxidized form of flavin adenine dinucleotide
$FADH_2$	reduced form of flavin adenine dinucleotide
GC	gas chromatograph
H^+	proton
HEC	2-(2-hydroxyethylthio)ethanesulfonate
HPC	2-(2-hydroxypropylthio)ethanesulfonate
HPCDH	2-(2-hydroxypropylthio)ethanesulfonate dehydrogenase
HPLC	high performance liquid chromatography
Leu	leucine, (L)
Lys	lysine, (K)
MDR	medium-chain dehydrogenase/reductase

Met	methionine, (M)
M-HPC	2-(2-methyl-2-hydroxypropylthio)ethanesulfonate
NAD^+	oxidized form of nicotinamide adenine dinucleotide
NADPH	reduced form of nicotinamide adenine dinucleotide
NMR	nuclear magnetic resonance
R-HPC	2-[(*R*)-2-hydroxypropylthio]ethanesulfonate, (2-(*R*)-2-hydroxypropyl-CoM)
R-HPCDH	2-[(*R*)-2-hydroxypropylthio]ethanesulfonate dehydrogenase
rR-HPCDH	recombinant 2-[(*R*)-2-hydroxypropylthio]ethanesulfonate dehydrogenase
SDR	short-chain dehydrogenase/reductase
Ser	serine, (S)
S-HPC	2-[(*S*)-2-hydroxypropylthio] ethanesulfonate, ([2-(*S*)-2-hydroxypropyl-CoM)
S-HPCDH	2-[(*S*)-2-hydroxypropylthio]ethanesulfonate dehydrogenase
rS-HPCDH	recombinant 2-[(*S*)-2-hydroxypropylthio] ethanesulfonate dehydrogenase
SDS-PAGE	sodium dodecyl sulfate-polyacrylamide gel electrophoresis
K_m	Michaelis constant
K_i	inhibition constant
k_{cat}	rate constant

2-KPC	2-(2-ketopropylthio)ethanesulfonate (2-ketopropyl-CoM);
2-KPCC	2-(2-ketopropylthio)ethanesulfonate carboxylase/oxidoreductase
TR-I	tropinone reductase I
TR-II	tropinone reductase II
Tris tris	(hydroxymethyl)aminomethane
Tyr	tyrosine, (Y)

CHAPTER 1

INTRODUCTION

BACKGROUND AND SIGNIFICANCE

The increasing dependence of our society on industrial chemical processes results in large amounts of short-chain ($C_2 - C_4$) hydrocarbons being released to the surrounding environment. The biogenic sources of alkanes and alkenes further increase the global atmospheric non-methane pool of hydrocarbons. Of these compounds, alkenes, their halogenated counterparts and epoxides are especially reactive molecules with toxic, mutagenic and potentially carcinogenic properties that threaten ecosystems and pose serious risks to human health and development (*1, 2*). Several bacteria have been isolated over the years that can convert these toxic molecules into usable non-reactive metabolites (*3*). The current interest in biodegradation is rationalized not only by the applied aspects, but also by the general need to understand the mechanisms that living systems utilize to detoxify and/or metabolize these compounds and their biological intermediates. In the case of applied technologies, both the whole organisms and the homogeneously purified enzymes that comprise the bacterial pathways of alkane and alkene metabolism have biotechnological potential. *Xanthobacter autotrophicus* strain Py2 is one of several bacteria capable of growing on propylene and epoxypropane as the primary carbon and energy source (*4*).

The research efforts described in the subsequent chapters of this dissertation have been focused on the elucidation of the mechanism by which the enzymes of the epoxide degradation pathway in *X. autotrophicus* Py2 catalyze the conversion of toxic epoxides to useful metabolites. Of particular interest are two enantiocomplementary dehydrogenases which allow bacteria to grow on both the *(R)*- and *(S)*- enantiomeric forms of epoxypropane.

Sources of Propylene and Epoxides. Propylene is produced primarily as a by-product of petroleum refining and of ethylene production by steam cracking of hydrocarbon feedstocks (*5*). Propylene is a major chemical intermediate. The most important derivatives of propylene are:

polypropylene, acrylonitryle, propylene oxide, isopropanol, acetone and cumene. Propylene oxide, also known as epoxypropane, is a versatile chemical intermediate used in a wide range of industrial and commercial products (*6*). By volume, it is among the top 50 chemicals produced in the world. About 4 billion pounds of epoxypropane is manufactured annually by Dow Chemical Company (*7*) as a starting material in the synthesis of versatile products like polyether polyols for urethanes, propylene glycol (mainly for polyester fibres), polypropylene glycol, dipropylene glycol, glycol ethers and surfactants (*6*). In addition, aliphatic epoxides such as epoxyethane and epoxypropane have been used extensively as sterilizing agents for the medical and food industries (*8*). Chlorinated epoxides such as epichlorohydrin (3-chloro-1,2-epoxypropane) are produced in large quantities as starting materials for the production of glycerol and epoxy resins (*9*). Epoxides are also generated in vivo through the epoxidation of alkenes by a number of enzymes with monooxygenase activity as shown in Scheme 1-1.

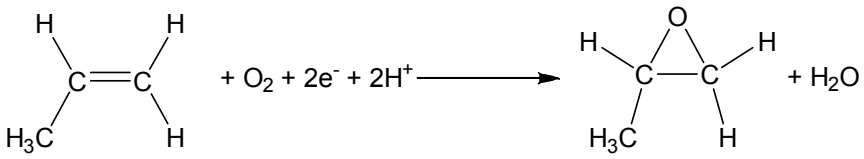

Scheme 1-1.

These monooxygenases can be divided into two general categories depending on the fate of their epoxide products. One consists of enzymes which metabolize epoxides for a source of carbon and energy, while the other is composed of enzymes converting epoxides for all other purposes (e.g., detoxification). An example of the monooxygenase-generated epoxides further metabolized for use as a carbon and energy source are found in alkene-utilizing organisms such as *X. autotrophicus* Py2 (*10*) and *R. rhodochrous* B-276 (*11*). In contrast, a number of

cytochrome P-450 monooxygenases represent enzymes that produce epoxides not metabolized for use by the organism. The heme-containing cytochrome P-450 monooxygenase family of isozymes (found ubiquitously in animals, plants, and microorganisms) are well known to nonselectively metabolize foreign compounds in the detoxification process (*12, 13*) . Although detoxification is an obvious benefit to organisms containing P-450 enzymes, in the case of alkenes, oxidation results in the generation of more toxic and reactive species, namely epoxides (*14*). The other enzymes of this category encompass the non-heme bacterial monooxygenases such as toluene monooxygenase (*15*), methane monooxygenase (*16*), ammonia monooxygenase (*17*), and alkane monooxygenase (*18*).

An interesting example of the biological source of epoxides are found in bacterial pathways of haloalkane metabolism via the action of halohydrin dehalogenases (*19*). These enzymes can convert a halohydrin, such as 1-chloro-2-propanol, into the corresponding epoxide (epoxypropane) and halide ion with a high enantioselectivity. Moreover, this reaction is thought to proceed via mechanism strategy similar to that of the SDR superfamily of enzymes, which will be discussed at a later point in this introduction.

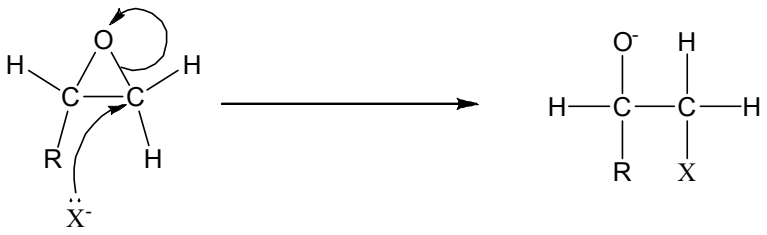

Scheme 1-2.

Biological Reactivity of Epoxides. Aliphatic epoxides are highly reactive, toxic compounds with mutagenic and in some cases carcinogenic properties (*1, 20*). The reactivity of

these molecules derives from their electrophilic nature and strained three-member ring. The general mechanism of elecrophilic addition of an epoxide is shown in Scheme 1-2. The biological nucleophile X^- attacks the epoxide, subsequently opening the ring and generating the alkylated product. Epoxides can react with a variety of cellular nucleophiles abundantly found on DNA, RNA, and proteins. In DNA and RNA, the principal reactive nucleophiles include the nitrogen atoms of the purines and pyrimidine bases. In proteins, epoxides react with sterically accessible

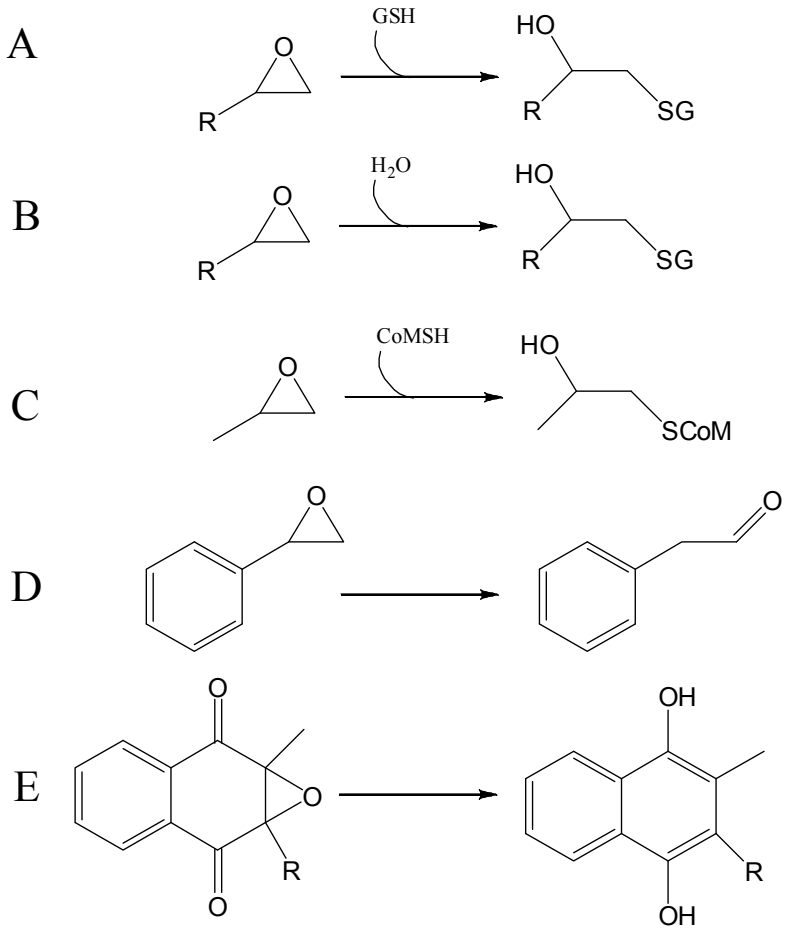

Figure 1-1. Biological strategies of epoxide metabolism. (A) glutathione transferase; (B) epoxide hydrolase; (C) epoxyalkane:CoM transferase; (D) styrene oxide isomerase; (E) vitamin K epoxide reductase.

cysteine thiol groups, methionine sulfurs or the histidine ring nitrogens. Biological systems have devised numerous strategies for converting epoxides into less detrimental species. Five known biological strategies have been described to date of epoxides metabolism/detoxification (Figure 1-1). All cases include opening of the epoxide ring via nucleophilic addition or isomerization, thus rendering the compounds inactive as electrophiles. The major differences in the examples described below lay in a type of nucleophile used in the reaction. The enzymes representing various strategies include: glutathione transferases, found in higher organisms to detoxifiy epoxides by converting them to less toxic glutathione conjugates (*21*); epoxide hydrolases, catalyzing the hydration of epoxides to the corresponding diols (*22-24*); epoxyalkane:coenzyme M transferase, an enzyme identified in both *X. autotrophicus* Py2 (*25*), and by extension *R. rhodochrous* B276 (*26, 27*), which detoxifies epoxypropane by converting it to a coenzyme M conjugate for further metabolism; styrene oxide isomerase, that catalyzes isomerization of styrene oxide to phenylacetaldehyde (*28*); and finally vitamin K epoxide reductase, a central enzyme in the vertebrate vitamin K cycle where it functions to regenerate the dihydroquinone form of vitamin K for use by vitamin K carboxylase (*29, 30*).

Epoxypropane Metabolism by Propylene-Oxidizing Bacteria. Many biological systems have developed mechanisms for dealing with epoxides. Among several bacteria capable of growing on epoxides as the only carbon and energy source are *X. autotrophicus* Py2 (*31*), *R. rhodochrous* strain B276 (*32*), and *Nocardia* strain A60 (*33*). Previous studies determined that the first step in the metabolism of propylene by *X. autotrophicus* Py2 and *R. rhodochrous* B276 occurs via an oxidative conversion to epoxypropane. The alkene monooxygenase (AMO) enzymes from these organisms have been homogenously purified and characterized. Both enzymes are NADH-dependent and highly stereoselective in their conversion of propylene to (*R*)-expoxypropane (*X. autotrophicus* Py2 AMO 95%, *R. rhodochrous* B276 AMO 92%) (*26, 34*). The *X. autotrophicus* Py2 AMO is a four component complex made up of an epoxygenase with 58-, 38-, and 10-kDa subunits arranged in an $\alpha_2\beta_2\gamma_2$ configuration that contains 4 moles of

nonheme iron, a 35-kDa monomeric reductase that contains FAD and a 2Fe-2S cluster, a homodimeric 13-kDa ferredoxin containing two Rieske-type 2Fe-2S clusters, and an 11-kDa effector protein (*35*). The *R. rhodochrous* B276 AMO is a three-component complex made up of an epoxygenase with 53- and 35-kDa subunits arranged in an αβ quarternary structure and containing two moles of non-heme iron, a 40-kDa monomeric reductase that contains FAD and a 2Fe-2S cluster, and a 14-kDa effector protein (*11*).

Overview of Epoxide Carboxylation. The conversion of epoxypropane to acetoacetate in the organisms *X. autotrophicus* Py2 is carried out by a four protein enzyme complex known as the epoxide carboxylase system (*26*). This enzyme complex is dependent on CO_2, NAD^+, NADPH, and an unusual cofactor, coenzyme M (CoM or 2-mercaptoethanesulfonate). The discovery of CoM, the smallest known biological cofactor, as being involved in the epoxides metabolism was both unprecedented and surprising. CoM was previously thought to be exclusively utilized during methanogenesis in archaebacteria where it plays a central role in reductive methane production (*25, 36, 37*). Bromoethanesulfonate (BES), a small molecule which is a structural analog of 2-mercaptoethanesulfonate (CoM), has been shown to be a potent inhibitor of methanogenesis (*38*) (Scheme 1-3 highlights structural similarities of both molecules). The enzymes involved in epoxide carboxylation utilize CoM to facilitate the opening

2-mercaptoethanesulfonate Bromoethanesulfonate

Scheme 1-3.

of the reactive epoxide ring and as a carbon carrier in the subsequent reactions as depicted in Figure 1-2. The thiol moiety of CoM (illustrated in Scheme 1-3) has proven to be a potent nucleophile capable of efficiently opening the epoxide ring, and the sulfonate moiety has been

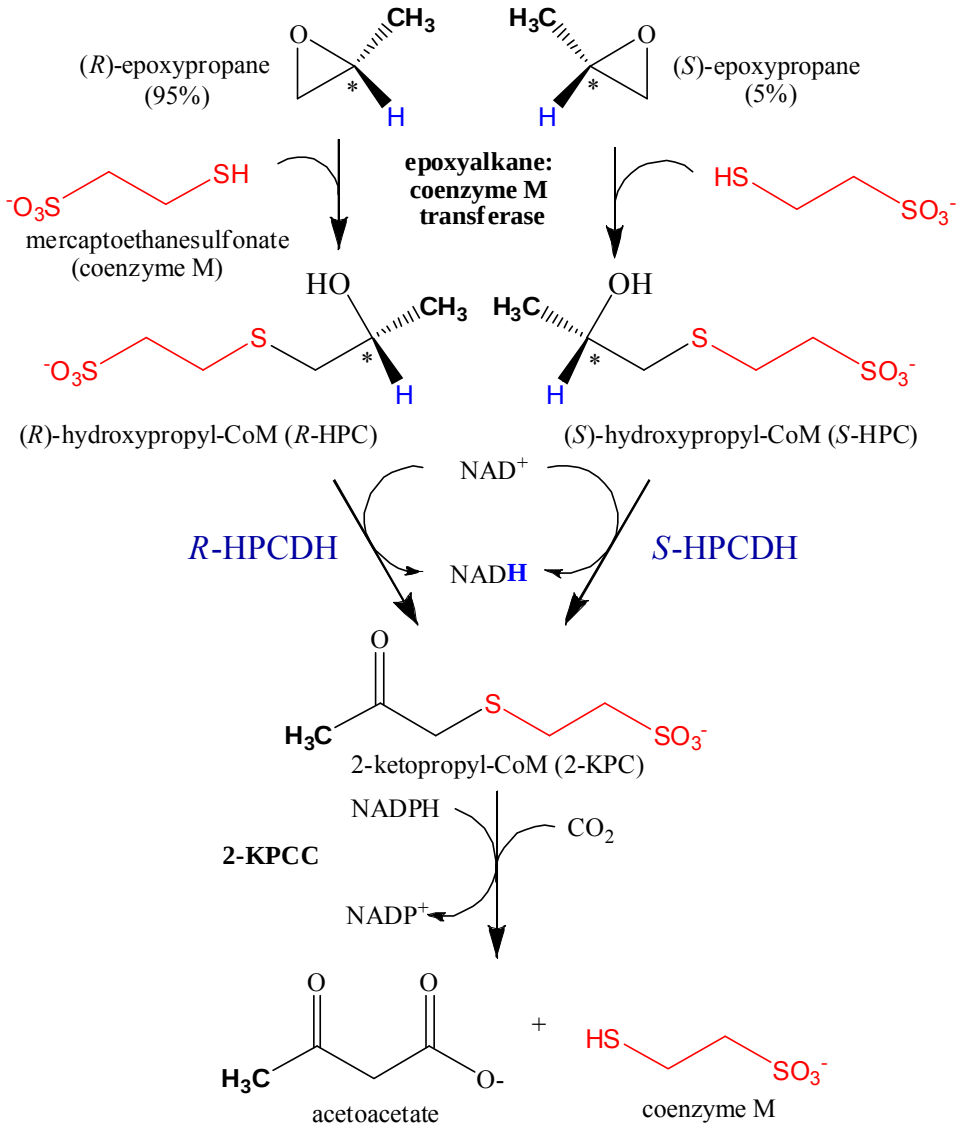

Figure 1-2. Pathway of aliphatic epoxide carboxylation in *X. autotrophicus* strain Py2. The enzymes catalyzing the subsequent reactions are: epoxypropane:CoM transferase, *(R)*-hydroxypropyl-CoM dehydrogenase (*R*-HPCDH), *(S)*-hydroxypropyl-CoM dehydrogenase (*S*-HPCDH) and 2-ketopropyl-CoM oxidoreductase/carboxylase (2-KPCC).

demonstrated to act as an effective binding "handle" for the enzymes (*39-42*). Recent studies show that BES is also a strong inhibitor of propylene metabolism in *X. autotrophicus* Py2 (*39*). The inhibitory effect of BES on the individual components of the epoxide carboxylase system is examined in more detail in Chapter 3 of this dissertation. The first step of the epoxide carboxylation pathway involves the opening of the epoxide ring, a reaction catalyzed by epoxyalkane:CoM transferase. In this reaction CoM is conjugated to either *(R)*- or *(S)*-epoxypropane thus producing the corresponding alcohols, namely *(R)*- or *(S)*-hydroxypropyl-CoM (*R*-HPC and *S*-HPC) (*25*). In the next step, two enantiocomplementary dehydrogenases, *(R)*- and (*S)*-hydroxypropyl-CoM dehydrogenases (*R*-HPCDH and *S*-HPCDH, respectively) catalyze the NAD^+ dependant oxidation of enantiomeric alcohols to a common achiral product, 2-ketopropyl-CoM (2-KPC) (*26*). In the final step, a novel carboxylase, 2-ketopropyl carboxylase/reductase (2-KPCC) catalyzes the NADPH-dependent reduction, cleavage and carboxylation of 2-KPC, forming acetoacetate and CoM. CoM is thus regenerated and recycled for the next round of reactions (*39*).

Enzymes of the Epoxide Degradation Pathway. Recently, the genome of *X. autotrophicus* Py2 was sequenced, assembled, and annotated (http://genome.jgi-psf.org/xanau/xanau.home.html). The genes encoding all components of the epoxide carboxylation pathway have been cloned and the corresponding enzymes purified (*26, 27, 39-42*). Amino acid sequence analysis of these enzymes along with biochemical, spectroscopic, and kinetic studies have helped further elucidate their mechanisms of action. Below is a summary of each of the enzymes involved in the pathway. The overall pathway is presented in Figure 1-2, while the stoichiometry of epoxypropane carboxylation is shown in Equation 1:

$$\textbf{epoxypropane} + CO_2 + NADPH + NAD^+ \rightarrow \textbf{acetoacetate} + H^+ + NADP^+ + NAD \quad \textit{(Eq. 1)}$$

Epoxyalkane:CoM Transferase. The first step in epoxide carboxylation is the ring opening of the epoxide by the nucleophilic addition of CoM catalyzed by epoxyalkane:CoM transferase (EaCoMT) (*25, 42*). Multiple sequence alignments have revealed that EaCoMT contains a characteristic zinc-binding motif similar to that of other zinc enzymes such as cobalamin-independent methionine synthase (MetE) (*43*) and methylcob(III)alamin:CoM methyltransferase-2 (MT2) (*42, 44*). Both of these homologous enzymes, as well as others within this family of Zn-containing alkyl-transferase enzymes, catalyze the nucleophilic substitution of an activated thiolate. Members of the Zn-containing alkyl-transferase family utilize thiols as nucleophiles that are activated by coordination to a zinc atom (*43*). In the case of EaCoMT the sulfhydryl group of CoM is proposed to coordinate zinc. This lowers the p*K*a of the thiol and thus activates it for alkylation, as shown in Figure 1-3. Three permanent ligands of the metal center are Cys and His residues, with the fourth coordination site occupied by an exchangeable ligand that is removed upon thiol binding. When the apo EaCoMT was reconstituted with Co^{2+} for spectroscopic studies it gave a normal spectrum corresponding to the tetrahedral state of the metal center. Upon CoM addition to the enzyme, the spectrum was altered dramatically suggesting that the thiol of CoM directly ligates the Co^{2+} center, either by displacing an exchangeable ligand or by increasing the coordination number about Co^{2+} (*45*). EaCoMT is an α_6 homohexameric protein with 1 mole of zinc per 41.7-kDa monomer (*45*). The enzyme has a modest k_{cat} (6.5 sec^{-1}) but a high affinity for propylene oxide (1.8 μM) (*42*). The native enzyme is expressed in high amounts (4% of the cellular protein) when *X. autotrophicus* Py2 is grown on propylene, additionally compensating for the modest k_{cat} (*40*). Regarding the highly reactive nature of epoxypropane, its accumulation in the cell would likely have a detrimental effect for the organism. This corresponds with an observation that epoxypropane does not accumulate in the assay or growth medium of *X. autotrophicus* Py2. Increased abundance of EaCoMT and its high affinity for epoxypropane aid in its efficient metabolism by a bacterium, thus preventing unnecessary and dangerous reactions with the cellular nucleophiles.

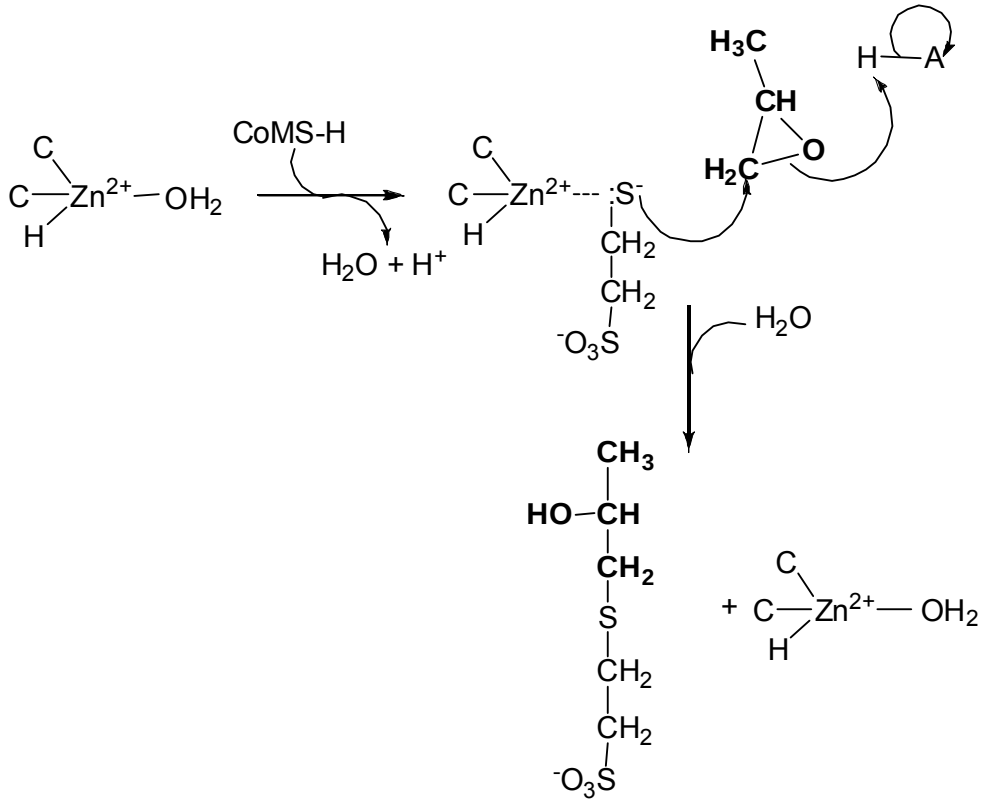

Figure 1-3. Activation of CoM by epoxyalkane-CoM transferase through coordination to a metal ion and the subsequent addition to propylene oxide.

(R)- and (S)- Hydroxypropyl-CoM Dehydrogenases. In the second step of the epoxide carboxylation pathway an enantiomeric mixture of *(R)*- and *(S)*-alcohols (in 95:5 ratio) is oxidized in a NAD^+ dependent manner to form a common β-keto acid (Figure 1-2). Specifically, two homologous enzymes *R*-HPCDH and *S*-HPCDH catalyze the reversible oxidation of *R*-HPC and *S*-HPC to yield an achiral product 2-KPC (*26, 41*). The *R*-HPCDH and *S*-HPCDH enzymes are highly stereoselective for their respective substrates, exhibiting only 0.5 to 1% activity with the opposing enantiomer (*26*). Biochemical and molecular studies showed that these enzymes belong to the "classical" short-chain dehydrogenase/reductase family of alcohol dehydrogenases

(*25, 26, 40*). The *R*- and *S*-HPCDH enzymes share a relatively high degree of sequence identity (41%) and are composed of subunits with molecular weights of 26 and 25 kDa, respectively (*40*). Although *R*-HPCDH has been cloned and expressed in a fully active form, many trials to purify *S*-HPCDH have not been successful due to its tendency to form inclusion bodies in the heterologous expression systems. Therefore, the kinetic, mechanistic and structural characterization of *S*-HPCDH is lagging behind that of *R*-HPCDH. Sequence alignments along with kinetic studies of the site directed mutants have revealed the identity and function of the catalytic triad residues for *R*-HPCDH (Tyr155, Lys159, Ser142) (*41*). Studies of the pH dependence of the kinetic parameters for *R*-HPC oxidation indicated a single ionizable residue of catalytic importance, Tyr155 with a pK_a of 6.9 (*41*). By analogy to other members of the SDR family, Tyr155 is believed to serve the role of a general acid/base. The oxidation of R-HPC was found to follow a compulsory-ordered ternary complex mechanism, where coenzymes are the outer substrates. Inhibition studies showed that the opposite enantiomer *S*-HPC and the substrate analog M-HPC are competitive inhibitors of *R*-HPC with K_{ic} values close to the K_m for *R*-HPC (*41*). Interestingly, other molecules containing sulfonate moieties, 2-mercaptoethanesulfonate (CoM), ethanesulfonate and methanesulfonate, were mixed or non-competitive inhibitors. The arginine modifying agents (2,3-butadione and phenylglyoxal) were capable of inactivating the protein in a time-dependent manner (*46*). These modifications affected the ability of the enzyme to oxidize *R*-HPC much more dramatically than similar substrates lacking the sulfonate moiety (*46*). These studies suggested that arginine residues in the enzyme active site interact with the negatively charged sulfonate moiety in order to orient the molecule for catalysis. Indeed, site-directed mutagenesis of the C-terminal arginine residues of *R*-HPCDH identified Arg152 and Arg196 as essential for catalysis of the natural substrates (*R*-HPC and 2-KPC) but not the substrates lacking the sulfonate moiety (*47*). Short-chain alkylsulfonates and CoM were found to modulate the enantioselectivity and kinetic properties for 2-butanone reduction by *R*-HPCDH. In the presence of 1 mM of additives, the enantioselectivity of 2-butanone reduction increased from

70% *(S)*-butanol and 30% *(R)*-butanol (produced in the absence of the additives) to a theoretical value of 100% *(S)*-butanol. The strongest modulating effects were observed for ethanesulfonate and propanesulfonate (*47*). However, these effects were abolished for the alanine mutants of Arg152 and Arg196 thereby confirming their role in the sulfonate binding. The length of the substrate alkyl chain was shown to be important in substrate affinity. When aliphatic alcohols were substrates for *R*-HPCDH, the K_m value decreased by 1700-fold upon going from 2-propanol to *(R)*-2-octanol (*47*). The *(S)*-alcohols with the chain length exceeding five carbons were sufficiently poor substrates that their kinetic parameters could not be determined. This suggested that the "methyl binding pocket" cannot accommodate groups longer than the propyl group presumably due to the steric clashes with the active site residues.

The uniqueness of the HPCDH enzymes along with their prospective industrial applications has prompted more detailed studies on the basis of their enantioselectivity. The recent successful cloning and expression of the *S*-HPCDH enzyme has allowed for the complementary kinetic and mechanistic studies, the results of which are presented in Chapter 2 of this dissertation.

SDR Family of Enzymes. As mentioned earlier, *R*- and *S*-HPC dehydrogenases belong to the short-chain dehydrogenase/reductase (SDR) family of enzymes. SDR enzymes play a critical role in amino acid, carbohydrate, cofactor, lipid, hormone and xenobiotic metabolism as well as in redox sensor mechanisms. Their importance and functional diversity is reflected in the physiology of various organisms ranging from viruses, archea, bacteria, yeast to eukaryotes and higher mammals (*48*). They constitute a large, evolutionarily old protein family of NAD(P)(H)-dependent enzymes with over 70 genes found in the human genome (*49-52*). The SDR enzymes are 250 - 350 amino acids in length, exist as dimers or tetramers, and carry out catalysis in the absence of a metal cofactor. The enzymes have three distinct domains: a conserved N-terminal NAD^+ (or $NADP^+$) binding domain, a central domain with three highly conserved catalytic triad residues (serine, tyrosine, and lysine) and a variable C-terminal domain responsible for substrate

recognition. Recent mutagenic and structural studies have extended the knowledge of the general reaction mechanism and have established a catalytic tetrad of the Asn, Ser, Tyr and Lys residues (*53*). The SDR enzymes constitute one of the largest enzyme superfamilies with presently over 46,000 members annotated in databases (*52*). The term "short-chain" alcohol dehydrogenases has traditionally been used to distinguish members of this family on the basis of primary sequence length and catalytic mechanism from the classical zinc-dependent "medium-chain" alcohol dehydrogenases (MDR), such as liver alcohol, glyceraldehyde or lactate dehydrogenases.

Primary Structure of SDR Enzymes. Since SDR family represents one of the oldest families of enzymes with its members showing early divergence, there is a relatively low sequence identity between different SDR enzymes (typically 15-30%). Despite that some highly conserved motifs are observed in their primery sequence (Figure 1-4). The first being a strictly conserved segment of the YxxxK sequence, known as the active-site motif. In addition to the Tyr and Lys residues, a Ser residue (13 residues upstream of Tyr) has been shown to be conserved in some SDR enzymes. Another characteristic motif is the N-terminal GxxxGxG sequence, which represents the nucleotide binding region (*54*). Spacing between the glycines is variable and depends on the specific subfamily. The two main types of SDR enzymes are denoted as "classical" and "extended." The "classical" type has a chain length of about 250 amino acids, while the "extended" family has an additional 100-residue domain in the C-terminal region. Three further types known as "intermediate," "complex" and "divergent" (*55*), can be distinguished based on the specific sequence motif of the cofactor and the active site residues (Table 1-1). Further, frequent sequence motifs are NNAG (around position 86 -89), a single Asn residue located around position 111, and a single Asp (around position 60) (*49, 56-58*). The latter is typical for the NAD^+(H)-dependent enzymes and is not present in $NADP^+$(H)-dependent enzymes (*55*).

Table 1-1. Cofactor and active site sequence motifs for the different SDR superfamilies[a]. This table was adopted from Kavanagh et al. (*59*).

Subfamily	Cofactor binding	Active site
classical	TGxxx[AG]xG	YxxxK
extended	[ST]GxxGxxG	YxxxK
intermediate	[GA]xxGxx[GA]	YxxxK
divergent	GxxxxxxSxA	YxxMxxxK
complex	GGxGxxG	YxxxN

[a]Abbrevaiations: x, any amino acid residue; [ ] denote alternatives that can be present or absent.

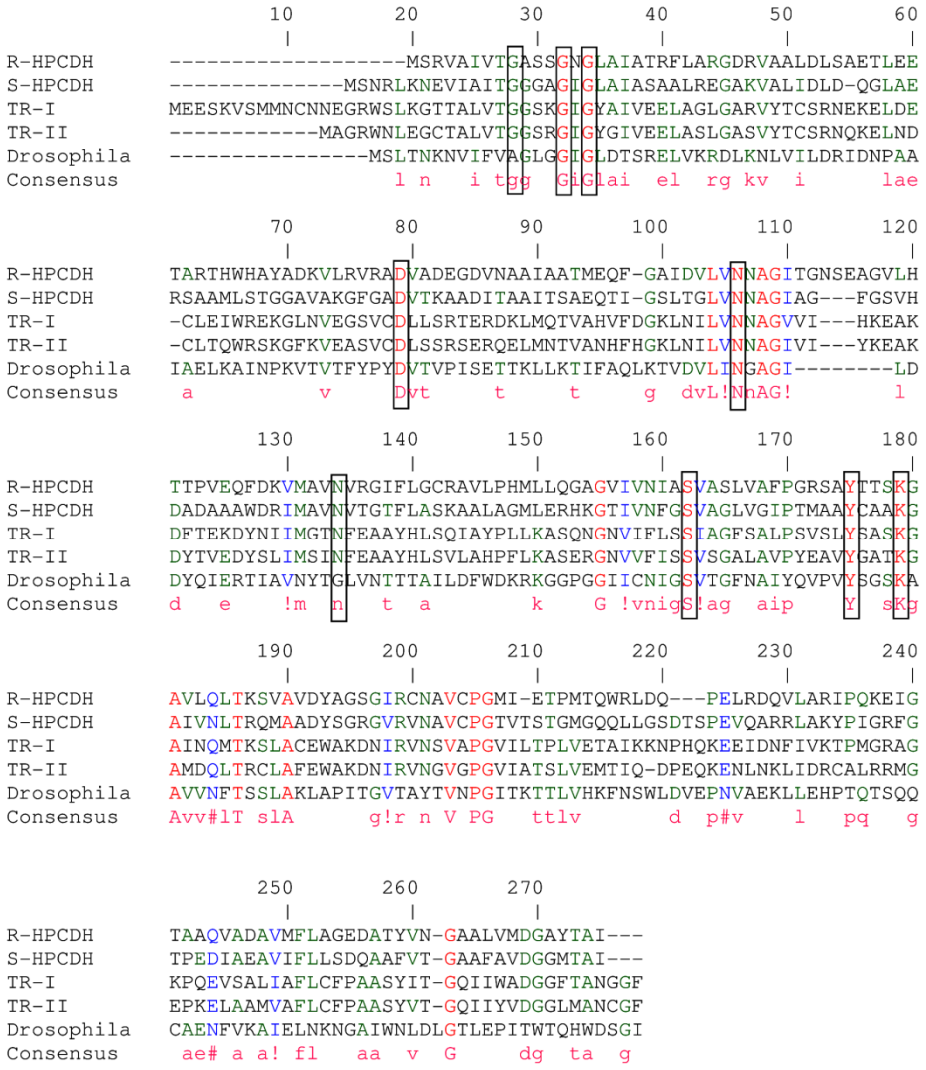

Figure 1-4. Multiple-sequence alignment of some of the SDR enzymes showing conserved motifs of the catalytic triad and the nucleotide binding region.

Tertiary Structure of the Enzymes of SDR Family. Regardless of the low primary sequence identity, the tertiary structures of the SDR enzymes display high structural similarities. Comparison of the 3D structures of enzymes representing the SDR family (82 structures deposited in PDB) reveals that the most common feature among all available structures is of a α/β folding pattern known as the Rossmann-fold (*60*). It is a dinucleotide cofactor binding motif composed of a central, twisted parallel β-sheet (typically consisting of 6-7 β-strands), which is surrounded by 6-8 α-helices (*61*) (Figure 1-5). The Gly-rich sequence pattern of this motif plays an essential role in the structural integrity of the protein and allows for binding of the pyrophosphate portion of the nucleotide cofactor (*61*). The NAD(H) specificity of the enzyme is determined by an acidic residue (typically Asp) binding to the 2' and 3' hydroxyls of the adenine ribose which is located about 20 residues downstream of the Gly-rich motif.

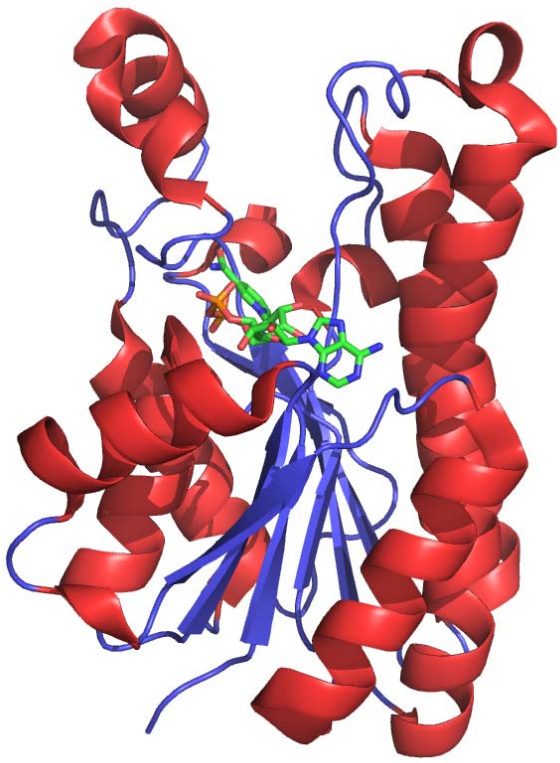

Figure 1-5. General fold of the SDR enzymes with the cofactor bound.

In contrast NADP(H)-dependent enzymes contain a basic residue (typically Asn) within the Gly-rich segment (61). The N-terminal nucleotide binding domain consists of the classic Rossmann-fold and the nucleotide binding sequence GxxxGxG (Figure 1-4). The central catalytic domain contains a strictly conserved catalytic motif YxxxK. The substrate binding domain is the most variable although various SDR enzymes show some similarities in this region. The substrate binding domain is generally composed of the loops between the last two β strands (generally βF and βG) of a subunit on one side and the loop between the previous two β strands (βD and βE) on the other side (*62*).

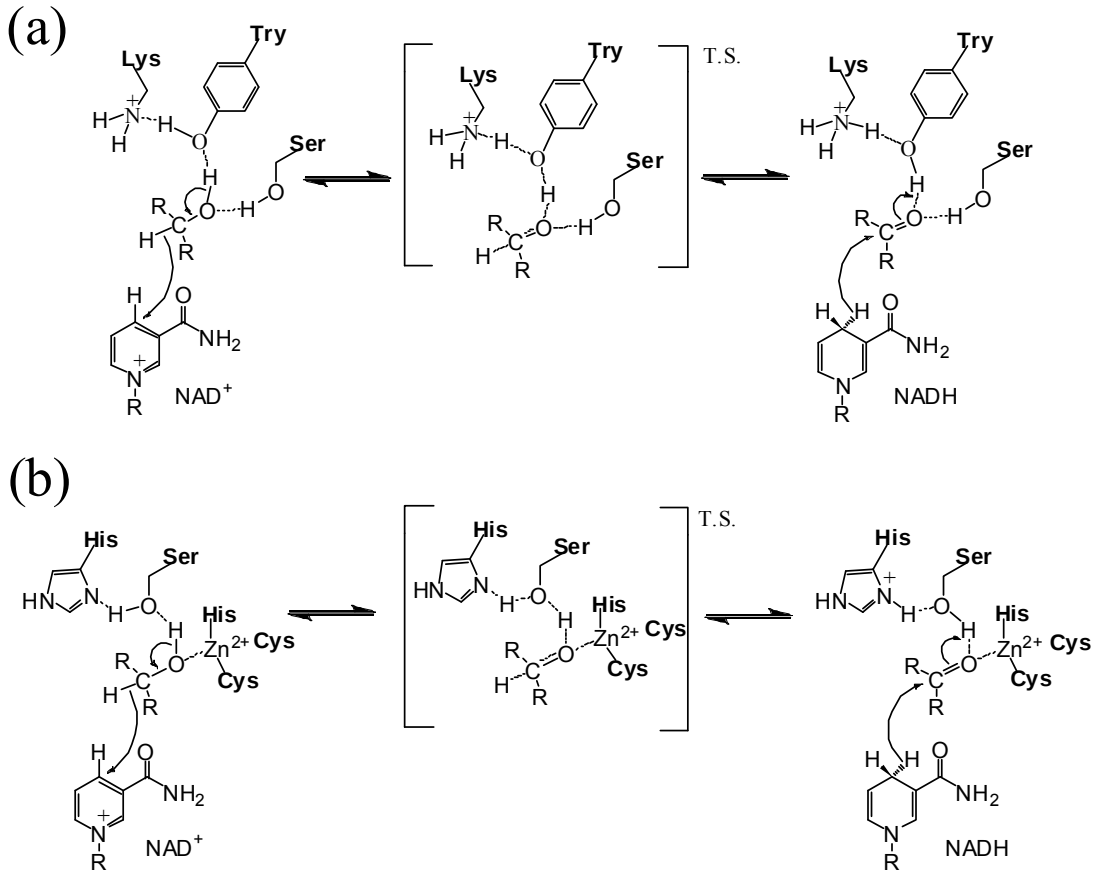

Figure 1-6. General mechanisms of catalysis for the SDR enzymes (a) and the zinc-dependent MDR enzymes (b).

General Mechanism of SDR Enzymes. Extensive structural, kinetic, and mechanistic characterization of SDR enzymes has resulted in the formulation of a general mechanism of action (*49, 63-65*). Comparison of this mechanism with the corresponding mechanism of the zinc-dependent MDR enzymes (*66-68*) is shown Figure 1-6. During oxidation, the Tyr residue of the catalytic triad is deprotonated and serves as a general base for proton abstraction from the substrate. The Lys residue binds the sugar moiety of NAD^+ and stabilizes the deprotonated tyrosyl group of the general base. The Ser residue is thought to increase the acidity of the substrate hydroxyl group through hydrogen bonding and to stabilize the developing charge on the alcohol oxygen in the transition state. Although present in most SDR enzymes, the Ser residue is not obligatory as demonstrated for some enzymes where it was either replaced with Thr or absent (*49, 69*). Recent studies have extended the catalytic triad by an Asn residue (*56, 70*), therefore establishing a tetrad which is thought to form a proton relay system, similar to that previously reported for horse liver ADH (*71*).

Enantiocomplementary SDR Enzymes. Among a large number of SDR enzymes annotated in databases [(46,000 (*52*)], there are very few examples of enzyme pairs which in a common pathway catalyzes the same reaction but with opposite stereoselectivity. To our knowledge, these enzymes are limited to a set of plant tropinone reductases (*72, 73*) and bacterial HPC dehydrogenases (*26, 41*). A multiple sequence alignment containing *R*- and *S*- HPC dehydrogenases from *X. autotrophicus* Py2 and the two reductases from *Datura stramonium* is shown in Figure 1-4. Tropinone reductase I and II (TR-I and TR-II) catalyze the reversible stereoselective reduction of the 3-keto group of tropinone to form the enantiomers tropine (α-hydroxy) and pseudotropine (β-hydroxy), respectively. Kinetic and structural analysis of TR-I and TR-II has helped establish their mechanism of stereoselectivity. According to this mechanism electrostatic interaction between the substrates and the charged amino acids underlie substrate binding and orientation for catalysis (*72, 73*). A positively charged histidine (His-112) in TR-I repels the positively charged nitrogen on the tropinone (Figure 1-7). In case of TR-II, the

negatively charged glutamate carboxylate (Glu-156) attracts the substrate nitrogen and thus fixes its position (Figure 1-7). Based on these results it is conceivable that a similar charge attraction/repulsion mechanism, involving interactions with the negatively charged sulfonate moiety of the coenzyme M, controls proper binding of *R*- and *S*-HPC to the respective dehydrogenases.

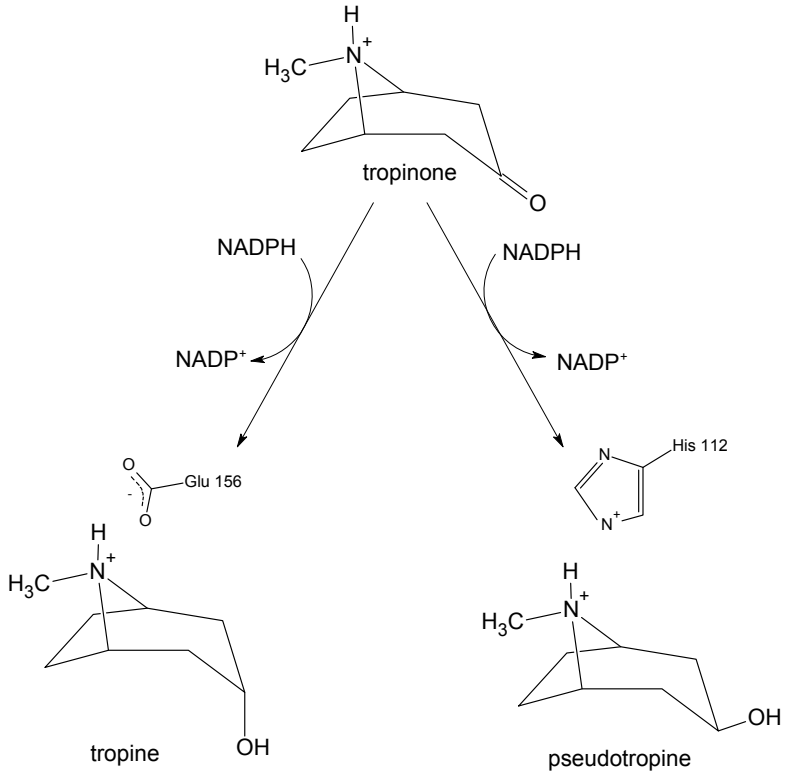

Figure 1-7. Mechanism of stereoselective discrimination and catalysis of pseudotropine and tropine by TR-I and TR-II, respectively.

Structural Basis for Stereoselectivity in R-HPCDH and S-HPCDH. The molecular structure of *R*-HPCDH has been determined using X-ray diffraction method and refined to 1.8 Å resolution (*74*). The overall fold shown in Figure 1-8, is consistent with the structures of the other members of the SDR family, including mannitol dehydrogenase (*75*) and halo alcohol

dehydrogenase (*76*). Although the previous results of size exclusion chromatography suggested that *R*-HPCDH exists as dimer (*41*), the X-ray structure suggests that it is a tetramer (*74*). The NAD^+ binding domain consists of a standard Rossmann motif of a large twisted β sheet surrounded by 7 α helices (Figure 1-8 B). Excellent quality of the electron density maps for the sulfonate portion of the bound product (2-KPC) helped to identify two arginine residues interacting with the sulfonate (Arg152 and Arg196). This confirms the results of the previous biochemical and mechanistic studies proposing that the interactions between the sulfonate of CoM and the specific arginines are crucial for the high enantioselectivity and catalytic efficiency of *R*-HPCDH (47).

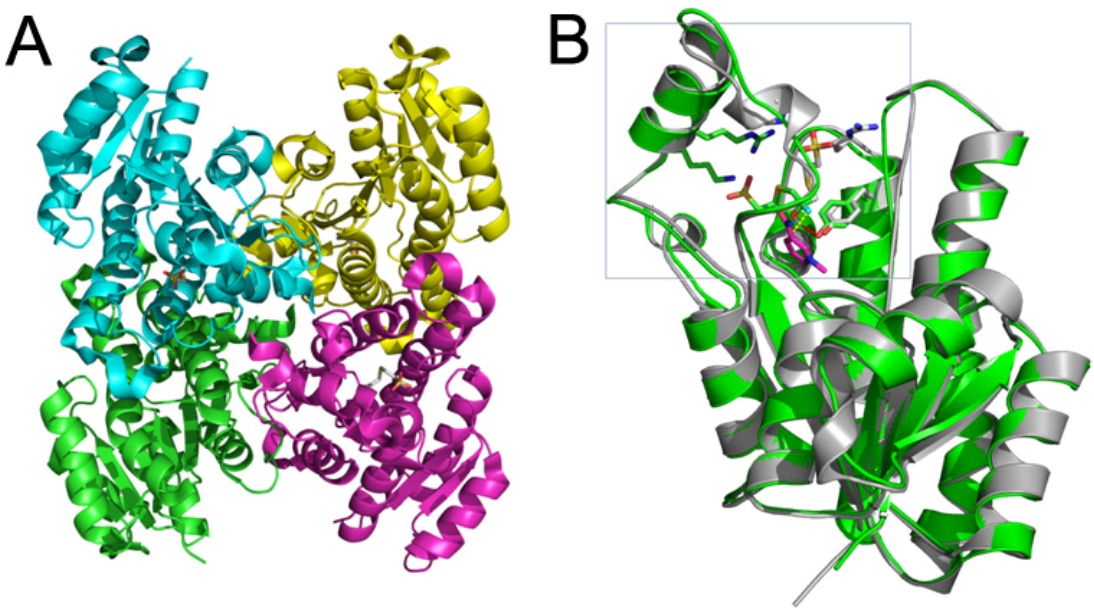

Figure 1-8. X-ray structure of *R*-HPCDH and the homology model of *S*-HPCDH; (A) The overall tertiary structure of *R*-HPCDH with the individual subunits colored differently. (B) Superimposition of the *R*-HPCDH structure (grey) with a homology model of *S*-HPCDH (green).

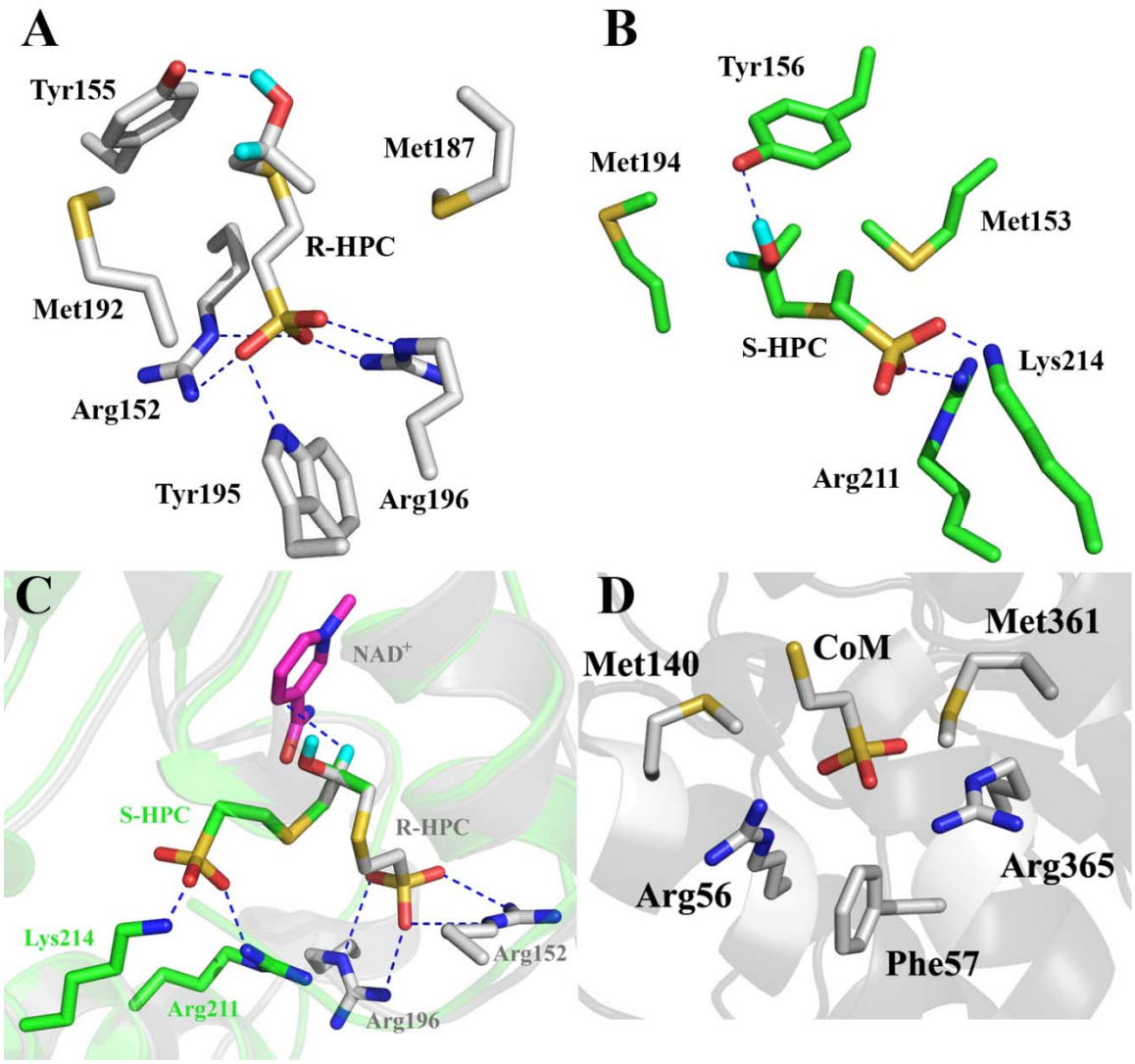

Figure 1-9. Comparison of the active sites architecture for *R*-HPCDH, *S*-HPCDH and 2-KPCC: (A) Active site of *R*-HPCDH with *R*-HPC. (B) Active site of *S*-HPCDH with *S*-HPC based on the homology model. (C) Superimposed structure of *R*-HPCDH (grey) with the homology model of *S*-HPCDH (green) to show different special orientation of the sulfonate binding site. (D) Active site of 2-KPCC with CoM.

The active site of *R*-HPCDH with the substrate bound *R*-HPC presented in Figure 1-9A shows that besides the electrostatic interactions of Arg152 and Arg196 with the sulfonate group, also Trp195 contributes to the substrate binding through hydrogen bonding. This residue is positioned at the back of the binding pocket and presumably acts as a backstop preventing

movement of the substrate during catalysis. An interesting feature of the active site is the presence of two methionines flanking the substrate. The architecture of the CoM binding pocket in *R*-HPCDH resembles that of 2-KPCC which also shows two arginines (Arg56 and Arg365) interacting with the sulfonate moiety, two methionines flanking the substrate (Met140 and Met361) and Phe57 acting as a backstop (Figure 1-9D). A homology model of *S*-HPCDH was constructed based on the structure of *R*-HPCDH. Superimposition of both structures reveals differences in the substrate binding region and suggests the reorientation of the sulfonate binding site with respect to the CoM binding pocket (Figure 1-9C). It is proposed that in S-HPCDH enzyme two positively charged residues Arg211 and Lys214 are involved in the sulfonate binding. Similar to *R*-HPCDH and 2-KPCC the substrate flanking methionines (Met153 and Met194) are also suggestes in the active site of *S*-HPCDH (Figure 1-9B).

Kinetic analysis showed that *S*-HPC is a strong competitive inhibitor of *R*-HPCDH with K_i similar to the K_m of the *R*-HPC (41). Although *S*-HPC binds to *R*-HPCDH with high affinity, the activity is only 0.1 % of that with *R*-HPC. To visualize the binding mode, *S*-HPC was modeled in the active site of the *R*-HPCDH. Positioning of the hydroxyl group of *S*-HPC exactly over that of the *R*-HPC orients the hydrogen atom of the *S*-HPC away from the NAD^+. This provides the structural basis for the strong inhibition observed with *S*-HPC (Figure 1-10). Furthermore, the comparison of the structures of *R*-HPCDH with the homology model of *S*-HPCDH suggests that the differential placement of the positively charged residues on each of the stereoselective enzymes is key to the proper orientation of the substrate for hydride abstraction, and thus brings about chiral discrimination of the *R*- and *S*-HPC substrates.

Although *R*-HPCDH has been extensively characterized up to date, there are still certain questions regarding its structural features which remain unanswered. For example, nothing is known about the role of the methionines flanking the substrate in the active site of *R*-HPCDH. Chapter 4 presents the efforts aimed towards elucidating their role in substrate binding and

stereoselective catalysis. The kinetic and mechanistic studies of the *R*-HPCDH site directed mutants are complemented by similar studies of the methionine mutants of *S*-HPCDH.

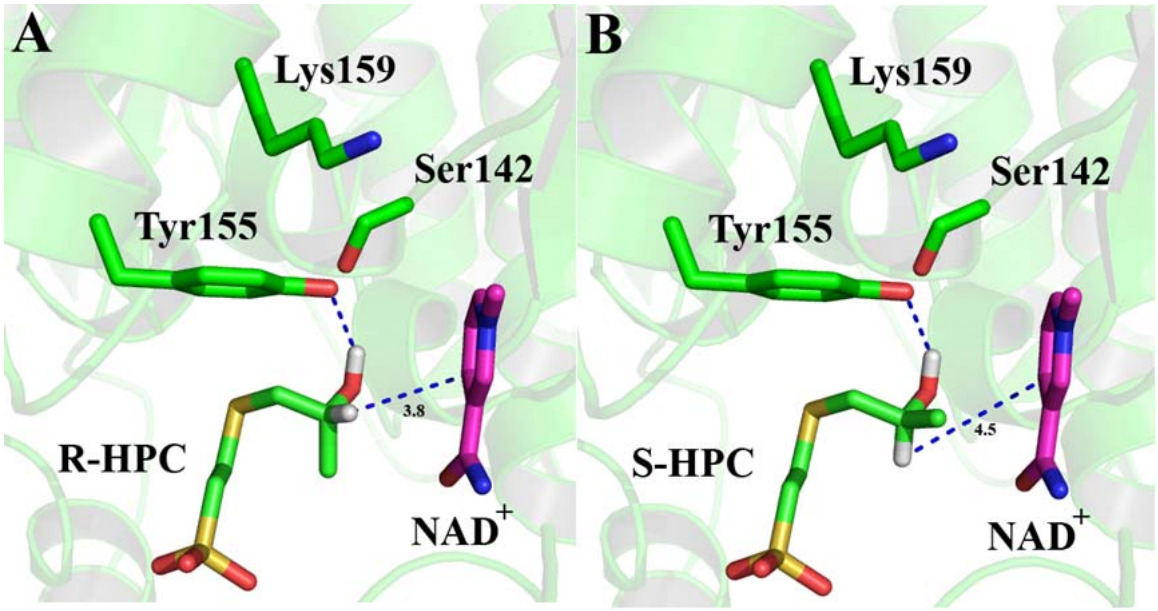

Figure 1-10. Binding mode of HPC enantiomers in the active site of *R*-HPCDH: (A) Active site of *R*-HPCDH with the substrate *R*-HPC bound. (B) Active site of *R*-HPCDH with the inhibitor *S*-HPC bound.

NADPH:2-Ketopropyl-CoM Carboxylase/Oxidoreductase. The final step in the pathway of reductive epoxide carboxylation is catalyzed by the enzyme NADPH:2-ketopropyl-CoM carboxylase/oxidoreductase (2-KPCC) (*39, 40*). This reaction is an NADPH-dependent carboxylation of 2-ketopropyl-CoM (2-KPC) to regenerate CoM and produce acetoacetate. It is also the actual CO_2 fixation step in epoxide metabolism (*40*). 2-KPCC is a homodimeric protein consisting of 57-kDa subunits with one FAD bound per subunit. Amino acid sequence analysis shows that 2-KPCC is a member of the FAD containing NADPH:disulfide oxidoreductase (DSOR) family of enzymes (*44*). Other members of this family include trypanothione reductase,

glutathione reductase, thioredoxin reductase, mercuric reductase and dihydrolipoamide dehydrogenase. All members of this family are NADPH and FAD dependent and catalyze the two-electron reduction of a disulfide bond (*44*). The exceptions are: mercuric reductase and 2-KPCC which catalyze the reduction of the mercuric ion to elemental mercury and the reduction of a thioether bond, respectively. An important feature of the DSOR enzymes is the presence of two highly conserved redox cysteines critical in the substrate reduction. The kinetic and structural characterization of 2-KPCC from *X. autotrophicus* Py2 resulted in the elucidation of the mechanism presented in Figure 1-11 (*39*).

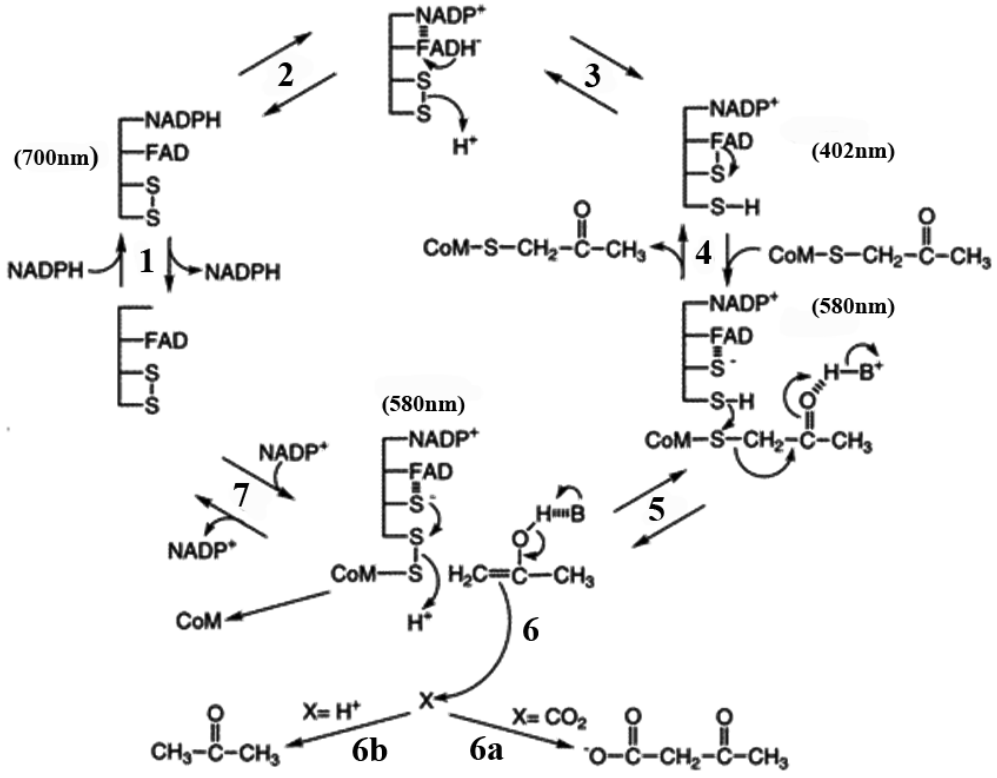

Figure 1-11. Proposed catalytic mechanism for the reductive cleavage and carboxylation of 2-KPC by 2-KPCC. The numbers refer to the steps of the cycle of 2-ketopropyl-CoM carboxylation. This figure was adapted from Ensign (*3*).

The catalytic mechanism includes two half-reactions. The first, reductive half is conserved among all true members of DSOR family and involves transfer of the reducing equivalents from NADPH to FAD and further to one of the cysteines forming a redox disulfide bond. In the second half the substrate is reductively cleaved and the enzyme regenerated. Specifically, in step 1 of the proposed mechanism, NADPH binds to the oxidized enzyme. In step 2 FAD is reduced. In step 3 the redox active disulfide is reduced by $FADH_2$ to form the interchange thiol-FAD covalent complex. During step 4, the electron transfer from FAD to the interchange thiol occurs resulting in the formation of the charge-transfer complex with the negative charge residing on the proximal thiol. At the same time the substrate 2-KPC binds to the enzyme. In step 5 the thioether bond of 2-KPC is reductively cleaved by the nucleophilically attack of the thiol of Cys82, forming enolacetone and the heterodisulfide bond between the thiols of CoM and the distal Cys82. The enolacetone is stabilized through its tautomerization to form the carbanion which can either attack CO_2 forming acetoacetate or a proton forming acetone. When CO_2 is present little or no acetone is formed. In the final step CoM and $NADP^+$ are released from the enzyme and the redox active disulfide is reconstituted. Experimental evidence indicated that all six reaction steps are fully reversible. Outlined in Scheme 1-4 are the five different catalytic activities associated with 2-KPCC, and in each, enolacetone is a proposed intermediate (*39*).

(1) $H_3CCOCH_2S\text{-}CoM + NADPH + \mathbf{CO_2} \rightarrow H_3CCOCH_2\mathbf{COO^-} + NADP^+ + CoM$

(2) $H_3CCOCH_2\mathbf{S\text{-}CoM} + NADPH + H+ \rightarrow H_3CCOCH_3 + NADP^+ + \mathbf{CoM}$

(3) $H_3CCOCH_2\mathbf{COO^-} + NADP^+ + \mathbf{CoM} \rightarrow H_3CCOCH_2\mathbf{S\text{-}CoM} + NADPH + \mathbf{CO_2}$

(4) $H_3CCOCH_2\mathbf{COO^-} + H^+ \rightarrow H_3CCOCH_3 + \mathbf{CO_2}$

(5) $H_3\mathbf{C}COCH_2COO^- + {}^{14}\mathbf{C}O_2 \rightarrow 1\text{-}[{}^{14}\mathbf{C}]\text{-}H_3CCOCH_2COO^-$

Scheme 1-4.

The molecular structure of 2-KPCC was recently solved and provided further insights into the mechanism of reductive cleavage of 2-KPC (*77*). The overall structure of 2-KPCC is similar to the dimeric structures observed for the classic members of the DSOR family (Figure 1-12) namely glutathione reductase (*78*), trypanothione reductase (*79*) and lipoamide dehydrogenase (*80*). Each monomer consists of three domains, including the FAD-binding domain, the NADPH binding domain, and the dimerization domain, or the interface domain.

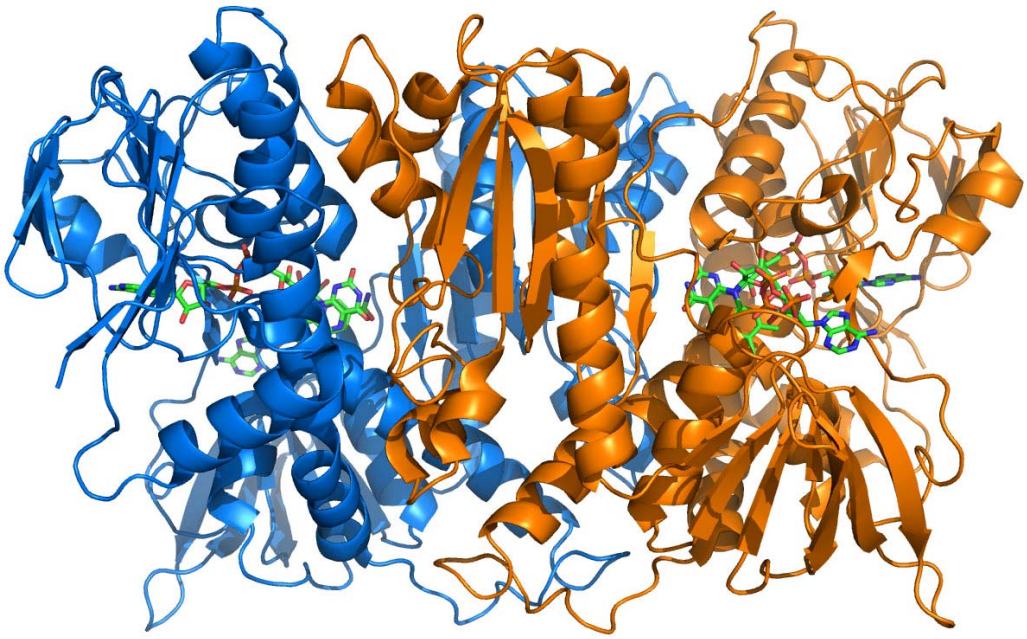

Figure 1-12. The overall fold of 2-KPCC with NADP and FAD bound (green). Individual subunits are depicted in orange and blue.

The FAD and NADPH binding domain consists of the standard Rossmann nucleotide binding motifs, as observed for the SDR enzymes discussed above. The structure of 2-KPCC with the substrate bound suggests a conformational change follows binding of 2-KPC, which is belived to prevent protonation of the substrate (*77*). In this way the enzyme also assures that there is a

linear pathway for electron pair transfer between FAD, the redox active disulfide and the thioether bond of the substrate. Again, as with the R-HPCDH, the substrate is bound and oriented by two arginines (Arg56 and Arg365) which bind the substrate with both hydrogen bonds and ionic interactions (81). The structure of the enzyme with 2-KPC bound revealed a linear reduction pathway between NADPH, FAD, the distal and proximal cysteine thiols, and the thioether linkage of 2-KPC. Structural analysis of the native and the substrate bound structures supports the mechanism of the reaction as proposed by Clark and Ensign (shown in Figure 1-11).

Concluding Remarks. The central goal of the research presented in the following chapters of this dissertation was to extend the kinetic, mechanistic and structural characterization of *R*- HPCDH and *S*-HPCDH in the context of their high degree of enantioselectivity. Both enzymes represent a unique example of the complementary SDR enzymes present in a common metabolic pathway, thus allowing the organism to utilize enantiomeric mixtures of epoxides as the carbon and energy source. Since *R*- and *S*-HPC dehydrogenases are an integral part of the epoxide carboxylase system, it is essential to present them in the broader context of the other enzymes in the pathway. The substrate flow and the physiological background are of great relevance to understanding both their role and the mechanism of action. Thereby this introduction has gone into great detail on topics ranging from the biological reactivity of epoxides, propylene metabolism and biochemical characterization of the enzymes constituting the epoxide carboxylase system to mechanistic and structural details of the SDR enzymes. This was done in order to introduce the relevance of this research, orient the reader on the work that has previously been conducted, and give an extensive introduction to the following chapters. The interested reader is referred to the many review articles cited in the text for a more in-depth understanding of the presented topics.

REFERENCES

1. Wade, D. R., Airy, S. C., and Sinsheimer, J. E. (1978) Mutagenicity of aliphatic epoxides. *Mutat. Res.-Genet. Tox. 58*, 217-223.

2. Voogd, C. E., Van der Stel, J. J., and Jacobs, J. (1981) The mutagenic action of aliphatic epoxides. *Mutat. Res.-Genet. Tox. 89*, 269-282.

3. Ensign, S. A. (2001) Microbial metabolism of aliphatic alkenes. *Biochemistry 40*, 5845-5853.

4. Allen, J. R., and Ensign, S. A. (1996) Carboxylation of epoxides to beta-keto acids in cell extracts of *Xanthobacter* strain Py2. *J. Bacteriol. 178*, 1469.

5. Calamur, N., and Carrera M. (1996) Propylene, in *Encyclopedia of Chemical Technology* (Howe-Grant, M., Ed.), pp 249-271, John-Wiley and Sons, Inc., New York.

6. Trent, D. L. (1996) Propylene oxide, in *Encyclopedia of Chemical Technology* (Howe-Grant, M., Ed.), pp 271-302, John-Wiley and Sons, Inc., New York.

7. (2010) Propylene oxide, Dow Chemical Company.

8. Hart, A., and Brown, M. W. (1974) Propylene oxide as sterilizing agent. *Appl. Microbiol. 28*, 1069.

9. Krijgsheld, K. R., and Van der Gen, A. (1986) Assessment of the impact of the emission of certain organochlorine compounds on the aquatic environment: Part III: Epichlorohydrin. *Chemosphere 15*, 881-893.

10. Small, F., and Ensign, S. (1997) Alkene monooxygenase from Xanthobacter strain Py2. *J. Biol. Chem. 272*, 24913.

11. Miura, A., and Dalton, H. (1995) Purification and characterization of the alkene monooxygenase from Nocardia corallina B-276. *Biosci. Biotechnol. Biochem. 59*, 853-859.

12. Guengerich, F. P. (1991) Reactions and significance of cytochrome P-450 enzymes. *J. Biol. Chem. 266*, 10019.

13. Guengerich, F. P., Liebler, D. C., and Reed, D. L. (1985) Enzymatic activation of chemicals to toxic metabolites. *Crit. Rev. Toxicol. 14*, 259-307.

14. Maples, K. R., and Dahl, A. R. (1991) Blood levels of propylene oxide during propylene inhalation and effect on hepatic and nasal cytochrome P-450 concentrations. *Drug Metab. Dispos. 19*, 835-837.

15. McClay, K., Fox, B. G., and Steffan, R. J. (2000) Toluene monooxygenase-catalyzed epoxidation of alkenes. *Appl. Environ. Microbiol. 66*, 1877.

16. Lipscomb, J. D. (1994) Biochemistry of the soluble methane monooxygenase. *Annu. Rev. Microb. 48*, 371-399.

17. Hooper, A. B., Vannelli, T., Bergmann, D. J., and Arciero, D. M. (1997) Enzymology of the oxidation of ammonia to nitrite by bacteria. *Antonie Van Leeuwenhoek 71*, 59-67.

18. Staijen, I. E., van Beilen, J. B., and Witholt, B. (2001) Expression, stability and performance of the three-component alkane mono-oxygenase of Pseudomonas oleovorans in Escherichia coli. *Eur. J. Biochem. 267*, 1957-1965.

19. van Hylckama Vlieg, J. E. T., Tang, L., Lutje Spelberg, J. H., Smilda, T., Poelarends, G. J., Bosma, T., van Merode, A. E. J., Fraaije, M. W., and Janssen, D. B. (2001) Halohydrin dehalogenases are structurally and mechanistically related to short-chain dehydrogenases/reductases. *J. Bacteriol. 183*, 5058.

20. Ehrenberg, L., and Hussain, S. (1981) Genetic toxicity of some important epoxides* 1. *Mutat. Res.-Rev. Genet. 86*, 1-113.

21. Salinas, A. E., and Wong, M. G. (1999) Glutathione S-transferases--a review. *Curr. Med. Chem. 6*, 279.

22. Armstrong, R. N., and Cassidy, C. S. (2000) New structural and chemical insights into the catalytic mechanism of epoxide hydrolases. *Drug Metab. Rev. 32*, 327-338.

23. Morisseau, C., and Hammock, B. D. (2004) Epoxide hydrolases: mechanisms, inhibitor designs, and biological roles.

24. Fretland, A. J., and Omiecinski, C. J. (2000) Epoxide hydrolases: biochemistry and molecular biology. *Chem. Biol. Interact. 129*, 41-59.

25. Allen, J. R., Clark, D. D., Krum, J. G., and Ensign, S. A. (1999) A role for coenzyme M (2-mercaptoethanesulfonic acid) in a bacterial pathway of aliphatic epoxide carboxylation. *Proc. Natl. Acad. Sci. U.S.A. 96*, 8432-8437.

26. Allen, J. R., and Ensign, S. A. (1999) Two short-chain dehydrogenases confer stereoselectivity for enantiomers of epoxypropane in the multiprotein epoxide carboxylating systems of *Xanthobacter* strain Py2 and *Nocardia corallina* B276. *Biochemistry 38*, 247-256.

27. Krum, J. G., and Ensign, S. A. (2000) Heterologous expression of bacterial Epoxyalkane: coenzyme M transferase and inducible coenzyme M biosynthesis in *Xanthobacter* strain Py2 and *Rhodococcus rhodochrous* B276. *J. Bacteriol. 182*, 2629-2634.

28. Hartmans, S., Smits, J. P., Van der Werf, M. J., Volkering, F., and De Bont, J. A. M. (1989) Metabolism of styrene oxide and 2-phenylethanol in the styrene-degrading Xanthobacter strain 124X. *Appl. Environ. Microbiol. 55*, 2850.

29. Wallin, R., Sane, D. C., and Hutson, S. M. (2002) Vitamin K 2, 3-epoxide reductase and the vitamin K-dependent [gamma]-carboxylation system. *Thromb. Res. 108*, 221-226.

30. Wallin, R., and Guenthner, T. M. (1997) Purification of warfarin-sensitive vitamin K epoxide reductase. *Methods Enzymol.*, 395-407.

31. Allen, J., and Ensign, S. (1996) Carboxylation of epoxides to beta-keto acids in cell extracts of Xanthobacter strain Py2. *J. Bacteriol. 178*, 1469.

32. Allen, J. R., and Ensign, S. A. (1998) Identification and characterization of epoxide carboxylase activity in cell extracts of Nocardia corallina B276. *J. Bacteriol. 180*, 2072.

33. De Bont, J. A. M., Van Dijken, J. P., and Van Ginkel, K. G. (1982) The metabolism of 1, 2-propanediol by the propylene oxide utilizing bacterium Nocardia A60. *BBA-Gen. Subjects 714*, 465-470.

34. Gallagher, S. C., Cammack, R., and Dalton, H. (1997) Alkene monooxygenase from Nocardia corallina B-276 is a member of the class of dinuclear iron proteins capable of stereospecific epoxygenation reactions. *Eur. J. Biochem. 247*, 635-641.

35. Small, F. J., and Ensign, S. A. (1997) Alkene monooxygenase from Xanthobacter strain Py2. *J. Biol. Chem. 272*, 24913.

36. Thauer, R. K. (1998) Biochemistry of methanogenesis: a tribute to Marjory Stephenson. *Microbiology 144*, 2377-2406.

37. Wolfe, R. S. (1991) My kind of biology. *Annu. Rev. Microbiol. 45*, 1-36.

38. Gunsalus, R. P., Romesser, J. A., and Wolfe, R. S. (1978) Preparation of coenzyme M analogs and their activity in the methyl coenzyme M reductase system of Methanobacterium thermoautotrophicum. *Biochemistry 17*, 2374-2377.

39. Clark, D. D., Allen, J. R., and Ensign, S. A. (2000) Characterization of five catalytic activities associated with the NADPH:2-ketopropyl-coenzyme M [2-(2-ketopropylthio)ethanesulfonate] oxidoreductase/carboxylase of the *Xanthobacter* strain Py2 epoxide carboxylase system. *Biochemistry 39*, 1294-1304.

40. Allen, J. R., and Ensign, S. A. (1997) Purification to homogeneity and reconstitution of the individual components of the epoxide carboxylase multiprotein enzyme complex from *Xanthobacter* strain Py2. *J. Biol. Chem. 272*, 32121-32128.

41. Clark, D. D., and Ensign, S. A. (2002) Characterization of the 2-[(R)-2-hydroxypropylthio]ethanesulfonate dehydrogenase from *Xanthobacter* strain Py2: product inhibition, pH dependence of kinetic parameters, site-directed mutagenesis, rapid equilibrium inhibition, and chemical modification. *Biochemistry 41*, 2727-2740.

42. Krum, J. G., Ellsworth, H., Sargeant, R. R., Rich, G., and Ensign, S. A. (2002) Kinetic and microcalorimetric analysis of substrate and cofactor interactions in epoxyalkane:CoM transferase, a zinc-dependent epoxidase. *Biochemistry 41*, 5005-5014.

43. Zhou, Z. S., Peariso, K., Penner-Hahn, J. E., and Matthews, R. G. (1999) Identification of the zinc ligands in cobalamin-independent methionine synthase (MetE) from Escherichia coli. *Biochemistry 38*, 15915-15926.

44. Ensign, S. A., and Allen, J. R. (2003) Aliphatic epoxide carboxylation. *Annu. Rev. Biochem. 72*, 55-76.

45. Boyd, J. M., and Ensign, S. A. (2005) Evidence for a metal-thiolate intermediate in alkyl group transfer from epoxypropane to coenzyme M and cooperative metal ion binding in epoxyalkane:CoM transferase. *Biochemistry 44*, 13151-13162.

46. Clark, D. D., and Ensign, S. A. (2002) Characterization of the 2- (R)-2-hydroxypropylthio ethane sulfonate dehydrogenase from Xanthobacter strain Py2: product inhibition, pH dependence of kinetic parameters, site-directed mutagenesis, rapid equilibrium inhibition, and chemical modification. *Biochemistry 41*, 2727-2740.

47. Clark, D. D., Boyd, J. M., and Ensign, S. A. (2004) The stereoselectivity and catalytic properties of *Xanthobacter autotrophicus* 2-[(R)-2-Hydroxypropylthio]ethanesulfonate dehydrogenase are controlled by interactions between C-terminal arginine residues and the sulfonate of coenzyme M. *Biochemistry 43*, 6763-6771.

48. Jörnvall, H., Höög, J. O., and Persson, B. (1999) SDR and MDR: completed genome sequences show these protein families to be large, of old origin, and of complex nature. *FEBS Lett. 445*, 261-264.

49. Joernvall, H., Persson, B., Krook, M., Atrian, S., Gonzalez-Duarte, R., Jeffery, J., and Ghosh, D. (1995) Short-chain dehydrogenases/reductases (SDR). *Biochemistry 34*, 6003-6013.

50. Oppermann, U. C. T., Filling, C., and Jörnvall, H. (2001) Forms and functions of human SDR enzymes. *Chem. Biol. Interact. 130*, 699-705.

51. Kallberg, Y., Oppermann, U., Jörnvall, H., and Persson, B. (2002) Short-chain dehydrogenase/reductase (SDR) relationships: a large family with eight clusters common to human, animal, and plant genomes. *Protein Sci. 11*, 636-641.

52. Persson, B., Kallberg, Y., Bray, J. E., Bruford, E., Dellaporta, S. L., Favia, A. D., Duarte, R. G., Jörnvall, H., Kavanagh, K. L., and Kedishvili, N. (2009) The SDR (short-chain dehydrogenase/reductase and related enzymes) nomenclature initiative. *Chem. Biol. Interact. 178*, 94-98.

53. Oppermann, U., Filling, C., Hult, M., Shafqat, N., Wu, X., Lindh, M., Shafqat, J., Nordling, E., Kallberg, Y., Persson, B., and Jörnvall, H. (2003) Short-chain dehydrogenases/reductases (SDR): the 2002 update. *Chem. Biol. Interact. 143-144*, 247-253.

54. Wierenga, R. K., Terpstra, P., and Hol, W. G. J. (1986) Prediction of the occurrence of the ADP-binding [beta][alpha][beta]-fold in proteins, using an amino acid sequence fingerprint. *J. Mol. Biol. 187*, 101-107.

55. Kallberg, Y., Oppermann, U., Jornvall, H., and Persson, B. (2002) Short-chain dehydrogenases/reductases (SDRs): Coenzyme-based functional assignments in completed genomes. *Eur. J. Biochem. 269*, 4409.

56. Filling, C., Berndt, K. D., Benach, J., Knapp, S., Prozorovski, T., Nordling, E., Ladenstein, R., Jornvall, H., and Oppermann, U. (2002) Critical residues for structure and catalysis in short-chain dehydrogenases/reductases. *J. Biol. Chem. 277*, 25677-25684.

57. Oppermann, U. C. T., Filling, C., Berndt, K. D., Persson, B., Benach, J., Ladenstein, R., and Joernvall, H. (1997) Active site directed mutagenesis of 3 beta/17 beta-hydroxysteroid dehydrogenase establishes differential effects on short-chain dehydrogenase/reductase reactions. *Biochemistry 36*, 34-40.

58. Filling, C., Nordling, E., Benach, J., Berndt, K. D., Ladenstein, R., Jörnvall, H., and Oppermann, U. (2001) Structural role of conserved Asn179 in the short-chain dehydrogenase/reductase scaffold. *Biochem. Biophys. Res. Commun. 289*, 712-717.

59. Kavanagh, K. L., Jörnvall, H., Persson, B., and Oppermann, U. (2008) The SDR superfamily: functional and structural diversity within a family of metabolic and regulatory enzymes. *Cell. Mol. Life Sci. 65*, 3895-3906.

60. Kallberg, Y., and Persson, B. (2006) Prediction of coenzyme specificity in dehydrogenases/reductases. *FEBS Journal 273*, 1177-1184.

61. Lesk, A. M. (1995) NAD-binding domains of dehydrogenases. *Curr. Opin. Struct. Biol. 5*, 775-783.

62. Tanaka, N., Nonaka, T., Nakamura, K. T., and Hara, A. (2001) SDR structure, mechanism of action, and substrate recognition. *Curr. Org. Chem. 5*, 89-111.

63. McKinley-Mckee, J. S., Winberg, J. O., and Pettersson, G. (1991) Mechanism of action of *Drosophila melanogaster* alcohol dehydrogenase. *IUBMB Life 25*, 879-885.

64. Benach, J., Atrian, S., Gonzàlez-Duarte, R., and Ladenstein, R. (1999) The catalytic reaction and inhibition mechanism of *Drosophila* alcohol dehydrogenase: observation of an enzyme-bound NAD-ketone adduct at 1.4 Å resolution by X-ray crystallography. *J. Mol. Biol. 289*, 335-355.

65. Duax, W. L., Ghosh, D., and Pletnev, V. (2000) Steroid dehydrogenase structures, mechanism of action, and disease. *Vitam. Horm. 58*, 121-148.

66. Vallee, B. L., and Auld, D. S. (1990) Zinc coordination, function, and structure of zinc enzymes and other proteins. *Biochemistry 29*, 5647-5659.

67. Leskovac, V., Trivi , S., and Anderson, B. M. (1999) Comparison of the chemical mechanisms of action of yeast and equine liver alcohol dehydrogenase. *Eur. J. Biochem. 264*, 840-847.

68. Al-Karadaghi, S., Cedergren-Zeppezauer, E. S., Hovmoller, S., Petratos, K., Terry, H., and Wilson, K. S. (1994) Refined crystal structure of liver alcohol dehydrogenase-NADH complex at 1.8 A resolution. *Acta Crystallogr., Sect. D: Biol. Crystallogr. 50*, 793-807.

69. Krozowski, Z. (1994) The short-chain alcohol dehydrogenase superfamily: variations on a common theme. *J. Steroid Biochem. 51*, 125-130.

70. Liao, D. I., Thompson, J. E., Fahnestock, S., Valent, B., and Jordan, D. B. (2001) A structural account of substrate and inhibitor specificity differences between two naphthol reductases. *Biochemistry 40*, 8696-8704.

71. Eklund, H., Plapp, B. V., Samama, J. P., and Branden, C. I. (1982) Binding of substrate in a ternary complex of horse liver alcohol dehydrogenase. *J. Biol. Chem. 257*, 14349-14358.

72. Nakajima, K., Hashimoto, T., and Yamada, Y. (1993) Two tropinone reductases with different stereospecificities are short-chain dehydrogenases evolved from a common ancestor. *Proc. Natl. Acad. Sci.U.S.A. 90*, 9591-9595.

73. Nakajima, K., Hashimoto, T., and Yamada, Y. (1994) Opposite stereospecificity of two tropinone reductases is conferred by the substrate-binding sites. *J. Biol. Chem. 269*, 11695-11698.

74. Krishnakumar, A. M., Nocek, B. P., Clark, D. D., Ensign, S. A., and Peters, J. W. (2006) Structural basis for stereoselectivity in the (R)- and (S)-hydroxypropyl thioethanesulfonate dehydrogenases. *Biochemistry 45*, 8831-8840.

75. Horer, S., Stoop, J., Mooibroek, H., Baumann, U., and Sassoon, J. (2001) The crystallographic structure of the mannitol 2-dehydrogenase NADP+ binary complex from Agaricus bisporus. *J. Biol. Chem. 276*, 27555.

76. de Jong, R. M., Tiesinga, J. J. W., Rozeboom, H. J., Kalk, K. H., Tang, L., Janssen, D. B., and Dijkstra, B. W. (2003) Structure and mechanism of a bacterial haloalcohol dehalogenase: a new variation of the short-chain dehydrogenase/reductase fold without an NAD (P) H binding site. *The EMBO Journal 22*, 4933.

77. Nocek, B., Jang, S. B., Jeong, M. S., Clark, D. D., Ensign, S. A., and Peters, J. W. (2002) Structural basis for CO_2 fixation by a novel member of the disulfide oxidoreductase family of enzymes, 2-ketopropyl-coenzyme M oxidoreductase/carboxylase. *Biochemistry 41*, 12907-12913.

78. Karplus, P. A., Pai, E. F., and Schulz, G. E. (1989) A crystallographic study of the glutathione binding site of glutathione reductase at 0.3-nm resolution. *Eur. J. Biochem. 178*, 693-703.

79. Kuriyan, J., Kong, X. P., Krishna, T. S., Sweet, R. M., Murgolo, N. J., Field, H., Cerami, A., and Henderson, G. B. (1991) X-ray structure of trypanothione reductase from Crithidia fasciculata at 2.4-A resolution. *Proc. Natl. Acad. Sci. 88*, 8764.

80. Schierbeek, A. J., Swarte, M. B. A., Dijkstra, B. W., Vriend, G., Read, R. J., Hol, W. G. J., Drenth, J., and Betzel, C. (1989) X-ray structure of lipoamide dehydrogenase from Azotobacter vinelandii determined by a combination of molecular and isomorphous replacement techniques. *J. Mol. Biol. 206*, 365-379.

CHAPTER 2

MOLECULAR BASIS FOR ENANTIOSELECTIVITY IN THE *(R)*- AND *(S)*-HYDROXYPROPYLTHIOETHANESULFONATE DEHYDROGENASES, A UNIQUE PAIR OF STEREOSELECTIVE SHORT-CHAIN DEHYDROGENASES/REDUCTASES INVOLVED IN ALIPHATIC EPOXIDE CARBOXYLATION[1]

ABSTRACT

(*R*)- and *(S)*-2-hydroxypropyl-CoM (*R*-HPC and *S*-HPC) are produced as intermediates in bacterial propylene metabolism from the nucleophilic addition of coenzyme M to *(R)*- and *(S)*-epoxypropane, respectively. Two highly enantioselective dehydrogenases (*R*-HPCDH and *S*-HPCDH) belonging to the short-chain dehydrogenase/reductase family catalyze the conversion of *R*-HPC and *S*-HPC to 2-ketopropyl-CoM (2-KPC), which undergoes reductive cleavage and carboxylation to produce acetoacetate. In the present study, one of three copies of *S*-HPCDH enzymes present on a linear megaplasmid in *Xanthobacter autotrophicus* strain Py2 has been cloned and overexpressed, allowing the first detailed side by side characterization of the *R*-HPCDH and *S*-HPCDH enzymes. The catalytic triad of *S*-HPCDH was found to consist of Y156, K160, and S143. R211 and K214 were identified as the amino acid residues coordinating the sulfonate of CoM in *S*-HPC. R211A and K214A mutants were severely impaired in the oxidation of *R*-HPC or reduction of 2-KPC but were largely unaffected in the oxidation and reduction of aliphatic alcohols and ketones. Kinetic analyses using *(R)*- and *(S)*-HPC as substrates revealed that enantioselectivity in *R*-HPCDH (value, 944) was dictated largely by differences in k_{cat} while enantioselectivity for *S*-HPCDH (value, 658) was dictated largely by changes in K_m. *S*-HPCDH had an inherent high enantioselectivity for producing (*S)*-2-butanol from 2-butanone that was *S*-had an inherent high enantioselectivity for producing *(S)*-2-butanol from 2-butanone that was unaffected by modulators that interact with the sulfonate binding site. The tertiary alcohol 2-methyl-2-hydroxypropyl-CoM (M-HPC) was a competitive inhibitor of *R*-HPCDH-catalyzed *R*-

[1]Coauthored by Dariusz A. Sliwa, Arathi M. Krishnakumar, John W. Peters and Scott A. Ensign.

HPC oxidation, with a K_{is} similar to the K_m for *R*-HPC, but was not an inhibitor of *S*-HPCDH. The primary alcohol 2-hydroxyethyl-CoM was a substrate for both *R*-HPCDH and *S*-HPCDH with identical K_m values. The pH dependence of kinetic parameters suggests that the hydroxyl group is a larger contributor to *S*-HPC binding to *S*-HPCDH than for *R*-HPC binding to *R*-HPCDH. It is proposed that active site constraints within the *S*-HPCDH prevent proper binding of *R*-HPC and M-HPC due to steric clashes with the improperly aligned methyl group on the C2 carbon, resulting in a different mechanism for controlling substrate specificity and enantioselectivity than present in the *R*-HPCDH.

INTRODUCTION

Alcohol dehydrogenases that catalyze the interconversion of secondary alcohols and ketones are often highly stereoselective with regard to the enantiomer of the alcohol oxidized or produced during the course of catalysis (*1-3*). However, there are very few examples of pairs of alcohol dehydrogenases expressed simultaneously by an organism to deal with both the *(R)*- and *(S)*-enantiomers of an alcohol produced during a metabolic pathway. One such unique pair was discovered in the pathway of propylene oxidation by the hydrocarbon-oxidizing bacteria *Xanthobacter autotrophicus* Py2 and *Rhodococcus rhodochrous* B276 (*4-8*). As shown in Figure 2-1, these bacteria initiate propylene oxidation by epoxidation to produce a mixture of the *(R)*- and *(S)*-enantiomers of epoxypropane. The atypical thiol cofactor Coenzyme M (2-mercaptoethanesulfonate, CoM) then acts a nucleophile to convert these epoxides to the chiral alcohols *(R)*- and *(S)*-hydroxypropyl-CoM (*R*- and *S*-HPC) (Figure 1-1). *R*- and *S*-HPC are the substrates for the unique pair of dehydrogenases that convert these alcohols to the ketone 2-ketopropyl-CoM (2-KPC), which subsequently undergoes reductive cleavage and carboxylation to produce acetoacetate (*4*).

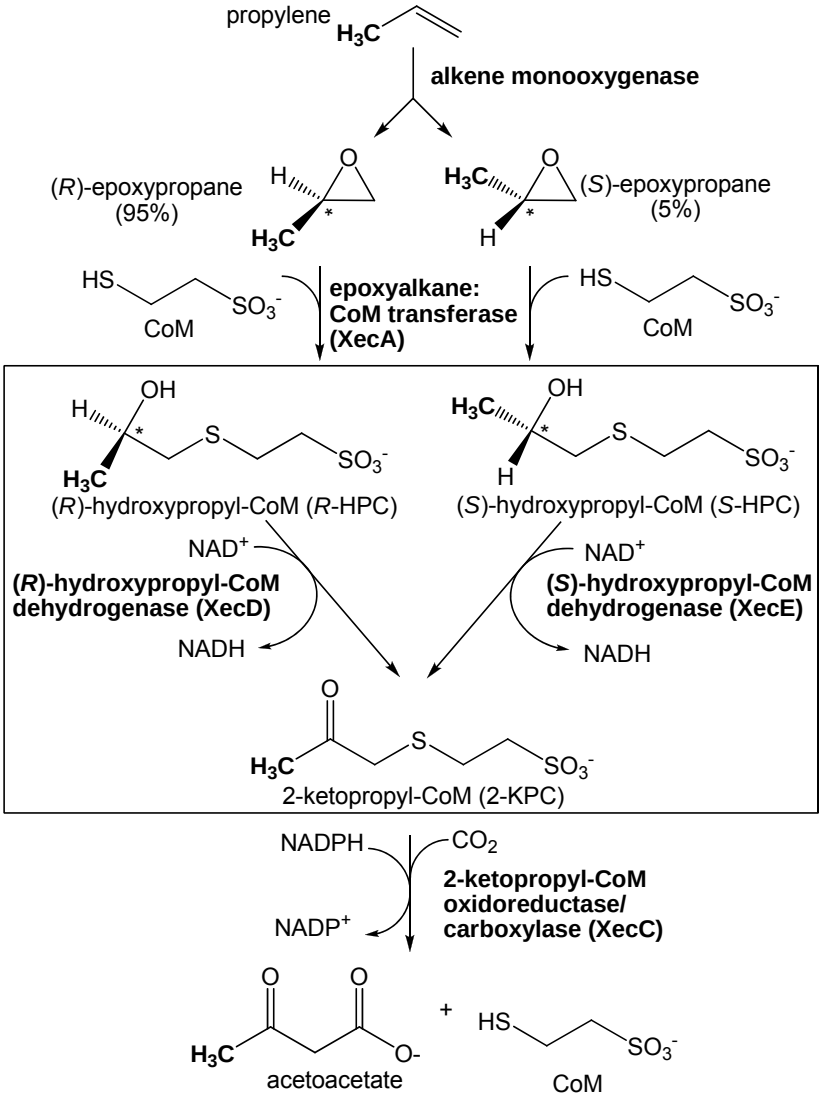

Figure 2-1. Pathway of propylene oxidation in *X. autotrophicus* Py2. The reactions catalyzed by *R*-HPCDH and *S*-HPCDH are shown in the boxed region.

Biochemical and molecular characterization of the *R*- and *S*-HPCDH enzymes showed that they are members of the "classical" short-chain dehydrogenase/reductase (SDR) family of alcohol dehydrogenases (*4-6*). Classical SDR enzymes typically contain a single polypeptide chain of about 25 kDa and are active as dimers or tetramers (*9-13*). They are further defined by a conserved NAD^+-binding motif in the N-terminal portion of the protein and a catalytic triad (or tetrad) within the central portion, with a conserved tyrosine of this tetrad serving as the general

base (or acid) for alcohol oxidation (or ketone reduction) (*9-13*). The C-terminal domains of the SDR families diverge to confer specificity for different substrates. Close to 10,000 dehydrogenases have been assigned to this SDR family, while more than 46,000 have been annotated in gene databases (*10, 12*).

The *R*- and *S*-HPCDH enzymes from *X. autotrophicus* are homologous enzymes that share high sequence identity but with notable sequence differences within their C-terminal regions (*5-8*). These enzymes are highly specific for their respective enantiomers of HPC, exhibiting less that 0.5% activity with the opposite isomer (*4*). Thus, side by side comparative studies of this enzyme pair promise to reveal important details into the mechanistic strategies that confer stereoselectivity for secondary alcohol enantiomers.

The *R*-HPCDH from *X. autotrophicus* has been extensively characterized mechanistically and structurally, culminating in the formulation of a mechanism of catalysis and stereoselectivity shown on the left side of Scheme 2-1 (*14-16*). Stereoselectivity is conferred in large part by two positively charged arginine residues that form salt bridges with the CoM moiety of the substrate within the CoM-binding pocket of the enzyme (*14, 16*). This strong ionic interaction orients the hydroxyl group and hydrogen atom of the alcohol functional group in the proper orientation for general base abstraction and hydride transfer (Scheme 2-1) (*16*). By analogy, a similar mechanistic strategy is believed to operate in the *S*-HPCDH, wherein the spatial orientations of the CoM- and methyl-binding pockets are reversed relative to the hydroxyl group and hydrogen atom to be transferred (Scheme 2-1, right side) (*14, 16, 17*). To date, this model has not been tested for the *S*-HPCDH due to difficulties encountered in attempting to express the enzyme in an active form in *Eschericia coli (14, 15)*.

Recently, the complete genome of *X. autotrophicus* was sequenced (http://genome.jgi-psf.org/xanau/xanau.home.html). An analysis of the genome reveals that multiple copies of the genes that encode the key enzymes of epoxide carboxylation are present. These homologs share high sequence identity but are not identical. In the present work, one of the additional copies of

the *S*-HPCDH homologs that had not been identified earlier was successfully cloned and over-expressed in *E. coli*, providing the necessary system for construction of site-directed mutants and kinetic and mechanistic studies to test the tenets of Scheme 2-1. Some unexpected and surprising results have come from these studies, which show that the *R*- and *S*-HPCDH enzymes share some common mechanistic features, but differ significantly in the strategies for controlling enantioselectivity for the *S*- and *R*-HPC natural substrates, as well as nonphysiological aliphatic alcohols and ketones. These studies provide the first detailed "side by side" kinetic and mechanistic analysis of such a novel pair of highly enantioselective dehydrogenases.

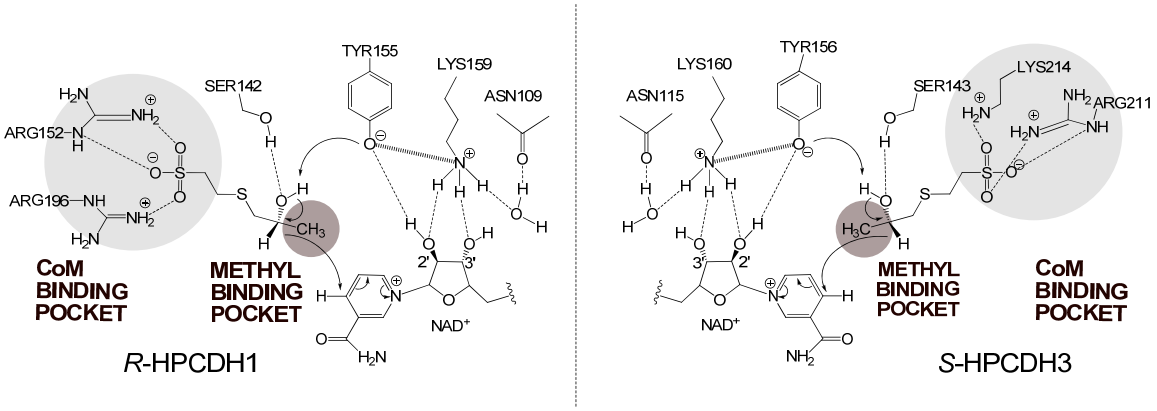

Scheme 2-1.

EXPERIMENTAL PROCEDURES

Materials. All commercially available chemicals were purchased from Sigma-Aldrich Chemicals, Acros Organics or Fisher Scientific, and were of analytical grade. 2-KPC, *R*-HPC *S*-HPC, HEC and M-HPC were synthesized as described previously (*15*). Chemical structures of the compounds were confirmed using ^{1}H NMR. The spectra of HPC enantiomers and 2-KPC were identical to those reported previously (*4, 15*). Purity of the synthesized chemicals as determined by reverse-phase HPLC was estimated to be ≥98%.

Cloning of the S-HPCDH Genes (xecE1, xecE2, and xecE3). Total genomic DNA was isolated from propylene-grown cells of *X. autotrophicus* strain Py2 using the Epicentre MasterPure DNA purification kit. Each of the three *xecE* genes was PCR amplified using the FailSafe PCR PreMix Selection Kit (Epicentre). Primers were designed such that the forward and reverse primers contained *BamH*I and *Sac*I restriction site overhangs, respectively. The primers were as follows:

xecE1: forward, GCAGGATCCAATGCTGGACGCAGAGG; reverse, CGTGAGCTCTCATATGGCGGTCATCC; *xecE2:* forward, TAGGATCCAGTGGCGCGCGCCGCGGT; reverse, ATGAGCTCTCATATGGCGGTCATCCCTC; *xecE3:* forward, GCAGGATCCAATGTCGAATCGCTTGAAG; reverse, GCAGAGCTCTCATATCGCCGTCATC.

The reactions contained 200 ng of *X. autotrophicus* genomic DNA, 1.0 μM primers, FailSafe PCR Enzyme Mix (1.25 Units), and the manufacturers buffer H. PCR was performed using the following cycling parameters: stage 1, (95 °C x 5 min) x 1; stage 2, (94 °C x 1min, 60 °C x 1 min, 72 °C x 50 s) x 35; stage 3, (72 °C x 10 min) x 1; The PCR products were analyzed on 1% (w/v) agarose gels, and *xecE1, xecE2* and *xecE3* DNA (0.75 kb, 0.69 kb, and 0.77 kb respectively) were purified using the QIAquick gel extraction kit (Qiagen). Purified DNA along with pET28-b (Novagen) and pRSFDuet-1 expression vectors were simultaneously subjected to a double digest with *Bam*HI and *Sac*I, resolved on 1% agarose gel and purified with the QIAquick gel extraction kit. Digested *xecE* genes and pET28-b DNA were mixed and ligated with T4 DNA ligase for 2h at 25ºC. The resulting plasmids were designated: pDS41, pDS42 and pDS43, and carried the *xecE1, xecE2* and *xecE3* genes, respectively. Likewise, digested *xecE* genes and pRSFDuet-1 DNA were mixed and ligated with T4 DNA ligase for 2h at 25ºC, to result in pDS51, pDS52 and pDS53 plasmids with *xecE1, xecE2* and *xecE3* genes, respectively.

Subsequent to DNA sequencing, all constructs were transformed into *E.coli* DH5α for plasmid maintenance and into *E. coli* BL21 - (DE3) CodonPlus (Stratagene) cells for protein expression.

Site-Directed Mutagenesis (SDM). All primers used to introduce point mutations were purchased from IDT. SDM of pDS53 was carried out utilizing the QuickChange Site-Directed Mutagenesis Kit (Stratagene) according to the manufacturer's protocols. All mutations were confirmed by DNA sequencing. The sequences of the mutagenic primer pairs used for each codon substitution in *xecE3* are as follows:

S143A, GATCGTCAATTTTGGCGCCGTCGCTGGCCTC and

GAGGCCAGCGACGGCGCCAAAATTGACGATC; Y156A,

GACCATGGCGGCCGCCTGCGCAGCCAAG and

CTTGGCTGCGCAGGCGGCCGCCATGGTC; Y156F,

CCATGGCGGCCTTCTGCGCAGCCAAGG and

CCTTGGCTGCGCAGAAGGCCGCCATGG; K160A,

CCTACTGCGCAGCCGCGGGCGCAATCGTCA and

TGACGATTGCGCCCGCGGCTGCGCAGTAGG; R211A,

GAAGTTCAGGCTCGCGCGCTGGCGAAATATCC and

GGATATTTCGCCAGCGCGCGAGCCTGAACTTC; K214A,

CTCGCCGGCTGGCGGCATATCCGATCGGGC and

GCCCGATCGGATATGCCGCCAGCCGGCGAG.

DNA Sequencing. Sequencing was performed on an AB 3730 DNA Analyzer at the Utah State University CIB DNA sequencing laboratory. The following sequencing primers were used to confirm all mutations to pDS53; ACYCDuetUP1 Primer (Novagen), GGATCTCGACGCTCTCCCT and DuetDOWN1 Primer (Novagen), GATTATGCGGCCGTGTACAA.

Media and Growth of Bacteria. *X. autotrophicus* was grown on propylene (10% (v/v) gas phase) in a 15L semicontinuous microferm fermenter as described previously (*18*). *E.coli*

DH5α was grown in standard Luria-Bertani (LB) broth supplemented with kanamycin (50 $\mu g \cdot mL^{-1}$). *E. coli* BL21-(DE3) CodonPlus was grown in LB media that contained both kanamycin (50 $\mu g \cdot mL^{-1}$) and chloramphenicol (50 $\mu g \cdot mL^{-1}$). All other procedures were performed as described previously (*15*).

Preparation of Cell-Free Extracts. About 60 grams of frozen cell paste was thawed at room temperature in 2 volumes of lysis buffer (20 mM Tris, 20% glycerol, 500 mM NaCl, 25 mM imidazole, 0.1% (w/v) Tween20, 0.03 $mg \cdot mL^{-1}$ DNase I, at pH 8.0). Homogenized cell suspension was passed twice through a French press at 15000 psi and the crude lysate was clarified by centrifugation at 244,717*g* for 45 min. The supernatant was further used for purification.

Purification of S-HPCDH1, rS-HPCDH1, rS-HPCDH3 and rS-HPCDH3 Mutants. *S*-HPCDH was purified from propylene-grown *X. autotrophicus* as described previously (*5*). For the purification of *rS*-HPCDH1, *rS*-HPCDH3 and *rS*-HPCDH3 mutants, clarified cell extract was applied to a 2.6 x 4.7 cm column of Ni Sepharose 6 Fast Flow (Amersham) at 3.0 $mL \cdot min^{-1}$ (33.9 $cm \cdot h^{-1}$). The column was rinsed at 6.0 $mL \cdot min^{-1}$ (67.8 $cm \cdot h^{-1}$) with 2 column volumes of lysis buffer, followed by 80 column volumes of rinse buffer (20 mM Tris, 20% glycerol, 500 mM NaCl, 50 mM imidazole, 0.1% (w/v) Tween20, pH 8.0). *rS*-HPCDH was eluted at 4.0 $mL \cdot min^{-1}$ (45.2 $cm \cdot h^{-1}$) with a linear gradient of 19.2 column volumes of 0-100% elution buffer (20 mM Tris, 20% glycerol, 500 mM NaCl, 500 mM imidazole, pH 8.0). Fractions containing *rS*-HPCDH were concentrated over a 30000 MW cutoff membrane, diluted in a 1:20 ratio with dialysis buffer (20 mM Tris, 10% glycerol, 100 mM NaCl, pH 8.2) and concentrated again (this procedure was repeated twice). Procedures for overnight dialysis against 5L buffer, described previously for *rR*-HPCDH1 (*15*), couldn't be followed due to protein precipitation. Dialyzed *rS*-HPCDH was flash frozen and stored in liquid nitrogen. All steps were performed at 4 °C, and all buffers used had the pH adjusted at 4 °C. Protein concentrations were determined on a NanoDrop

spectrophotometer using theoretical extinction coefficients (ϵ_{280} = 10033 M^{-1} cm^{-1} for *S*-HPCDH3, ϵ_{280} = 15595 M^{-1} cm^{-1} for *S*-HPCDH1, and ϵ_{280} = 18512.5 M^{-1} cm^{-1} for *R*-HPCDH1), with dialysis flow-through buffers as blanks.

SDS-PAGE and Native PAGE Analysis. SDS-PAGE (12% T) and native PAGE (4-20% T BioRad) were performed according to the Laemmli procedure (*19*). The apparent molecular masses of polypeptides on a SDS-PAGE gel were determined by comparison to R_f values of standard proteins. Migration of *rS*-HPCDH3 mutants was also compared directly to wild-type *rS*-HPCDH3, wild-type *rR*-HPCDH1, native *S*-HPCDH and *R*-HPCDH (isolated from *X. autotrophicus*). The apparent molecular masses of polypeptides on a native PAGE gel were determined from a standard curve. The standard curve was constructed by plotting R_f values on against the log of the native molecular mass for the following standards: β-amylase (200 kDa), alcohol dehydrogenase (150 kDa), bovine serum albumin (66 kDa) and ovalbumin (43 kDa).

Gel Filtration Chromatography. The native molecular masses of *rS*-HPCDH3 and *rS*-HPCDH3 mutants were estimated by gel filtration chromatography using HPLC (Shimadzu SLC-10A) with a fluorescence detector (Shimadzu RF-10AXL) set up for excitation and emission wavelengths at 280 nm and 350 nm, respectively. The gel filtration column (BioSep-SEC S-2000, 300 x 7.8 mm, Phenomenex) was equilibrated in 50 mM Na_2HPO4, 200 mM NaCl, pH 7.5, containing 10% glycerol and 1 mM NAD^+. The following molecular mass standards were used for calibration: β-amylase (200 kDa), aldolase (158 kDa), conalbumin (75 kDa), bovine serum albumin (66 kDa), ovalbumin (43 kDa), carbonic anhydrase (29 kDa), and myoglobin (18.8 kDa). All separations were performed at 4 ºC, at a flow rate of 0.5 mL min^{-1}. A calibration curve was constructed by plotting the retention time against the log of the native molecular mass for standards. This plot was fit using a second order polynomial, and the equation of this line was used to determine the log native molecular masses for *rS*-HPCDH3 and *rS*-HPCDH3 mutants using their experimentally determined retention times.

Circular Dichroism (CD). CD spectra were recorded at 25 °C on an AVIV Model 410 CD Spectrophotometer, using 1 nm spectral bandwidth and a 0.1 cm path length. Stock peptide solutions were desalted on Sephadex G-25 (PD-10) columns and diluted in 10 x buffer to a final concentration of 10% glycerol, 10 mM KH2PO4 and 100 mM KF at pH 7.0. Total enzyme concentration was approximately 0.3 mg•mL^{-1} (10 μM). Typically, five scans were acquired over the wavelength range 190-260 nm. The residue ellipticity (Θ) was calculated using *rS*-HPCDH3 molecular weight of 27085.5 Da and N_A (number of amino acid in the protein) of 268 residues.

Spectrophotometric Enzyme Assays. Assays with 2-KPC, *S*-HPC, *R*-HPC and 2-propanol as substrates were performed in 50 mM glycine, 50 mM NaH_2PO_4, and 50 mM Tris base (GPT buffer mix) at a pH of 7.5 (adjusted at 30 °C), as described previously (*15*). Assays with all other substrates (C_4 to C_6 in carbon chain length) were carried out in 50 mM GPT buffer containing 15% (v/v) glycerol. Stock solutions of synthesized substrates were standardized, as described previously (*15*) All enzyme assays were performed in triplicates at 30 °C in a Shimadzu model UV160U spectrophotometer containing a water-jacketed cell holder for thermal control. Alcohol or ketone production was monitored by measuring the change in absorbance at 340 nm using the extinction coefficient for NADH (ϵ_{340} = 6.22 mM^{-1} cm^{-1}). For alcohol oxidation assays, the following ranges of alcohol concentrations were used in determining kinetic constants for *R*-HPCDH1: *R*-HPC, 0.020 – 1.0 mM; *S*-HPC, 0.074-11 mM; 2-propanol, 65-3900 mM; (*S*)-2-butanol, 10.9-381 mM; (*R*)-2-butanol, 43.6-490 mM. For *S*-HPCDH3 the concentrations were: *R*-HPC, 0.038-48 mM; *S*-HPC, 0.016 – 0.310 mM; 2-propanol, *(S)*-2-butanol and *(R)*-2-butanol, the same as for *R*-HPCDH1. The concentration of NAD^+ for all assays was 10 mM (26 x value of K_{mNAD+}). For assays of ketone reduction, the following concentration ranges were used in determining kinetic constants: 2-KPC, 0.050-2.6 mM; 2-butanone, 10-300 mM. The concentration of NADH for these assays was 0.16 mM, (4.4 x value of K_{mNADH}). On average, seven concentrations of substrates within the ranges indicated were chosen for the kinetic

analyses. All samples were degassed/flushed with nitrogen and incubated at 30 ºC water-bath for 5 min prior to the enzyme addition. To determine kinetic parameters (apparent K_m and V_{max}) initial rate values were plotted as a function of substrate concentration and data points were fitted to the Michaelis-Menten equation using SigmaPlot 11.0.

pH Dependence of Kinetic Parameters. All assays were performed in GPT buffer mix or APT buffer mix (50 mM CH_3COONa, 50 mM NaH_2PO_4, and 50 mM Tris base) at ten different pH values (5.0 – 10.0) adjusted to the desired pH at 30 ºC, as described previously (*15*). The assay results were used to construct a plot of k_{cat}/K_m vs pH, which was then fit to Equation 1:

$$\log k_{cat}/K_m = \log(C/(1 + [H^+]/ K_a)) \quad \text{(Eq1)}$$

where C is the maximal log k_{cat}/K_m value and K_a is the acid dissociation constant of the catalytically important ionizing residue. Plots of log k_{cat} and log K_m vs pH were constructed in a point-to-point manner. Stability of the enzyme at a pH 5.0 and 10.0 was tested according to the pH-jump method (*20*). The stock solution of *rS*-HPCDH3 was diluted to 0.1 mg•mL^{-1} in 10 mM APT or GPT buffer mix containing 15% glycerol, at pH values of 5.0 and 10.0, respectively. The enzyme was equilibrated on ice at the desired pH (adjusted at 4 ºC) for 5 min prior to its addition to the reaction mixture (total of 0.3 µg of *rS*-HPCDH3). Activity assays were performed for 30 sec in 100 mM GPT buffer mix, pH 7.5, at 30 °C.

Inhibition Studies. All assays were performed in GPT buffer mix at pH 7.5 with saturating concentration of NAD^+ (5 mM). Inhibition assays for *R*-HPCDH1 were performed at variable concentrations of *R*-HPC (31, 72, 144, 287 and 615 µM) or HEC (0.8, 2.0, 4.0, 8.0 and 1.6 mM). Each assay was performed at several fixed concentrations of M-HPC: (0, 0.2, 0.4, 0.8 and 1.6 mM). Initial rate data for *rR*-HPCDH1 were fit to Equation 2 describing competitive inhibition of enzymatic activity:

$$\upsilon = V_{max}[S]/(\alpha K_m + [S]) \quad \text{(Eq 2)}$$

where S is the substrate, I is the inhibitor, $\alpha = 1 + ([I]/K_{is})$. The type of inhibition exhibited by M-HPC was determined by graphing initial rate data in the form of double reciprocal plots ($1/\upsilon$ vs 1/[S] at various [I]). Numerical value of K_{is} was calculated from equation 2 using SIGMA-PLOT. Inhibition assays for *S*-HPCDH3 were performed at varying concentrations of *S*-HPC (16, 31, 62, 155 and 310 μM) or HEC (0.4, 0.8, 2.0, 4.0, 8.0, and 1.6 mM) and three fixed concentrations of M-HPC: (0, 1.2 and 4.9 mM). Initial rate data were fit to a rectangular hyperbola described by the standard form of the Michaelis-Menten equation.

Chiral Gas Chromatographic Assay for 2-Butanone Reduction. All assays were performed in GPT buffer mix, pH 7.5 (adjusted at 30 ºC), containing 15% (v/v) glycerol. Assay components in 1 mL reaction volume were: NADH (15 mM), 2-butanone (56 mM), and 0.64 mg of enzyme. Serum vials (3 mL) were crimp-sealed and degassed/flushed with nitrogen three times and allowed to equilibrate for 20 min at 30 ºC in a shaking water-bath (200 rpm). The assay was initiated by adding enzyme. After 1 h incubation 250 μL of headspace gas was removed and injected into a Shimadzu GC-8A gas chromatograph outfitted with a Supelco β-Dex 225 (30 m × 0.53 mm) column. GC parameters used were as previously described (*14*).

RESULTS AND DISCUSSION

Genetic and Bioinformatic Analysis of the Enzymes of Alkene and Epoxide Metabolism. A previous study demonstrated that the genes of alkene and epoxide metabolism are present on a 320 kb linear megaplasmid in *X. autotrophicus* Py2 (*21*). Furthermore, the genes encoding the enzymes of epoxide carboxylation were found to be clustered in an operon where *xecA, xecC, xecD,* and *xecE* encode the key enzymes shown in Figure 2-1 (*5, 22*). Of significance to the present work, *xecD* encodes *R*-HPCDH, while *xecE* encodes *S*-HPCDH. All four of the enzymes of epoxide carboxylation were purified and characterized in some detail from the native

bacterium (*4-6, 23*). Of relevance to our interest in determining the molecular basis for enantioselectivity in the dehydrogenation reactions of Figure 2-1, the *xecD* gene was successfully cloned into an *E. coli* expression vector and the enzyme was over-expressed and purified in a fully active state (*15*). This allowed for the production of the necessary amounts of protein for kinetic, mechanistic, and structural characterization, and the construction of site-directed mutants that provided valuable insights into the catalytic mechanism and the roles of key amino acid residues in catalysis and controlling enantioselectivity (*14-16*). Unfortunately, all attempts to clone and express the counterpart *S*-HPCDH in a soluble and active form were unsuccessful despite numerous attempts (*15*), and the mechanistic and structural characterization of this enzyme has thus lagged behind that of the *R*-HPCDH.

Recently, the genome of *X. autotrophicus* Py2 was sequenced, assembled, and annotated (http://genome.jgi-psf.org/xanau/xanau.home.html). Unexpectedly, an analysis of the linear megaplasmid of *X. autotrophicus* shows the presence of multiple copies of the *xec* genes, as well as for the putative enzymes of coenzyme M biosynthesis. In contrast, only a single copy of the genes encoding the alkene monooxygenase multicomponent enzyme system that converts propylene to epoxypropane *(xamoABCDEF)* are present. The *xec* paralogs are distributed among three apparent operons and share high identities. The *xecD* and *xecE* genes whose protein sequences were reported previously (*5, 22*) are those located in an operon approximately 10.4 kbp downstream of the *xamo* operon, while the additional copies are located about 197 and 223 kbp downstream of this first operon. For naming purposes, these copies are now referred to as *xecD1* and *xecE1*, to designate they are found in the first gene cluster, while the additional copies are referred to as *xecD2*, *xecE2*, *xecD3* and *xecE3* based on which of the additional two clusters they are found within. Since the abbreviations *R*- and *S*-HPCDH has been used previously, these proteins will also be affixed with the numbers 1, 2, and 3 for naming purposes (i.e., XecD1 is *R*-HPCDH1 while XecD2 is *R*-HPCDH2 and so on).

The identification of multiple copies of the *xec* genes in the linear plasmid genome rationalizes some previous unexplained observations. Most notably, we were unsuccessful in using a highly efficient transposon mutagenesis system optimized for *X. autotrophicus* to obtain mutants defective in growth with epoxides as the carbon source, although the same system allowed for the identification of the enzymes of carotenoid biosynthesis, acetone metabolism, and alkene oxidation (*24, 25*). Since the transposon mutagenesis system relies on insertional inactivation of a single gene with a kanamycin cassette, no phenotype will be observed where multiple redundant copies are present in the genome, which the sequence of the linear megaplasmid has now revealed is the case for the genes and enzymes of epoxide carboxylation (but not alkene oxygenation).

Cloning, Expression, and Biochemical Characterization of xecE Homologs. Each of the three *S*-HPCDH homologs identified on the linear megaplasmid was expressed using an optimized expression system with the inclusion of N-terminal six-histidine tags. Only small amounts (<0.1 mg/g cell paste) of the XecE1 (*S*-HPCDH1) protein were present in the soluble fraction, with most of the protein being in inclusion bodies. The small amount of soluble protein, when purified, had a specific activity nearly identical to the native enzyme, demonstrating that the enzyme can be expressed in an active form, albeit at levels too low for detailed biochemical and structural characterization. The second copy, XecE2 (*S*-HPCDH2), contained apparent mutations in the N-terminal region, most notably the lack of the classic GXXXGXG cofactor sequence motif that is found within the Rossman fold (*10*). This protein was expressed with more protein in the soluble fraction (~50%), but was completely inactive, as expected due to the lack of key NAD^+-binding residues. The third copy, XecE3 (*S*-HPCDH3), was very similar to xecE1, with 74% identity, and with all of the conserved SDR sequences intact (Figure 2-2). XecE3 was expressed in high yields in a soluble form (>4 mg enzyme/g cell paste), and when purified, had a specific activity nearly identical to that of *S*-HPCDH1 and *S*-HPCDH purified from *X. autotrophicus*.

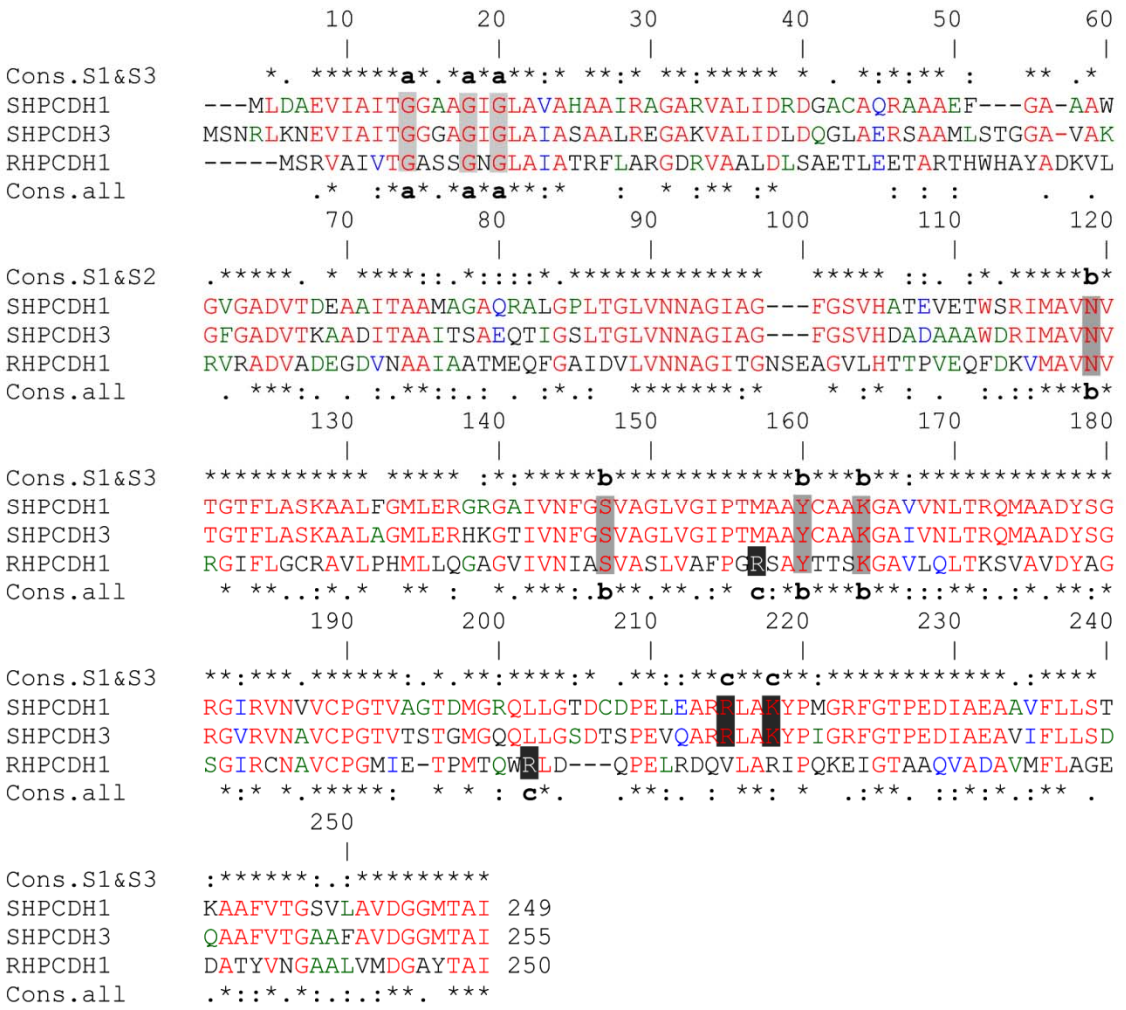

Figure 2-2. Multiple-sequence alignment of *S*-HPCDH1, *S*-HPCDH3 and *R*-HPCDH1 enzymes from *X. autotrophicus* Py2. Abbreviations: Cons.S1&3, consensus amino acid alignment for *S*-HPCDH1 and *S*-HPCDH3; Cons.all, consensus of *S*-HPCDH1, *S*-HPCDH3 and *R*-HPCDH1 Letter designations: **a,** Classic GXXXGXG glycine-rich NAD^+ binding motif. **b,** Catalytic tetrad residues of Asn, Ser, Tyr and Lys. **c,** Positively charged residues that have been shown (*R*-HPCDH1) or are proposed (*S*-HPCDH) to interact with the sulfonate group of CoM in the substrate. The alignment was generated using MULTALIN with default parameters, while the consensus was derived using ClustalW2. The following symbols mean that the residues are: (*) identical; (:) conserved ; (.) semi-conserved.

The *rS*-HPCDH3 was subjected to gel filtration chromatography and eluted as a single peak with an apparent molecular mass of 70.2 kDa. By comparison, native *S*-HPCDH and *rR*-HPCDH1 eluted from the same column with apparent molecular masses of 49.6 kDa and 64.7

kDa, respectively, results that are identical to those reported previously when the proteins were analyzed using a different (Superose-12) gel filtration column (*5, 15*). The molecular masses of the *R*- and *S*-HPCDH polypeptides are all in the 25-26 kDa range, and each of the native *S*-HPCDH, *rR*-HPCDH1, *rS*-HPCDH1, and *rS*-HPCDH3 proteins migrated as single bands on SDS-PAGE gels at the expected positions based on their molecular masses.

It is unclear why *rS*-HPCDH3 elutes with a higher apparent molecular weight on the gel filtration column than native *S*-HPCDH and more similarly to how *R*-HPCDH migrates. The discrepancy could be due to the likelihood that the *S*-HPCDH we purified from the native organism is a homogeneous (or nearly homogeneous) preparation of the XecE1 homolog (*S*-HPCDH1), and that this protein elutes differently from that of XecE3. This idea is supported by the results of N-terminal sequence analysis of native *S*-HPCDH by Edman degradation, which provided the sequence MLDNEVIAIT (*5*). As shown in Figure 2-2, XecE1 is identical at the N-terminus to that sequence except for one amino acid (the N at position 4). In contrast, the N-terminus of XecE3 has the N-terminal sequence MSNRLKN before converging with XecE1 at EVIAIT (Figure 2-2). Clearly, the presence of three homologs of each of the HPCDH enzymes emphasizes the importance of expressing specific enzymes in a defined expression system.

Originally, both *R*- and *S*-HPCDH were proposed to be dimers based on their elution profiles on gel filtration (*5*). However, the crystal structure of *rR*-HPCDH1 clearly showed a tetrameric structure (*16*), as has been seen for some other members of the SDR family of enzymes (*26-28*). Thus, as for many proteins, the HPCDH enzymes may migrate anonymously on gel filtration columns and we are hesitant to predict the quaternary state of *rS*-HPCDH3 based on the gel filtration results.

Native PAGE, gel filtration chromatography, and CD spectrapolarimetric analyses were performed with wild-type *rS*-HPCDH3 and the mutants described subsequently (S143A, Y156A, Y156F, K160A, R211A, K214A). Native PAGE and gel filtration revealed that all of the *rS*-HPCDH3 mutants migrated in a similar manner to that of the wild-type *rS*-HPCDH. CD analysis

of the *rS*-HPCDH3 mutants generated spectra that are indistinguishable from that of the wild-type enzyme. Collectively, these data suggest that elimination or alteration of the activity of *rS*-HPCDH3 mutants is not due to major structural changes in the protein, but a result of a change in the chemical environment surrounding substituted residues.

Kinetic Parameters for rS-HPCDH1, rS-HPCDH3, and rR-HPCDH with Physiological Substrates. Native *S*-HPCDH1 was previously shown to be highly specific for *S*-HPC as the substrate, exhibiting only 0.5% activity when *R*-HPC was used as the substrate, but the kinetic parameters for the enzyme were not investigated (*4*). In the present work, the kinetic analysis of *rR*-HPCDH1 performed previously (*14*) was repeated in side by side experiments with the two active XecE homologs so that the three enzymes can be compared directly. Although expressed only at very low levels, *rS*-HPCDH1 was included in these analyses in order to see if the two XecE homologs had any significant differences in catalytic properties. For these analyses, varying concentrations of *R*-HPC, *S*-HPC, or 2-KPC and fixed concentrations of NAD^+ and NADH several times higher than K_m were used to determine the apparent K_m, V_{max}, and k_{cat} values for each enzyme in the forward (oxidative) and reverse (reductive) directions under conditions identical to those done previously (*14*). These results are presented in Table 2-1.

The apparent k_{cat} and K_m values determined for *R*-HPC and *S*-HPC oxidation, and 2-KPC reduction, by *rR*-HPCDH1 are similar to those reported previously (*14*). With regard to *rS*-HPCDH1 and *rS*-HPCDH3, the apparent k_{cat} values for *S*-HPC oxidation are nearly identical to each other, while the apparent K_m is seven-fold lower for *rS*-HPCDH3. For 2-KPC reduction, *rS*-HPCDH1 exhibits a two-fold higher k_{cat} but nearly identical K_m relative to *rS*-HPCDH3. As noted above, *S*-HPCDH1 and *S*-HPCDH3 share high identity (74%) but are not identical enzymes, so it is not surprising that some differences in kinetic parameters are observed.

The most surprising results of the kinetic analyses are the large relative differences in k_{cat} and K_m for the *opposite enantiomers* when characterized as substrates for the *R*- and *S*-dehydrogenases. As shown in Table 2-1, *rR*-HPCDH1 catalyzed the oxidation of *S*-HPC with a

Table 2-1. Kinetic Parameters for *R*- and *S*-HPCDH with physiological substrates in the forward and reverse directions[a]

Substrate	***rR*-HPCDH1**			***rS*-HPCDH1**			***rS*-HPCDH3**		
	K_m (μM)	k_{cat} (s^{-1})	k_{cat}/K_m ($M^{-1}\ s^{-1}$)	K_m (μM)	k_{cat} (s^{-1})	k_{cat}/K_m ($M^{-1}\ s^{-1}$)	K_m (μM)	k_{cat} (s^{-1})	k_{cat}/K_m ($M^{-1}\ s^{-1}$)
R-HPC	95.5 ± 7.5	47.9 ± 1.1	5.0×10^5	5230 ± 350	2.41 ± 0.057	4.6×10^2	9110 ± 1120	5.48 ± 0.23	1.2×10^3
S-HPC	224 ± 72	0.119 ± 0.0099	5.3×10^2	222 ± 23	28.2 ± 0.80	1.3×10^5	31.4 ± 0.89	24.8 ± 0.17	7.9×10^5
2-KPC	67.9 ± 12	28.9 ± 1.6	4.2×10^5	241 ± 11	20.0 ± 0.24	8.3×10^4	275 ± 13	10.8 ± 0.15	3.9×10^4

[a]Assay for *R*-HPC and *S*-HPC oxidation by *rR*-HPCDH1 contained 1.0 µg and 46 µg of enzyme, respectively. Assay for *R*-HPC and S-HPC oxidation by *rS*-HPCDH1 and *rS*-HPCDH3 contained 5.0 µg and 1.0 µg of enzyme, respectively. Assay for 2-KPC reduction contained 1 µg of enzyme. Apparent k_{cat} and K_m values are reported as means ± standard deviations. All assays were performed in triplicates at 30 ˚C with fixed concentrations of NAD^+ (10 mM) or NADH (0.17 mM). Apparent kinetic constants were determined by fitting experimental data to the standard form of the Michaelis-Menten equation.

k_{cat} that is 402-times less than that for *R*-HPC. In contrast, *rS*-HPCDH1 and *rS*-HPCDH3 catalyzed the oxidation of *R*-HPC with k_{cat} values only 11 and 4.5-times less than that for *S*-HPC, but with substantially higher K_m values (24 and 290-times higher) (Table 2-1).

A comparison of the catalytic efficiencies (k_{cat}/K_m) of the three enzymes for the *(R)*- and *(S)*-enantiomers provides additional insights. The catalytic efficiencies for the "natural" enantiomers for each enzyme are in the range of 1 to 8 x 10^5. By comparison, the catalytic efficiencies for the opposite enantiomers are about three orders of magnitude lower. When enantioselectivity *(E)* is defined as the ratio of k_{cat}/K_m for the natural enantiomer to k_{cat}/K_m for the opposite enantiomer, the following values are obtained: E_{RHPCDH1} = 944, E_{SHPCDH1} = 283, and E_{SHPCDH3} = 658. Thus, the HPCDH enzymes are highly efficient at discriminating between the HPC enantiomers, with enantioselectivity controlled largely by differences in k_{cat} for *R*-HPCDH, and predominantly by differences in K_m for the two *S*-HPCDH enzymes.

The *rS*-HPCDH1 and *rS*-HPCDH3 homologs are similar but not identical in terms of their catalytic properties, verifying that the homologs are redundant *S*-HPC specific enzymes. The subsequent studies of *S*-HPCDH are focused on *rS*-HPCDH3, since only this protein could be expressed in sufficient amounts for the detailed analyses described below.

The apparent K_m values for NAD^+ and NADH with *R*-HPC and 2-KPC as substrates were determined for *rS*-HPCDH3 and gave the following values: K_{m} for NAD^+, 191 ± 21 μM; K_{m} for NADH, 8.42 ± 1.58 μM. By comparison, the K_m values for *rR*-HPCDH1 using a complete bisubstrate kinetic analysis were previously reported to be 457 μM and 36.6 μM for NAD^+ and NADH, respectively (*15*).

pH Dependence of the Kinetic Parameters for rS-HPCDH3. Kinetic parameters were determined for the oxidation of *S*-HPC by *rS*-HPCDH3 at a range of pH values and plotted as log k_{cat} vs pH, log $k_{\mathrm{cat}}/K_{\mathrm{m}}$ vs pH and log K_{m} vs pH as was done previously for oxidation of *R*-HPC by

rR-HPCDH1 (*15*). These results are presented in Figure 2-3. The overall trends are similar to those reported for *rR*-HPCDH1 but with some important differences (*15*) suggesting a similar fundamental chemical mechanism for substrate oxidation. The differences in the pH analyses for the two enzymes are highlighted below.

Figure 2-3A shows a fairly steady increase in log k_{cat} as the pH increases (slope 0.08) suggesting that isomerization of the enzyme-NAD^+ complex could be a major rate-determining step, as described for other dehydrogenases (*29*). The same effect was seen for *rR*-HPCDH1 (*15*), although the change in k_{cat} was more pronounced (over six-fold increase vs. three-fold increase for *rS*-HPCDH3). Linear regression of the plot of log k_{cat}/K_m vs. pH from pH 5.0 – 8.0 (Figure 2-3B) gave a slope of 0.998 with an R^2 value of 0.980, suggesting the importance of a single ionizable residue that must be deprotonated for catalysis. A fit of the data in Figure 2-3B to Equation 1 provides a pK_a value for this residue of 7.9. Based on pH studies of other SDR enzymes, the ionizable residue most likely represents the tyrosine of the catalytic triad, which serves as the general acid/base for catalysis. For comparison, the pK_a value for the corresponding ionizable group of *rR*-HPCDH1 was reported to be a lower value of 6.9 (*15*), while the prototype alcohol dehydrogenases from *Drosophila melanogaster* and *D. lebanonensis* were reported to be 7.1 and 7.6, respectively (*30, 31*).

The data presented in Figure 2-3C show a dramatic decrease in K_m (321-fold decrease from pH 5.0 to pH 9.0) as the pH is increased. Taken together with the above results, this suggests that the deprotonated tyrosine general base plays an important role in both alcohol binding (K_m effect) and catalysis (k_{cat} and k_{cat}/K_m effects). The increase in K_m from pH 9 to pH 10 could reflect deprotonation of another functional group important in coordinating the sulfonate of CoM (K214, as described below). The decrease in K_m for *rS*-HPCDH3 was much greater than that observed for *rR*-HPCDH1, where only a 14-fold decrease in K_m was observed (*15*). This suggests that the general acid/base of *S*-HPCDH3 is more important for binding of the alcohol

substrate in the *(S)*-dehydrogenase than the *(R)*-dehydrogenase, an idea that is supported by the further studies described below.

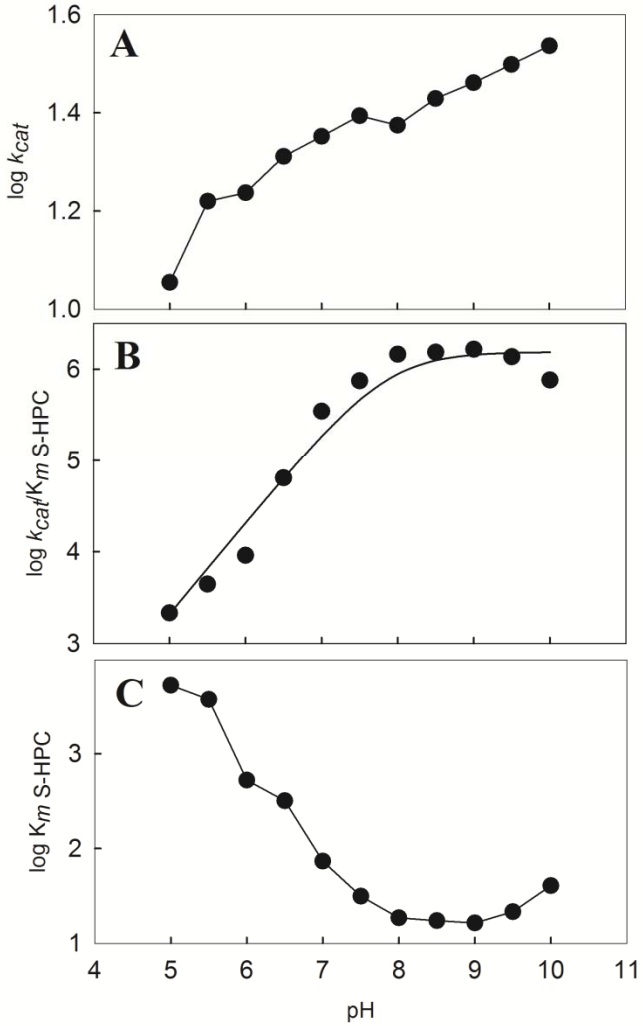

Figure 2-3. Changes of kinetic parameters with pH for *rS*-HPCDH3 catalyzed oxidation of *S*-HPC. (A) k_{cat} vs. pH, (B) $k_{cat}/K_{mS\text{-}HPC}$ vs. pH, (C) $K_{mS\text{-}HPC}$ vs. pH, represented in log scale. The plots in (A) and (C) are shown as simple line plots. The line in plot (B) was generated by a fit of the experimental data to equation 1.

Site-Directed Mutagenesis of the Catalytic Triad. As noted in the Introduction, members of the SDR family of enzymes contain a catalytic triad consisting of a serine, a tyrosine, and a lysine (or, as more recently described, a tetrad, with the fourth residue being an asparagine) (*10, 11*). As shown in Figure 2-2, the positions of these residues in the primary sequences are conserved between the *R*- and *S*-HPCDH enzymes. To confirm the importance of the key residues, site-directed mutants were constructed. As shown in Table 2-2, the Y156F and K160A mutants were completely inactive. The S143A mutant exhibited a small amount of activity but with a catalytic efficiency that was reduced by more than five orders of magnitude relative to wild-type. Interestingly, the Y156A mutant exhibited a k_{cat} that was 2.6% of the activity of the wild-type enzyme, with a K_m value 60-fold higher than wild-type. The observation that the Y156A, but not Y156F mutant retains some activity suggests that the removal of the bulky phenyl group allows the enzyme to facilitate hydrogen atom abstraction from the hydroxyl group by another mechanism. An analysis of the primary sequences of the HPCDH enzymes shows that a cysteine residue is next to the tyrosine base in the *S*-enzymes but not the *R*-enzyme (Figure 2-2). A cysteine is also adjacent to the catalytic triad in the SDR 17β-hydroxysteroid dehydrogenase, and the Y to A substitution in that enzyme also exhibits a small amount of activity (*32*). It is conceivable that C157 substitutes as the general base in the Y156A mutant, albeit with a reduced catalytic efficiency, although this possibility has not been pursued further in this study.

Identification and Site-Directed Mutagenesis of the Sulfonate Binding Residues. For *rR*-HPCDH1, two arginine residues, R156 and R196, were shown to interact with the sulfonate of CoM via ionic interactions (Scheme 1, left side) (*14, 16*). Site-directed mutagenesis of either of these residues to alanine resulted in substantially reduced k_{cat} values and increased K_m values for 2-KPC reduction. Importantly, the same amino acid substitutions did not significantly alter k_{cat} or K_m when 2-butanone, a non-physiological substrate lacking the sulfonate, was used as the

substrate (*14*). Thus, the sulfonate-coordinating arginine residues of *R*-HPCDH1 are only required for effective catalysis with the natural substrate. By analogy, positively charged residues within a pocket are believed to interact with the sulfonate moiety of 2-KPC and *S*-HPC in *S*-HPCDH, but with differential placement relative to the methyl binding pocket such that the hydroxyl group and hydrogen atom of the substrate are oriented properly for catalysis (*14, 16*). To facilitate the identification of these residues, a homology model was constructed for *S*-HPCDH3 based on the *R*-HPCDH1 structure, as was done previously for *S*-HPCDH1 (at the time it was thought that there was only one copy of this enzyme) (*16*). The physiological substrates for each enzyme were modeled into the active sites of the enzymes using the crystal structure that was obtained for *rR*-HPCDH1 bound to *S*-HPC (*16*). As shown in Figure 2-4A, the positioning of the catalytic triad residues, verified for *S*-HPCDH3 by the mutational analyses in Table 2-2, are conserved between the two *S*-HPCDH enzymes. As predicted, the active sites of the enzymes differ in the spatial orientations of the CoM and methyl groups, with the positions of the hydrogen atom and hydroxyl group being fixed relative to NAD^+ and the tyrosine general base. Figure 2-4B shows a different view of the active sites, highlighting the interactions known (for *rR*-HPCDH1) and proposed (for *rS*-HPCDH3) to be important in binding the sulfonate of CoM. While two arginines coordinate the sulfonate within *R*-HPCDH1, the model suggests coordination by an arginine and a lysine for *S*-HPCDH3 (as well as *S*-HPCDH1 as seen in the multiple sequence alignment of Figure 2-2). To verify the importance of these residues, they were mutated to alanines, and the effects on enzymatic activity were determined. As shown in Table 2-3, substitution of either R211 or K214 by alanine resulted in substantially reduced catalytic efficiencies for *S*-HPCDH3 with the natural substrates in both the forward (oxidative, S-HPC as substrate) and reverse (reductive, KPC as substrate) directions. Interestingly, the most dramatic effects of the mutations were on K_m values, which were 50-74 times higher in the oxidative

Table 2-2. Summary of Amino Acid Substitutions Made to the Putative *rS*-HPCDH35 Catalytic Residues Using Site-Directed Mutagenesis [a]

amino acid	postulated catalytic role(s) [b]	substitution	V_{max} (units•mg^{-1})	K_m (μM S-HPC)	k_{cat} (s^{-1})	k_{cat}/K_m (M^{-1} s^{-1})
		none	54.8 ± 0.37	31.4 ± 0.89	24.8	7.49 x 10^5
S143	H-bond donor to substrate/charge stabilization of the transition state	S143A	0.0290 ± 0.0030[ca]	9480 ± 2500	0.0131	1.38 x 10^0
Y156	general acid/base	Y156A	1.44 ± 0.045[ca]	1850 ± 180	0.652	3.52 x 10^2
		Y156F	no activity[d]			
K160	lowers pK_a of Y156/coenzyme binding	K160A	no activity[d]			

[a]Abbreviations: *S*-HPC, 2-[(*S*)-2-hydroxypropylthio]ethanesulfonate. [b]Postulated catalytic roles are based on a general trend found in most SDR enzymes (including *R*-HPCDH). [c]Assays contained 66 μg of S143A or 20 μg of Y156A, 5 mM NAD+ and variable concentration of *S*-HPC. [d]No activity was defined as no measurable change in the absorbance at 340 nm (for NADH) in assays containing 100 μg of the protein, 2.5 mM of *S*-HPC and 20 mM NAD^+. Apparent V_{max} and K_m values are reported as means ± standard deviations. All other values are reported as means only. All assays were performed in triplicate at 30 ºC with fixed concentrations of NAD^+. Apparent kinetic constants were determined by fitting experimental data to the standard form of the Michaelis-Menten equation.

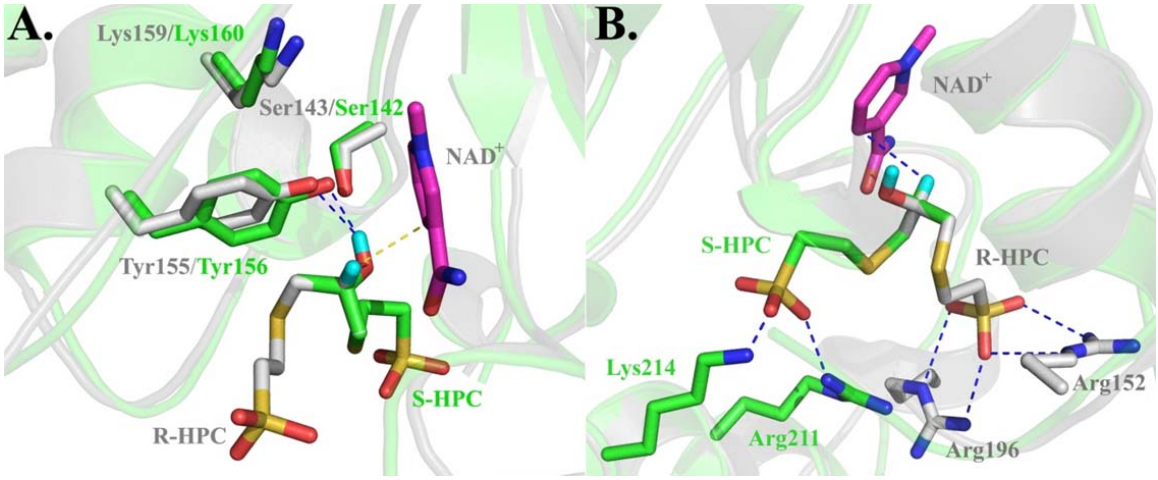

Figure 2-4. Superimposed active sites of *R*-HPCDH1 and *S*-HPCDH3 based on the crystal structure of *R*-HPCDH1 and a homology model of *S*-HPCDH3. The cartoon structures and carbon atoms of amino acid residues of *R*-HPCDH1 (pdb ID 2cfc) and the homology model for *S*-HPCDH3 are colored grey and green, respectively. NAD^+ is shown in magenta. *R*-HPC and *S*-HPC were modeled using the crystal structure for *S*-HPC bound at the active site of *R*-HPCDH1 as described previously (*16*). In both views, *R*-HPC (grey carbon atoms) and *S*-HPC (green carbon atoms) are modeled at the active sites such that the positions of the hydroxyl group and hydrogen atom occupy the same positions. The methyl groups and the methylene groups linking the hydroxypropyl groups to CoM are overlayed on top of each other to highlight the different spatial orientations of these groups in *R*- and *S*-HPC. Panel A, Superimposed structures highlighting the interactions of substrates with the catalytic triads. Panel B, Superimposed structures highlighting the interactions of substrates with the amino acids that coordinate the sulfonate of CoM.

direction and 41-43 times higher in the reductive direction. There was a significant (40-80%) decrease in k_{cat} due to the mutations for the forward reaction, but very little change for the reductive direction. By comparison, 2-KPC reduction by the R152A and R196A mutants of *R*-HPCDH1 were impaired sizably in both K_m and k_{cat} values (*14*). The k_{cat} and K_m values measured for the reduction of the aliphatic ketone 2-butanone and the oxidation of the aliphatic alcohol 2-propanol were largely unaffected by the amino acid changes in *S*-HPCDH3 (Table 2-3). These aliphatic substrates had dramatically higher K_m values and lower k_{cat} values relative to the natural

substrates, highlighting the importance of the CoM moiety in catalysis. The fact that the kinetic parameters did not change substantially in the site-directed mutants demonstrates that the

Table 2-3. Kinetic Parameters for wild-type *rS*-HPCDH3 and R211A and K214A with various substrates [a]

Enzyme	K_m (mM)	Change in K_m (x-fold)	k_{cat} (s^{-1})	Change in k_{cat} (x-fold)	k_{cat}/K_m (M^{-1} s^{-1})
Substrate: *S*-HPC					
wild-type	0.0314 ± 0.00089	1.0	24.8 ± 0.17	1.0	7.9×10^5
R211A	1.55 ± 0.12	49	16.0 ± 0.42	0.64	1.0×10^4
K214A	2.30 ± 0.094	73	5.78 ± 0.090	0.23	2.5×10^3
Substrate: 2-KPC					
wild-type	0.275 ± 0.013	1.0	10.8 ± 0.15	1.0	3.9×10^4
R211A	11.4 ± 0.48	41	8.59 ± 0.18	0.80	7.5×10^2
K214A	11.8 ± 0. 94	43	9.62 ± 0.34	0.89	8.1×10^2
Substrate: 2-butanone					
wild-type	118 ± 5.3	1.0	0.0438 ± 0.00086	1.0	3.7×10^2
R211A	179 ± 26	1.5	0.0718 ± 0.054	1.6	4.0×10^2
K214A	71.9 ± 6.1	0.61	0.0387 ± 0.0012	0.90	5.4×10^2
Substrate: 2-propanol					
wild-type	1410 ± 59	1.0	2.02 ± 0.54	1.0	1.4×10^3
R211A	724 ± 36	0.51	1.72 ± 0.035	0.85	2.4×10^3
K214A	951 ± 18	0.67	1.73 ± 0.19	0.86	1.8×10^3

[a]Assay for *S*-HPC oxidation contained 0.20 μg of wild-type *rS*-HPCDH3, or 4.0 μg of R211A and K214A while assay for 2-KPC reduction contained 0.20 μg of wild-type *rS*-HPCDH3, 5.0 μg of R211A and 2.0 μg of K214A. Assay for 2-butanone reduction contained 197 μg of enzyme while assay for 2-propanol oxidation contained 8.0 μg of enzyme. Apparent k_{cat} and K_m values are reported as means ± standard deviations. All other values are reported as means only. All assays were performed in triplicates at 30 ºC with fixed concentrations of NAD^+ (10 mM) or NADH (0.17 mM). Apparent kinetic constants were determined by fitting experimental data to the standard form of the Michaelis-Menten equation.

sulfonate-binding residues are not important for aliphatic substrates where no favorable interaction with the positively charged residues would occur. Similar results were obtained when 2-butanone was analyzed as a substrate for wild-type *R*-HPCDH1 and the R152A and R196A mutants (*14*).

S-HPCDH3 Has an Inherent Stereoselectivity for 2-Butanone Reduction not Present in R-HPCDH1. To gain further information on the stereoselectivity of *S*-HPCDH3, the chiral products of 2-butanone reduction (*(R)*- and *(S)*-2-butanol) were quantified. As shown in Table 2-4, *S*-HPCDH3 has a very high inherent stereoselectivity, producing *(S)*-2-butanol with a 98.4% enantioexcess (ee). These results are dramatically different than those observed for *R*-HPCDH1, where *(S)*-2-butanol is also produced in higher amounts than *(R)*-2-butanol, but in only a 44% enantioexcess (Table 2-4 and (*14*)). Thus, even though the *R*- and *S*-HPCDH enzymes are highly specific for production of *R*-HPC and *S*-HPC from 2-KPC reduction, they both form excesses of *(S)*-2-butanol from 2-butanone, a result that seems contradictory to what one might expect from the stereoselectivity observed for the natural substrates and products.

An interesting feature of the *R*-HPCDH1 is that the enantioselectivity of 2-butanone reduction can be "modulated" to produce higher amounts of *(S)*-2-butanol by including CoM, methanesulfonate, ethanesulfonate, or propanesulfonate in the assay (*14*). These "enantioiselective modulators" modulated stereospecificity in a saturable fashion, with a theoretical yield of 100% *(S)*-2-butanol at the saturation points (*14*). The effects of these enantioselective modulators were abolished in mutants in the sulfonate-coordinating arginines (R152A and R196A) (*14*). These results were interpreted as follows: the alkylsulfonates bind in the CoM binding pocket, constraining 2-butanone to bind in the active site with the methyl group rather than the ethyl group oriented towards the bound alkylsulfonate to prevent steric clashes. In this orientation, the sp^2 hybridized carbonyl of 2-butanone is necessarily constrained for hydride transfer to the plane that produces *(S)*-2-butanol (*14*).

Table 2-4. Enantioselectivity of 2-butanone reduction by wild-type *rS*-HPCDH3, *rS*-HPCDH3 mutants, and *rR*-HPCDH1[a]

	no additions			+ 1 mM ethanesulfonate		
Enzyme	% (*S*)-2-butanol	% (*R*)-2-Butanol	*ee* (*S*)-2-butanol	% (*S*)-2-butanol	% (*R*)-2-butanol	*ee* (*S*)-2-butanol
rS-HPCDH3	99.18 ± 0.15	0.82 ± 0.15	98.36	98.03 ± 0.08	1.97 ± 0.08	96.06
rS-HPCDH3 R211A	99.42 ± 0.22	0.58 ± 0.22	98.84	99.36 ± 0.15	0.64 ± 0.15	98.72
rS-HPCDH3 K214A	91.59 ± 0.31	8.41 ± 0.31	83.18	90.88 ± 0.20	9.12 ± 0.20	81.76
rR-HPCDH1	71.94 ± 1.34	28.06 ± 1.34	43.88	92.67 ± 0.05	7.33 ± 0.05	85.34

All assays were performed in triplicate at 30 °C using 0.64 mg enzyme, 15 mM NADH, and 56 mM 2-butanone. Percent yields are reported as means ± standard deviations.

Table 2-5. Kinetic Parameters for *rS*-HPCDH3 and *rR*-HPCDH1 catalyzed oxidation of 2-butanol[a]

Substrate	K_m (mM)	V_{max} (units/mg)	k_{cat} (s^{-1})	k_{cat}/K_m (M^{-1} s^{-1})	Change in k_{cat} (x-fold)	Change in K_m (x-fold)	enantio-selectivity (*E*)
			rS-HPCDH3				
(R)-2-butanol	67.6 ± 3.4	2.23 ± 0.03	1.00	14.8	1.00	1.00	0.16
(S)-2-butanol	28.1 ± 1.5	5.77 ± 0.07	2.60	92.8	2.60	0.42	6.27
			rR-HPCDH1				
(R)-2-butanol	215 ± 11	3.77 ± 0.06	1.87	8.69	1.00	1.00	0.33
(S)-2-butanol	353 ± 45	18.8 ± 0.9	9.34	26.4	4.99	1.64	3.04

[a]All assays were performed in triplicate at 30 ˚C with fixed concentrations of NAD^+ (10 mM). Assays of 2-butanol oxidation catalyzed by *rS*-HPCDH3 and *rR*-HPCDH1 contained 25 and 21 μg of enzyme, respectively. Apparent kinetic constants were determined by fitting experimental data to the standard form of the Michaelis-Menten equation. Apparent V_{max} and K_m values are reported as means ± standard deviations. All other values are reported as means only. Enantioselectivity was defined as $(k_{cat}/K_m)_{R\text{-enantiomer}}/(k_{cat}/K_m)_{S\text{-enantiomer}}$ for *(R)*-2-butanol oxidation and as $(k_{cat}/K_m)_{S\text{-enantiomer}}/(k_{cat}/K_m)_{R\text{-enantiomer}}$ for *(S)*-2-butanol oxidation.

As shown in Table 2-4, the addition of 1 mM ethanesulfonate to *rS*-HPCDH3 had very little effect on the stereochemical outcome of 2-butanone reduction relative to the effect observed with *rR*-HPCDH1. No effect of ethanesulfonate was seen in the *rS*-HPCDH3 wild-type or R211A mutant. Interestingly, the enantioselectivity decreased somewhat for the *rS*-HPCDH3 K214A mutant, an effect that was not changed when ethanesulfonate was added. Perhaps the substitution of lysine by the smaller alanine opens the active site to allow 2-butanone to bind in an orientation producing more of the *(R)*-product. In any event, the high inherent stereoselectivity for production of *(S)*-2-butanol from 2-butanone reduction by *rS*-HPCDH3, the same enantiomer produced in excess by *rR*-HPCDH1 and that can be increased by the addition of alkysulfonates, highlights a significant difference in how the two enzymes act on non-physiological aliphatic ketones.

Dehydrogenation of 2-Butanol Enantiomers by rR- and rS-HPCDH Enzymes. The studies of 2-butanone reduction were expanded to examine the kinetic parameters for the reverse reaction, i.e., *(R)*- and *(S)*-2-butanol oxidation to 2-butanone. These results are summarized in Table 2-5. Both enzymes exhibited a preference for *(S)*-2-butanol as the substrate, with enantioselectivity values of 6.23 and 3.04 for *rS*-HPCDH3 and *rR*-HPCDH1, respectively. These results are in agreement with the studies showing *(S)*-2-butanol to be the preferred product of 2-butanone reduction for both enzymes. The K_m values for 2-butanone reduction were about 1000-times higher than for 2-KPC. Clearly, the sulfonate of CoM is a determining factor in the exquisite stereoselectivity for *(R)*- and *(S)*- enantiomers for the natural substrates.

2-(2-methyl-2-hydroxypropylthio)ethanesulfonate is a Competitive Inhibitor of Natural Substrate Oxidation by rR-HPCD1H but not rS-HPCDH3. Referring back to the studies of Table 2-1, *rR*-HPCDH1 exhibits a K_m for *S*-HPC in the same range as *R*-HPC, while *rS*-HPCDH3 exhibits a K_m for *R*-HPC that is nearly 300-times higher than for *S*-HPC. If K_m is a measure of binding affinity, these results indicate that *rR*-HPCDH1 is able to bind either enantiomer with

high affinity, although for the improper enantiomer, the hydroxyl and hydrogen of the substrate are misaligned, resulting in lower turnover (Table 2-1). In contrast, the high K_m value for *R*-HPC with *rS*-HPCDH3 suggests that the other enantiomer does not bind well in the first place, possibly due to steric constraints when the methyl group is misaligned. As shown in Chart 2-1, 2-(2-methyl-2-hydroxypropylthio)ethanesulfonate (M-HPC) is an achiral analog of both *R*-HPC and *S*-HPC where the hydrogen atoms of each alcohol are replaced by a methyl group, resulting in a tertiary alcohol that cannot undergo oxidation. M-HPC is thus an equivalent mimic of both HPC enantiomers and can be studied as a possible inhibitor of both enzymes to shed light on the K_m differences for the opposite enantiomers discussed above.

As shown in Figure 2-5A, M-HPC was a competitive inhibitor of *R*-HPC oxidation by *rR*-HPCDH1, with a K_{is} of 289 ± 14 μM. This value is in the range of the K_m for the natural substrate *R*-HPC (96 μM) and the opposite enantiomer *S*-HPC (224 μM), demonstrating that all three compounds bind *rR*-HPCDH1 with comparable affinities. In marked contrast to these results, no detectable inhibition was observed for M-HPC vs. the natural substrate *S*-HPC with *rS*-HPCDH3 (Figure 2-5B). This result correlates with the observation that *R*-HPC has a dramatically higher K_m for *S*-HPCDH3 relative to the natural substrate (9110 vs. 31.4 μM). This experiment was repeated with *rS*-HPCDH1 and the same result was obtained: no detectable inhibition was seen with M-HPC (Figure 2-5C). Thus, the addition of the methyl group in the improper position relative to the CoM and hydroxyl groups has profound effects on binding affinity for the *R*- and *S*-specific dehydrogenases, further highlighting an important distinction between these enzymes.

2-(2-hydroxyethylthio)ethanesulfonate (HEC) is a Substrate for Both the R- and S-HPCDH Enzymes with Identical K_m Values. As shown in Chart 2-1, HEC is an achiral mimic of both *R*-HPC and *S*-HPC in which the methyl group is replaced by a hydrogen. HEC was found to be a substrate for both *rR*-HPCDH1 (k_{cat} = 0.55 ± 0.015 μM, K_m = 959 ± 107 μM) and *rS*-

HPCDH3 (k_{cat} = 3.8 ± 0.25 μM, K_m = 975 ± 248 μM). Thus, the loss of the methyl groups imparting chirality resulted in an enzyme substrate with identical (within experimental error) K_m values for both enzymes, suggesting that for this substrate, the CoM moiety and hydroxyl group have become equal determinants in binding affinity (assuming K_m approximates affinity). As a final experiment, M-HPC was investigated as an inhibitor of HEC oxidation to see if the result of Figure 2-5 would hold with the achiral substrate. As shown in Figure 2-6, M-HPC was a competitive inhibitor of HEC oxidation by *rR*-HPCDH1 with a K_{is} of 114 ± 12 μM, but was not an inhibitor of HEC oxidation by *rS*-HPCDH3, further highlighting the specificity of M-HPC as a reversible competitive inhibitor of only the *(R)*-dehydrogenase.

Different Strategies of Controlling Enantioselectivity in the R- and S-HPCDH Enzymes. To summarize, the results presented above demonstrate that enantioselectivity in *rR*-HPCDH1 is controlled largely by differences in k_{cat} for the two HPC enantiomers, while enantioselectivity in *rS*-HPCDH3 is controlled by differences in K_m (Table 2-1). In the opposite direction, both enzymes reduce 2-KPC with comparable efficiencies. The tertiary alcohol M-HPC is a competitive inhibitor that binds to *rR*-HPCDH1 with an affinity similar to *R*-HPC and *S*-HPC, but does not bind to *rS*-HPCDH3. The primary alcohol HEC exhibits an identical K_m value for both enzymes. The simplest interpretation of these results is that *rR*-HPCDH1 can bind either enantiomer of HPC with the CoM moiety oriented properly in the sulfonate-binding pocket consisting of R152 and R196 (Figure 2-4), but that *rS*-HPCDH3 is unable to bind *R*-HPC in this fashion, presumably due to steric clashes imposed by the presence of the misaligned methyl group on the C2 atom. Both enzymes bind HEC with identical affinities since no methyl group is present. Thus, a high affinity ternary complex of *S*-HPC, NAD^+, and *rR*-HPCDH1 forms, but the misalignment of the hydrogen and hydroxyl groups on C2 relative to NAD^+ and the tyrosine general base results in a 403-fold lower turnover rate. Indeed, this model has been confirmed by the x-ray crystal structure of the complex of *S*-HPC and NAD^+ with *rR*-HPCDH1 (*16*).

Alcohol	Corresponding ketone or aldehyde
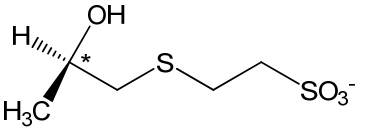 (*R*)-hydroxypropyl-CoM (*R*-HPC)	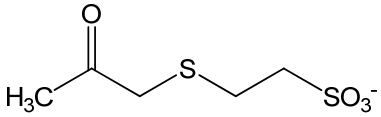 2-ketopropyl-CoM (2-KPC)
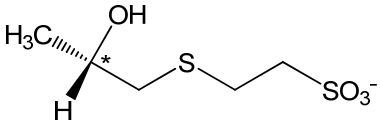 (*S*)-hydroxypropyl-CoM (*S*-HPC)	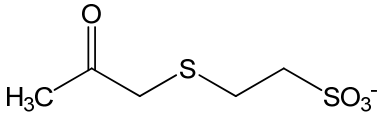 2-ketopropyl-CoM (2-KPC)
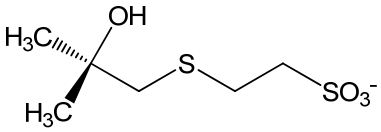 methylhydroxypropyl-CoM (M-HPC)	none
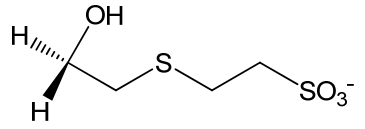 hydroxyethyl-CoM (HEC)	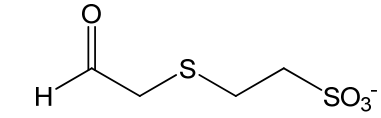 formylmethyl-CoM
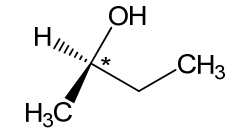 (*R*)-2-butanol	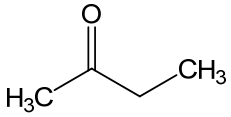 2-butanone
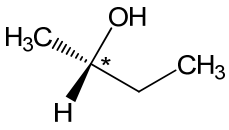 (*S*)-2-butanol	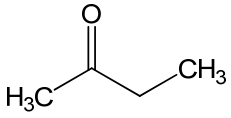 2-butanone
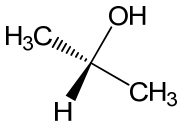 2-propanol	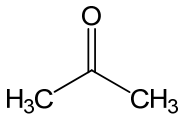 acetone

Chart 2-1.

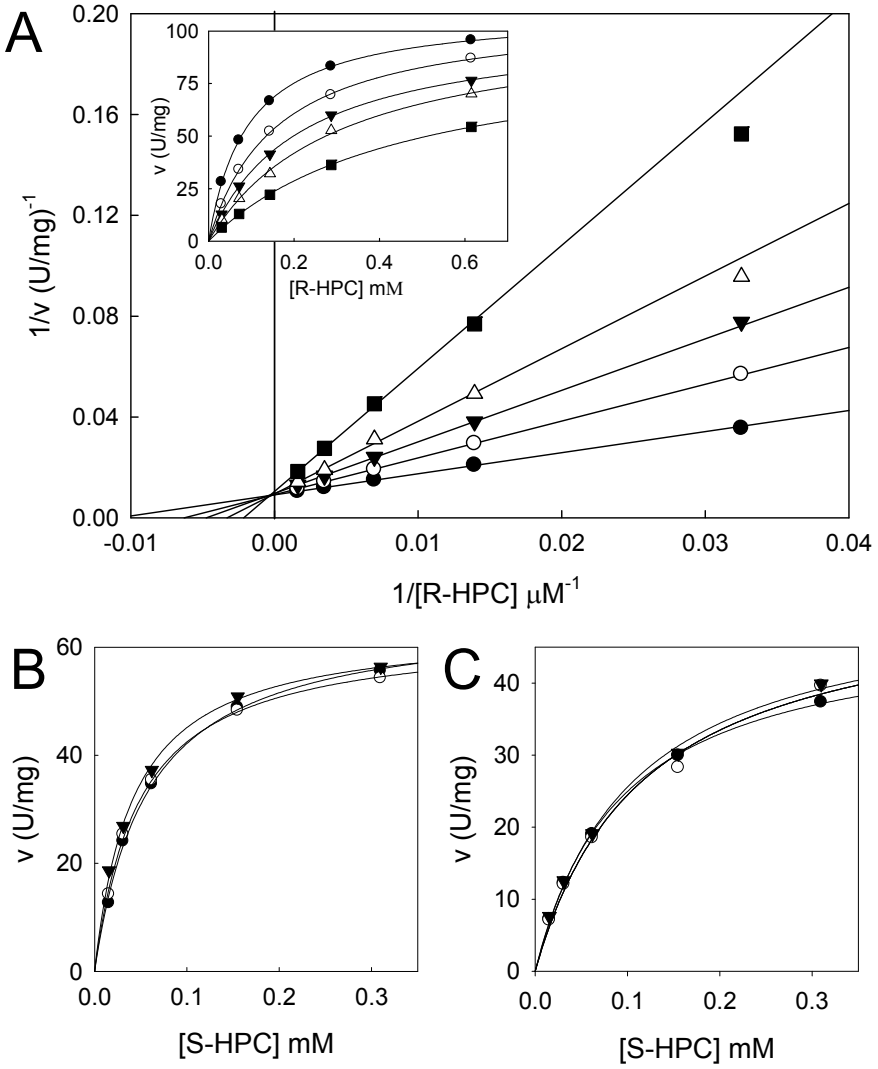

Figure 2-5. Effects of 2-(2-methyl-2-hydroxypropylthio)ethanesulfonate (M-HPC) on *R*- and *S*-HPC oxidation by *R*-HPCDH1, *S*-HPCDH3, and *S*-HPCDH1. Panel A, Competitive inhibition of *R*-HPCDH1-catalyzed *R*-HPC oxidation by M-HPC. The double reciprocal plots for assays performed in the presence of different concentrations of M-HPC are shown in the main diagram. Data points represent the average of triplicate experiments. The solid lines were generated by nonlinear least-square fits of the *v* vs. S data, shown in the *inset*, to the equation for a rectangular hyperbola using Sigmaplot. M-HPC concentrations: (●) 0 mM, (○) 0.2 mM, (▼) 0.4 mM, (Δ) 0.8 mM, (■) 1.6 mM. Panels B and C, *v* vs. S plots for S-HPC oxidation by *S*-HPCDH3 and *S*-HPCDH1, respectively, in the presence of different concentrations of M-HPC. The lines were generated by fitting the data to the standard form of the Michaelis-Menten equation. M-HPC concentrations: (●) 0 mM, (○) 1.2 mM, (▼) 4.9 mM

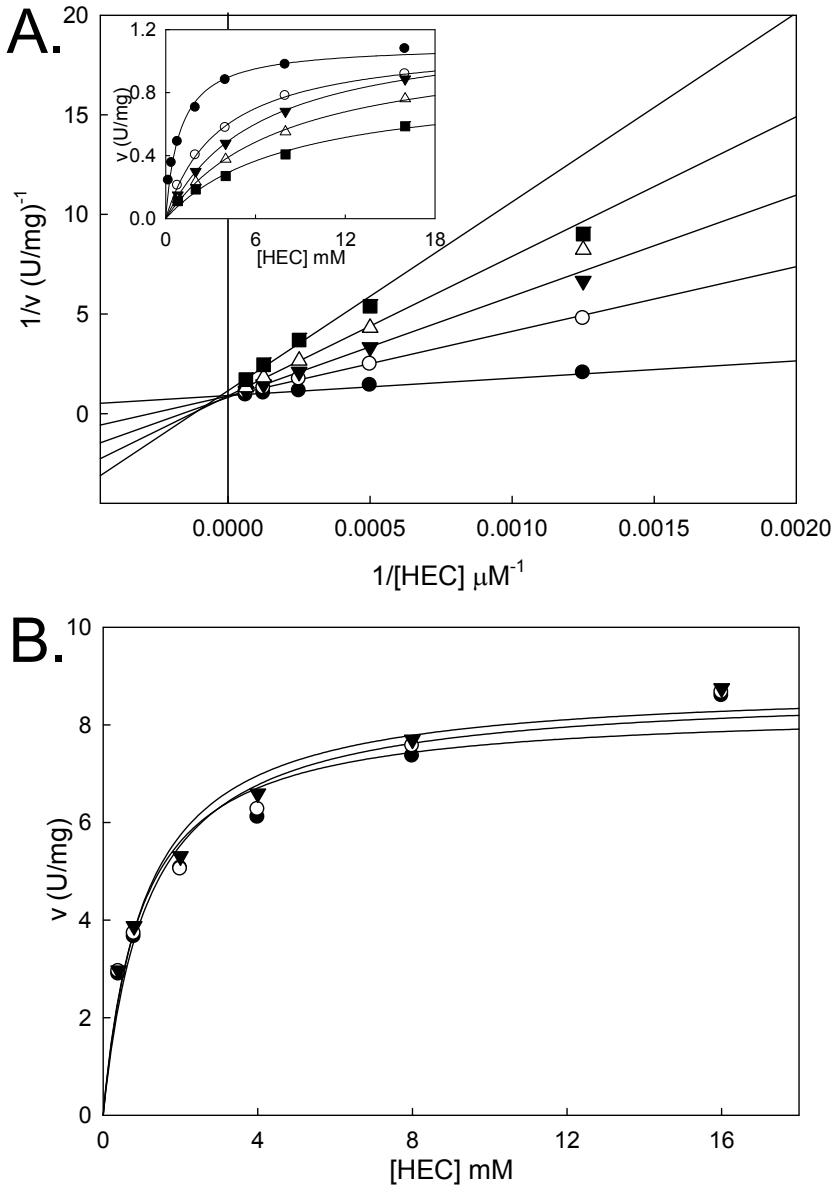

Figure 2-6. Effects of 2-(2-methyl-2-hydroxypropylthio)ethanesulfonate (M-HPC) on 2-(2-hydroxyethylthio) ethanesulfonate (HEC) oxidation by *R*-HPCDH1 and *S*-HPCDH3. Panel A, Competitive inhibition of *R*-HPCDH1-catalyzed HEC oxidation by M-HPC. The double reciprocal plots for assays performed in the presence of different concentrations of M-HPC are shown in the main diagram. Data points represent the average of triplicate experiments. The solid lines were generated by nonlinear least-square fits of the *v* vs. S data, shown in the *inset*, to the equation for a rectangular hyperbola using Sigmaplot. M-HPC concentrations: (●) 0 mM, (○) 0.2 mM, (▼) 0.4 mM, (Δ) 0.8 mM, (■) 1.6 mM. Panel B, *v* vs. S plots for HEC oxidation by *S*-HPCDH3 in the presence of different concentrations of M-HPC. The lines were generated by fitting the data to the standard form of the Michaelis-Menten equation. M-HPC concentrations: (●) 0 mM, (○) 1.2 mM, (▼) 4.9 mM.

In contrast to *rR*-HPCDH1, *rS*-HPCDH3 apparently cannot bind *S*-HPC analogs (*R*-HPC and M-HPC) with CoM oriented properly in the sulfonate-binding pocket that consists of R122 and K214. The most logical explanation for this is that the misaligned methyl groups on C2 required for this high affinity binding are not accommodated due to steric clashes with amino acid side chain(s). Thus, *R*-HPC binds to *rS*-HPCDH3 with a 290-fold lower affinity, but in an orientation where the hydroxyl and hydrogen on C2 can be more properly aligned with tyrosine 156 and NAD^+, such that k_{cat} only decreases by 4.5-fold relative to the natural substrate *S*-HPC. The limited studies done with the other *S*-HPCDH homolog (*rS*-HPCDH1) support a similar strategy for controlling enantioselectivity.

The results of the pH studies further indicate that the hydroxyl group at C2 is a larger determinant in the binding of *S*-HPC to *rS*-HPCDH3 than for binding of *R*-HPC to *rR*-HPCDH1. Note that the K_m for the natural substrate is three-fold lower for *S*-HPCDH3 than for *rR*-HPCDH1, which could be due to higher affinity binding of the hydroxyl group. However, the K_m values for HEC, lacking the methyl group, are identical for both enzymes. Thus, the methyl group of *S*-HPC may facilitate the alignment of the hydroxyl group in this higher affinity position.

While the homology model of *rS*-HPCDH3 proved useful for predicting the catalytic triad and sulfonate-binding residues verified experimentally in this paper, it is not sufficient for testing the tenets of this model by definitively identifying steric clashes with a modeled substrate or inhibitor. The verification of this model for differential control of enantioselectivity will require solving the three-dimensional structure of *rS*-HPCDH3, work that is currently in progress, followed by further biochemical, mutational, and kinetic characterization of the enzyme.

Physiological Implications of These Studies. The differential control of enantioselectivity in the *R*- and *S*-HPCDH enzymes may have evolved to reflect the roles these enzymes play in propylene metabolism. As shown in Figure 2-1, alkene monooxygenase from *X. autotrophicus* produces a mixture of *(R)* and *(S)*-epoxypropane, although *(R)*-epoxypropane is produced in a

90% enantioexcess (*4*). Both *(R)*- and *(S)*-epoxypropane are substrates for epoxyalkane:CoM transferase, which results in the production of *R*- and *S*-HPC, respectively. Although *(S)*-epoxypropane (and by extrapolation, *S*-HPC) are the minor products of the metabolic pathway, it is still essential for these compounds to be further metabolized by the bacterium, since epoxides are highly toxic. While epoxyalkane:CoM transferase detoxifies *(S)*-epoxypropane by conversion to *S*-HPC, *S*-HPC must proceed through the pathway of epoxide carboxylation to regenerate free CoM; if it did not, the CoM pool would be wastefully sequestered. Since *R*-HPC is the more abundant enantiomer, *R*-HPCDH will still operate efficiently even with a similar K_m value for the opposite enantiomer, since *S*-HPC is predicted to be produced at about 20-fold lower concentrations. In contrast, in order for *S*-HPCDH to be efficient at the lower concentrations of *S*-HPC encountered in the cell, it needs to have a lower K_m for the natural substrate and substantially higher K_m for the opposite enantiomer to work efficiently. To summarize, the different amounts of *R*- and *S*-HPC that accumulate in the cells due to the inherent stereoselectivity of the alkene monooxygenase appears to have led to the evolution of different strategies for controlling efficient substrate flux through the pathway. *R*-HPC oxidation is controlled by k_{cat}, since *R*-HPCDH does not need to discriminate substrate binding at the much lower concentrations of the opposite enantiomer present, while control of *S*-HPC oxidation is controlled by K_m, since discrimination of substrate binding is crucial with the higher concentrations of the inhibitory enantiomer present. In the context of this physiological discussion it should be noted that *R*- and *S*-HPCDH were found to have comparable specific activities in cell extracts of *X. autotrophicus* when grown on propylene, with each predicted to account for about 1% of soluble cell protein (*4-6*). This observation reiterates that substrate flux is controlled by differences in mechanisms of these enzymes and not by differences in levels of expression.

The fact that *X. autotrophicus* has redundant copies of the dehydrogenases (as well as the other enzymes of epoxide metabolism) further highlights the importance of these enzymes to the

bacterium. The results of Table 2-1 suggest some differences in the kinetic properties for two of the redundant *S*-enzymes. It will be interesting to see if there are any kinetic differences in the redundant *R*-enzymes, as well as to determine at what relative levels the individual enzymes are expressed. The copies we purified from *X. autotrophicus* in our previous studies (*4-6, 18, 23*) consisted primarily (or wholly) of the enzymes in the first operon based on yields from the purification schemes and their biochemical properties. Now that we have a greater understanding of the organization of the epoxide carboxylation genes we can apply molecular genetics to determine how important the individual copies are to bacterial growth and survival under different conditions.

Summary. To our knowledge, this paper provides the first side by side characterization of a pair of SDR enzymes expressed simultaneously to act on two enantiomers of the same alcohol produced in a metabolic pathway. These dehydrogenases are distinguished from all other known members of the SDR family in using the novel sulfonate functional group of coenzyme M as a handle for chiral discrimination. The differential control of enantioselectivity by k_{cat} vs. K_m is a surprising yet explainable result in the context of cellular metabolism. These results provide a standard for examining the molecular basis of stereoselectivity in other such enzyme pairs.

REFERENCES

1. Kroutil, W., Mang, H., Edegger, K., and Faber, K. (2004) Recent advances in the biocatalytic reduction of ketones and oxidation of sec-alcohols. *Curr. Opin. Chem. Biol. 8*, 120-126.

2. Nakamura, K., Yamanaka, R., Matsuda, T., and Harada, T. (2003) Recent developments in asymmetric reduction of ketones with biocatalysts. *Tetrahedron: Asymmetry 14*, 2659-2681.

3. Goldberg, K., Schroer, K., Lütz, S., and Liese, A. (2007) Biocatalytic ketone reduction—a powerful tool for the production of chiral alcohols—part I: processes with isolated enzymes. *Appl. Microbiol. Biotechnol. 76*, 237-248.

4. Allen, J. R., Clark, D. D., Krum, J. G., and Ensign, S. A. (1999) A role for coenzyme M (2-mercaptoethansulfonic acid) in a bacterial pathway of aliphatic epoxide carboxylation. *Proc. Natl. Acad. Sci. U.S.A. 96*, 8432-8437.

5. Allen, J. R., and Ensign, S. A. (1997) Purification to homogeneity and reconstitution of the individual components of the epoxide carboxylase multiprotein enzyme complex from *Xanthobacter* strain Py2. *J. Biol. Chem. 272*, 32121-32128.

6. Allen, J. R., and Ensign, S. A. (1999) Two short-chain dehydrogenases confer stereoselectivity for enantiomers of epoxypropane in the multiprotein epoxide carboxylating systems of *Xanthobacter* strain Py2 and *Nocardia corallina* B276. *Biochemistry 38*, 247-256.

7. Ensign, S. A. (2001) Microbial metabolism of aliphatic alkenes. *Biochemistry 40*, 5845-5853.

8. Ensign, S. A., and Allen, J. R. (2003) Aliphatic epoxide carboxylation. *Ann. Rev. Biochem. 72*, 55-76.

9. Jörnvall, H., Persson, B., Krook, M., Atrian, S., Gonzàlez-Duarte, R., Jeffery, J., and Ghosh, D. (1995) Short-chain dehydrogenases/reductases. *Biochemistry 34*, 6003-6013.

10. Kavanagh, K. L., Jornvall, H., Persson, B., and Oppermann, U. (2008) The SDR superfamily: functional and structural diversity within a family of metabolic and regulatory enzymes. *Cell. Mol. Life Sci. 65*, 3895-3906.

11. Oppermann, U., Filling, C., Hult, M., Shafqat, N., Wu, X., Lindh, M., Shafqat, J., Nordling, E., Kallberg, Y., Persson, B., and Jörnvall, H. (2003) Short-chain dehydrogenases/reductases (SDR): the 2002 update. *Chem.-Biol. Interact. 143-144*, 247-253.

12. Persson, B., Kallberg, Y., Bray, J. E., Bruford, E., Dellaporta, S. L., Favia, A. D., Duarte, R. G., Jornvall, H., Kavanagh, K. L., Kedishvili, N., Kisiela, M., Maserk, E., Mindnich, R., Orchard, S., Penning, T. M., Thornton, J. M., Adamski, J., and Oppermann, U. (2009) The SDR (short-chain dehydrogenase/reductase and related enzymes) nomenclature initiative. *Chem.-Biol. Interact. 178*, 94-98.

13. Persson, B., Krook, M., and Jörnvall, H. (1991) Characteristics of short-chain alcohol dehydrogenases and related enzymes. *Eur. J. Biochem. 200*, 537-543.

14. Clark, D. D., Boyd, J. M., and Ensign, S. A. (2004) The stereoselectivity and catalytic properties of *Xanthobacter autotrophicus* 2-[(R)-2-Hydroxypropylthio]ethanesulfonate dehydrogenase are controlled by interactions between C-terminal arginine residues and the sulfonate of coenzyme M. *Biochemistry 43*, 6763-6771.

15. Clark, D. D., and Ensign, S. A. (2002) Characterization of the 2- (R)-2-hydroxypropylthio ethane sulfonate dehydrogenase from *Xanthobacter* strain Py2: product inhibition, pH dependence of kinetic parameters, site-directed mutagenesis, rapid equilibrium inhibition, and chemical modification. *Biochemistry 41*, 2727-2740.

16. Krishnakumar, A. M., Nocek, B. P., Clark, D. D., Ensign, S. A., and Peters, J. W. (2006) Structural basis for stereoselectivity in the (R)- and (S)-hydroxypropylthioethanesulfonate dehydrogenases. *Biochemistry 45*, 8831-8840.

17. Krishnakumar, A. M., Sliwa, D., Endrizzi, J. A., Boyd, E. S., Ensign, S. A., and Peters, J. W. (2008) Getting a handle on the role of coenzyme M in alkene metabolism. *Microbiol. Mol. Biol. Rev. 72*, 445.

18. Allen, J. R., and Ensign, S. A. (1997) Characterization of three protein components required for functional reconstitution of the epoxide carboxylase multienzyme complex from *Xanthobacter* strain Py2. *J. Bacteriol. 179*, 3110-3115.

19. Laemmli, U. K. (1970) Cleavage of structural proteins during the assembly of the head of bacteriophage T4. *Nature 227*, 680-685.

20. Cook, P. F., and Cleland, W. W. (2007) *Enzyme Kinetics and Mechanism*, Garland Science, New York.

21. Krum, J. G., and Ensign, S. A. (2001) Evidence that a linear megaplasmid encodes enzymes of aliphatic alkene and epoxide metabolism and Coenzyme M (2-mercaptoethanesulfonate) biosynthesis in *Xanthobacter* strain Py2. *J. Bacteriol. 183*, 2172-2177.

22. Swaving, J., Weijers, C. A., van Ooyen, A. J., and de Bont, J. A. M. (1995) Complementation of *Xanthobacter* Py2 mutants defective in epoxyalkane degradation, and expression and nucleotide sequence of the complementing DNA fragment. *Microbiology 141*, 477-484.

23. Clark, D. D., Allen, J. R., and Ensign, S. A. (2000) Characterization of five catalytic activities associated with the NADPH : 2-ketopropyl-coenzyme M [2-(2-ketopropylthio)ethanesulfonate] oxidoreductase/carboxylase of the *Xanthobacter* strain Py2 epoxide carboxylase. *Biochemistry 39*, 1294-1304.

24. Larsen, R. A., Wilson, M. M., Guss, A. M., and Metcalf, W. W. (2002) Genetic analysis of pigment biosynthesis in *Xanthobacter autotrophicus* Py2 using a new, highly efficient transposon mutagenesis system that is functional in a wide variety of bacteria. *Arch. Microbiol. 178*, 193-201.

25. Sluis, M. K., Larsen, R. A., Krum, J. G., Anderson, R., Metcalf, W. W., and Ensign, S. A. (2002) Biochemical, molecular, and genetic analyses of the acetone carboxylases from *Xanthobacter autotrophicus* strain Py2 and *Rhodobacter capsulatus* strain B10. *J. Bacteriol. 184*, 2969-2977.

26. de Jong, R. M., Kalk, K. H., Tang, L., Janssen, D. B., and Dijkstra, B. W. (2006) The X-ray structure of the haloalcohol dehalogenase HheA from *Arthrobacter* sp strain AD2: Insight into enantioselectivity and halide binding in the haloalcohol dehalogenase family. *J. Bacteriol. 188*, 4051-4056.

27. Horer, S., Stoop, J., Mooibroek, H., Baumann, U., and Sassoon, J. (2001) The crystallographic structure of the mannitol 2-dehydrogenase NADP(+) binary complex from *Agaricus bisporus*. *J. Biol. Chem. 276*, 27555-27561.

28. Hoffken, H. W., Duong, M., Friedrich, T., Breuer, M., Hauer, B., Reinhardt, R., Rabus, R., and Heider, J. (2006) Crystal structure and enzyme kinetics of the (S)-specific 1-

phenylethanol dehydrogenase of the denitrifying bacterium strain EbN1. *Biochemistry 45*, 82-93.

29. Grimshaw, C. E., Cook, P. F., and Cleland, W. W. (1981) Use of isotope effects and pH studies to determine the chemical mechanism of *Bacillus subtilis* L-alanine dehydrogenase. *Biochemistry 20*, 5655-5661.

30. Winberg, J. O., Brendskag, M. K., Sylte, I., Lindstad, R. I., and McKinley-McKee, J. S. (1999) The catalytic triad in *Drosophila* alcohol dehydrogenase: pH, temperature and molecular modelling studies. *J. Mol. Biol. 294*, 601-616.

31. Brendskag, M. K., McKinley-McKee, J. S., and Winberg, J. O. (1999) *Drosophila lebanonensis* alcohol dehydrogenase: pH dependence of the kinetic coefficients. *Biochim. Biophys. Acta, Protein Struct. Mol. Enzymol. 1431*, 74-86.

32. Puranen, T. J., Poutanen, M. H., Peltoketo, H. E., Vihko, P. T., and Vihko, R. K. (1994) Site-directed mutagenesis of the putative active site of human 17β-hydroxysteroid dehydrogenase type. *Biochem. J 304*, 289-293.

CHAPTER 3

THE ENANTIOSELECTIVITY AND KINETIC PROPERTIES OF (*R*) - AND (*S*) – HYDROXYPROPYL COM DEHYDROGENASES FROM *XANTHOBACTER AUTOTROPHICUS* STRAIN PY2

ABSTRACT

The 2-(*R*)- and 2-[(*S*)-2-hydroxypropylthio]ethanesulfonate (HPC) dehydrogenases (DH) represent a unique set of enantioselective short-chain dehydrogenase/reductase (SDR) enzymes, catalyzing the reversible oxidation of *R*-HPC and *S*-HPC to produce 2-(2-ketopropylthio)ethanesulfonate (2-KPC). Recent successful cloning and expression of *rS*-HPCDH3 allowed for the comparison studies with the previously characterized *rR*-HPCDH1 counterpart. Both enzymes are highly enantioselective for their corresponding substrates, exhibiting 0.14% to 1.0% activity with the opposite enantiomer. The enantioselectivity was shown to be controlled differently in the HPCDH enzymes, either through changes in the K_m or the k_{cat} (*1*). The kinetic and mechanistic studies of *R*- and *S*-HPCDH enzymes in the context of their high degree of enantioselectivity are reported. The reduction of 2-butanone by *rR*-HPCDH1 produced 30% *(R)*-2-butanol and 70% *(S)*-2-butanol, while in the same reaction *rS*-HPCDH3 produced 99% *(S)*-2-butanol. The enantioselectivity and the kinetic parameters in the reduction of the aliphatic ketones can be modulated by the addition of the short-chain alkylsulfonates as observed for *rR*-HPCDH1. This modulating effect was abolished for *rS*-HPCDH3, regardless of the direction of the reaction and the chain-length of the additive. The absolute enantioselectivity towards the *(S)*-alcohol is observed for *rS*-HPCDH3 in the reduction of 2-butanone, 2-pentanone and 2-hexanone. The ability of *rS*-HPCDH3 to oxidize the *(R)*- and *(S)*-enantiomers the long-chain aliphatic alcohols (C_4-C_8) suggests that chirality of the alcohol is not a sufficient determinant for the high degree of enantioselectivity displayed by *rS*-HPCDH3. There is a clear requirement for the sulfonate moiety on the substrate to provide strong binding affinity and the

proper orientation of the substrate for the hydride abstraction. Inhibitors were investigated as probes of the molecular features of the substrate contributing to its binding. Ethanesulfonate, propanesulfonate and butanesulfonate were found to be uncompetitive inhibitors of *S*-HPC oxidation by *rS*-HPCDH3, while methanesulfonate and CoM were mixed inhibitors. This suggested that the length of the substrate carbon chain is an important determinant in the recognition by the HPCDH enzymes. Bromoethanesulfonate (BES) is a structural analog of CoM and has been shown to be a potent inhibitor of methanogenesis. The effect of BES on the oxidation of *S*-HPC by *rS*-HPCDH3 was examined to complement the previous studies with other enzymes of the epoxide carboxylation pathway. BES was found to be a strong uncompetitive inhibitor with respect to *S*-HPC. This study provides an important insight into the mechanism of enantioselectivity among the SDR enzymes, with emphasis of on *rS*-HPCDH3.

INTRODUCTION

Chiral alcohols are valuable intermediates in the synthesis of a large number of fine chemicals and pharmaceuticals. Thus, the production of optically pure alcohols by the reduction of the corresponding ketones represents one of the most fundamental and practical chemical transformations. The biocatalytic approach to these transformations is finding an increasing number of industrial applications (*2*) due to its efficiency, high optical purity of resulting products and low environmental impact (*3, 4*). For this reasons biocatalysis offers an attractive alternative to chemical synthesis. Alcohol dehydrogenases (ADHs) are of special interest due to their high degree of enantioselectivity and substrate specificity (*5*). Since their early use in the biocatalytic production of secondary *(S)*- and *(R)*-alcohols (*6*), screening efforts have been made towards isolation and characterization of novel ADHs with high thermostability and chemo-, regio- and stereoselectivity. Of particular demand are enantiocomplementary enzymes, which catalyze the same reaction, but with an opposite stereoselectivity. A unique example of such enzymes constitute a pair of 2-*(R)*- and 2-[*(S)*-2-hydroxypropylthio]ethanesulfonate (HPC) dehydrogenases

(DH) from *Xanthobacter autotrophicus* strain Py2. The *R*- and *S*-HPCDH are an integral part of the three step epoxide degradation pathway in *X. autotrophicus* Py2, where they act in concert to catalyze the reversible oxidation of *R*- and *S*-HPC to a common achiral product 2-(2-ketopropylthio)ethanesulfonate (2-KPC) (Scheme 3-1) (*7, 8*). This pathway requires CoM as a cofactor for the epoxide ring opening and as a carrier of 2-hydroxypropyl- and 2-ketopropyl-CoM intermediates (*9*). *R*- and *S*-HPCDH belong to the short-chain dehydrogenase/reductase (SDR) superfamily. The X-ray structures determined for members of this family display highly similar α/β folding pattern with a Rossmann-fold for nucleotide binding. The SDR enzymes represent one of the oldest protein families found in all forms of life, where they display great functional diversity (*10-12*).

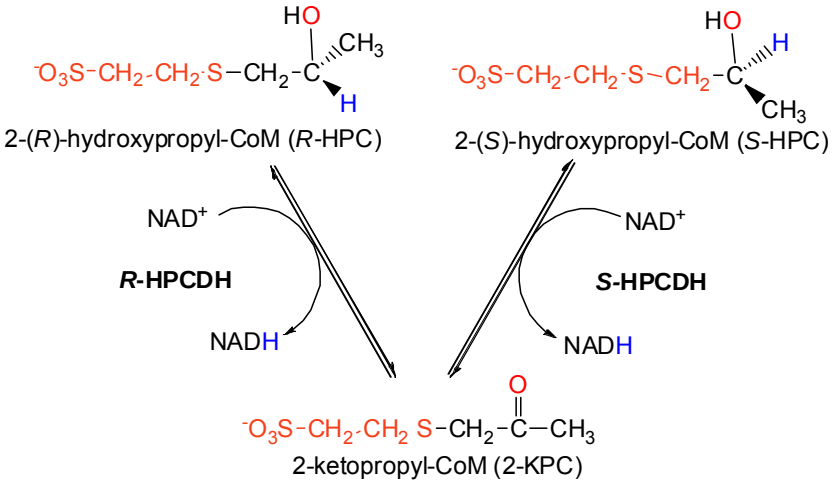

Scheme 3-1.

Among a large number of SDR enzymes annotated in databases (*13*), there are very few stereoselective enzymes present in a common pathway that catalyze the same reaction but with an opposite stereoselectivity. The only known examples include a pair of tropinone reductases (*14, 15*) and the *R*- and *S*-HPC dehydrogenases (*8, 16*). The uniqueness of the HPCDH enzymes,

along with their prospective industrial applications has prompted more detailed studies on the basis of their enantioselectivity. Besides biocatalytical implications of this research for the production of enantiopure alcohols, in its broader context this study may also prove useful in the bioremediation of toxic compounds such as alkenes, ketones and epoxides. Furthermore, understanding the mechanism of enantioselectivity may prove useful in engineering other stereoselective enzymes for biocatalytical purposes, either through the rational design or directed evolution.

The central goal of the research presented in this chapter is to extend the kinetic and mechanistic characterization of HPCDH enzymes in the context of their high degree of enantioselectivity. This work is complementary to the research described in Chapter 2 and is intended to investigate in the greater detail differences in the enantioselectivity observed for *rS*-HPCDH3 and *rR*-HPCDH1. Side by side kinetic experiments in the presence of short-chain alkylsulfonates as potential modulators of the enzyme activity and enantioselectivity were carried out to aid better understanding of the mechanism of chiral discrimination. Results of the inhibition studies supported by the structural analysis further define similarities and differences between *rS*-HPCDH3 and *rR*-HPCDH1. As reported previously, the amino acid sequence comparison of both enzymes revealed a number of differences in their respective C-terminal domains. The most striking being the differential placement of positively charged residues (Arg, Lys) that play an important role in binding of the sulfonate of CoM (*1, 16*). Based on the available kinetic and structural data for *rR*-HPCDH1 and *rS*-HPCDH3 a model has been proposed in which the differential placement of the sulfonate binding residues and the steric clashes of the terminal methyl group of the substrate are responsible for proper binding and orientation of *R*-HPC and *S*-HPC alcohols to their respective enzymes. This hypothesis has been investigated by examining the catalytic properties and stereoselectivity of the HPCDH enzymes with their physiological substrates (*R*-HPC, *S*-HPC, and 2-KPC) and non-physiological substrates (aliphatic alcohols and ketones lacking the sulfonate moiety). The effect of linear alkylsulfonates on the

kinetic parameters of the aliphatic ketone reduction catalyzed by *rS*-HPCDH3 was also investigated.

EXPERIMENTAL PROCEDURES

Materials. All commercially available chemicals were purchased from Sigma-Aldrich Chemicals, Acros Organics or Fisher Scientific, and were of analytical grade. Substrates for enzymatic assays: 2-KPC, *R*-HPC and *S*-HPC were synthesized as described previously (*16*). Chemical structures of the compounds were confirmed using ^{1}H NMR. The spectra of HPC enantiomers and 2-KPC were identical to those reported previously (*16, 17*). Purity of the synthesized chemicals was estimated by reverse-phase HPLC to be ≥98%.

Cloning of the rR-HPCDH3 and rS-HPCDH1 Genes (xecD1 and xecE3). As described previously (*1*), three sets of genes encoding *R*- and *S*-HPCDH enzymes were identified on the linear megaplasmid of *X. autotrophicus* Py2. The operon in which they occur were designated as 1, 2 and 3, accordingly to order in which they appear in the DNA sequence and with respect to the first discovered and characterized operon of the epoxide degradation pathway genes (assigned with number 1). The *xecD1* gene encoding *R*-HPCDH1 (from the first operon) and *xecE3* gene encoding *S*-HPCDH3 (from the third operon) were amplified using genomic DNA of propylene-grown *X. autotrophicus* Py2 as a template. The PCR primers and cloning procedures were identical to those described previously (*1*). Plasmids pXD28 and pDS53 containing *xecD1* and *xecE3* genes, respectively, were transformed into *Escherichia coli* BL21 - (DE3) CodonPlus (Stratagene) cells for protein expression.

DNA Sequencing. All the sequencing was performed on an AB 3730 DNA Analyzer at the Utah State University CIB DNA sequencing laboratory with the following primers: for pXD28; T7 promoter primer, TAATACGACTCACTATAGGG (Novagen), and T7 terminator primer, GCTAGTTATTGCTCAGCGG (Novagen), and for pDS53; ACYCDuetUP1 Primer

(Novagen), GGATCTCGACGCTCTCCCT and DuetDOWN1 Primer (Novagen), GATTATGCGGCCGTGTACAA.

Media and Growth of Bacteria. E. coli BL21- (DE3) CodonPlus was grown in a 15L semicontinuous microferm fermenter with LB media that contained both kanamycin (50 μg mL^{-1}) and chloramphenicol (50 μg mL^{-1}). All other procedures were performed as described previously (*16*).

Purification of rR-HPCDH1 and rS-HPCDH3. The recombinant enzymes *rR*-HPCDH1 and *rS*-HPCDH3 were purified on IMAC column with Ni Sepharose 6 Fast Flow (Amersham) resin as described previously (*1*). Protein concentrations were determined on a NanoDrop spectrophotometer using theoretical extinction coefficients (ϵ_{280} = 10033 M^{-1} cm^{-1} for *S*-HPCDH3 and ϵ_{280} = 18512.5 M^{-1} cm^{-1} for *R*-HPCDH1), with dialysis flow-through buffers as blanks.

Molecular Mass of rR-HPCDH1 and rS-HPCDH3, and Native State Evaluation. The apparent molecular masses of polypeptides were determined on a SDS-PAGE gel (12% T) by comparison to R_f values of standard proteins. The native molecular masses of *rR*-HPCDH1 and *rS*-HPCDH3 were estimated by native PAGE (4-20% T BioRad) and gel filtration chromatography using HPLC (Shimadzu SLC-10A) with a fluorescence detector (Shimadzu RF-10AXL) adjusted for excitation at 280 nm and emission 350 nm. The gel filtration column (BioSep-SEC S-2000, 300 x 7.8 mm, Phenomenex) was used in conditions described previously (*1*). SDS-PAGE and native PAGE were performed according to the Laemmli procedure (*18*). Circular dichroism (CD) spectrapolarimetric analysis were performed to ensure that the tertiary structure of the proteins remains intact. CD spectra were recorded at 25 °C on an AVIV Model 410 CD Spectrophotometer, as described previously (*1*).

Spectrophotometric Enzyme Assays. Assays with 2-KPC, *S*-HPC and *R*-HPC as substrates were performed in 50 mM glycine, 50 mM NaH_2PO_4, and 50 mM Tris base (GPT buffer mix) at pH 7.5, as described previously (*16*). Assays with all other substrates (C_4 to C_8 in carbon chain-length) were carried out in 50 mM GPT buffer containing 15% (v/v) glycerol. Stock solutions of

synthesized substrates were standardized, as described previously (*16*). All assays were performed at 30 °C in a Shimadzu model UV160U spectrophotometer containing a water-jacketed cell holder for thermal control. Alcohol or ketone production was monitored by measuring the change in absorbance at 340 nm using the extinction coefficient for NADH (ϵ_{340} = 6.22 mM^{-1} cm^{-1}). For alcohol oxidation assays, the following ranges of alcohol concentrations were used in determining kinetic constants: *R*-HPC, 0.035-1.4 mM; *S*-HPC, 0.096-1.9 mM; (*S*)-2-butanol, 10.9-381 mM; (*R*)-2-butanol, 43.6-490 mM. The oxidation of 2-butanol in the presence of 1 mM alkylsulfonates was carried out with 227 mM of (*R*)-2-butanol or 174 mM of (*S*)-2-butanol (Table 2-4). Activity assay of *rS*-HPCDH3 with *(S)*- and *(R)*-enantiomers of C_4 to C_8 alcohols was performed at concentrations ranging from 50 mM to 74 mM (Table 2-5). The concentration of NAD^+ for all assays was 10 mM (26 x value of K_{mNAD+}). For assays of ketone reduction, the following concentration ranges were used in determining kinetic constants: 2-KPC, 0.050-2.6 mM; 2-butanone, 10-300 mM; 2-pentanone, 47-470 mM; 3-pentanone, 18.8-564 mM; 2-hexanone, 16.2-162 mM. In the assay of 2-ketone reduction catalyzed by *rS*-HPCDH3 all additives tested for their ability to modify kinetic parameters were present at an overall concentration of 1 mM (Table 2-7). All assays contained the following concentrations of the substrate: 558 μM of 2-butanone; 225 mM of 2-pentanone and 122 mM of 2-hexanone. The concentration of NADH for these assays was 0.16 mM, (4.4 x value of K_{mNADH}). On an average, seven concentrations of the substrates within the ranges indicated were chosen for the kinetic analyses. The assays were performed in duplicates or triplicates, unless otherwise stated. All samples were degassed/flushed with nitrogen and incubated in the 30 ºC water-bath for 5 min prior to the enzyme addition. To determine kinetic parameters (apparent K_m and V_{max}) initial rate values were plotted as a function of substrate concentration and data points were fitted to a Michaelis-Menten equation using SigmaPlot 11.0.

Standardization of Stock Solutions. Stock solutions of *R*-HPC and 2-KPC were standardized with *rR*-HPCDH1, whereas stock solutions of *S*-HPC were standardized by use of *rS*-HPCDH3. Standardization assays for *R*-HPC and *S*-HPC oxidation were performed in GPT buffer (50 mM glycine, 50 mM NaH_2PO_4, and 50 mM Tris base) at pH 11.0 with 50 μg of enzyme and 10 mM of NAD^+. Standardization assay for 2-KPC reduction was performed in GPT buffer at pH 7.5 with 50 μg of enzyme and 0.2 mM of NADH. All assays were carried out at 30 ºC for 2 min and repeated 3 to 6 times. The average absorbance measured at 340 nm was correlated with micromoles of the substrate used in the assay using the extinction coefficient for NADH (ϵ_{340} = 6.22 mM^{-1} cm^{-1}). Calculations of the final stock concentration of 2-KPC were done using the equilibrium constant determined from the Haldane equation, as described previously (*16*). Calculations of the final stock concentration of *R*-HPC and *S*-HPC were based on assumption that the reactions went to completion, since pH 11.0 renders both enzymes irreversible. Stock solutions of NAD^+ and NADH were standardized by measuring absorbance of aliquoted solutions at 260 nm and 340 nm, respectively, using the appropriate extinction coefficients (NAD^+ ϵ_{260} = 18.0 mM^{-1} cm^{-1} and NADH ϵ_{340} = 6.22 mM^{-1} cm^{-1}).

Inhibition Studies. All assays were performed in GPT buffer mix at pH 7.5 with saturating concentration of NAD^+ (10 mM). Inhibition assays for *rR*-HPCDH1 were performed at variable concentrations of *R*-HPC (31, 72, 144, 287 and 615 μM). Each assay was performed at several fixed concentrations of propanesulfonate (0, 1, 2, 4 and 8 mM) or butanesulfonate (0, 0.25, 0.5, 1.0 and 2.0 mM). Inhibition assays for S-HPCDH3 were performed at variable concentrations of *S*-HPC (16, 31, 62, 155, 310 and 645 μM) and several fixed concentrations of the inhibitor: *R*-HPC (0, 1.2, 2.4, 4.9 and 9.7 mM), methanesulfonate (0, 40, 80, 160 and 300 mM), ethanesulfonate (0, 10, 20, 50 and 100 mM), propanesulfonate (0, 10, 20, 40 and 80 mM), butanesulfonate (0, 1.25, 2.5, 5, and 10 mM), 2-mercaptoethanesulfonate (0, 1, 2, 4 and 8 mM), bromoethanesulfonate (BES) (0, 0.5, 1.0, 1.5 and 3.0) and Na_2SO_4 (0, 10, 20, 50, 100, 200 and

300 mM). Assay with BES was carried out in the presence of 1 mM EDTA. Initial rate data for each inhibitor were fitted to the following equations describing enzyme activity in the presence of competitive (Eq 1), uncompetitive (Eq 2) and mixed (Eq 3) inhibitors:

$$\upsilon = V_{max}[S]/(\alpha K_m + [S]) \quad \text{(Eq 1)}$$

$$\upsilon = V_{max}[S]/(K_m + \alpha'[S]) \quad \text{(Eq 2)}$$

$$\upsilon = V_{max}[S]/(\alpha K_m + \alpha'[S]) \quad \text{(Eq 3)}$$

where S is the substrate, I is the inhibitor, $\alpha = 1 + ([I]/K_{is})$ and $\alpha' = 1 + ([I]/K_{ii})$. The type of inhibition exhibited by each compound was determined based on the visual evaluation of the lines pattern displayed on the double reciprocal plots ($1/\upsilon$ vs 1/[S] at various [I]) and by fitting data to each of the inhibition models described by equations 1 – 3. All calculations and graphing were done in SigmaPlot 11.0. Final inhibition mode was decided upon the best data fit defined by the smallest value of standard deviation for K_{is} and/or K_{ii} following the appropriate graphical pattern. Initial rate data were fit to a rectangular hyperbola described by the standard form of Michaelis-Menten equation.

Chiral Gas Chromatographic Assay for 2-Ketone Reduction. All assays were performed in GPT buffer mix, pH 7.5 (adjusted at 30 ºC), containing 15% (v/v) glycerol. Assay components in 1ml reaction volume were: 15 mM NADH, 0.64 mg of enzyme (wild-type or mutant *rS*-HPCDH3) and 56 mM of the substrate (2-butanone, 2-prentanone or 2-hexanone). Additionally, assays examining the ability of alkylsulfonates to modulate the enantioselectivity of *rS*-HPCDH3 contained 1 mM of additives (methanesulfonate, ethanesulfonate, propanesulfonate, butanesulfonate or 2-mercaptoethanesulfonate). All other procedures were performed as described previously (*1*).

RESULTS AND DISCUSSION

Genetic Analysis of Genes Encoding Enzymes Involved in Aliphatic Epoxide Carboxylation. It was reported previously that the genes encoding the key enzymes of the epoxide carboxylase system were clustered in a single operon located on a 320 kbp linear megaplasmid (*19*). The DNA analysis of the recently published genome of *X. autotrophicus* Py2 (http://genome.jgi-psf.org/xanau/xanau.home.html) revealed the presence of two additional operons shown in Figure 3-1. For the naming purposes the previously characterized operon was designated as number one, while the newly discovered operons are designated as two and three, according to the order of appearance in the DNA sequence. The additional operons are not complete and contain genes which are highly homologous, but not identical. Interestingly, the genes appearing in all three operons are those encoding *R*-HPCDH and *S*-HPCDH enzymes (*xecD1- xecD3* and *xecE1 - xecE3,* respectively) (*1*).

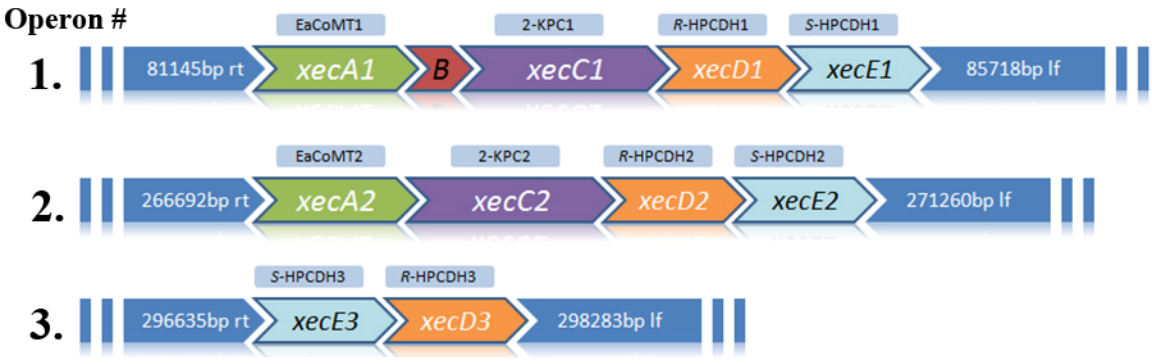

Figure 3-1. Fragment of 320 kb linear megaplasmid of *X. autotrophicus* Py2 showing multiple copies of *xecD* and *xecE* genes encoding *R*- and *S*-HPCDH, respectively.

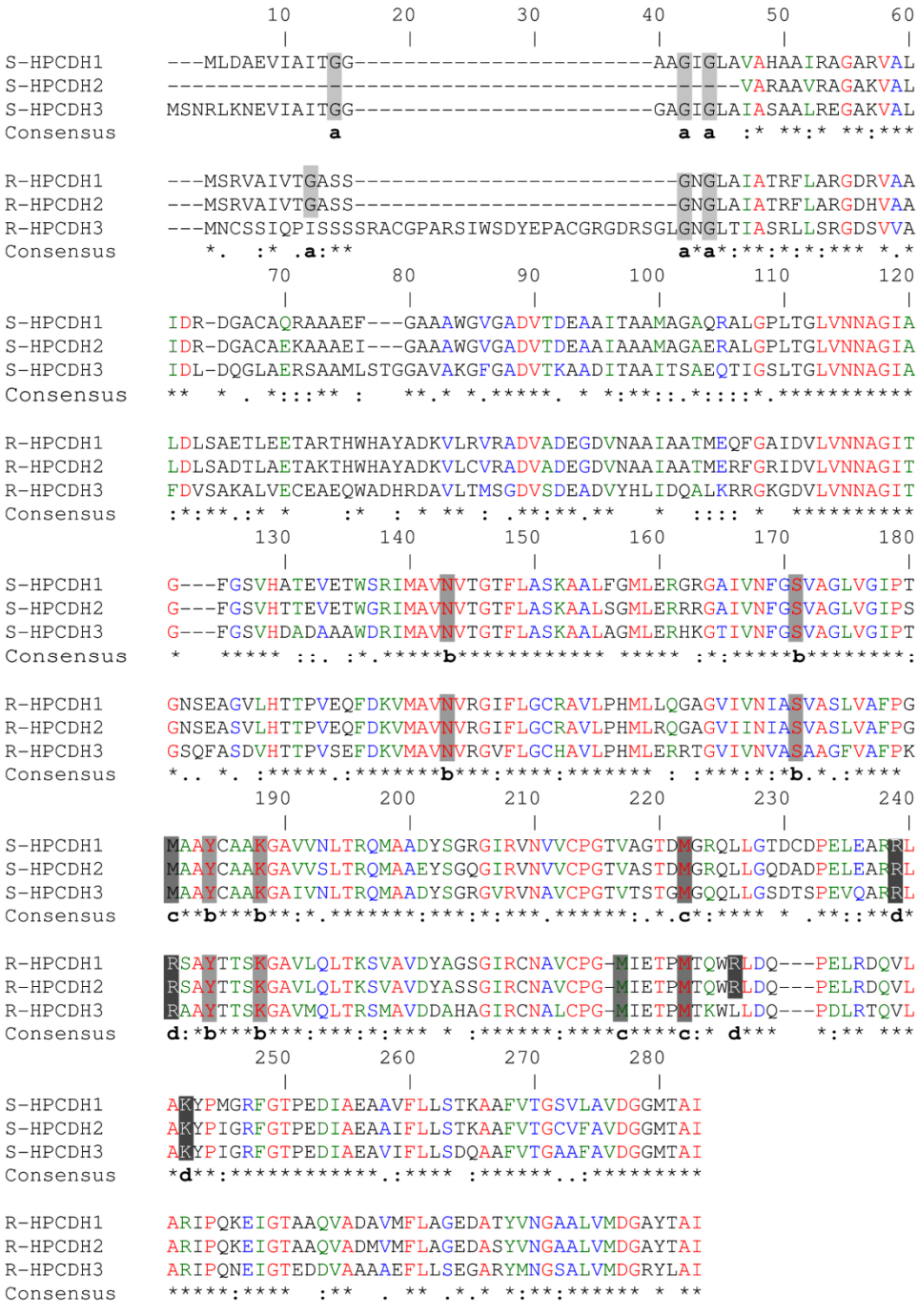

Figure 3-2. Multiple sequence alignment of *S*-HPCDH and *R*-HPCDH enzymes homologs from *X. autotrophicus* Py2. Letter designations: **a**, classic GXXXGXG glycine-rich NAD^+ binding motif; **b,** catalytic tetrad residues of Asn, Ser, Tyr and Lys; **c**, substrate flanking Met residues; **d**, positively charged residues that have been shown in *R*-HPCDH1 and *S*-HPCDH3 to interact with the sulfonate group of the substrate. The alignment was generated using MULTALIN with default parameters, while consensus was derived using ClustalW2. The following symbol means that the residues are: (*) identical; (:) conserved ; (.) semi-conserved.

Production of rR-HPCDH1 and rS-HPCDH3. The presence of multiple copies of genes encoding *R*- and *S*-HPCDH could explain the previous results showing that *R*-HPCDH1 isolated from *X. autotropicus* Py2 migrated in a form of two bands on the SDS-PAGE gels, despite many efforts of their chromatographic separation (*20*). The calculated molecular weights of the proteins encoded by *xecD1*, *xecD2* and *xecD3* are 26.1 kDa, 29.5 kDa and 26.2 kDa, respectively. Mixture of all homologs resolved on the SDS-PAGE gel could therefore account for the appearance of two bands. With regard to *S*-HPCDH enzymes, further analysis show that *S*-HPCDH1, *S*-HPCDH2 and *S*-HPCDH3 (encoded by *xecE1*, *xecE2* and *xecE3* genes, respectively) share 76% to 88% of amino acid identity. The *S*-HPCDH2 lacked the NAD^+ binding motive GXXXGXG and when purified was found to be inactive (data not shown). The catalytic triad residues (Ser, Tyr, Lys), the CoM binding residues (Arg and Lys) as well as two substrate flanking methionines were highly conserved between all homologs of *S*-HPCDH (Figure 3-2). Amino acid sequence alignment of the *S*-HPCDH homologs and *R*-HPCDH1 reveal only 40% to 41% identity. This is not surprising given that low sequence identity is common among SDR enzymes and typically ranges between 15% to 30% (*21*). Examination of the codon usage in *xecE* genes shows that *xecE1* and *xecE3* contain 7 and 10 rare codons, respectively. This suggests that codon usage could have contributed to even more troublesome expression of *rS*-HPCDH1 than of its counterpart *rR*-HPCDH1. Indeed, the expression of *rS*-HPCDH1 was minimal (< 0.1 mg/g of cell paste), as most of the protein remained insoluble. The highest expression was obtained for the *rS*-HPCDH3 homolog cloned in pRSF Duet vector and expressed in BL21-CodonPlus(DE3) strain (*1*). Therefore, only *rR*-HPCDH1 and *rS*-HPCDH3 were used in the subsequent kinetic and structural studies. Purification of the native form of *S*-HPCDH1 from *X. autotrophicus* Py2 allowed for comparison studies which showed that the specific activity of *rS*-HPCDH3 and *S*-HPCDH1 are nearly identical (*1*).

Molecular Mass of rR-HPCDH1 and rS-HPCDH3, and Native State Evaluation. The *rS*-HPCDH3 was subjected to gel filtration chromatography and eluted as a single peak with an apparent molecular mass of 70.2 kDa. By comparison, native *S*-HPCDH1 and recombinant *R*-HPCDH1 eluted from the same column with apparent molecular masses of 49.6 kDa and 64.7 kDa, respectively. These results are identical to those reported previously when the proteins were analyzed using a different (Superose-12) gel filtration column (*22, 23*). It is unclear why *rS*-HPCDH3 elutes with a higher apparent molecular weight on the gel filtration column than native *S*-HPCDH1 and more similarly to how *rR*-HPCDH1 migrates. The discrepancy could be due to the likelihood that the *S*-HPCDH we purified from the native organism is a homogeneous (or nearly homogeneous) preparation of the *S*-HPCDH1 homolog, and that this protein elutes differently from that of *S*-HPCDH3. This idea is supported by the results of N-terminal sequence analysis of native *S*-HPCDH by Edman degradation, which provided the sequence MLDNEVIAIT (*22*). As shown in Figure 3-2, *S*-HPCDH1 is identical at the N-terminus to that sequence except for one amino acid (the N at position 4). In contrast, the N-terminus of *S*-HPCDH3 has the N-terminal sequence MSNRLKN before converging with *S*-HPCDH1 at EVIAIT (Figure 3-2). Clearly, the presence of three homologs of each of the HPCDH enzymes emphasizes the importance of expressing specific enzymes in a defined expression system.

Originally, both *R*- and *S*-HPCDH were proposed to be dimers based on their elution profiles on gel filtration (*16, 20*). However, the crystal structure of *rR*-HPCDH1 clearly showed a tetrameric structure (*22*), as has been reported for other members of the SDR family (*23-25*). Thus, as for many enzymes, the HPCDH homologs can migrate anonymously on gel filtration columns and we are hesitant to predict the quaternary state of *rS*-HPCDH3 based on the gel filtration results.

SDS-PAGE analysis of *rR*-HPCDH1 and *rS*-HPCDH3 mutants estimated the average purities of the enzymes used in this work to be ≥98%. All proteins migrated on a SDS-PAGE gel

as single bands with the predicted molecular masses. Results of gel filtration chromatography and CD analysis suggested that the oligomerization state of the recombinant proteins is unaffected.

Spectrophotometric Enzyme Assays. Difficulties in the heterologous expression of a soluble and an active form of *rS*-HPCDH1 resulted in cloning and purification of the *rS*-HPCDH3 homolog. Both enzymes share a high amino acid identity (78%) and high structural similarities, based on their homology models. All kinetic parameters in the reaction with *S*-HPC, 2-KPC and *R*-HPC were very similar (*1*). As revealed in Chapter 2, the *rS*-HPCDH3 and *rR*-HPCDH1 enzymes control their enantioselectivity via different mechanisms. The enantioselectivity of *rR*-HPCDH1 was shown to be dictated by changes in k_{cat}, while the enantioselectivity of *rS*-HPCDH3 was mostly controlled by changes in K_m (*1*).

Activity assays for *rS*-HPCDH3 performed with varied concentrations of NAD^+ and NADH, when HPC and 2-KPC were saturating, respectively, revealed the following kinetic parameters: K_m for NAD^+, 191 ± 21 μM; K_m for NADH, 8.42 ± 1.58 μM. The equilibrium constant (K_{eq}) determined using the Haldane relationship for a bisubstrate reaction (Eq 4) was 88.9 x 10^{-2} at 30 ºC and pH 7.5. By comparison K_{eq} determined in the same conditions for *rR*-HPCDH1 was 7.5 x 10^{-2} (*16*).

$$K_{eq} = (V^f_{max} K_{mNADH} K_{m2\text{-}KPC}) / (V^r_{max} K_{mNAD^+} K_{mS\text{-}HPC}) \qquad \text{(Eq 4)}$$

where V^f_{max} and V^r_{max} are the maximal rates for the forward and reverse reactions, respectively, when substrates are at saturating concentration.

The product inhibition studies for the oxidation of *R*-HPC by *rR*-HPCDH1 demonstrated that NADH was a competitive inhibitor for NAD^+, while 2-KPC was found to be a mixed inhibitor. This suggests that only coenzymes can productively bind to the free enzyme (*16*). The same was observed for other members of the SDR family and is believed to apply also for *rS*-HPCDH3. If that is the case, then based on the K_m values for the cofactors it appears that NADH

is a stronger inhibitor for NAD^+ in *rS*-HPCDH3, as compared to *rR*-HPCDH1. The difference in the K_m values between the two cofactors increased significantly and was 23-fold for *rS*-HPCDH3, and 12-fold for *rR*-HPCDH1. Additionally, with respect to *rS*-HPCDH3, lower K_m values for NAD^+ (457 vs. 191 μM) and NADH (37 vs. 8 μM) indicated that the formation of the binary enzyme complex might be easier in case of *rS*-HPCDH3 than for *rR*-HPCDH1.

Chiral Gas Chromatographic Assay for 2-Butanone Reduction by rR-HPCDH1 and rS-HPCDH3 in the Presence of Short-Chain Alkylsulfonates. Chiral gas chromatography was employed to analyze enantiomeric products of 2-butanone reduction. Since, short-chain alkylsulfonates were found to modulate kinetic parameters and product distribution of 2-butanone reduction in *rR*-HPCDH1 enzyme (with ethanesulfonate having the strongest effect) (*26*), this possibility was also examined for *rS*-HPCDH3. Results of 2-butanone reduction presented in Table 3-1 indicate that *rS*-HPCDH3 is highly enantioselective in oxidizing 2-butanone to (*S*)-2-butanol, exhibiting 98% enantiomeric excess (ee). Interestingly, the same reaction catalyzed by *rR*-HPCDH1 also results in an excess of (*S*)-2-butanol, however at a lower value of ee (44%). While the presence of 1 mM ethanesulfonate in the reaction mixture increases ee for *rR*-HPCDH1 to 85%, no effect on the enantioselectivity of 2-butanone reduction is observed for *rS*-HPCDH3. The enantioselectivity of *rS*-HPCDH3 remains unaffected even at higher concentrations of the alkylsulfonates (up to 5 mM) as close to 100% of (*S*)-2-butanol is produced in the reduction of 2-butanone. It was previously proposed (*26*) that binding of ethanesulfonate in the CoM binding pocket of *rR*-HPCDH1 influences both the orientation in which 2-butanone binds and the rate of the reaction. Thus, the presence of ethanesulfonate could result in the substrate binding preferentially in the orientation that leads to the formation of (*S*)-2-butanol, due to steric clashes between the bound alkylsulfonate and the ethyl side chain of 2-butanone. If the proposed mechanism holds true for *rS*-HPCDH3, one would expect the reverse preference for 2-butanone binding in the presence of ethanesulfonate, namely a change in the enantioselectivity towards the production of (*R*)-2-butanol. This would be expected especially with longer chain alkylsulfonates,

which would introduce increasing steric hindrance and in turn increasing selectivity for (*R*)-2-butanol. To test this possibility, the *rS*-HPCDH3 catalyzed reduction of 2-butanone was performed with the addition of C_1 to C_4 alkylsulfonates and with CoM (at a total concentration of 1 mM). For comparison, the same assay was carried out with *rR*-HPCDH1. As reported previously (*1*) (Table 2-6), the amount of (*S*)-2-butanol produced by *rS*-HPCDH3 remain unchanged and close to 100% of the *(S)*-enantiomer regardless of the used additive. At the same time, total concentration of 2-butanol produced in the assay decreases with the increasing carbon chain-length of the modulator molecule, and is the lowest for butanesulfonate (21% less than the control reaction without the additive). Although alkylsulfonates had no effect on modulating enantioselectivity of *rS*-HPCDH3, change in the product yield for 2-butanone reduction suggests binding of the modulator molecule at the active site of *rS*-HPCDH3. In contrast, *rR*-HPCDH1 exhibits a significant increase in the enantioselectivity in the presence of a modulator molecule, enhancing the production of *(S)*-2-butanol from 70% for the control reaction (without the additive) to 91% with 1 mM of ethanesulfonate. This was accompanied by up to 3.7-fold increase in the total amount of 2-butanol produced in the assays containing methanesulfonate or ethanesulfonate. The modulating effect of the effector molecule on the product distribution and yield of *rR*-HPCDH1 was decreasing with an increase in its chain-length. This trend was observed only for alkylsulfonates longer than ethanesulfonate. Thus, 2-butanone reduction in the presence of propanesulfonate and butanesulfonate resulted in a decreasing amount of the *(S)*-enantiomer (although still higher than without the additive) and decreasing total yield of 2-butanol. Free CoM used in the assay gave similar results to the same chain-length propanesulfonate. Structural studies of the active site of *rR*-HPCDH1 and *rS*-HPCDH3 revealed a differential spatial orientation of the positively charged residues in the CoM binding pocket. In *rS*-HPCDH3 these residues (Arg211 and Lys214) are found to occupy one side of the substrate binding pocket rather than approach the sulfonate group from both sides, as in the case of *rR*-HPCDH1 (Arg152 and Arg196). Additionally, the active site of *rR*-HPCDH1 shows a presence

Table 3-1. Additives tested for their ability to modulate enantioselectivity of *rR*-HPCDH1 and *rS*-HPCDH3 in the asymmetric reduction of 2-butanone – GC assay[a]

	rS-HPCDH3				*rR*-HPCDH1			
modifier	% (*S*)-2-butanol	% (*R*)-2-butanol	Total conc. [mM]	Change in total conc. (x-fold)	% (*S*)-2-butanol	% (*R*)-2-butanol	Total conc. [mM]	Change in total conc. (x-fold)
None	99.18 ± 0.2	0.82 ± 0.2	1.49 ± 0.2	1.00	70.21 ± 1.0	29.79 ± 1.0	1.65 ± 0.4	1.00
methanesulfonate	99.50 ± 0.5	0.50 ± 0.5	1.59 ± 0.1	1.07	90.84 ± 0.4	9.16 ± 0.4	5.32 ± 0.3	3.22
ethanesulfonate	98.03 ± 0.1	1.97 ± 0.1	1.38 ± 0.1	0.93	91.46 ± 0.1	8.54 ± 0.1	6.05 ± 0.2	3.67
propanesulfonate	99.25 ± 0.2	0.75 ± 0.2	1.41 ± 0.2	0.95	89.96 ± 0.5	10.04 ± 0.5	2.09 ± 0.3	1.27
butanesulfonate	100.0 ± 0.00	0.00 ± 0.00	1.18 ± 0.1	0.79	79.75 ± 1.0	20.25 ± 1.0	1.08 ± 0.01	0.65
CoM	100.0 ± 0.00	0.00 ± 0.00	1.32 ± 0.1	0.89	88.90 ± 0.4	11.10 ± 0.4	2.92 ± 0.1	1.77

[a]All additives were used at the overall concentration of 1mM. All assays were performed in triplicate at 30 °C using 0.64 mg *rS*-HPCDH3 or *rR*-HPCDH1, NADH (15 mM), and 2-butanone (56 mM). Assay time was 60 min. All values are given as means ± standard deviations.

Table 3-2. Enantioselectivity of 2-ketone reduction by *rS*-HPCDH3 and *rR*-HPCDH1- GC assay[a]

	rS-HPCDH3				*rR*-HPCDH1			
Substrate	% (*S*)-alcohol	% (*R*)-alcohol	Total conc. [mM]	Change in total conc. (x-fold)	% (*S*)-alcohol	% (*R*)-alcohol	Total conc. [mM]	Change in total conc. (x-fold)
2-butanone	98.80	1.20	1.49	1.00	71.94	28.06	2.13	1.00
2-pentanone	100.0	0.00	4.92	3.30	36.30	63.70	5.24	2.46
2-hexanone	100.0	0.00	2.94	1.97	37.22	62.78	14.66	6.88

[a]All substrates were used at the overall concentration of 56 mM. All assays were performed in 50 mM GPT buffer with 15% glycerol at 30°C using 0.64 mg *rS*-HPCDH3 or *rR*-HPCDH1 and NADH (15 mM). Assay time was 60 min. A single assay was performed for each of the substrates.

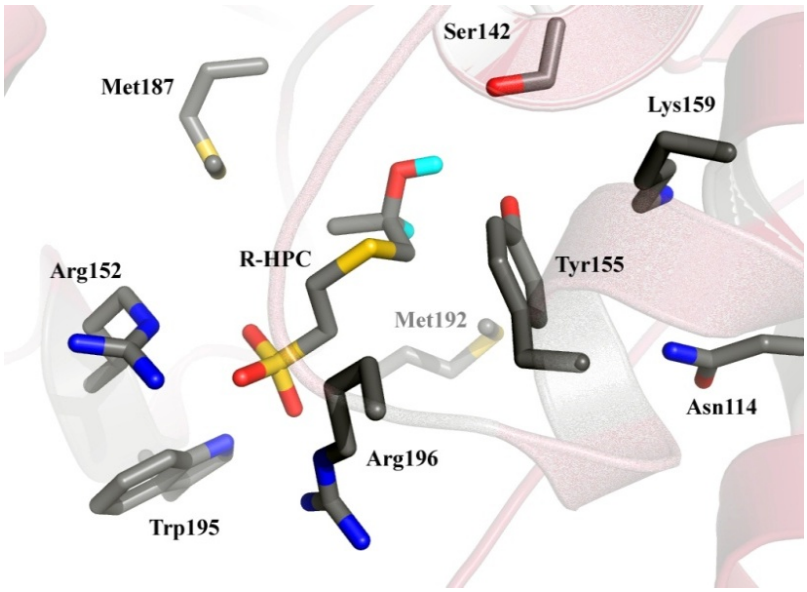

Figure 3-3. Active site of *rR*-HPCDH1 with the bound substrate *R*-HPC showing the catalytic tetrad (Asn114, Ser142, Tyr155, Lys159) and residues interacting with the sulfonate moiety of the substrate (Arg152, Arg196 and Trp195).

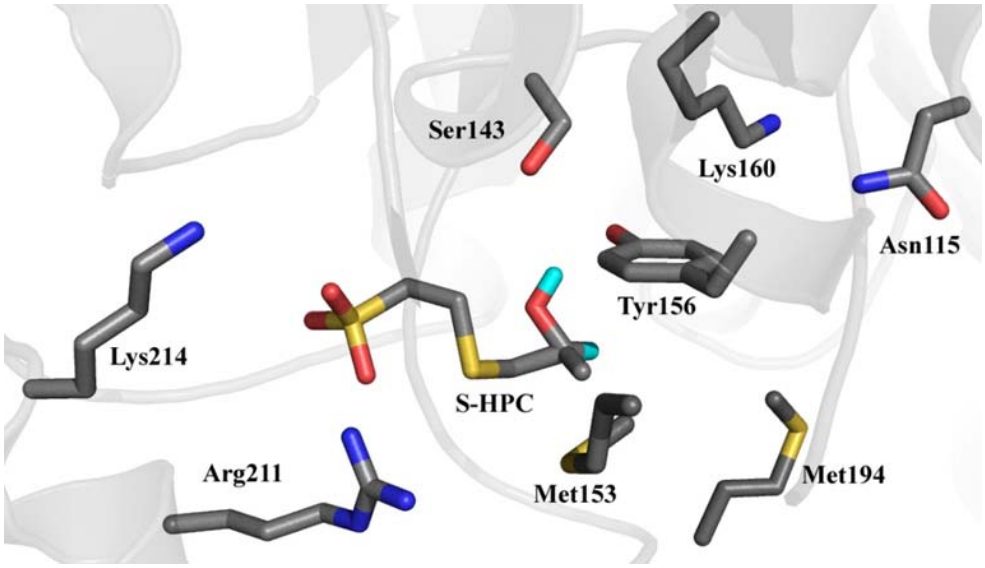

Figure 3-4. Active site of *rS*-HPCDH3 (homology model) with the bound substrate *S*-HPC, showing the catalytic tetrad (Asn115, Ser143, Tyr156, Lys160) and positively charged residues (Arg211, Lys214) proposed to coordinate the sulfonate moiety of the substrate.

of the Trp195 residue, missing in *rS*-HPCDH3, which not only serves as a back-stop to prevent the substrate from further translation, but also contributes to binding of the sulfonate group (Figure 3-3). This spatially even distribution of Arg152, Arg196 and Trp195 residues could provide a larger contact surface and thus allow *rR*-HPCDH1 to orient the substrate more precisely than is observed for *rS*-HPCDH3 (Figure 3-4). It is somewhat intriguing why such different effects of "modulating" enantioselectivity of 2-butanone reduction by alkylsulfonates are observed for *rR*-HPCDH1 and *rS*-HPCDH3. Although both enzymes are highly homologous, with many structural and mechanistic similarities, they are clearly not identical. Careful analysis of the molecular structure of *rS*-HPCDH3, once available, may aid in better understanding of this phenomena.

Chiral Gas Chromatographic Assay for 2-Penatone and 2-Hexanone Reduction by rR-HPCDH1 and rS-HPCDH3. Chiral gas chromatography studies of 2-butanone reduction were expanded to examine if the distribution of products observed for 2-butanone reduction also holds for longer chain ketones, namely 2-pentanone and 2-hexanone. As shown in Table 3-2, *rS*-HPCDH3 exhibits absolute enantioselectivity in the reduction of 2-pentanone and 2-hexanone producing only the *(S)*-enantiomer of the respective alcohols (within detection levels). In contrast, reduction of the same ketones by *rR*-HPCDH1 results in a mixture of about 36% of the *(S)*-alcohol and 64% of the *(R)*-alcohol. This is an unexpected change from the results observed for 2-butanone reduction where 72% of the produced alcohol is in form of the *(S)*-enantiomer (Table 3-2). Comparison of the total product concentration shows that both enzymes are more efficient (by at least two-fold) in reducing aliphatic ketones with longer than C_4 carbon chains (Table 3-2). An interesting observation made during the course of 2-hexanone reduction assay with *rR*-HPCDH1 is that the product distribution of resulting 2-hexanol seems to be time dependent (Table 3-3). Specifically, it was noticed that the ratio of *S/R* enantiomers is changing over time towards 1:1 ratio with a concurrent decrease in the total concentration of the products. Although the concentration of *(S)*-2-hexanol remains relatively constant, the amount of *(R)*-2-hexanol

Table 3-3. Time dependent asymmetric reduction of 2-hexanone by *rS*-HPCDH3 and *rR*-HPCDH1- GC assay[a]

Assay time [h]	peak area [units]		peak area [%]		conc. [mM]		total conc. [mM]
	(S)-2-hexanol	*(R)*-2-hexanol	*(S)*-2-hexanol	*(R)*-2-hexanol	*(S)*-2-hexanol	*(R)*-2-hexanol	2-hexanol
				rS-HPCDH3			
1	29403	ND[a]	100.00	0.00	2.94	ND[a]	2.94
2	65472	ND[a]	100.00	0.00	6.55	ND[a]	6.55
3	94885	ND[a]	100.00	0.00	9.49	ND[a]	9.49
				rR-HPCDH1			
1	54586	92054	37.22	62.78	5.46	9.21	14.66
2	54099	75593	41.71	58.29	5.41	7.56	12.97
3	51358	55191	48.20	51.80	5.14	5.52	10.65

[a]All assays were performed in 50 mM GPT buffer with 15% glycerol at 30 °C and contained 15 mM NADH, 56 mM 2-hexanone and 0.64 mg *rS*-HPCDH3 or *rR*-HPCDH1. Single point measurements were taken at various time intervals for each of the assays.

decreases by 40% within a 2h period. It is unclear what causes this change, however it appears that *(R)*-2-hexanol gets further converted to a compound other than 2-hexanone or *(S)*-2-hexanol. Interestingly enough, a similar observation was made for the reduction of 2-butanone by *rR*-HPCDH1 (unpublished data).

Aliphatic Alcohols as Substrates for rR-HPCDH1 and rS-HPCDH3. It was shown previously that electrostatic interactions between the sulfonate moiety of the substrate and the positively charged residues within the C-terminal substrate binding domain of *rR*-HPCDH1 and *rS*-HPCDH3 are major determinants of binding affinity and chiral discrimination (*1, 22, 26*). Moreover, kinetic assays with *(R)*- and *(S)*-2-butanol revealed that both enzymes are stereoselective towards *(S)*-2-butanol (*1*). Although enantioselectivity of *rR*-HPCDH1 for *(S)*-2-butanol is lower than that observed for *rS*-HPCDH3 (E = 3.0 vs. 6.2), it remains somewhat surprising that *rR*-HPCDH1 selects in favor of the *(S)*-enantiomer as a substrate, with five-fold higher k_{cat} value. To further investigate high enantioselectivity of *rS*-HPCDH3 for *(S)*-2-butanol observed in 2-butanone reduction, complementary studies were carried out in the reverse direction where *(R)*- and *(S)*-2-butanol oxidation was monitored in the presence of short-chain

alkylsulfonates (Table 3-4). First of all, specific activity of *(S)*-2-butanol oxidation by *rS*-HPCDH3 was 2.8-times higher than for *(R)*-2-butanol which confirms previously reported results of 2-butanol oxidation showing 2.6-fold ratio of *(S)*-2-butanol/*(R)*-2-butanol (*1*).

Table 3-4. Additives tested for their ability to modify kinetic parameters for *rS*-HPCDH3 catalyzed 2-butanol oxidation

Additive	*(S)*-2-butanol		*(R)*-2-butanol		
	Specific Activity (U/mg)	Activity change (x-fold)	Specific Activity (U/mg)	Activity change (x-fold)	Relative change S/R (x-fold)
none	4.92 ± 0.13	1.00	1.74 ± 0.010	1.00	2.83
methanesulfonate	4.97 ± 0.20	1.01	1.80 ± 0.013	1.04	2.76
ethanesulfonate	4.93 ± 0.15	1.00	1.87 ± 0.029	1.08	2.63
propanesulfonate	4.71 ± 0.13	0.96	1.72 ± 0.025	0.99	2.74
butanesulfonate	4.24 ± 0.085	0.86	1.62 ± 0.024	0.93	2.61
CoM	4.33 ± 0.076	0.88	1.52 ± 0.010	0.88	2.84
propionate	4.83 ± 0.022	0.98	1.75 ± 0.040	1.00	2.77

[a]All assays were performed at 30 ˚C in UV spectrophotometer with fixed concentrations of NAD^+ (10 mM). All additives were present at an overall concentration of 1 mM. All assays contained 25 μg of enzyme and 227 mM of (*R*)-2-butanol or 174 mM of (*S*)-2-butanol. All values are reported as means ± standard deviations.

Moreover, this ratio remains fairly constant regardless of the alkylsulfonate used in the assay, which corroborates well with the results of the 2-butanone reduction assay where identical additives had no effect on the stereochemical outcome of the reaction. Comparison of the results presented in Table 3-4 reveals that methanesulfonate and ethanesulfonate have no effect on the overall activity of *rS*-HPCDH3 at 1 mM concentration used in the assay. Beginning with propanesulfonate the enzyme activity decreases as the carbon chain of the "modulator" increases. The lowest value is observed for CoM for which the specific activity declines by 12% as compared to the control reaction without the additives. It is plausible that binding of the "modulator" molecule in the active site of *rS*-HPCDH3, determined by strong electrostatic interactions with its sulfonate group, affects the relatively weaker binding of the alcohol equipped with a single functional group. Thus prior binding of the alkylsulfonates with longer than C_3

carbon chain is thought to impose steric restrictions on the substrate. Interestingly, although this has no effect the overall enantioselectivity of *rS*-HPCDH3, it does change the enzyme's activity. In conclusion, these results suggest that the enantioselectivity of *rS*-HPCDH3 for *(S)*-2-butanol cannot be modulated regardless of the additive and the direction of the reaction (oxidative vs. reductive). Therefore the phenomena of modulating enantioselectivity by incorporating non-reactive molecules containing sulfonate moiety remains a unique feature limited only to *rR*-HPCDH1.

Table 3-5. Comparison of *rS*-HPCDH3 activity with *(S)*- and *(R)*-enantiomers of various chiral alcohols

	(S)-enantiomer	*(R)*-enantiomer		
Substrate	Specific Activity [U/mg]	Specific Activity [U/mg]	Activity change x-fold (S/R)	Activity difference [%]
2-butanol	3.65	1.10	3.3	232
2-pentanol	7.11	1.74	4.1	308
2-hexanol	5.11	1.16	4.4	341
2-heptanol	4.38	0.91	4.8	380
2-octanol	3.45	0.66	5.3	425

[a]All assays were performed at 30 ˚C in UV spectrophotometer with fixed concentrations of NAD^+ (10 mM). All assays contained 25 μg of enzyme. Single assays were performed for each of the substrates.

It was shown previously that *rS*-HPCDH3 is capable of oxidizing non-physiological substrates, such as short-chain secondary aliphatic alcohols (2-propanol, 2-butanol), although high concentrations of alcohols were required to give rates significantly lower than that observed for *S*-HPC (*1*). To further extend kinetic characterization of *rS*-HPCDH3 and to gain more insight into the mechanism of the enantioselectivity, the oxidation of long-chain chiral alcohols lacking the sulfonate moiety was investigated. In side by side experiments both enantiomers of each of the alcohols ranging from 2-butanol to 2-octanol were tested. As expected, *(S)*-alcohols are better substrates for *rS*-HPCDH3 with three- to five-fold higher activity than that of the corresponding *(R)*-alcohols (Table 3-5). Interestingly, the specific activity with longer chain *(S)*-alcohols (C_5 to

C_7) is greater than that with *(S)*-2-butanol, presumably due to their increasing affinity for the enzyme which in turn could aid in their better positioning for catalysis. Similar assays performed for *rR*-HPCDH1 revealed the importance of the alkyl chain-length of tested alcohols in binding affinity. Specifically, it was shown for *rR*-HPCDH1 that the K_m decreases significantly (1700-fold) when *(R)*-2-octanol is used as a substrate in place of 2-propanol *rR*-HPCDH1 (*26*). Interestingly, *rS*-HPCDH3 exhibits comparable activity for *(S)*-2-butanol and *(S)*-2-octanol, despite the 550-fold difference in the solubility (in aqueous solutions used in the assay). Furthermore, comparison of the results determined for *(R)*- and *(S)*-enantiomers of C_4 to C_8 alcohols reveals that the enantioselectivity (defined as specific activity of *(S)*-alcohol/ specific activity of *(R)*-alcohol) of *rS*-HPCDH3 towards the *(S)*-alcohol increases with an increasing chain-length of the substrates. This is a consequence of decreasing activity of *rS*-HPCDH3 with *(R)*-enantiomers and simultaneously increasing activity with *(S)*-enantiomers upon going from 2-butanol to 2-octanol. Although, the activity of *rS*-HPCDH3 towards *(R)*-alcohols lowers with each additional carbon in the substrate's chain, *(R)*-alcohols remain the relatively good substrates with activities comparable to those of the *(S)*-alcohols. This is an unexpected result given that in similar studies of *rR*-HPCDH1 the opposite enantiomers of alcohols longer than C_5 were sufficiently poor substrates that their kinetic parameters could not be determined (*26*). In case of *rS*-HPCDH3 the efficient catalysis of *(R)*-enantiomer requires its hydroxyl group and the hydrogen atom to be properly aligned with respect to NAD^+ and Tyr156. This can be accomplished when the position of the terminal methyl group and the remaining carbon chain are switched. How *rS*-HPCDH3 can accommodate up to six-carbon long aliphatic chain in a methyl binding pocket remains unknown. At this point *rS*-HPCDH3 is thought to be highly enantioselective only towards alcohols containing the sulfonate moiety and much more versatile in oxidizing enantiomeric mixtures of secondary alcohols lacking such a moiety.

Aliphatic Ketones as Substrates for rS-HPCDH3 and rR-HPCDH1. Results of the assays performed for *rS*-HPCDH3 with various aliphatic ketones, ranging from 2-butanone to 2-

hexanone, summarized in Table 3-6, confirm the trend previously observed for the aliphatic alcohols. Namely, the K_m value decreases as the alkyl chain-length increases, roughly two-fold for every additional carbon, thus suggesting again that hydrophobic interactions play an important role in binding of aliphatic ketones by *rS*-HPCDH3. Also in case of *rR*-HPCDH1 the K_m value decreases in a similar manner, however with a simultanous increase in the k_{cat} value (14-fold) upon going from 2-butanone to 2-hexanone. This increase in k_{cat} is likely due to the increasing binding affinity which in turn could result in the limited rotational motion of the substrate. Less degree of freedom could thus aid in proper alignment of the substrate for catalysis. Interestingly in case of *rS*-HPCDH3, the increase in k_{cat} is observed only in the reduction of 2-pentanone, while in the reduction of 2-hexanone the k_{cat} remains the same as in the reduction of 2-butanone. This was despite five-fold increase in affinity of 2-hexanone for the enzyme (assuming that K_m represents binding affinity of the substrate). Changes in the kinetic parameters for the reduction of 2-pentanone and 3-pentanone by *rR*-HPCDH1 and *rS*-HPCDH3 suggest that geometry of the substrate might be an important determinant of efficient catalysis. Both enzymes display about 6.5-fold higher catalytic efficiency (k_{cat}/K_m) for 2-pentanone relative to 3-pentanone. Interestingly this was accomplished differently for *rR*-HPCDH1 and *rS*-HPCDH3. While *rR*-HPCDH1 controls its specificity mostly through changes in K_m (2.3-fold increase from 2-pentanone to 3-pentanone), the specificity of *rS*-HPCDH3 is largly dictated by difference in the k_{cat} values for both substrates (five-fold decrease from 2-pentanone to 3-pentanone). It was shown previously that although a "methyl binding pocket" of *rR*-HPCDH1 can accommodate ethyl and propyl groups, their binding comes with a significant increase in the K_m values. Accordingly, similar increase in the K_m values for 3-pentanone is presumably a result of the ethyl group being forced to occupy the "methyl binding pocket" in the HPCDH active site. This in turn could cause steric hindrance and necessary misalignment of the carbonyl group of the substrate with respect to NAD^+ and the catalytic triad residues. Regardless of these differences, 3-pentanone proves to be

a better substrate than 2-butanone for *rR*-HPCDH1 (but not for *rS*-HPCDH3) with 2.4-fold specificity ratio for 3-pentanone as indicated by k_{cat}/K_m values (Table 3-6).

Table 3-6. Kinetic Parameters for *rS*-HPCDH3 – Catalyzed reduction of 2-ketones[a]

Substrate	K_m (mM)	V_{max} (units/mg)	k_{cat} (s^{-1})	k_{cat}/K_m (M^{-1} s^{-1})	Change in k_{cat} (x-fold)	Change in K_m (x-fold)
			rS-HPCDH3			
2-butanone	156.5 ± 13.8	0.14 ± 0.00	0.063	0.401	1.00	1.00
2-pentanone	62.13 ± 6.04	0.27 ± 0.01	0.123	1.981	1.95	0.40
3-pentanone	76.81 ± 8.68	0.05 ± 0.00	0.023	0.305	0.37	0.49
2-hexanone	33.69 ± 3.72	0.14 ± 0.00	0.061	1.821	0.97	0.22
			rR-HPCDH1			
2-butanone	51.9 ± 0.50	0.05 ± 0.00	0.027	0.520	1.00	1.00
2-pentanone	16.01 ± 1.68	0.25 ± 0.01	0.125	7.804	4.63	0.31
3-pentanone	47.18 ± 7.38	0.13 ± 0.00	0.058	1.229	2.15	0.91
2-hexanone	9.57 ± 0.54	0.79 ± 0.01	0.391	4.086	14.48	0.18

[a]All assays were performed in triplicates at 30 ˚C in UV spectrophotometer with fixed concentrations of NADH (0.17 mM). All assays contained 191 μg of enzyme. Apparent kinetic constants were determined by fitting experimental data to the standard form of Michaelis-Menten equation. Apparent V_{max} and K_m values are reported as means ± standard deviations. All other values are reported as means only.

Reduction of Aliphatic Ketones by rS-HPCDH3 in the Presence of Short-Chain Alkylsulfonates. As demonstrated above, short-chain alkylsulfonates were unable to modulate enantioselectivity of 2-butanone reduction catalyzed by *rS*-HPCDH3. The amount of produced *(S)*-2-butanol remained unchanged and close to 100% regardless of the used additive. It was also proposed that the steric clashes of the alkylsulfonate chain and the ethyl group of 2-butanone were responsible for the modulating effect of the 2-butanone reduction revealed by *rR*-HPCDH1. To examine the possibility of such steric effects in *rS*-HPCDH3, longer chain ketones (2-petnanone and 2-hexanone) were used in the assay along with the previously tested alkylsulfonates. For comparison purposes the reduction of 2-butanone was carried out under

identical conditions. In general, the results presented in Table 3-7 suggest that the longer the carbon chain of the sulfonate compound, the greater the effect it has on the specific activity of the enzyme in the reduction reaction. This effect is however minimal and noticeable only for longer than three carbon chain alkylsulfonates with the largest change (12%) observed for 2-pentanone reduction in the presence of butanesulfonate. As was shown in Table 3-2, *rS*-HPCDH3 is highly stereospecific in 2-ketone reduction producing exclusively *(S)*-2-alcohol as the final product. Thus it is plausible that any steric constraints introduced in the active site could only lower this stereospecificity. Since the production of *(R)*-enantiomer by *rS*-HPCDH3 would likely proceed with a lower activity (Table 3-5), any variation in the product ratio (less than 100% of *(S)*-enantiomer) should result in a decrease of the specific activity. Accordingly, if the addition of the alkylsulfonates can modulate enantioselectivity of the enzyme, as observed for *rR*-HPCDH1 then it would reflect in the values of the specific activity for the reduction of 2-ketones. Surprisingly, in the most extreme example of the reduction of 2-hexanone in the presence of 1 mM butanesulfonate or CoM, the specific activity exhibited by *rR*-HPCDH1 remains almost unchanged. It is unclear how both molecules can be simultaneously accommodated in the active site without causing additional steric restrictions. Undoubtly, crystallographic data of the *rS*-HPCDH3 structure with both molecules bound would be of great help. Nevertheless, these results provide further evidence for the unusual characteristics of *rS*-HPCDH3 which might be of special interest for the biocatalytical production of enantiopure secondary alcohols.

Inhibition Studies. It is generally accepted that the data from inhibition experiments can give a significant insight into an enzyme's kinetic mechanism. Determination of the inhibition constants for the analyzed compounds can also help to define the enzyme's active site and the relative contribution of the groups involved in substrate binding. As shown in Table 3-8, *R*-HPC was found to be an uncompetitive inhibitor of *S*-HPC oxidation catalyzed by *rS*-HPCDH3, with a

Table 3-7. Additives tested for their ability to modify kinetic parameters for *rS*-HPCDH3 catalyzed reduction of 2-ketones[a]

Additive	2-butanone		2-pentanone		2-hexanone	
	Specific Activity (U/mg)	Activity change (x-fold)	Specific Activity (U/mg)	Activity change (x-fold)	Specific Activity (U/mg)	Activity change (x-fold)
None	0.1115 ± 0.0021	1.00	0.2008 ± 0.0005	1.00	0.0975 ± 0.0008	1.00
methanesulfonate	0.1122 ± 0.0045	1.01	0.1984 ± 0.0165	0.99	0.1031 ± 0.0013	1.06
ethanesulfonate	0.1078 ± 0.0007	0.97	0.2073 ± 0.0003	1.03	0.0960 ± 0.0024	0.98
propanesulfonate	0.1019 ± 0.0062	0.91	0.1905 ± 0.0053	0.95	0.1008 ± 0.0101	1.03
butanesulfonate	0.1074 ± 0.0033	0.96	0.1777 ± 0.0081	0.88	0.0936 ± 0.0003	0.96
CoM	0.1068 ± 0.0010	0.96	0.1829 ± 0.0053	0.91	0.0925 ± 0.0042	0.95

[a]All assays were performed at 30 ˚C in UV spectrophotometer with fixed concentrations of NADH (0.17 mM). All additives were present at an overall concentration of 1 mM. All assays contained 191 μg of enzyme and the following concentrations of the substrate: 558 μM of 2-butanone; 225 mM of 2-pentanone and 122 mM of 2-hexanone. All values are reported as means ± standard deviations.

Table 3-8. Inhibition studies of *rS*-HPCDH3 and *rR*-HPCDH1-catalyzed oxidation of *S*-HPC and *R*-HPC, respectively[a]

inhibitor	*rS*-HPCDH3 with *S*-HPC			*rR*-HPCDH1 with *R*-HPC		
	Type of inhibition	K_{is} [μM]	K_{ii} [μM]	Type of inhibition	K_{is} [μM]	K_{ii} [μM]
R-HPC	Uncompetitive	NA[b]	13490 ± 1784	NA[b]	NA[b]	NA[b]
S-HPC	NA[b]	NA[b]	NA[b]	Competitive[c]	156 ± 7	NA[b]
methanesulfonate	Mixed	222300 ± 23610	830000 ± 91280	Mixed[c]	147800 ± 2600	122700 ± 5100
ethanesulfonate	Uncompetitive	NA[b]	180308 ± 10257	Mixed[c]	26700 ± 800	38900 ± 2300
propanesulfonate	Uncompetitive	NA[b]	11020 ± 640.8	Mixed	3131 ± 578	2981 ± 255
butanesulfonate	Uncompetitive	NA[b]	1264 ± 54.68	Mixed	264.8 ± 26.96	1685 ± 251
CoM	Mixed	1319 ± 204.70	1369 ± 101.30	Mixed[c]	2250 ± 130	3620 ± 170
BES	Uncompetitive	NA[b]	656 ± 33.66	Mixed[d]	1710 ± 280	2300 ± 200
Na_2SO_4	ND[e]	ND[e]	ND[e]	ND[ce]	ND[ce]	ND[ce]

[a]Abbreviations: BES, bromoethanesulfonate; All assays were performed at 30 °C, pH 7.5, with variable concentrations of *S*-HPC or *R*-HPC, 0.64 mg *rS*-HPCDH3 or *rR*-HPCDH1 and 10 mM NAD^+. All values are given as means ± standard deviations. [b]NA – not applicable. [c]Determined by Clark et al. (*16*). [d]Determined by Boyd, J.M. (*29*) [e]ND – not detected; Na_2SO_4 did not exhibit inhibitory effects at concentrations up to 300 mM.

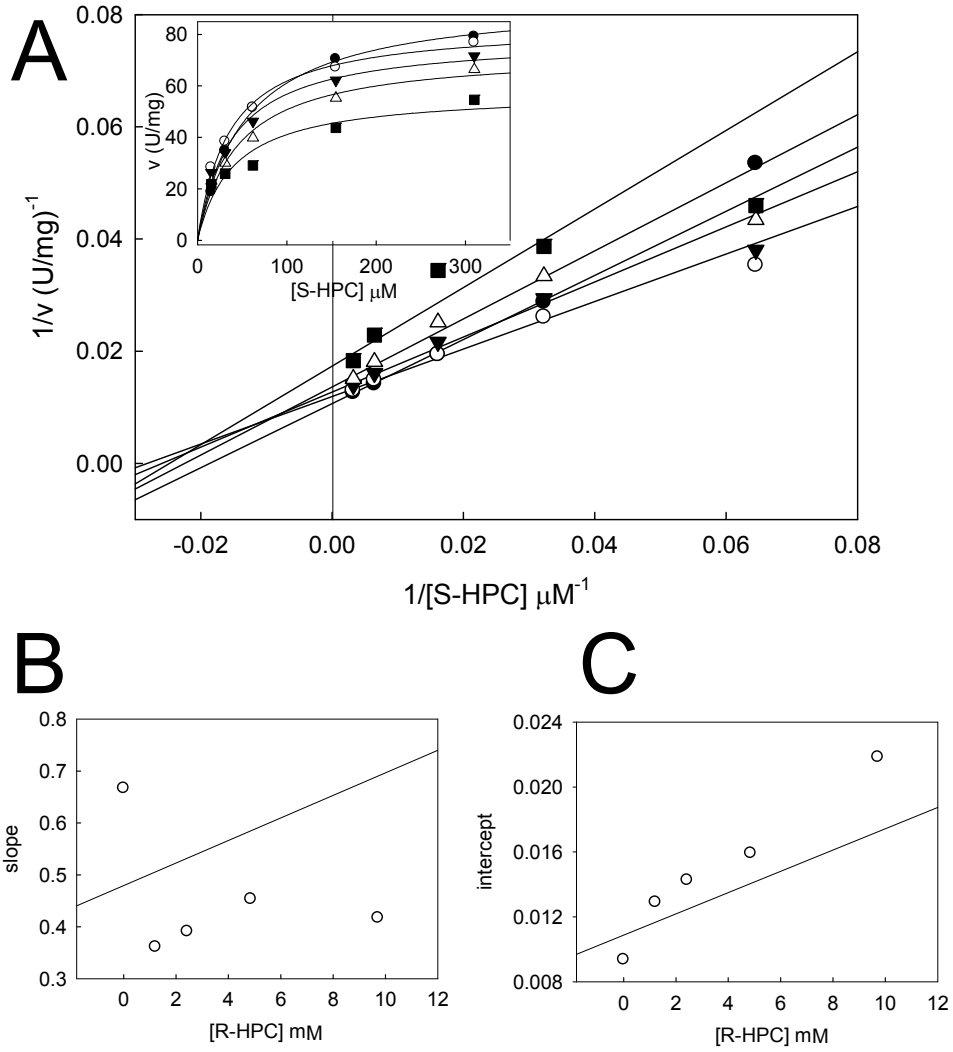

Figure 3-5. Effect of *R*-HPC on *rS*-HPCDH3 catalyzed oxidation of *S*-HPC at pH 7.5. (A) 1/*v* as a function of the inverse *S*-HPC concentration determined at several fixed concentrations of *R*-HPC: (●) 0 mM, (○) 1.2 mM, (▼) 2.4 mM, (Δ) 4.9 mM, (■) 9.7 mM. (B, C) Secondary plots of (A) illustrate data quality and fit to equation 1. (B) Slopes from plot A as a function of the *R*-HPC concentration. (C) Intercepts from plot A as a function of the *R*-HPC concentration. Data points represent the average of triplicate experiments. Shown in the inset is the nonlinear least-square fit of the *v* vs. S data to the equation for a rectangular hyperbola using SigmaPlot. In all cases lines represent theoretical data generated from experimental values by SigmaPlot.

K_{ii} value (13490 ± 1784 μM) 435-times higher than the K_m for *S*-HPC (31 ± 0.9 μM) but close to the K_m for *R*-HPC (9100 ± 1100 μM) (*1*). Because the fit of the initial rate data in a double reciprocal form (shown in Figure 3-5) does not reveal a typical pattern for uncompetitive

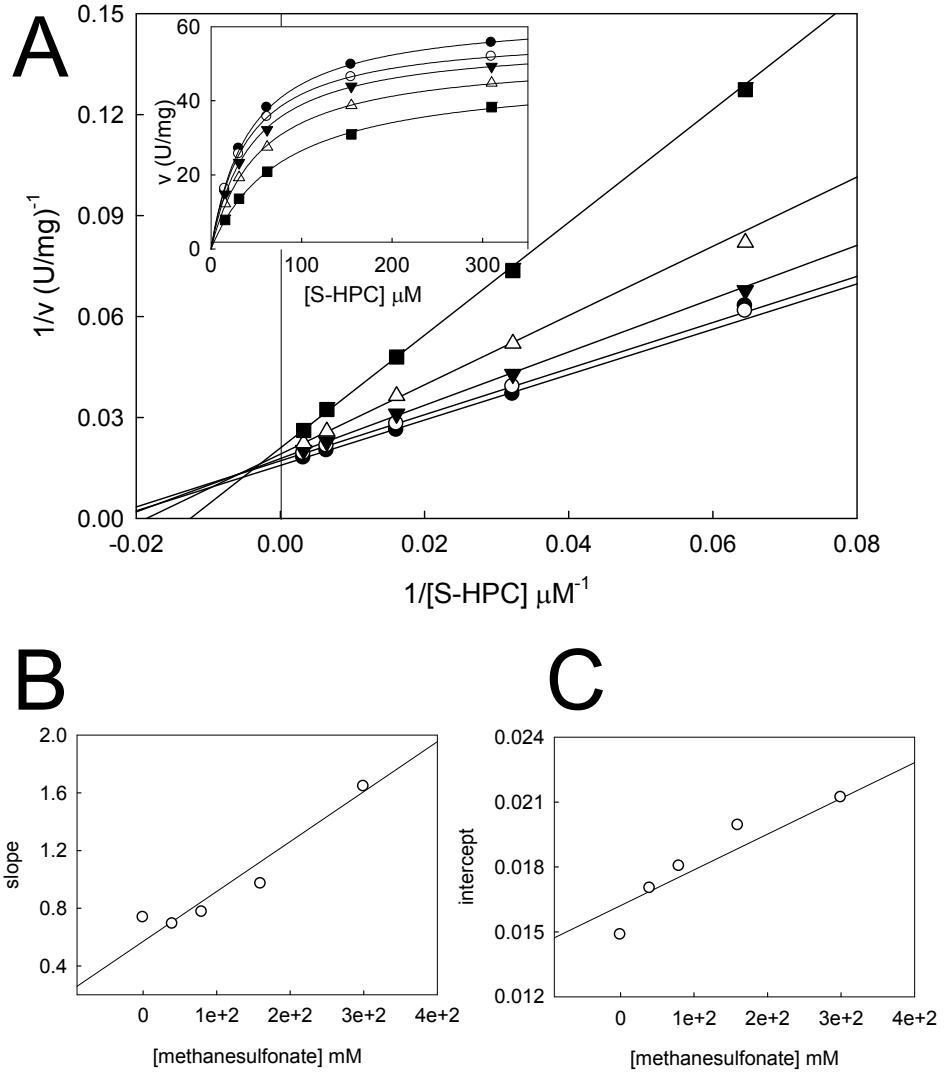

Figure 3-6. Effect of methanesulfonate on *rS*-HPCDH3 catalyzed oxidation of *S*-HPC at pH 7.5. (A) 1/*v* as a function of the inverse *S*-HPC concentration determined at several fixed concentrations of methanesulfonate: (●) 0 mM, (○) 40 mM, (▼) 80 mM, (Δ) 160 mM, (■) 300 mM. (B, C) Secondary plots of (A) illustrate data quality and fit to equation 1. (B) Slopes from plot A as a function of the methanesulfonate concentration. (C) Intercepts from plot A as a function of the methanesulfonate concentration. Data points represent the average of triplicate experiments. The inset represents the nonlinear least-square fit of the *v* vs. S data to the equation for a rectangular hyperbola using SigmaPlot. In all cases lines represent theoretical data generated from experimental values by SigmaPlot.

inhibition, other models were also considered. The only reasonable alternative fit was observed for competitive inhibition, although the determined value of K_{is} carried a significantly larger error

(5155 ± 1424 μM). It should be noted here that *R*-HPC is also a substrate for *rS*-HPCDH3 (typified by 290-fold higher K_m and 4.5-fold lower k_{cat} than those of *S*-HPC) and as such cannot be considered as a "true" inhibitor. Therefore, any conclusions drawn from this study should be as a substrate (400-times lower k_{cat} than that of *R*-HPC). As determined previously, *S*-HPC is a strong competitive inhibitor with a K_{is} value close to the K_m for *R*-HPC (105 ± 2 μM) (*16*). With regard to alkylsulfonates, methanesulfonate was found to be a mixed inhibitor of *S*-HPC oxidation catalyzed by *rS*-HPCDH3 which agrees with the pattern observed in Figure 3-6.

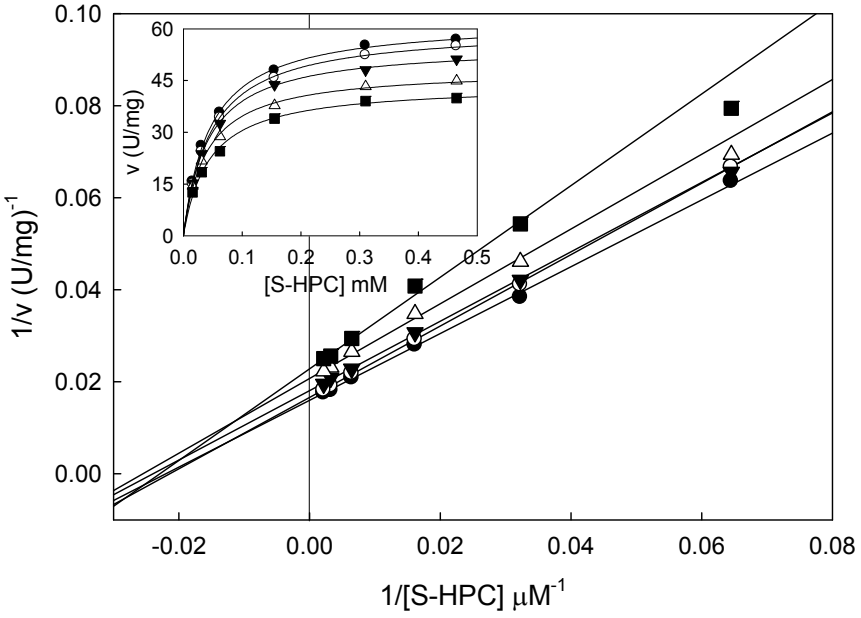

Figure 3-7. Effect of ethanesulfonate on *rS*-HPCDH3 catalyzed oxidation of *S*-HPC at pH 7.5. (A) 1/*v* as a function of the inverse *S*-HPC concentration determined at several fixed concentrations of ethanesulfonate: (●) 0 mM, (○) 10 mM, (▼) 20 mM, (Δ) 50 mM, (■) 100 mM. The inset represents the nonlinear least-square fit of the *v* vs. S data to the equation for a rectangular hyperbola using SigmaPlot. In all cases lines represent theoretical data generated from experimental values by SigmaPlot.

An ambiguous situation is observed for ethanesulfonate as the double reciprocal plot of the inhibition assay does not reveal any distinct pattern, but rather resembles a combination of multiple inhibition models (Figure 3-7). Calculations performed in SigmaPlot 11.0 show the best fit of the experimental data to the uncompetitive model with 18% standard deviation on the determined value of K_{ii}, followed by the competitive model with 37% error for calculated value of $K_{is.}$ Mixed inhibition, somewhat suggested by the graphical representation of the experimental data, was typified by 7% and 27% error of K_{is} and K_{ii} value, respectively. Propanesulfonate is an

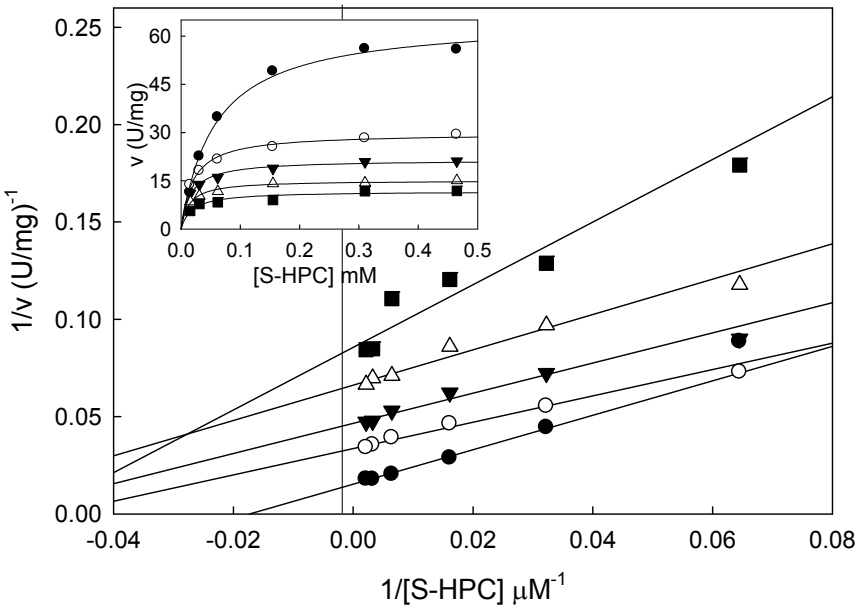

Figure 3-8. Effect of propanesulfonate on *rS*-HPCDH3 catalyzed oxidation of *S*-HPC at pH 7.5. (A) 1/*v* as a function of the inverse *S*-HPC concentration determined at several fixed concentrations of propanesulfonate: (●) 0 mM, (○) 10 mM, (▼) 20 mM, (Δ) 40 mM, (■) 80 mM. The inset represents the nonlinear least-square fit of the *v* vs. S data to the equation for a rectangular hyperbola using SigmaPlot. In all cases lines represent theoretical data generated from experimental values by SigmaPlot.

uncompetitive inhibitor with respect to *S*-HPC as determined by fitting the experimental data to the equation 2. This result agrees with the graphical pattern displayed on the double reciprocal

plot (Figure 3-8). Likewise, butanesulfonate is an uncompetitive inhibitor of *S*-HPC oxidation by *rS*-HPCDH3 showing the appropriate line pattern, although somewhat distorted as the slope values are not identical (Figure 3-9). In contrast, propanesulfonate and butanesulfonate were found to be mixed inhibitors of *R*-HPC oxidation by *rR*-HPCDH1 showing a very clear and characteristic pattern typically observed for this type of inhibition (Figure 3-11 and 3-12). Also CoM is a mixed inhibitor with values comparable to the inhibition constants determined for both enzymes (Table 3-8 and Figure 3-10). Comparison of the K_{ii} values shown in Table 3-8 reveals

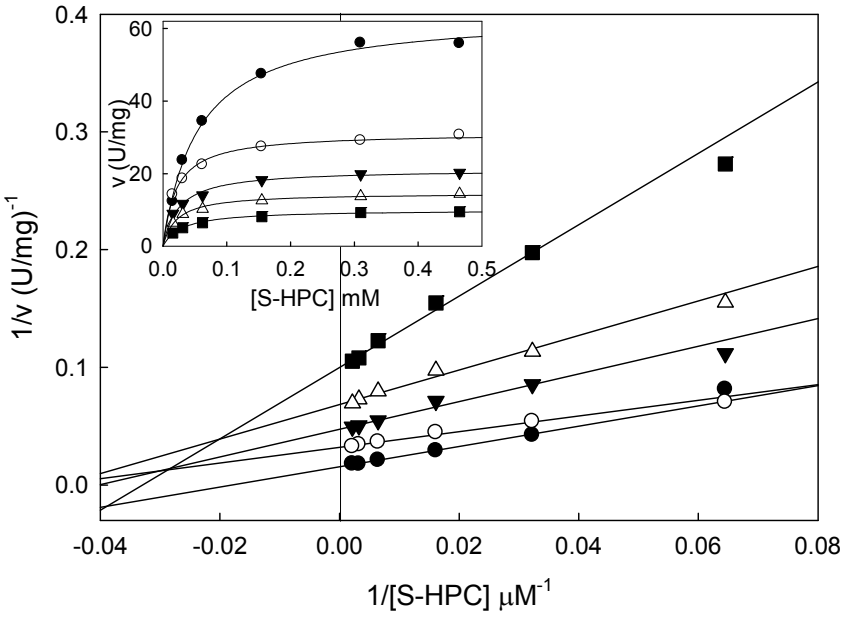

Figure 3-9. Effect of butanesulfonate on *rS*-HPCDH3 catalyzed oxidation of *S*-HPC at pH 7.5. (A) 1/*v* as a function of the inverse *S*-HPC concentration determined at several fixed concentrations of butanesulfonate: (●) 0 mM, (○) 1.25 mM, (▼) 2.5 mM, (Δ) 5.0 mM, (■) 10 mM. The inset represents the nonlinear least-square fit of the *v* vs. S data to the equation for a rectangular hyperbola using SigmaPlot. In all cases lines represent theoretical data generated from experimental values by SigmaPlot.

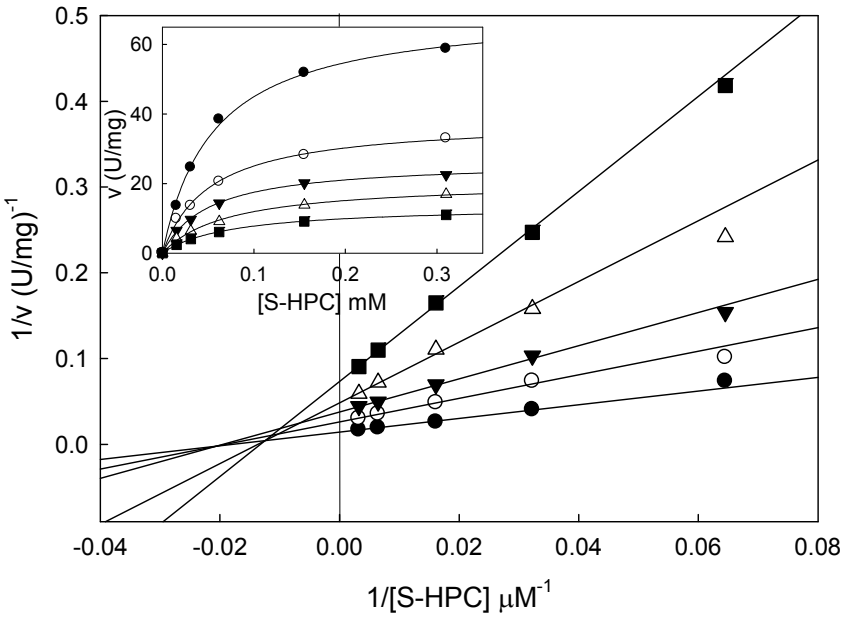

Figure 3-10. Effect of CoM (mercaptoethanesulfonate) on *rS*-HPCDH3 catalyzed oxidation of *S*-HPC at pH 7.5. (A) 1/*v* as a function of the inverse *S*-HPC concentration determined at several fixed concentrations of CoM: (●) 0 mM, (○) 1.0 mM, (▼) 2.0 mM, (Δ) 4.0 mM, (■) 8.0 mM. Data points represent the average of triplicate experiments. The inset represents the nonlinear least-square fit of the *v* vs. S data to the equation for a rectangular hyperbola using SigmaPlot. In all cases lines represent theoretical data generated from experimental values by SigmaPlot.

that the addition of a single methyl group to methanesulfonate increases its binding affinity to *rS*-HPCDH3 by five-fold. Similarly, the addition of a methyl group to ethanesulfonate increases its binding affinity by 16-fold, while the addition of the ethyl group to ethanesulfonate results in a more significant increase (143-fold). Together, these results suggest that the length of the substrate carbon chain is an important determinant in the recognition by *rS*-HPCDH3. Although a similar trend is observed for *rR*-HPCDH1, where the K_{ii} value decreases upon going from methanesulfonate to butanesulfonate by 73-fold, this change is not as pronounced as for *rS*-

HPCDH3 where the corresponding K_{ii} values decrease by 657-fold. Moreover, it appears that the addition of a thiol group to ethanesulfonate also increases recognition by *rR*-HPCDH1 and *rS*-HPCDH3 as the K_{ii} values for CoM (2-mercaptoethanesulfonate) decrease by 11- and 132-fold, respectively. This contribution, however, is difficult to extrapolate to any added affinity afforded by the *S*- or *R*-HPC thioether, because of the possibility that CoM is binding directly with the deprotonated Tyr residue of the catalytic triad through the thiol. In an attempt to estimate the binding contribution of the sulfonate group alone, sodium sulfonate was used in the assay, however no inhibitory effect was detected at concentrations up to 300 mM. Comparison of the

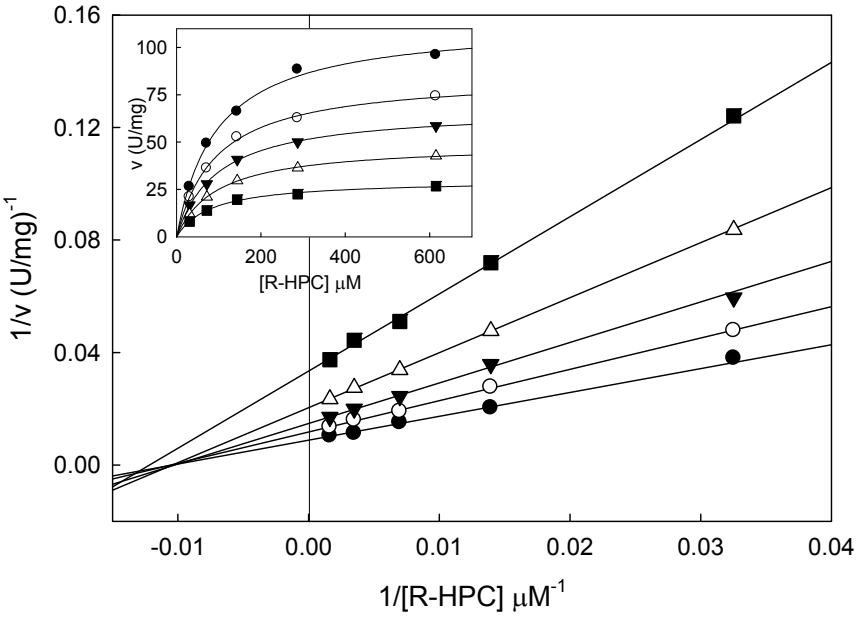

Figure 3-11. Effect of propanesulfonate on *R*-HPC oxidation by *rR*-HPCDH1. The double reciprocal plot illustrating mixed inhibition is shown in the main diagram. The solid lines were generated by nonlinear least-square fits of the *v* vs. S data (shown in the *inset*) to the equation for a rectangular hyperbola using SigmaPlot. The assay of *R*-HPC oxidation was performed in the presence of different concentrations of propanesulfonate: (●) 0 mM, (○) 1.0 mM, (▼) 2.0 mM, (Δ) 4.0 mM, (■) 8.0 mM.

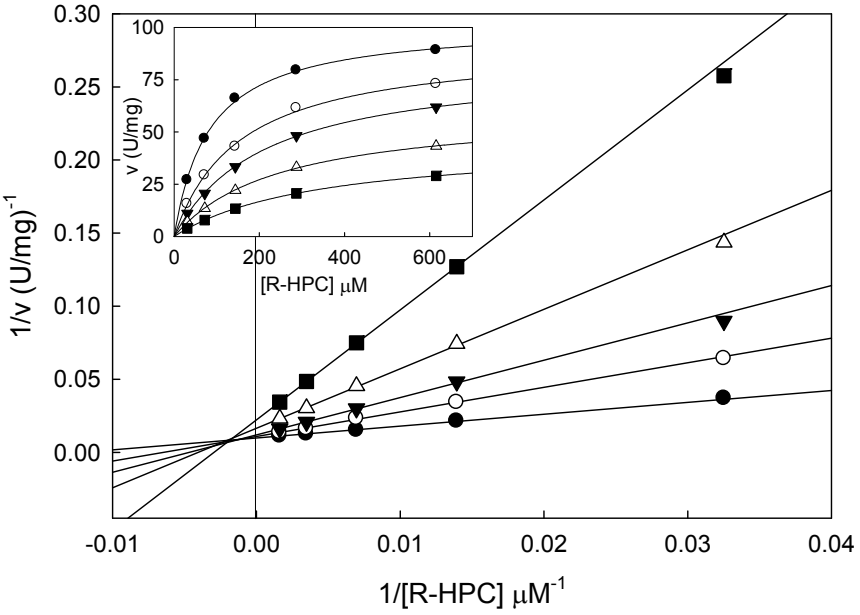

Figure 3-12. Effect of butanesulfonate on *R*-HPC oxidation by *rR*-HPCDH1. The double reciprocal plot illustrating mixed inhibition is shown in the main diagram. The solid lines were generated by nonlinear least-square fits of the *v* vs. S data (shown in the *inset*) to the equation for a rectangular hyperbola using SigmaPlot. The assay of *R*-HPC oxidation was performed in the presence of different concentrations of butanesulfonate: (●) 0 mM, (○) 0.25 mM, (▼) 0.50 mM, (Δ) 1.0 mM, (■) 2.0 mM.

results summarized in Table 3-8 and the double reciprocal plots for different carbon chain-length alkylsulfonates reveals a trend for *rS*-HPCDH3 enzyme, where the type of inhibition "transitions smoothly" from a mixed inhibition determined for methanesulfonate through an uncompetitive inhibition and back to the mixed inhibition for CoM. Note that the best fit of the experimental data for an uncompetitive model is observed for propanesulfonate, while both ethanesulfonate and butanesulfonate show an uncompetitive fit with traits of a mixed inhibition. Interestingly, all alkylsulfonates (but not *S*-HPC) were found to be mixed inhibitors for *R*-HPC oxidation by *rR*-HPCDH1, which indicates that they can bind to multiple forms of the enzyme. Conversely, uncompetitive inhibitors (ethanesulfonate, propanesulfonate and butanesulfonate with respect to

S-HPC oxidation by *rS*-HPCDH3) can only bind to the enzyme•subtrate binary complex and affect the V_{max} of the reaction rather than the substrate's K_m. In summary, if these inhibitors bind in a manner similar to that of the mercaptoethanesulfonate (CoM) portion of the substrate (*R*-HPC or *S*-HPC), then these results provide an insight to the binding contribution of the substrate's CoM moiety methylenes.

Effect of 2-Bromoethanesulfonate on rS-HPCDH3. Bromoethanesulfonate (BES), a structural analog of CoM, is a well known inhibitor of methanogenesis (*28*) and bacterial growth on propylene and propylene oxide (*27*). Both BES and CoM contain a sulfonate moiety which has proven to be a powerful binding determinate in all four epoxide carboxylase enzymes (*1, 16, 22, 29, 30*). The electrophilic bromine moiety of BES also makes it a potent alkylating agent or affinity label. Therefore, BES has been shown to affect the activity of two out of the four enzymes involved in epoxide metabolism, namely *rR*-HPCDH1 and 2-KPCC (*27*). Both enzymes were non-competitively inhibited by BES with respect to their sulfonate containing substrates. In addition to being a rapid equilibrium non-competitive (mixed) inhibitor, BES was demonstrated to be a reversible inhibitor of *rR*-HPCDH1 and an irreversible inactivator of 2-KPCC (*31*). As demonstrated previously, BES is not an inhibitor of the first enzyme in epoxypropane metabolism, epoxyalkane:CoM transferase (EaCoMT) (*31*). This study examines the inhibitory effect of BES on *rS*-HPCDH3, thereby complementing the previous studies and completing the picture of the overall effect of BES on all enzymes involved in CoM-dependent bacterial epoxide carboxylation. To determine which type of inhibition occurs, the rate of *S*-HPC oxidation was measured at different concentrations of BES. The experimental data was fit to equations 1 – 3, and double reciprocal plots were constructed (Figure 3-13). The results presented in Table 3-8 indicate that BES is an uncompetitive inhibitor with respect to *S*-HPC with the K_{ii} value of 656 ± 33.7 μM. The line pattern observed in Figure 3-13 is consistent with this type of inhibition. The parallel lines with an identical slope are observed for all different concentrations of BES examined in the assay with an exception of the line representing 3 mM BES. Even when this line

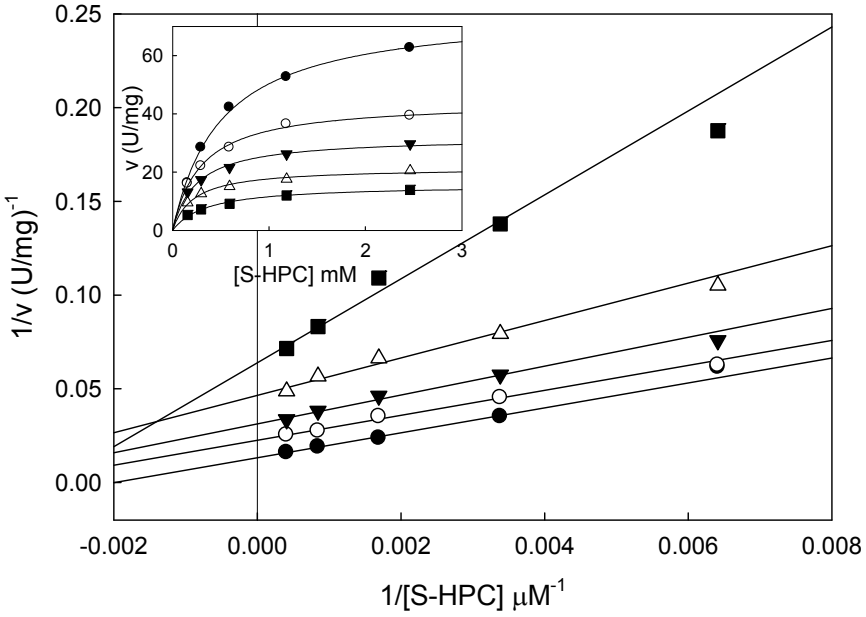

Figure 3-13. Effect of BES (bromoethanesulfonate) on *rS*-HPCDH3 catalyzed oxidation of *S*-HPC at pH 7.5. (A) 1/*v* as a function of the inverse *S*-HPC concentration determined at several fixed concentrations of BES: (●) 0 mM, (○) 0.5 mM, (▼) 1.0 mM, (Δ) 1.5 mM, (■) 3.0 mM. Data points represent the average of duplicate experiments. The inset represents the nonlinear least-square fit of the *v* vs. S data to the equation for a rectangular hyperbola using SigmaPlot. In all cases lines represent theoretical data generated from experimental values by SigmaPlot.

is excluded from the calculations of the theoretical values (using Eq 1) the determined value of K_{ii} remains very similar (693.4 ± 26.1 μM). By way of comparison, the BES inhibition assay of *R*-HPC oxidation by *rR*-HPCDH1 revealed non-competitive (mixed) inhibition suggesting that BES can bind to any form of the enzyme thus altering its activity. Furthermore, the inhibition constants (K_{ii} and K_{is}) determined for *rR*-HPCDH1 were significantly higher than that of *rS*-HPCDH3. The 3.5-fold difference in the K_{ii} value indicates that BES has a greater inhibitory effect on *S*-HPC oxidation carried out by *rS*-HPCDH3. Because of the close similarities between BES and CoM, it is not surprising that both the HPCDH enzymes are inhibited by its presence. However, since HPC substrates also contain the sulfonate moiety it was thought that inhibition of BES and CoM would be competitive. As shown in Table 3-8, this is not the case for either of the enzymes. The

rR-HPCDH1 exhibited mixed inhibition with both BES and CoM showing similar values of the inhibition constants, whereas *rS*-HPCDH3 revealed uncompetitive and mixed inhibition, respectively, with significantly different K_{ii} values. Considering the latter, it is intriguing why such different mechanisms of *rS*-HPCDH3 inhibition are observed for the two similar molecules and why the HPCDH enzymes exhibit such different inhibitory effects in the presence of the same set of alkylsulfonate compounds.

Summary and Concluding Remarks. Although biocatalysis holds a tremendous potential particularly for the pharmaceutical and agriculture industry, it has not been spared from its own weaknesses. One of them is the lack of enantiocomplementary enzymes to produce a desired enantiomer in an asymmetric synthesis. There are however examples of naturally occurring enantioselective enzymes catalyzing the same reaction in a common pathway but with opposite stereospecificity. One obvious evolutionary advantage of this approach is the ability to use both enantiomers as a carbon and energy source, and prevent wasteful, and in case of toxic compounds dangerous, accumulation of the other enantiomer. Epoxide carboxylation pathway of *X. autotrophicus* Py2 is one of very few examples where a pair of enantioselective enzymes is found to be integrated in the same pathway allowing the organism to individually metabolize both enantiomeric forms of epoxypropane. Moreover, since *R*-HPCDH and *S*-HPCDH represent one of only two known pairs of the SDR enzymes, they can be considered as an excellent model for studying enantioselectivity within the SDR family. The results presented in this chapter can aid in a better understanding of the mechanism underlying the high degree of chiral discrimination observed for *R*- and *S*-HPCDH.

The results of the chiral gas chromatography assay for 2-butanone reduction confirmed the previous results (*26*), showing again that the enantioselectivity and the product yield of *rR*-HPCDH1 can be significantly enhanced by the presence of short-chain alkylsulfonates in the assay reaction. This is a novel and unprecedented phenomenon in the biocatalytic production of chiral alcohols. In contrast, the modulating effect of the alkylsulfonates was abolished for 2-

butanone reduction catalyzed by *rS*-HPCDH3, as the enzyme revealed nearly absolute enantioselectivity towards *(S)*-2-butanol (ee 98 %) regardless of the additive used. A similar observation was made for the reduction of higher ketones, namely 2-penatnone and 2-hexanone. Moreover, results presented in Table 3-3 show that the reduction of 2-hexanone to 100% of *(S)*-2-hexanol is consistent throughout the time of the assay and not affected by the increasing concentrations of the product. This appears as an important and valuable feature of a good biocatalyst, not exhibited by *rR*-HPCDH1. The results of the oxidation of *(R)*- and *(S)*-2-butanol show that the enantioselectivity of *rS*-HPCDH3 cannot be modulated regardless of the additive used and the direction of the reaction (oxidative vs. reductive). Thus the phenomena of modulating enantioselectivity of *rR*-HPCDH1 by incorporating non-reactive molecules containing CoM moiety remains a unique feature limited only to *rR*-HPCDH1.

The assay with the long-chain aliphatic alcohols (C_4-C_8) revealed that *rS*-HPCDH3 is capable of oxidizing both *(R)*- and *(S)*-enantiomers of tested alcohols, which is not observed for *rR*-HPCDH1. Additionally, these results demonstrate that chirality of the alcohol is not a sufficient determinant of the high degree of enantioselectivity displayed by *rS*-HPCDH3, and to some extent by *rR*-HPCDH1. Clearly, there is a requirement for the sulfonate moiety on the substrate which provides a strong binding affinity and more importantly serves as a useful handle in orienting the substrate for hydride abstraction. This is consistent with a 1000-fold increase in the K_m value and an over 100-fold decrease in the enantioselectivity value (*E*) for *(R)*- and *(S)*-2-butanol, as compared to the corresponding natural substrates (*R*-HPC, *S*-HPC). Lack of negatively charged groups on 2-butanol allows it to assume one of two possible orientations with either a methyl or an ethyl group residing in a "methyl binding pocket", thus leading to poor enantioselectivity. Results of the kinetic assays performed for *rS*-HPCDH3 with various aliphatic alcohols and ketones showed that substrate affinity increases with the increasing chain-length of the substrate. This could suggest that hydrophobic interactions play an important role in substrate binding for both HPCDH enzymes. The position of the carbonyl group on the substrate is also of

some importance, given that 2-pentanone was demonstrated to be a better substrate than 3-pentanone for both enzymes. Results of activity assays of the aliphatic ketone reduction catalyzed by *rS*-HPCDH3 and *rR*-HPCDH1 (Table 3-8) indicated that both enzymes were up to 230-fold more active in the oxidation of 2-butanol than in the reduction of 2-butanone. This is in agreement with the corresponding reactions of HPC oxidation and 2-KPC reduction, where k_{cat}/K_m values were lower for the reduction reaction catalyzed by *rS*-HPCDH3 and *rR*-HPCDH1 (*1*). The K_m value exhibited by *rS*-HPCDH3 for the reduction of 2-butanone was two- to six-times higher than the K_m values for 2-butanol, suggesting that the hybridization state (planar sp^2 vs. tetrahedral sp^3) of the substrate can have an effect on its binding affinity for the enzyme. In contrast, *rR*-HPCDH1 showed an opposite correlation, where K_m value for 2-butanol was four- to seven-fold higher, as compared to 2-butanone. Inhibitors were investigated as probes of the molecular features of *R*- and *S*-HPC that contribute to substrate binding. Ethanesulfonate, propanesulfonate and butanesulfonate were found to be uncompetitive inhibitors of *S*-HPC oxidation by *rS*-HPCDH3 suggesting that they can only bind to the enzyme•subtrate binary complex and affect the V_{max} of the reaction rather than the substrate's K_m. Methanesulfonate and CoM were mixed inhibitors with respect to *S*-HPC, the result similar to that determined for the oxidation of *R*-HPC by *rR*-HPCDH1. Mixed inhibition was also observed for propanesulfonate and butanesulfonate in the oxidation of *R*-HPC by *rR*-HPCDH1, thus showing that all short-chain alkylsulfonates are mixed inhibitors with respect to *R*-HPC and can bind to any form of the enzyme. Together, these results provide an insight to the binding contribution of the mercaptoethanesulfonate methylenes of the substrates and suggest that the length of the substrate carbon chain is an important determinant in recognition by the HPCDH enzymes (more for *rS*-HPCDH3 than for *rR*-HPCDH1). Finally, the effect of BES on the oxidation of *S*-HPC by *rS*-HPCDH3 was examined completing the picture of the overall effect of BES on all enzymes involved in CoM-dependent bacterial epoxide carboxylation. BES was found to be an

uncompetitive inhibitor with respect to *S*-HPC. The determined values of the inhibition constants suggest that BES has a greater inhibitory effect on *rS*-HPCDH3 than on *rR*-HPCDH1.

Although both enzymes share a high degree of structural homology and are highly stereoselective for their respective substrates, they differ in many aspects. The most significant differences are observed in the inhibition studies and in the reaction with the non-physiological substrates (aliphatic alcohols and ketones lacking the CoM moiety). Most importantly, they employ different mechanisms of controlling their enantioselectivity. Although both enzymes are highly enantioselective and hold high potential for the biocatalytic production of optically pure alcohols, the *rS*-HPCDH3 is especially noteworthy for its near absolute stereospecificity towards *(S)*-alcohols.

REFERENCES

1. Sliwa, D. A., Krishnakumar, A. M., Peters, J. W., and Ensign, S. A. (2010) Molecular basis for enantioselectivity in the (R)- and (S)-hydroxypropylthioethanesulfonate dehydrogenases, a unique pair of stereoselective short-chain dehydrogenases/reductases involved in aliphatic epoxide carboxylation. *Biochemistry 49*, 3487-3498.

2. Goldberg, K., Schroer, K., Lütz, S., and Liese, A. (2007) Biocatalytic ketone reduction—a powerful tool for the production of chiral alcohols—part I: processes with isolated enzymes. *Appl. Microbiol. Biotechnol. 76*, 237-248.

3. Cherry, J. R., and Fidantsef, A. L. (2003) Directed evolution of industrial enzymes: an update. *Curr. Opin. Biotechnol. 14*, 438-443.

4. Rubin-Pitel, S. B., and Zhao, H. (2006) Recent advances in biocatalysis by directed enzyme evolution. *Comb. Chem. High T. Scr. 9*, 247-257.

5. Nakamura, K., Yamanaka, R., Matsuda, T., and Harada, T. (2003) Recent developments in asymmetric reduction of ketones with biocatalysts. *Tetrahedron: Asymmetry 14*, 2659-2681.

6. Keinan, E., Hafeli, E. K., Seth, K. K., and Lamed, R. (1986) Thermostable enzymes in organic synthesis. 2. Asymmetric reduction of ketones with alcohol dehydrogenase from *Thermoanaerobium brockii*. *J. Am. Chem. Soc. 108*, 162-169.

7. Ensign, S. A. (2001) Microbial metabolism of aliphatic alkenes. *Biochemistry 40*, 5845-5853.

8. Allen, J. R., and Ensign, S. A. (1999) Two short-chain dehydrogenases confer stereoselectivity for enantiomers of epoxypropane in the multiprotein epoxide

carboxylating systems of *Xanthobacter* strain Py2 and *Nocardia corallina* B276. *Biochemistry 38*, 247-256.

9. Krishnakumar, A. M., Sliwa, D., Endrizzi, J. A., Boyd, E. S., Ensign, S. A., and Peters, J. W. (2008) Getting a Handle on the Role of Coenzyme M in Alkene Metabolism. *Microbiol. Mol. Biol. Rev. 72*, 445.

10. Joernvall, H., Persson, B., Krook, M., Atrian, S., Gonzalez-Duarte, R., Jeffery, J., and Ghosh, D. (1995) Short-chain dehydrogenases/reductases (SDR). *Biochemistry 34*, 6003-6013.

11. Kallberg, Y., Oppermann, U., Jornvall, H., and Persson, B. (2002) Short-chain dehydrogenases/reductases (SDRs): Coenzyme-based functional assignments in completed genomes. *Eur. J. Biochem. 269*, 4409.

12. Oppermann, U., Filling, C., Hult, M., Shafqat, N., Wu, X., Lindh, M., Shafqat, J., Nordling, E., Kallberg, Y., and Persson, B. (2003) Short-chain dehydrogenases/reductases (SDR): the 2002 update. *Chem. Biol. Interact. 143*, 247-253.

13. Persson, B., Kallberg, Y., Bray, J. E., Bruford, E., Dellaporta, S. L., Favia, A. D., Duarte, R. G., Jörnvall, H., Kavanagh, K. L., and Kedishvili, N. (2009) The SDR (short-chain dehydrogenase/reductase and related enzymes) nomenclature initiative. *Chem. Biol. Interact. 178*, 94-98.

14. Nakajima, K., Hashimoto, T., and Yamada, Y. (1993) Two tropinone reductases with different stereospecificities are short-chain dehydrogenases evolved from a common ancestor. *Proc. Natl. Acad. Sci. USA 90*, 9591-9595.

15. Nakajima, K., Hashimoto, T., and Yamada, Y. (1994) Opposite stereospecificity of two tropinone reductases is conferred by the substrate-binding sites. *J. Biol. Chem. 269*, 11695-11698.

16. Clark, D. D., and Ensign, S. A. (2002) Characterization of the 2-[(R)-2-hydroxypropylthio]ethanesulfonate dehydrogenase from *Xanthobacter* strain Py2: product inhibition, pH dependence of kinetic parameters, site-directed mutagenesis, rapid equilibrium inhibition, and chemical modification. *Biochemistry 41*, 2727-2740.

17. Allen, J. R., Clark, D. D., Krum, J. G., and Ensign, S. A. (1999) A role for coenzyme M (2-mercaptoethanesulfonic acid) in a bacterial pathway of aliphatic epoxide carboxylation. *Proc. Natl. Acad. Sci. U.S.A. 96*, 8432-8437.

18. Laemmli, U. K. (1970) Cleavage of structural proteins during the assembly of the head of bacteriophage T4. *Nature 227*, 680-685.

19. Krum, J. G., and Ensign, S. A. (2001) Evidence that a linear megaplasmid encodes enzymes of aliphatic alkene and epoxide metabolism and coenzyme M (2-mercaptoethanesulfonate) biosynthesis in *Xanthobacter* strain Py2. *J. Bacteriol. 183*, 2172-2177.

20. Allen, J. R., and Ensign, S. A. (1997) Purification to homogeneity and reconstitution of the individual components of the epoxide carboxylase multiprotein enzyme complex from *Xanthobacter* strain Py2. *J. Biol. Chem. 272*, 32121-32128.

21. Oppermann, U., Filling, C., Hult, M., Shafqat, N., Wu, X., Lindh, M., Shafqat, J., Nordling, E., Kallberg, Y., Persson, B., and Jörnvall, H. (2003) Short-chain dehydrogenases/reductases (SDR): the 2002 update. *Chem. Biol. Interact. 143-144*, 247-253.

22. Krishnakumar, A. M., Nocek, B. P., Clark, D. D., Ensign, S. A., and Peters, J. W. (2006) Structural basis for stereoselectivity in the (R)- and (S)-hydroxypropyl thioethanesulfonate dehydrogenases. *Biochemistry 45*, 8831-8840.

23. de Jong, R. M., Kalk, K. H., Tang, L., Janssen, D. B., and Dijkstra, B. W. (2006) The X-ray structure of the haloalcohol dehalogenase HheA from *Arthrobacter* sp strain AD2: Insight into enantioselectivity and halide binding in the haloalcohol dehalogenase family. *J. Bacteriol. 188*, 4051-4056.

24. Horer, S., Stoop, J., Mooibroek, H., Baumann, U., and Sassoon, J. (2001) The crystallographic structure of the mannitol 2-dehydrogenase NADP(+) binary complex from *Agaricus bisporus*. *J. Biol. Chem. 276*, 27555-27561.

25. Hoffken, H. W., Duong, M., Friedrich, T., Breuer, M., Hauer, B., Reinhardt, R., Rabus, R., and Heider, J. (2006) Crystal structure and enzyme kinetics of the (S)-specific 1-phenylethanol dehydrogenase of the denitrifying bacterium strain EbN1. *Biochemistry 45*, 82-93.

26. Clark, D. D., Boyd, J. M., and Ensign, S. A. (2004) The stereoselectivity and catalytic properties of *Xanthobacter autotrophicus* 2-[(R)-2-Hydroxypropylthio]ethanesulfonate dehydrogenase are controlled by interactions between C-terminal arginine residues and the sulfonate of coenzyme M. *Biochemistry 43*, 6763-6771.

27. Boyd, J. M. (2005) Mechanistic studies of the enzymes involved in bacterial acetone and propylene oxide metabolism, Dissertation, Utah State University, Logan.

28. Sparling, R., and Daniels, L. (1987) The specificity of growth inhibition of methanogenic bacteria by bromoethanesulfonate. *Can. J. Microbiol. 33*, 1132-1136.

29. Krum, J. G., Ellsworth, H., Sargeant, R. R., Rich, G., and Ensign, S. A. (2002) Kinetic and microcalorimetric analysis of substrate and cofactor interactions in epoxyalkane:CoM transferase, a zinc-dependent epoxidase. *Biochemistry 41*, 5005-5014.

30. Nocek, B., Jang, S. B., Jeong, M. S., Clark, D. D., Ensign, S. A., and Peters, J. W. (2002) Structural basis for CO_2 fixation by a novel member of the disulfide oxidoreductase family of enzymes, 2-ketopropyl-coenzyme M oxidoreductase/carboxylase. *Biochemistry 41*, 12907-12913.

31. Boyd, J. M., Clark, D. D., Kofoed, M. A., and Ensign, S. A. Mechanism of inhibition of aliphatic epoxide carboxylation by the Coenzyme M analog 2-bromoethanesulfonate. *J. Biol. Chem. 285*, 25232.

CHAPTER 4

ROLE OF THE ACTIVE SITE METHIONINES IN THE SUBSTRATE RECOGNITION AND THE CATALYTIC MECHANISM OF THE *(R)*- AND *(S)*-HYDROXYPROPYLTHIOETHANESULFONATE DEHYDROGENASES; KINETIC AND STRUCTURAL STUDIES

ABSTRACT

The novel epoxide carboxylase pathway of *Xanthobacter autotrophicus* strain Py2 is characterized by a three-step, four enzyme conversion of a highly reactive epoxypropane to acetoacetate. Structural analysis of three of these enzymes (*R*-HPCDH, *S*-HPCDH and 2-KPCC) revealed striking similarities in their active site architecture. Highly conserved positively charged residues (Arg/Lys) lining the CoM binding pocket and two methionine residues flanking the substrate are a common feature. While, Arg and Lys residues were shown to be important in binding of the sulfonate moiety of the substrate through electrostatic interactions, the role of methionines remains unknown. The present study investigates the importance of the active site methionines in the *R*- and *S*-HPCDH enzymes. Site-directed mutagenesis of Met187 and Met192 of *R*-HPCDH1 to alanine and subsequently to leucine, followed by kinetic analysis with various substrates was carried out. Similar substitutions and kinetic studies were performed on Met153 and Met194 of *S*-HPCDH3. The most significant change in the kinetic parameters observed for methionine to alanine mutants was a dramatic increase in the apparent K_m values for the physiological substrates. The double mutant (Met187Ala/Met192Ala) of *R*-HPCDH1 showed minimal catalytic activity with negligible k_{cat} and K_m values. In contrast, kinetic parameters for methionine to leucine mutants were similar to those obtained for the wild-type enzyme, but with some differences. For example, Met187Leu and Met192Leu of *R*-HPCDH1 showed a substrate dependent increase of k_{cat} values, while Met194Leu of *S*-HPCDH3 showed a substrate dependent increase in K_m values. The primary alcohol 2-hydroxyethyl-CoM (HEC) was a substrate for the

wild-type enzyme and Met to Leu mutants of both *R*-HPCDH1 and *S*-HPCDH3 with similar K_m values (except for Met192Leu of *R*-HPCDH1). Interestingly, Met192Leu mutant showed 42% increase in k_{cat} value and over seven-fold increase in the K_m value. The apparent k_{cat} and apparent K_m values exhibited by Met187Leu mutant and wild-type *rR*-HPCDH1 were identical and suggested that Met187 plays an important role in binding and catalysis of the physiological substrates (*R*- and *S*-HPC), but not substrates analogs lacking the terminal methyl group (e.g., HEC). Inhibition studies show that the tertiary alcohol, 2-methyl-2-hydroxypropyl-CoM (M-HPC) is a competitive inhibitor of *R*-HPC oxidation by Met187Leu and Met192Leu of *R*-HPCDH1, with a K_{is} similar to the K_m values for *R*-HPC. No inhibition of *S*-HPC oxidation by M-HPC was detected for any of Met mutants of *S*-HPCDH3. The X-ray structures for Met187Ala and Met192Ala of *R*-HPCDH1 were determined to 1.5 Å and 2.0 Å, respectively. A large solvent accessible pocket near the CoM binding site was revealed in the Met187Ala mutant structure. The sulfonate moiety of the substrate was not visible in this region, thus suggesting non-productive interaction of the arginine residues involved in the sulfonate binding with the surrounding solvent molecules. The Met192Ala mutant structure revealed electron density for the sulfonate moiety. The Met192 is in close proximity to the chiral carbon of the substrate molecule where chemistry occurs and appears to be shielding the interactions of the substrate with the active site residues from the surrounding environment. These results highlight the important role of the substrate flanking methionines in the active site of enzymes involved in the epoxide carboxylase pathway. Additionally a general architecture of the active site with the substrate flanking methionines and positively charged amino acids interacting with the sulfonate moiety, observed in *R*- and *S*-HPCDH, and 2-KPCC, may prove useful in identifying new CoM-dependent enzymes. On the basis of the kinetic analysis it is proposed that steric clashes of the terminal methyl group of the HPC substrates with the nicotinamide ring of NAD^+ are a major determinant of the enantioselectivity in *rS*-HPCDH3.

INTRODUCTION

In the three-step mechanism of epoxide degradation in *X. autotrophicus* Py2 an enantiomeric mixture of *R*- and *S*-epoxypropane is converted into a common metabolite acetoacetate by the action of four enzymes (*1, 2*). Integral to the versatility of this four-enzyme pathway are two enantioselective *R*- and *S*-dehydrogenases that individually allow for the oxidation of a single epoxypropane enantiomer (*3*). Collectively, however, these enzymes enable *X. autotrophicus* Py2 to utilize enantiomeric mixtures of epoxypropane, including those produced in vivo by an alkene monooxygenase during growth on gaseous propylene (*4*). The (*R*)- and (*S*)-hydroxypropyl-CoM dehydrogenases (*R*-HPCDH and *S*-HPCDH) are highly homologous enzymes catalyzing the reversible oxidation of (*R*)- and (*S*)-hydroxypropyl-CoM (*R*- and *S*-HPC) to an achiral product 2-ketopropyl-CoM (2-KPC) (*3*). Based on BLAST analysis and the amino acid sequence alignment, both enzymes belong to the class of short-chain dehydrogenase/reductase super-family (SDR). Analogous to other members of SDR family, *R*- and *S*-HPCDH enzymes are about 250 amino acids in length and carry out catalysis in the absence of a metal cofactor (*2*). Site-directed mutagenesis studies allowed for the identification of the catalytic triad residues (Ser, Tyr and Lys) in both enzymes (*5, 6*). Kinetic analysis of *R*- and *S*-HPCDH homologs (namely *R*-HPCDH1 and *S*-HPCDH3) revealed that both are highly enantioselective in discriminating their respective enantiomeric substrates. In *R*-HPCDH1 this enantioselectivity was shown to be mostly dictated by changes in k_{cat} while in *S*-HPCDH3 enantioselectivity was dictated largely by differences in K_m (*6*). Analysis of the X-ray structure of *R*-HPCDH1 along with a homology model of *S*-HPCDH3 shed light on the structural basis for stereoselectivity (*7*). In order for the alcohol to be effectively oxidized by HPCDH enzymes its hydroxyl group and the hydrogen atom have to be properly aligned with respect to the general base (Tyr155 or Tyr156) and the nicotinamide ring of NAD^+, respectively. In *R*-HPCDH1 the positively charged side chains of Arg152 and Arg196 were shown to coordinate the negatively

charged sulfonate group of the substrate (*5, 7, 8*). These strong electrostatic interactions are thought to be largely responsible for proper binding and positioning of the "business end" of the substrate with respect to the active site tyrosine and the NAD^+ cofactor. When the opposite enantiomer (*S*-HPC) was modeled in the active site of *R*-HPCDH1 by superimposing its hydroxyl group with that of *R*-HPC, the hydrogen atom of *S*-HPC was pointing away from the nicotinamide ring of NAD^+. This shows that binding of *S*-HPC in the same mode as *R*-HPC cannot support its proper orientation for catalysis (*7*). Indeed, kinetic analysis of *S*-HPC oxidation by *R*-HPCDH1 corroborates this observation, revealing that *S*-HPC is a strong competitive inhibitor of *R*-HPCDH1 with K_{is} close to the K_m of *R*-HPC (*5*). Together, these data suggested that binding of the substrate sulfonate via positively charged residues is crucial to orienting substrate for effective hydride transfer and provides the "switch" necessary for chiral discrimination in *R*-HPCDH1. Comparison of the X-ray structure of *R*-HPCDH1 with a homology model of *S*-HPCDH3 indicated different special orientation of the sulfonate binding site in *S*-HPCDH3 and suggested that Arg211 and Lys214 could be involved in binding of the CoM moiety (*7*). Site-directed mutagenesis studies confirmed this prediction, however kinetic analysis showed that enantioselectivity of *S*-HPCDH3 is not entirley controlled by the proper positioning of the substrate brought about by the electrostatic interactions with the positively charged residues in the CoM binding pocket. In contrast to *R*-HPCDH1, *S*-HPCDH3 was shown to catalyze oxidation of the opposite enantiomer (*R*-HPC) with only 4.5-times lower k_{cat} (as opposed to 402-times lower k_{cat} for *R*-HPCDH1) but with 290-times higher K_m (*6*). Based on these data and the results of the inhibition studies with the substrate analogs (M-HPC and HEC) it was proposed that the steric constraints in the active site of *S*-HPCDH3 prevent *R*-HPC from proper binding due to clashes of the terminal methyl group of the substrate with the active site residues. This could explain a different mechanism for controlling substrate specificity and enantioselectivity than that observed in *R*-HPCDH1 (*6*).

Despite a relatively low amino acid homology (41%), *R*-HPCDH and *S*-HPCDH reveal high structural similarities. Both enzymes share several important features that facilitate specific interactions with the substrate functional groups in order to bring about proper orientation of the substrate for catalysis. Common to both enzymes is a compact structure of the substrate binding region, which effectively isolates the active site residues from the immediate surroundings of the solvent environment. Moreover, one side of the binding pocket contains the catalytic triad residues (Ser, Tyr and Lys), while the opposite side of the pocket is lined with two arginine residues (in *R*-HPCDH1) or arginine and lysine residues (in *S*-HPCDH3), which again were shown to be important in binding of the substrate sulfonate group. In addition, the CoM binding pocket of *R*-HPCDH1 is typified by the presence of a tryptophan residue (Trp195), which appears to act as a "backstop" preventing movement of the substrate during catalysis (*5, 7*). Two substrate flanking methionines are another interesting feature common to both HPCDH enzymes. In *R*-HPCDH1 these are Met187 and Met192, while in *S*-HPCDH3 these are Met153 and Met194. Strikingly similar architecture of the active site is seen in the subsequent enzyme in the epoxide degradation pathway, namely 2-KPCC. This enzyme catalyzes the reductive cleavage and carboxylation of 2-ketopropyl-CoM to acetoacetate and CoM. Likewise, the compact substrate binding pocket of 2-KPCC is composed of the active site residues (Cys82 and Cys87) on one end, and arginines along with adjacent phenylalanine on the other end of the pocket. The crystal structure of 2-KPCC revealed that while Arg56 and Arg365 side chains are involved in binding of the CoM moiety, phenylalanine acts as a "backstop" restraining further translation of the substrate (*9*). Additionally two methionines (Met140 and Met361) flanking the sides of the pocket were identified in the active site of 2-KPCC (*9*). While the role of the active site residues and positively charged residues coordinating the sulfonate moiety is pretty evident based on the available biochemical data, the role of the methionines remains unknown and requires further investigation.

Unique properties of methionine residues make them useful building blocks in biological systems, as they are commonly found in practically all proteins. Despite this widespread

occurrence few studies have been done to investigate the importance of methionines in cellular processes and particularly in enzymatic reactions. Recent reports provide an increasing body of evidence suggesting that methionines might be critically important in facilitating specific functions of enzymes. The following literature review highlights only the most important findings in order to introduce the relevance of this research and orient the reader on the work that has previously been conducted, thus providing a context for understanding the possible roles of the substrate flanking methionines in HPCDH enzymes.

Methionine (Met) is one of the most readily oxidized amino acid constituents of proteins. Considering the reversibility of Met oxidation and the functional changes associated with its oxidation, it has been proposed that Met oxidation/reduction in proteins may be one of the means to control homeostasis in biological systems (*10*). Moreover, methionine residues may act as catalytic antioxidants, protecting both the protein where they are located and other macromolecules against oxidative stress (*11*). Oxidation of a single active site methionine to methionine sulfoxide can also result in a significant increase in the catalytic activity of an enzyme, as observed for α-galactosidase (12-fold increase) (*12*). Recently, a role of the methionine residues has also been proposed in substrate recognition. In a study investigating the structural basis of broad spectrum of specificity of the mammalian signal-recognition particle (SRP54), it was proposed that the clusters of methionine residues are essential in a recognition process of a wide variety of nonpolar peptide sequences. Similar mechanism has been suggested for other proteins interacting with a broad spectrum of substrates e.g., calmodulin (a calcium-binding regulatory protein), which contains eight methionines at the binding site, thus providing a plastic surface compatible with structurally diverse nonpolar surfaces on binding partners (*13*). This unique role of methionine residues was rationalized by the conformational flexibility of the Met side chain, which cannot be provided by other residues of similar polarity. For example leucine or isoleucine as the closest analogs of methionine, are branched and thus more rigid. This hypothesis was further modified by Gellman (*14*), who suggested that the structural flexibility of

methionines arises more from the presence of the sulfur atom rather than the lack of branching. A statistical survey of crystallized proteins showed that the distribution of the methionine torsion angles is practically flat over the entire range of possible values, in contrast to the periodicities observed for all other amino acids side chains (*15*). Thus small enthalpic discrimination among possible methionine rotamers could explain considerable freedom of adjusting themselves to accommodate nonpolar binding partners of different structures. Additionally, the significantly larger polarizability of sulfur in methionine, as compared to other hydrocarbon moieties, makes methionine residues even better candidates for binding extensive nonpolar surfaces. Based on the observed proximity of cysteine (Cys) and methionine (Met) to aromatic side chains in protein crystal structures (*16*) it has been proposed that the aryl–sulfur interactions are among the most favorable interactions. It has been further reported that Met and the phenylalanine aryl ring interactions are especially important and frequently observed. Substitution with Lys or Ile were shown to result in a less favorable value of the corresponding interactions (*17*). Furthermore, one study proposed that Met with Trp and Phe clusters are so important for protein-protein interactions (e.g., in p53, HIV transcriptase) that they should be considered as a target for drug design (*18*). Important roles of Met interactions with aromatic residues in a recognition process was further highlighted by the recent structural and functional studies on the influenza virus strain H5N1 (*19*). It was shown that Met54 was a key residue of hemagglutimin (H5) of the virus, making two aromatic interactions with Trp21 of the cell receptor via its sulfur atom.

Together, unique properties of methionine residue suggest that the thioether sulfur atom in the methionine side chain is more than a methylene equivalent. The conformational properties of thioether fragments and the unusually large polarizability of the sulfur atom itself prove to be useful in producing binding sites that are tailored for strong interactions with nonpolar surfaces of various shapes.

One example of an enzyme which utilizes Met residues to control substrate specificity is α-Lytic protease (*20*). Simple substitution of Met192 and Met213 to Ala in one of the substrate

binding pockets resulted in significant changes in the specificity profiles of the protease due to the reduction of unfavorable steric constraints. Further, Met213 was implied to play a significant role in effecting the precise positioning of substrates for optimal interactions with the enzyme. Another study shows that the presence of a single methionine residue in the binding pocket of a glutamate transporter is capable of controlling substrate selectivity (*21*). In particular, it is proposed that the side-chain of Met367 plays a steric role in the positioning of the substrate in a step subsequent to its initial binding.

In the present work, the role of active site methionines was investigated in a pair of enantioselective dehydrogenases (*R*- and *S*-HPCDH) involved in aliphatic epoxide carboxylation. Site-directed mutagenesis was carried out to convert each of the methionines in *R*-HPCDH1 (Met187 and Met192) and in *S*-HPCDH3 (Met153 and Met194) to alanine or leucine. As a result, nine different mutants were isolated and kinetically characterized to shed light on the effect of each of the methionines on the substrate binding and catalysis.

EXPERIMENTAL PROCEDURES

Materials. All commercially available chemicals were of analytical grade (Sigma-Aldrich Chemicals, Acros Organics, and Fisher Scientific). 2-KPC, *R*-HPC *S*-HPC, HEC and M-HPC were synthesized as described previously (*5, 8*). Chemical structures of the compounds were confirmed using ^{1}H NMR. The spectra of HPC enantiomers and 2-KPC were identical to those reported previously (*5, 22*). Purity of the synthesized chemicals as determined by reverse-phase HPLC was estimated to be ≥98%.

Cloning of the HPCDH Genes (xecD1 and xecE3). Three sets of genes encoding *R*- and *S*-HPCDH enzymes were identified on the linear megaplasmid of *X. autotrophicus* Py2 (*6*). These gene clusters are designated with numbers 1, 2 and 3, respectively, in the order in which they were discovered and subsequently studied. Thus, *xecD1* encodes *R*-HPCDH1 and refers to the first operon, whereas *xecE3* encodes *S*-HPCDH3 found in the third operon, downstream from

the first operon on the megaplasmid. Genes *xecD1 and xecE3* were cloned in pET28-b (Novagen) and pRSFDuet-1 (Novagen) expression vectors to yield pXD28 and pDS53 vectors, respectively. All procedures were performed as described previously (*6*).

Site-Directed Mutagenesis (SDM). Site-directed mutagenesis of *xecD1* (in pXD28) and *xecE3* (in pDS53) were carried out utilizing the QuickChange site-directed mutagenesis kit (Stratagene) according to the manufacturer's protocols. All mutations were confirmed by DNA sequencing. The sequences of the mutagenic primer pairs (purchased from IDT) used for each codon substitution in *xecD1* are as follows:

M187A, GCGGTCTGTCCGGGCGCCATCGAGACGCCCATG and
CATGGGCGTCTCGATGGCGCCCGGACAGAC; M192A,
CATGATCGAGACGCCCGCCACCCAGTGGCGCCTCG and
CGAGGCGCCACTGGGTGGCGGGCGTCTCGATCATG; M187L,
GCGGTCTGTCCGGGCCTGATCGAGACGCCCATG and
GTACCCGCAGAGCTAGTCCGGGCCTGTCTGGCG; M192L,
CATGATCGAGACGCCCCTGACCCAGTGGCGCCTCG and
GCTCCGCGGTGACCCAGTCCCCGCAGAGCTAGTAC.

Primers used for SDM of *xecE3* are as follows:

M153A, CGGCATCCCGACCGCGGCGGCCTACTGC and
GCAGTAGGCCGCCGCGGTCGGGATGCCG; M194A,
ACACCTCGACCGGCGCGGGGCAGCAGCTG and
CAGCTGCTGCCCCGCGCCGGTCGAGGTG; M153L,
GGCATCCCGACCTTGGCGGCCTACT and AGTAGGCCGCCAAGGTCGGGATGCC;
M194L, CCTCGACCGGCTTGGGGCAGCAG and CTGCTGCCCCAAGCCGGTCGAGG;

DNA Sequencing. Sequencing was performed on an AB 3730 DNA Analyzer at the Utah State University CIB DNA sequencing laboratory. The following sequencing primers were used to confirm all mutations in pXD28: T7 promoter primer, TAATACGACTCACTATAGGG

(Novagen), and T7 terminator primer, GCTAGTTATTGCTCAGCGG (Novagen). Primers used to confirm all mutations in pDS53 were as follows: ACYCDuetUP1 Primer (Novagen), GGATCTCGACGCTCTCCCT and DuetDOWN1 Primer (Novagen), GATTATGCGGCCGTGTACAA.

Media and Growth of Bacteria. E. coli BL21- (DE3) CodonPlus with pXD28 or pDS53 plasmids was grown in a 15L semicontinuous microferm fermenter with LB media supplemented with kanamycin (50 μg mL^{-1}) and chloramphenicol (50 μg mL^{-1}). All other procedures were performed as described previously (*5, 6*).

Preparation of Cell-Free Extracts. On average about 60 grams of frozen cell paste was thawed at room temperature in two volumes of lysis buffer (20 mM Tris, 20% glycerol, 500 mM NaCl, 20 mM imidazole, 0.03 mg mL^{-1} DNase I, at pH 8.0). For purification of *S*-HPCDH3 lysis buffer also contained 0.1% (w/v) Tween20. Homogenized cell suspension was subjected to two passes through a French pressure cell at 15000 psi and the crude lysate was clarified by centrifugation at 244,717*g* for 45 min. The supernatant was further retained for purification.

Purification of rR-HPCDH1, rR-HPCDH1 Mutants, rS-HPCDH3 and rS-HPCDH3 Mutants. All purification procedures were performed in identical conditions, as described previously (*5, 6*). All steps were carried out at 4 °C. All used buffers had the pH adjusted at 4 °C. Dialyzed proteins were concentrated over a 30000 MW cutoff membrane, flash frozen and stored in liquid nitrogen for future use. Protein concentrations were determined on a NanoDrop spectrophotometer using theoretical extinction coefficients (ϵ_{280} = 10033 M^{-1} cm^{-1} for *rS*-HPCDH3 and ϵ_{280} = 18512.5 M^{-1} cm^{-1} for *rR*-HPCDH1), with dialysis flow-through buffers as blanks.

SDS-PAGE and Native PAGE Analysis. SDS-PAGE (12% T) and native PAGE (4-20% T BioRad) were performed according to the Laemmli procedure (*23*). The apparent molecular masses of polypeptides on a SDS-PAGE gel were determined by comparison to R_f values of

standard proteins. Migration of *rS*-HPCDH3 mutants and *rR*-HPCDH1 mutants were also compared directly to wild-type *rS*-HPCDH3 and wild-type *rR*-HPCDH1.

Spectrophotometric Enzyme Assays. All enzymes assays were performed in 50 mM glycine, 50 mM NaH_2PO_4, and 50 mM Tris base (GPT buffer mix) at a pH of 7.5 (adjusted at 30 °C), as described previously (*5*). Assays were performed at 30 °C in a Shimadzu model UV160U spectrophotometer equipped with a water-jacketed cuvette holder for thermal control. Alcohol or ketone production was correlated to micromoles of NADH appearance or disappearance, respectively, measured at 340 nm using the extinction coefficient for NADH (ϵ_{340} = 6.22 mM^{-1} cm^{-1}). In determining kinetic constants for *R*-HPC oxidation by *rR*-HPCDH1 the following ranges of alcohol concentration were used in the assays: 0.025 – 1.0 mM (WT); 0.75 – 24 mM (M187A and M192A); 0.75 – 75 mM (M187A/M192A); 0.050 – 20 mM (M187L); 0.10 – 81 mM (M192L). For *S*-HPC oxidation the concentrations were: 0.078 – 7.8 mM (WT); 14 – 52 mM (M187A); 3.5 – 87 mM (M192A); 0.035 – 14 mM (M187L); 0.078 – 7.8 mM (M192L). For HEC oxidation the concentrations were: 0.20 – 16 mM (WT); 0.40 – 16 mM (M187L); 0.80 – 30 mM (M192L). In the assay of *S*-HPC oxidation by *rS*-HPCDH3 the following ranges of alcohol concentrations were used: 0.030 – 3.8 mM (WT); 3.5 – 87 mM (M153A); 1.6 – 52 mM (M194A); 0.21 – 6.7 mM (M194L). For *R*-HPC oxidation the concentrations were: 1.5 – 3.8 mM (WT); 12 – 45 mM (M153A); 30 – 121 mM (M194A); 1.5 – 3.8 mM (M194L). For HEC oxidation the concentrations were: 0.20 – 16 mM (WT); 0.40 – 16 mM (M194L). The concentration of NAD^+ for all assays was 10 mM (22 x value of $K_{mNAD}{}^+$ for *rR*-HPCDH1 and 52 x value of $K_{mNAD}{}^+$ for *rS*-HPCDH3). For assays of ketone reduction by *rR*-HPCDH1, the following ranges of 2-KPC concentration were used in determining kinetic constants: 0.016 – 0.50 mM (WT); 0.36 – 36 mM (M187A); 0.7 – 17 mM (M192A); 1.4 – 36 mM (M187A/M192A); 0.016 – 1.0 mM (M187L); 0.033 – 2.1 mM (M192L). In the assay of 2-KPC reduction by *rS*-HPCDH3 the following ranges of concentration were used: 0.10 – 32 mM (WT); 6.2 – 34 mM (M153A); 1.4 – 21 mM (M194A); 0.69 – 22 mM (M194L); The concentration of NADH for these assays was 0.16 mM, (4.4 x value

of K_{mNADH} for *rR*-HPCDH1 and 19 x value of K_{mNADH} for *rS*-HPCDH3). On an average, six concentrations of substrates within the ranges indicated were chosen for the kinetic analyses. All samples were degassed/flushed with nitrogen and incubated at 30 ºC water-bath for 5 min prior to the enzyme addition. To determine kinetic parameters (apparent K_m and V_{max}) initial rate values were plotted as a function of substrate concentration and data points were fitted to the Michaelis-Menten equation using SigmaPlot 11.0.

Standardization of Stock Solutions. Stock solutions of synthesized *R*-HPC and 2-KPC were standardized using wild-type *rR*-HPCDH1, whereas stock solutions of synthesized *S*-HPC were standardized with wild-type *rS*-HPCDH3. Standardization assays for *R*-HPC and *S*-HPC oxidation were performed in GPT buffer (50 mM glycine, 50 mM NaH_2PO_4, and 50 mM Tris base) at pH 11.0 with 50 μg of enzyme and 10 mM of NAD^+. Standardization assay for 2-KPC reduction was performed in GPT buffer at pH 7.5 with 50 μg of enzyme and 0.2 mM of NADH. All assays were repeated three to six times depending on the value of standard deviation obtained from triplicate experiments. Reactions were carried out at 30 ºC for 2 min. The average absorbance measured at 340 nm was correlated with micromoles of the substrate used in the assay using the extinction coefficient for NADH (ϵ_{340} = 6.22 mM^{-1} cm^{-1}). Calculations of the final stock concentration of 2-KPC were done using the equilibrium constant determined from the Haldane equation, as described previously (*5*). Calculations of the final stock concentration of *R*-HPC and *S*-HPC were based on assumption that the reactions went to completion, since pH 11.0 renders both enzymes irreversible. Stock solutions of NAD^+ and NADH were standardized by measuring absorbance of aliquoted solutions at 260 nm and 340 nm, respectively, using corresponding extinction coefficients (NAD^+ ϵ_{260} = 18.0 mM^{-1} cm^{-1}).

Inhibition Studies. All assays were performed in GPT buffer mix at pH 7.5 with saturating concentration of NAD^+ (10 mM). Inhibition assays for wild-type *rR*-HPCDH1 were performed at the following variable concentrations of *R*-HPC: 31, 72, 144, 287 and 615 μM. For

rR-HPCDH1 M187L concentrations of *R*-HPC were: 48, 96, 240, 480, 960 and 1920 μM, whereas for *rR*-HPCDH1 M192L concentrations of *R*-HPC were: 246, 491, 982, 1960, 3920 and 7840 μM. Each assay was performed at several fixed concentrations of M-HPC: 0, 0.2, 0.4, 0.8 and 1.6 mM. Inhibition assays for wild-type *rS*-HPCDH3 were performed at the following variable concentrations of *S*-HPC: 16, 31, 62, 155 and 310 μM and three fixed concentrations of M-HPC (0, 1.2 and 4.9 mM). Similar assays for *rS*-HPCDH3 methionine mutants were performed at the following concentrations of *S*-HPC: 0.10, 0.21, 0.42, 0.83, 17 and 34 mM and five fixed concentrations of M-HPC (0, 1.2, 2.4, 4.9 and 9.8 mM). Initial rate data were fit to a rectangular hyperbola described by the standard form of the Michaelis-Menten equation.

Crystallization Data for the Met187Ala and Met192Ala Mutants of rR-HPCDH1. The structural studies described below were conducted in collaboration with Dr. John Peters from Montana State University. Crystalization conditions for the Met187Ala and Met192Ala mutants were identical to those used for the wild-type enzyme (*7*). Crystal trays were set up with both substrates NAD^+ and *R*-HPC present at a concentration of 15 and 20 mM, respectively. After 2 weeks crystals of the average size of 0.2 x 0.3 x 0.2 mm were obtained. These crystals were harvested and flash frozen in liquid nitrogen. Diffraction data was collected at SSRL beam line 9-2 and further processed using HKL2000. Table 4-1 and 4-2 summarize data statistics obtained for each of the mutants. Both crystals were assigned to the space group $P2_1$ and revealed identical cell parameters as previously characterized crystals of the wild-type *R*-HPCDH (*7, 24*). The molecular replacement method was applied for solving the Met187Ala and Met192Ala mutant structures with the wild-type structure as the starting model. The refinement of these structures was carried out. Several cycles of refinement using the CNS suite of programs along with model building using the program O resulted in final models with 100% residues occupying allowed regions of a Ramachandran Plot, as calculated by PROCHECK. The refinement statistics are presented in Tables 4-3 and 4-4.

Table 4-1. Data statistics for the *R*-HPCDH mutant Met187Ala co-crystallized with *R*-HPC. Adopted from Krishnakumar (*25*).

Space group	$P2_1$				
Cell dimensions	a = 64.678 Å	b = 110.176 Å	c = 68.894 Å	α = γ = 90°	β = 93.855°
Resolution (Å)	20.00-1.46				
Completeness (%)	97.9(93.7)				
Observed reflections	1163058				
Unique reflections	161616				
I/σ	48 (7.5)				
R_{merge} [a]	0.042(0.301)				

Numbers in parentheses indicate values for the highest resolution bin.
[a]R_{merge} = ΣhklΣi|Ii - >|/ΣhklΣi|<I>|, where Ii is the intensity for the ith measurement of an equivalent reflection with indices h, k, l.

Table 4-2. Data statistics for the *R*-HPCDH mutant Met192Ala co-crystallized with *R*-HPC. Adopted from Krishnakumar (*25*).

Space group	$P2_1$				
Cell dimensions	a = 64.720 Å	b = 110.812 Å	c = 68.866 Å	α = γ = 90°	β = 93.710°
Resolution (Å)	20.00-2.08				
Completeness (%)	98.9(96.7)				
Observed reflections	503556				
Unique reflections	65222				
I/σ	30.1(15.5)				
R_{merge} [a]	0.111(0.264)				

Numbers in parentheses indicate values for the highest resolution bin.
[a]R_{merge} = ΣhklΣi|Ii - >|/ΣhklΣi|<I>|, where Ii is the intensity for the ith measurement of an equivalent reflection with indices h, k, l.

Table 4-3. Refinement statistics for the *R*-HPCDH mutant Met187Ala co-crystallized with *R*-HPC. Adopted from Krishnakumar (*25*).

Resolution (Å)	20.00-1.46
R_{free}	0.201
R_{cryst}	0.181
No. Non hydrogen atoms	
Protein	4004
Cofactor	176
Solvent	419
RMSD from target values	
Bond lengths (Å)	0.012
Bond angles (°)	1.55
Average isotropic B factor	
All atoms	18.71
Protein main chain	13.71
Protein side chain	18.41
NAD^+	47.25
Water	19.05

Table 4-4. Refinement statistics for the *R*-HPCDH mutant Met192Ala co-crystallized with *R*-HPC. Adopted from Krishnakumar (*25*).

Resolution (Å)	20.00-2.08
R_{free}	0.201
R_{cryst}	0.231
No. Non hydrogen atoms	
Protein	4004
Cofactor	176
Solvent	243
RMSD from target values	
Bond lengths (Å)	0.014
Bond angles (º)	1.59
Average isotropic B factor	
All atoms	15.39
Protein main chain	19.66
Protein side chain	17.33
NAD^+	50.25
Water	15.05

RESULTS AND DISCUSSION

The Overall Structure of the Met187Ala and Met192Ala Mutants of rR-HPCDH1. The overall structure of the mutants is analogous to that of the wild-type *rR*-HPCDH1 (PDB ID 2cfc). The Met187Ala mutant structure was determined at resolution up to 1.46 Å and resulted in calculating high quality electron density maps. These maps indicate that the NAD^+ molecule is well ordered (Figure 4-1). In contrast to the previously determined structure of *rR*-HPCDH1, the present structure reveals clear electron density for the entire ribose molecule, thus confirming its positioning in the previously determined wild-type structure (*7*). Site directed mutagenesis studies of Met187 and Met192 in *rR*-HPCDH1 have revealed the importance of these residues for catalysis. Kinetic analysis, discussed in detail further in the text, revealed that substitution of the methionines to alanine significantly altered both k_{cat} and K_m in the reaction with all tested substrates. To gain further insigh into the role of the active site methionines in the substrate binding and catalysis crystal structures of the methionine mutants were determined.

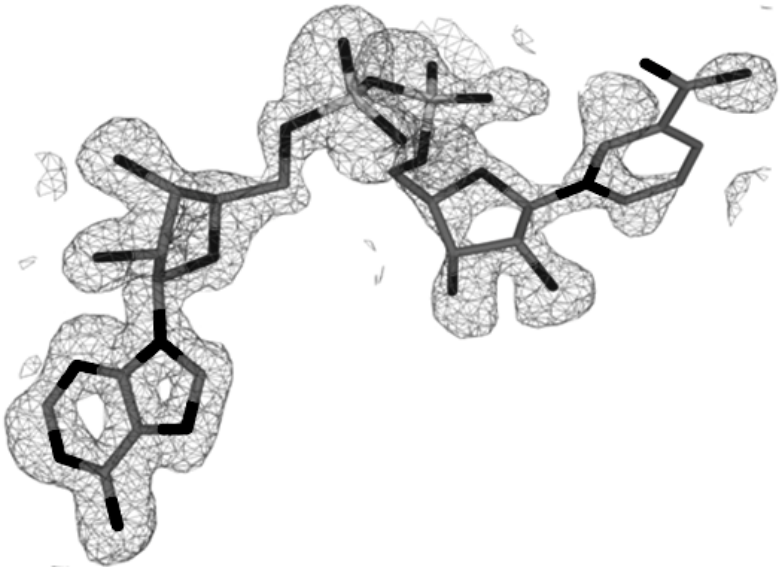

Figure 4-1. Electron density contoured at 1σ cutoff around NAD^+ in the structure of *R*-HPCDH1 Met187Ala mutant.

Structural Analysis of the Role of Met187 Residue in rR-HPCDH1. The X-ray structure of Met187Ala shows clear density of an alanine rather than a methionine residue at position 187, thus confirming the mutation. No electron density corresponding to the sulfonate group at the sulfonate binding site could be seen in the initial density maps. Instead, this position is occupied by what seems like solvent molecules, present in the electron density maps in form of disordered "blobs" (Figure 4-2). Comparison of the wild-type *rR*-HPCDH1 structure with the Met187Ala mutant structure reveals structural implications in the substrate binding pocket brought about by the mutation. Based on the structural data it is proposed that the Met187 plays a role in shielding the sulfonate moiety of the substrate from the ambient solvent and in separating/shielding charges of the sulfonate moiety from the charges developing in the active site during catalysis. The Met187 residue in the wild-type *rR*-HPCDH1 is positioned close to the sulfonate moiety of the substrate and forms a part of the solvent protected substrate binding pocket. Superimposition of the wild-type *rR*-HPCDH1 and the Met187Ala mutant structures reveals a large solvent

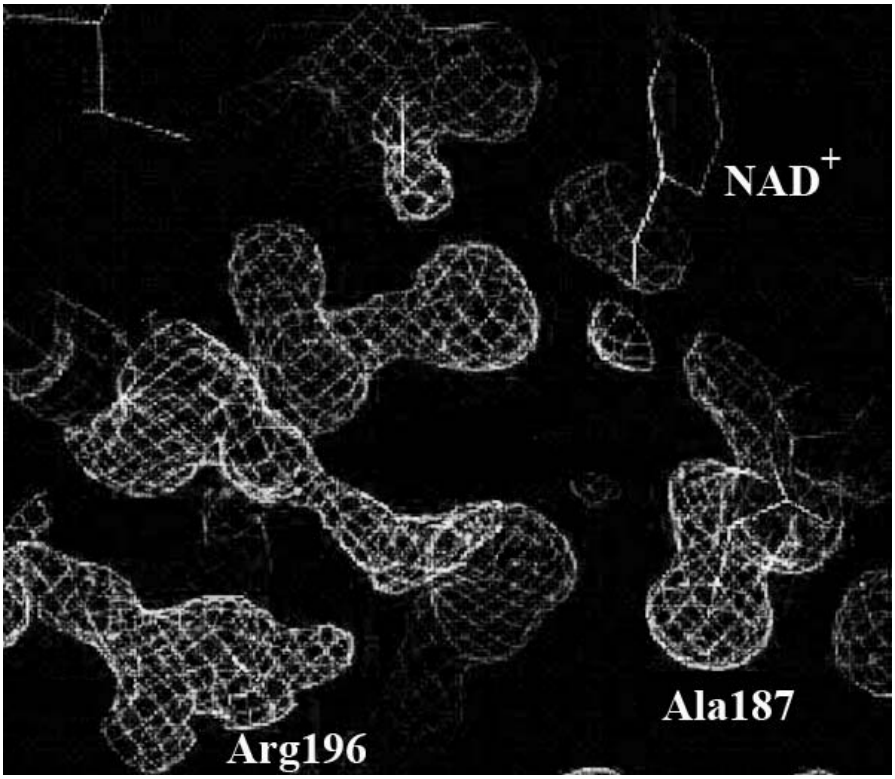

Figure 4-2. Electron density contoured at 1σ cutoff at the sulfonate biding region in the Met187Ala mutant structure of *R*-HPCDH1. Adopted from Krishnakumar (*25*).

accessible pocket created around the sulfonate binding pocket. As a result non-productive interactions of the solvent molecules with the arginine residues impair/prevent interactions of these residues with the sulfonate moiety of the substrate (Figure 4-3). Another important difference is the altered conformation of the side chain of Phe149 in the mutant structure. Analysis of the wild-type structure revealed that the side chain of Phe149 forms several hydrophobic interactions with the C1, C2 and C3 carbons of the product 2-KPC (Figure 4-4) clearly contributing to its binding. Also, a terminal methyl group of Met187 side chain is oriented towards Phe149 making a single hydrophobic contact. Position and orientation of Met187 and Phe149 in the wild-type structure suggest that both residues contribute to the compact active site architecture and appear to be shielding the substrate from behind. Substitution of Met187 to

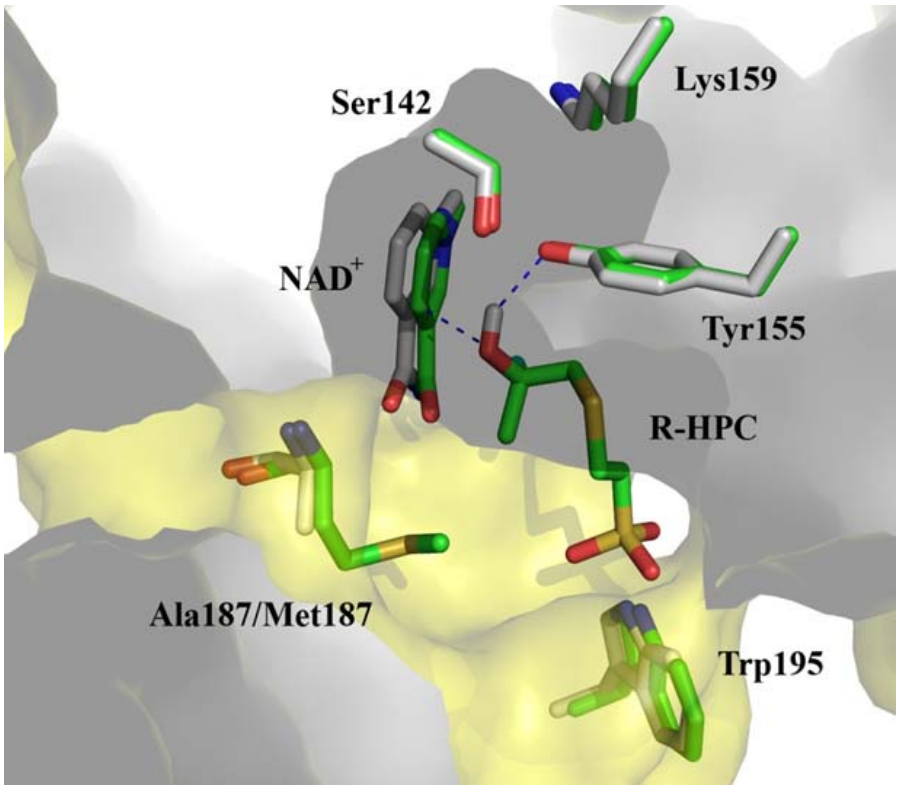

Figure 4-3. Superimposed structures of the Met187Ala mutant (grey) and wild-type *rR*-HPCDH1 (green) highlighting alignment of NAD^+ and the active site residues, and showing a position of Met187 in a channel leading to the active site cavity. Surface representation of Met187Ala mutant (yellow) shows a large opening of the active site as a result of Met187 to Ala substitution.

smaller in size alanine allows the side chain of Phe149 to assume a different conformation, thus creating a large solvent accessible pocket. Superimposition of Met187Ala mutant and the wild-type enzyme structures reveals that the phenolic ring of Phe149 in Met187Ala structure clashes with the product 2-KPC present in the wild-type structure (Figure 4-4). It is plausible that different confirmation of Phe149 side chain might be a direct result of the product absence, as observed for Met187Ala mutant. Lack of hydrophobic interactions between Phe149 and both the product and Met187 residue could provide the phenolic ring of Phe149 with more conformational freedom. Another important observation is that the catalytic triad residues of Ser142, Y155 and Lys159 along with the NAD^+ cofactor are well aligned with respect to each other in both the wild-type and the mutant structures (Figure 4-3). This is despite the fact that the Met187Ala

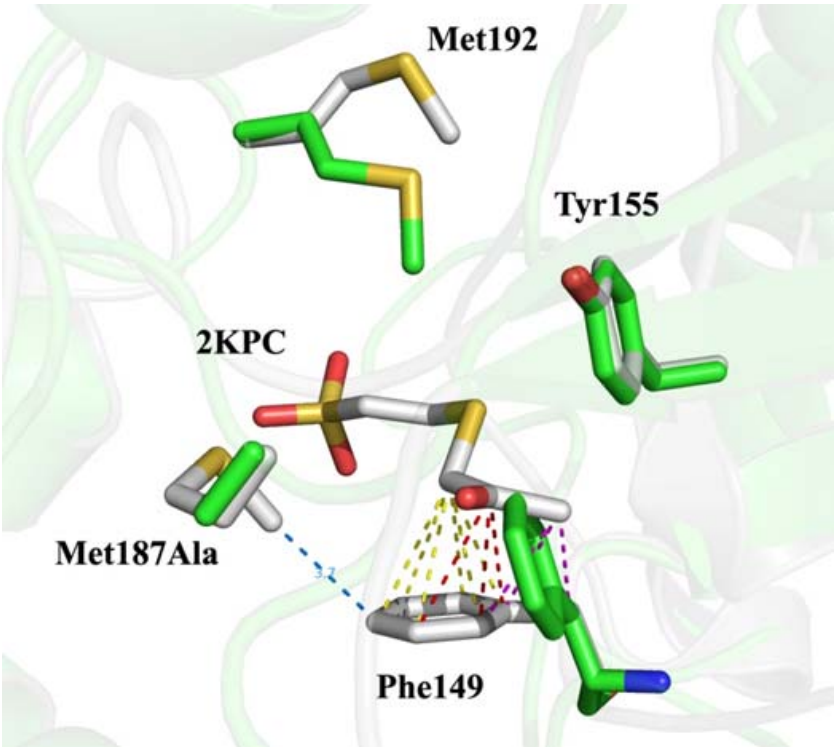

Figure 4-4. Superimposed structures of the Met187Ala mutant (green) and the wild-type *rR*-HPCDH1 (grey) highlighting hydrophobic interactions (dashed lines) of Phe149 with C1-C3 carbons of 2-KPC in the wild-type enzyme structure, and different conformation of Phe149 and Met192 residues in the Met187Ala mutant structure relative to that of the wild-type *rR*-HPCDH1.

mutant structure lacks the substrate *R*-HPC and thus represents an enzyme•NAD^+ binary complex, whereas the wild-type structure with the product 2-KPC bound represents enzyme•NAD^+•2-KPC ternary complex. Together it may suggest that there is no conformational change induced by the substrate binding to the enzyme•NAD^+ binary complex with respect to the active site residues. However the cofactor-induced conformational change reported for some members of the SDR family cannot be rule out at this point (*26*).

Structural Analysis of the Role of Met192 Residue in rR-HPCDH1. The crystal structure of Met192Ala determined at 2.08Å resolution clearly shows lack of the methionine residue at position 192, thus confirming the mutation (Figure 4-5). An electron density of the substrate bound in the active site is only observed for the sulfonate moiety. Lack of good electron density for the remaining part of the substrate prevents from its precise postioning relavite to the catalytic

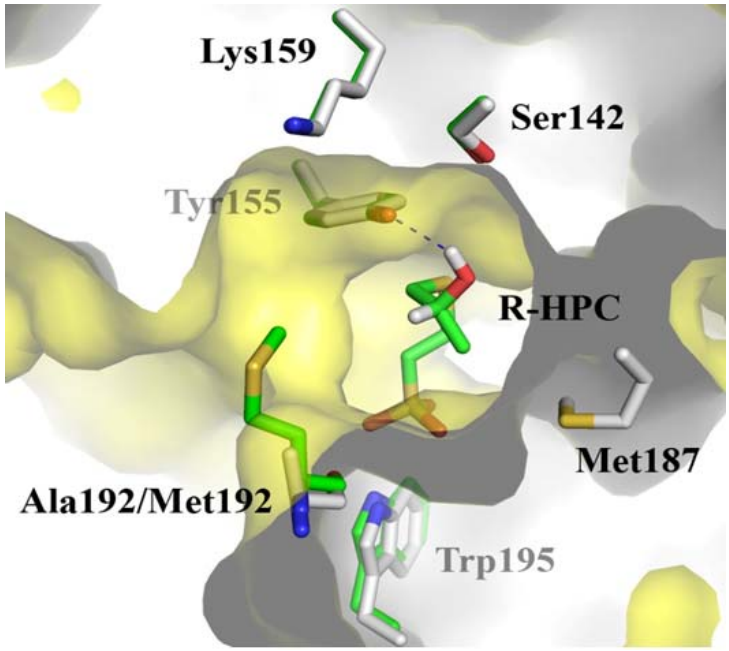

Figure 4-5. Superimposed structures of the Met192Ala mutant (grey) and the wild-type *rR*-HPCDH1 (green) highlighting alignment of NAD^+ and the active site residues, and showing a position of Met187 in a channel leading to the active site cavity. Surface representation of Met192Ala mutant (yellow) shows a large opening of the active site as a result of Met192 to Ala substitution.

triad residues. Nevertheless, the fact that the sulfonate group is present in these initial maps is somewhat surprising considering that the K_m value for *R*-HPC exhibited by Met192Ala mutant is higher than that for the Met187Ala mutant, which did not show electron density corresponding to the bound substrate. Superimposition of the Met192Ala mutant and the wild-type *rR*-HPCDH1 structures highlights further differences in the architechture of the two active sites thus providing insight into the possible role of Met192. The crystal structure of the wild-type enzyme reveals that Met192 is positioned in close proximity of the hydroxyl group and the hydrogen atom involved in the oxidation/reduction chemistry. This suggests a possible role of this residue in shielding the negative charge on the catalytic triad tyrosine from the non-productive interactions with the solvent molecules. The comparison of both structures corroborates with this prediction

and reveals a large solvent accessible pocket around the active site as a result of the Met192 substitiution to Ala (Figure 4-5).

Kinetic Analysis of Met187Ala and Met192Ala Mutants of rR-HPCDH1. The apparent k_{cat} and K_m values determined for *R*-HPC and *S*-HPC oxidation, and 2-KPC reduction, by *rR*-HPCDH1 were similar to those reported previously (*6*). In contrast, kinetic parameters of *rR*-HPCDH1 methionine mutants were significantly altered, suggesting an important role of Met187 and Met192 in substrate binding and/or catalysis. Specifically, in *R*-HPC oxidation catalyzed by Met187Ala and Met192Ala mutants the apparent K_m values increased by 18- and 24-fold, respectively, as compared to the wild-type *rR*-HPCDH1. These results are in agreement with the structural data showing that the substitution of Met187 and Met192 to alanine creates a large solvent accessible pocket, thus permitting non-productive interactions of the active site residues with the solvent molecules. The significance of both methionines was also reflected in the two- to four-fold decrease of the apparent turnover number (k_{cat}) exhibited by Met187Ala and Met192Ala mutants, respectively. The most substantial changes were observed for Met192Ala mutant suggesting a special role of Met192 in the catalytic activity of *rR*-HPCDH1. Indeed crystallographic data shows that Met192 in the wild-type enzyme shields the negative charge on Tyr155 of the catalytic triad from ambient solvent molecules, thereby bringing about effective catalysis. The trend of an increasing K_m and a decreasing k_{cat} was dramatically intensified in a double mutant of *rR*-HPCDH1 (Met187Ala/Met192Ala) where the apparent K_m was 876-fold higher and the apparent k_{cat} 22-fold lower than for the wild-type enzyme, thereby making the mutant enzyme practically inactive at the cellular concentration of *R*-HPC. A combined effect of the changes in K_m and k_{cat} was well reflected in the catalytic efficiencies (k_{cat}/K_m) of the analyzed mutants, which values decreased by 43-fold (Met187Ala), 96-fold (Met192Ala) and over 19,000-fold (Met187Ala/Met192Ala). Significant changes in kinetic parameters were also observed in 2-KPC reduction, where the apparent k_{cat} values decreased four-fold (Met187Ala), five-fold (Met192Ala) and 196-fold (Met187Ala/Met192Ala). This in turn translates to a further

Table 4-5. Kinetic parameters for *rR*-HPCDH1 WT and its Met187Ala and Met192Ala mutants at 30°C and pH 7.5[a]

Enzyme	K_m (μM)	Change in K_m (x-fold)	V_{max} (units•mg^{-1})	k_{cat} (s^{-1})	Change in k_{cat} (x-fold)	k_{cat}/K_m (M^{-1} s^{-1})
Substrate: *R*-HPC						
WT	82.7 ± 6.8	1.00	83.2 ± 1.9	41.2	1.0	4.98×10^5
M187A	1510 ± 92	18.3	35.2 ± 0.54	17.4	0.42	1.15×10^4
M192A	2020 ± 210	24.4	21.0 ± 0.61	10.4	0.25	5.16×10^3
M187/192A	72500 ± 10500	876	3.82 ± 0.33	1.89	0.046	2.61×10^1
Substrate: *S*-HPC						
WT	265 ± 72	1.00	0.226 ± 0.014	0.112	1.0	4.22×10^2
M187A	ND[b]		ND[b]	ND[b]		ND[b]
M192A	4840 ± 280	18.3	0.165 ± 0.0021	0.0815	0.73	1.68×10^1
M187/192A	ND[c]		ND[c]	ND[c]		ND[c]
Substrate: 2-KPC						
WT	72.4 ± 12	1.00	55.7 ± 2.9	27.6	1.0	3.81×10^5
M187A	1160 ± 120	16.0	12.5 ± 0.37	6.19	0.22	5.33×10^3
M192A	1890 ± 220	26.1	10.5 ± 0.34	5.20	0.19	2.75×10^3
M187/192A	8470 ± 1260	117	0.28 ± 0.015	0.141	0.0051	1.66×10^1

[a]Assay for *R*-HPC and *S*-HPC oxidation by *rR*-HPCDH1 WT, M187A and M192A mutants contained 1.0 μg and 46 μg of enzyme, respectively. Assay for *R*-HPC and *S*-HPC oxidation by M187A/M192A mutant contained 46 μg and 100 μg of enzyme, respectively. Assay for 2-KPC reduction by *rR*-HPCDH1 WT, M187A and M192A mutants contained 2.0 μg of enzyme and 70 μg of M187A/M192A mutant. Apparent k_{cat} and K_m values are reported as means ± standard deviations. All assays were performed at 30 ˚C with fixed concentrations of NAD^+ (10 mM) or NADH (0.16 mM). Apparent kinetic constants were determined by fitting experimental data to the standard form of the Michaelis-Menten equation. [b]ND, not determined; accurate steady-state kinetic data were unobtainable due to lack of saturation up to 52 mM of *S*-HPC. [c]ND – no detectable activity at concentrations up to 28 mM of *S*-HPC and 100 μg of enzyme.

decline in the k_{cat}/K_m values, which were 71-fold, 139-fold and 23,000-fold lower, respectively, than the corresponding values for the wild-type *rR*-HPCDH1. As previously demonstrated, *rR*-HPCDH1 enzyme is highly specific towards *R*-HPC, exhibiting only 0.5% activity with the opposite enantiomer (*5, 6*). It was further shown that enantioselectivity of *rR*-HPCDH1 enzyme is mostly controlled by k_{cat} values, while K_m values for both enantiomers remain similar. Results presented in Table 4-5 confirm this finding, showing 370-times lower k_{cat} for the opposite enantiomer (*S*-HPC) of *rR*-HPCDH1 and similar K_m values for both isomers. The reaction of *S*-HPC oxidation by Met192Ala mutant was characterized by 18-fold increase in the apparent K_m value, as compared to the wild-type *rR*-HPCDH1, and was analogous to the corresponding increase of the apparent K_m values (24-fold) for *R*-HPC oxidation. When enantioselectivity *(E)* is defined as the ratio of k_{cat}/K_m for the natural enantiomer to k_{cat}/K_m for the opposite enantiomer, the following values were obtained: $E_{RHPCDH1} = 1182$ and $E_{RHPCDH1\_M192A} = 307$. Thus, the Met192Ala mutant of *rR*-HPCDH1 is about four times less efficient in discriminating between the HPC enantiomers than its wild-type counterpart.

Although the enantioselectivity of both enzymes is still controlled largely by the differences in k_{cat} values for the reaction with *R*-HPC vs. *S*-HPC, this difference is significantly smaller for the Met192Ala mutant ($\Delta k_{cat} = 130$ vs. $\Delta k_{cat} = 370$ for *rR*-HPCDH1). Similar activity assays with *S*-HPC performed for Met187Ala / Met192Ala mutant showed no detectable activity, whereas accurate steady-state kinetic data for *S*-HPC oxidation by Met187Ala mutant were unobtainable due to lack of enzyme saturation. Interestingly, however, the Met187Ala mutant showed a specific activity which was four times lower than for Met192Ala mutant at 14 mM of the substrate and remained fairly constant with increasing concentrations of *S*-HPC (up to 52 mM).

Structural Analysis of Met187Leu and Met192Leu Mutants of rR-HPCDH1. To further investigate the importance of the substrate flanking methionines in the active site of *rR*-HPCDH1, Met187 and Met192 were substituted with leucines. This substitution was rationalized by the fact

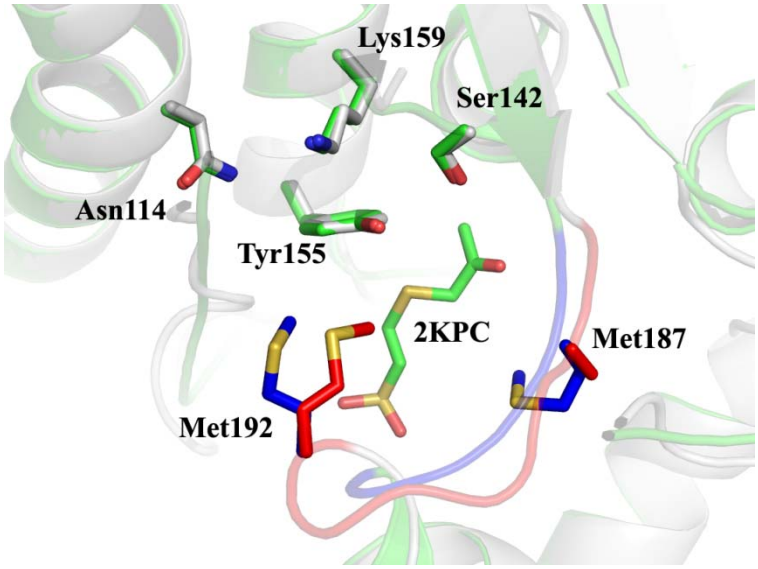

Figure 4-6. Superimposed structures of Met187Ala *rR*-HPCDH1 (grey) and wild-type *rR*-HPCDH1 (green) showing positions of Met187 and Met192 residues on the loop connecting *β*F sheet and αFF1 helix (Met187Ala *rR*-HPCDH1 loop – red, WT *rR*-HPCDH1 loop-blue).

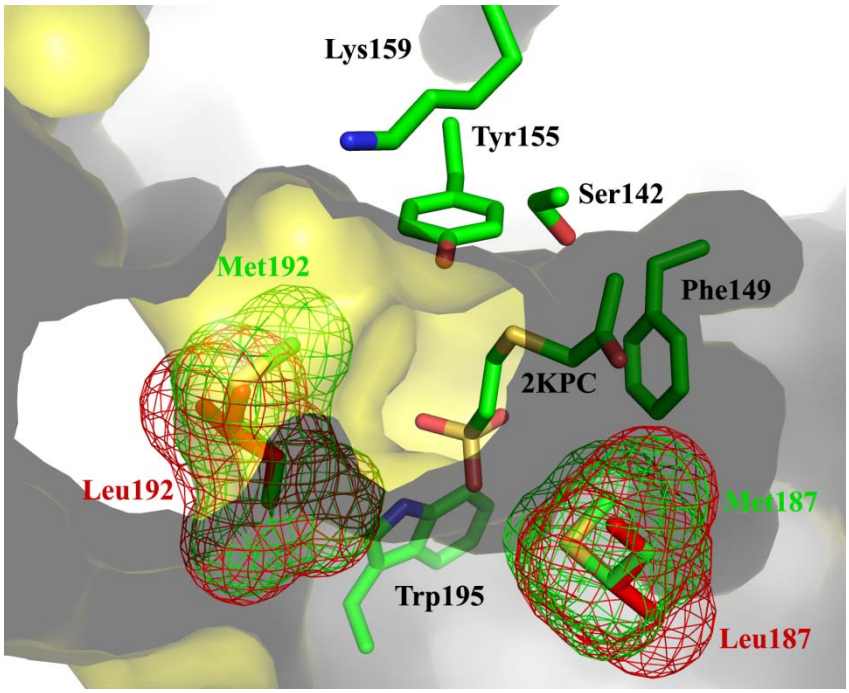

Figure 4-7. Structure of the wild-type *rR*-HPCDH1 showing a channel leading to the active site cavity. Positions of Met187 and Met192 residues (green) were superimposed on the modeled in PyMol Leu187 and Leu192 residues (red). Electron density around residues 187 and 192 highlights differences in shape of the occupied volume.

that the van der Waals volume occupied by leucine is the same as for methionine (*27*) and that the substitution of methionines with leucines within the interior of a enzyme has been reported to increase stability of the resulting mutants (*28*). If the methionines of interest had any role in the catalytic mechanism of the enzyme, these substitutions would allow us to test their contribution, at the same time preserving the compact and solvent protected structure of the active site. Analysis of the X-ray structure of the wild-type *rR*-HPCDH1 shows that methionines 187 and 192 are located on a loop between *β*F sheet and αFF1 short helix (Figure 4-6) in such a way that they approach the substrate from opposite sides. Additionally, Met192 is strategically positioned on a side of a channel leading to the active site cavity, which may suggest its role as a "gate keeper" (Figure 4-7). In the absence of the X-ray structures for Leu187 and Leu192 mutants, modeling studies were done in PyMol 1.2 to visualize possible structural changes resulting from these substitutions. Both residues (Met187 and Met192) were converted to leucines and the most plausible rotamers (in terms of steric clashes) were selected. Superimposition of the methionines with the corresponding leucines revealed noticeable differences in the shape of their electron density clouds. Although the overall volume occupied by leucine and methionine residues is the same (*27*), differences in its distribution, as seen in Figure 4-7, could potentially have some structural consequences. These could include enlargement of the channel leading to the active site, thus making it more accessible to solvent. It could also cause some small but noticeable rearrangement of the neighboring residues in order to accommodate the differently shaped residue, thereby remodeling the active site cavity and introducing different steric constrains posed on the substrate. All of the above could result in alteration of the kinetic parameters and thus should be considered for Met153Leu and Met194Leu mutants.

Analysis of the structural data for the wild-type *rR*-HPCDH1 shows that Met192 is in close proximity of the chiral carbon of the substrate and as such could impose steric constrains favoring only certain orientations of the terminal methyl group (Figure 4-8). This in turn would

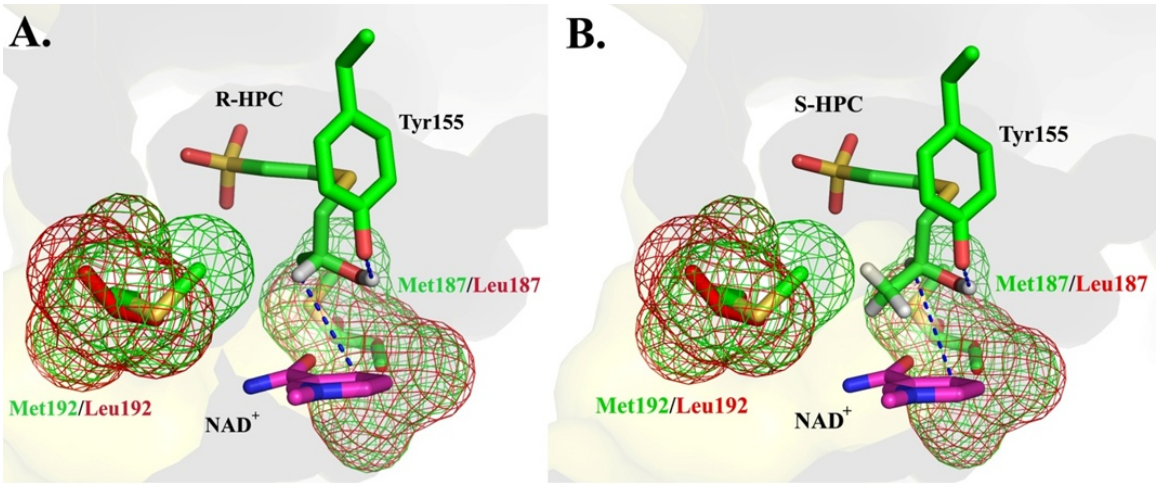

Figure 4-8. Active site of the wild-type *rR*-HPCDH1 with the substrate flanking Met187 and Met192. Superimposed are methionine 192 (green) and leucines 192 (red) to show differences in their electron density and possible interactions with the substrates: (A) *R*-HPC or (B) *S*-HPC. Alignment of the hydroxyl group and hydrogen atom of the substrate with respect to Tyr155 and the nicotinamide ring of NAD^+ is depicted in dashed lines.

determine orientation of the hydroxyl group and the hydrogen atom with respect to Tyr155 and the nicotinamide ring of NAD^+. It was reported previously and again confirmed in this study (Table 4-5), that even though *rR*-HPCDH1 enzyme binds both enantiomers of HPC with similar affinity, only *R*-HPC can be efficiently oxidized to 2-KPC, outcompeting *S*-HPC oxidation with over 400-fold higher k_{cat} (*6*). This difference in k_{cat} values results from a misalignment of the hydrogen atom on C2 carbon of *S*-HPC with respect to the nicotinamide ring of NAD^+, where it gets transferred in form of a hydride ion. Additionally, altered orientation of the hydrogen on *S*-HPC increases the distance of the hydride transfer to NAD^+ as compared to the corresponding distance for *R*-HPC (Figure 4-8).

Two enantiomers were modeled in the active site of *rR*-HPCDH1 in such a way that their hydroxyl groups were identically oriented with respect to the general base Tyr155. As a result, the terminal methyl group and the hydrogen atom at the chiral center switched their positions. When *R*-HPC is present at the active site its methyl group is located between residues 187 and 192, while the hydrogen atom points directly at Met192 (Figure 4-8A). The orientation of the

substrate is proper for catalysis and no steric clashes occur. In contrast, when *S*-HPC is bound in the active site (with identical orientation of the hydroxyl group), its methyl group assumes the position of the hydrogen atom in *R*-HPC which in turn may cause unfavorable steric clashes with Met192 (Figure 4-8B). With regard to Met192Leu mutant it is possible that the substitution of Met192 for shorter leucine could enlarge an otherwise compact active site and thus provide more room for the substrate to assume a proper orientation for catalysis (Figure 4-8). Accordingly, when *S*-HPC is bound in the active site with its terminal methyl group pointing at residue 192, leucine residue in place of methionine could lower steric hindrance necessary for the proper alignment of the hydroxyl group and the hydrogen atom with respect to Tyr155 and the nicotinamide ring of NAD^+. To visualize differences in the special orientation of the chiral center substituents with respect to Met187 and Met192, both enantiomers of HPC alcohol were modeled in the active site of *R*-HPCDH1 (Figure 4-8 and 4-9). Corresponding Leu residues were superimposed on Met residues to envision possible changes in steric constrains imposed on the substrate. Likewise, the achiral product of HPC alcohols oxidation (2-KPC) was analyzed in the active site of *R*-HPCDH1 to visualize possible interactions with methionines and leucines at positions 187 and 192 (Figure 4-10). The binding mode of 2-KPC is displayed as in the X-ray structure of *R*-HPCDH1. The carbonyl group of 2-KPC is shifted away from Tyr155 and the nicotinamide ring of NAD^+ in direction of Phe149 residue, with which it forms several hydrophobic interaction (Figure 4-4). As a result, this orientation brings 2-KPC close to Met187 and suggests that mutagenesis at this position could have a significant effect on the kinetic parameters of 2-KPC reduction catalyzed by *R*-HPCDH1.

Kinetic Analysis of Met187Leu and Met192Leu Mutants of rR-HPCDH1. Enzymatic assays with Met187Leu and Met192Leu mutants were performed in identical conditions as for the corresponding alanine mutants and the wild-type *rR*-HPCDH1. In general, kinetic parameters determined for *R*-HPC and *S*-HPC oxidation as well as for 2-KPC reduction were similar to those obtained for the wild-type enzyme, but with few potentially important differences. As shown

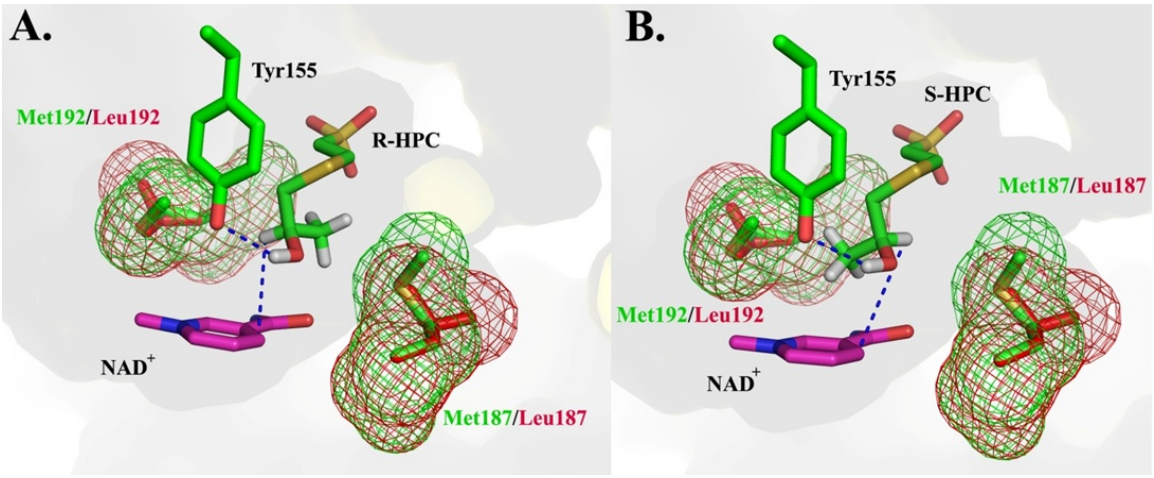

Figure 4-9. Active site of the wild-type *rR*-HPCDH1 with the substrate flanking Met187 and Met192. Superimposed are methionine 187 (green) and leucine 187 (red) to show differences in their electron density and possible interactions with the substrates: (A) *R*-HPC or (B) *S*-HPC. Alignment of the hydroxyl group and hydrogen atom of the substrate with respect to Tyr155 and the nicotinamide ring of NAD^+ is depicted in dashed lines.

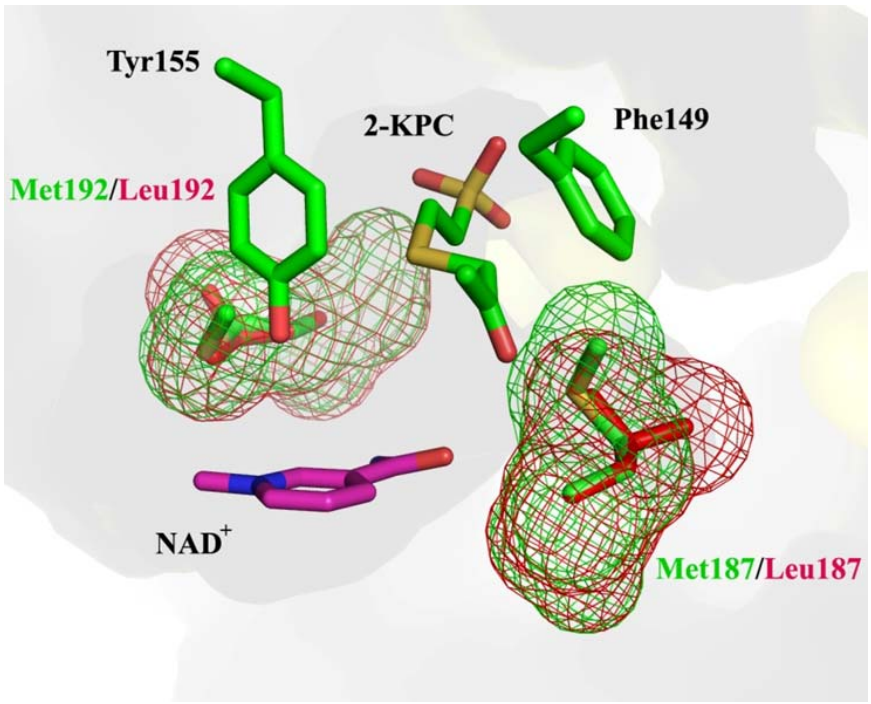

Figure 4-10. Active site of the wild-type *rR*-HPCDH1 with nicotinamide ring of NAD^+ and the substrate flanking Met187 and Met192. Superimposed are methionine 187 (green) and leucine 187 (red) to show differences in their electron density and possible interactions with 2-KPC.

in Table 4-6, the apparent K_m values for Met187Leu mutant with all tested substrates remained fairly similar to those of the wild-type enzyme, implying a structural role of Met187. It is speculated that alternative hydrophobic residues of similar volume (e.g., leucine, norleucine) could effectively substitute the role of Met187 in preserving a compact and solvent free environment of the active site. With respect to the kinetic parameters exhibited by Met192Leu mutant, the apparent K_m values increased three- to five-fold. Although this change was much less dramatic than for the corresponding Met192Ala mutant (18- to 26-fold), it suggested an important role for Met192 at its strategic position, susceptible to even small changes. This observation is supported by the structural data suggesting that differences in shape of the electron density of methionine and leucine at position 192 could result in a larger opening of the channel leading to the active site (Figure 4-7). This in turn would provide easier access for solvent molecules to enter the active site and competitively interact with charged residues otherwise involved in the substrate binding/catalysis. The overall comparison of the apparent K_m values for *R*-HPC, *S*-HPC and 2-KPC displayed by Met187Leu and Met192Leu mutants with respect to the wild-type *rR*-HPCDH1 implies that observed variations in K_m are not substrate dependent, but rather arise from changes inherited by the active site, as a consequence of the mutagenesis. For example, the increase in K_m for Met187Leu mutant is consistent across all tested substrates (1.4- to 1.7-fold), similar to the increase in K_m for Met192Leu mutant (3.3- to 5.2-fold). Surprisingly, in the reaction of *R*-HPC oxidation catalyzed by Met187Leu and Met192Leu mutants, the apparent k_{cat} values increased by 42% and 59%, respectively, as compared to the wild-type enzyme. However, the most significant change in k_{cat} was observed for *S*-HPC oxidation by Met192Leu mutant, where its value increased by almost three-fold. Interestingly, this enhancement of activity was abolished for 2-KPC reduction where the apparent k_{cat} value remained fairly similar to the corresponding value of the wild-type enzyme (Table 4-6). These results may suggest that chirality and/or oxidation state of the substrate are important factors in determining k_{cat} values exhibited by

Table 4-6. Kinetic parameters for *rR*-HPCDH1 WT and its Met187Leu and Met192Leu mutants at 30°C and pH 7.5[a]

Enzyme	K_m (μM)	Change in K_m (x-fold)	V_{max} (units•mg^{-1})	k_{cat} (s^{-1})	Change in k_{cat} (x-fold)	k_{cat}/K_m (M^{-1} s^{-1})
Substrate: *R*-HPC						
R-HPCDH1	82.7 ± 6.8	1.0	83.2 ± 1.9	41.2	1.0	4.98×10^5
M187L	144 ± 10	1.7	118 ± 2.1	58.3	1.4	4.05×10^5
M192L	431 ± 14	5.2	132 ± 1.1	65.4	1.6	1.52×10^5
Substrate: *S*-HPC						
R-HPCDH1	265 ± 72	1.0	0.226 ± 0.014	0.112	1.0	4.22×10^2
M187L	434 ± 69	1.6	0.195 ± 0.006	0.097	0.87	2.23×10^2
M192L	881 ± 54	3.3	0.632 ± 0.011	0.313	2.8	3.55×10^2
Substrate: 2-KPC						
R-HPCDH1	72.4 ± 12	1.0	55.7 ± 2.9	27.6	1.0	3.81×10^5
M187L	104 ± 11	1.4	72.2 ± 2.4	35.8	1.3	3.43×10^5
M192L	341 ± 38	4.7	48.0 ± 1.9	23.8	0.86	6.99×10^4

[a]Assay for *R*-HPC and *S*-HPC oxidation by *rR*-HPCDH1 WT and Met mutants contained 1.0 μg and 46 μg of enzyme, respectively. Assay for 2-KPC reduction contained 1.0 μg of enzyme. Apparent k_{cat} and K_m values are reported as means ± standard deviations. All assays were performed at 30 ˚C with fixed concentrations of NAD^+ (10 mM) or NADH (0.16 mM). Apparent kinetic constants were determined by fitting experimental data to the standard form of the Michaelis-Menten equation.

Met192Leu. Analysis of the structural data supports this observation showing that the steric constrains of Met192 in the active site of *rR*-HPCDH1 with the terminal methyl group of *S*-HPC might be involved (Figure 4-8). Accordingly it is speculated that the observed three-fold increase in k_{cat} exhibited by the Met192Leu mutant is caused by the substitution of Met192 with a shorter leucine which in turn could provide more degrees of freedom for *S*-HPC to assume proper orientation for catalysis (Figure 4-8). Lack of the similar increase in k_{cat} for the oxidation of *S*-HPC by the Met187Leu mutant seems to further support this hypothesis (Table 4-6). The same rationale is believed to apply in the case of the Met187Leu mutant catalyzed *R*-HPC oxidation

where the terminal methyl group of the substrate is oriented towards residue 187 (Figure 4-9). Substitution to leucine at this position would remove excessive steric restrictions and thus allow the enzyme to orient *R*-HPC in a fashion more favorable for catalysis. This could explain an increase in k_{cat} value revealed by Met187Leu (Table 4-6). Unexpectedly a similar increase in the k_{cat} value is observed for *R*-HPC oxidation by the Met192Leu mutant. Although this increase can be regarded as moderate compared to the corresponding increase in k_{cat} observed for *S*-HPC oxidation (59% vs. 280%, respectively), nevertheless this observation suggests an important role of Met192 in the catalytic function of *rR*-HPCDH1, which cannot be explained strictly in terms of steric effects. This increase in the apparent k_{cat} value is accompanied by over five-fold increase in the apparent K_m value. Consequently, despite the positive effect of Met192 to leucine substitution on the turnover number, the overall catalytic efficiency for *R*-HPC oxidation decreased by more than three-fold relative to the wild-type enzyme. Thus, choice of methionine in this particular position appears to be optimal and perfectly tuned by many rounds of evolutionary selection. It should be noted at this point that the Met192 residue is located only 4.6 Å away from the general acid/base residues (Tyr155) and thus any changes made to its closest environment could potentially have significant implications on the enzyme's catalytic activity (e.g., increase in k_{cat}). Once available, the X-ray structure of the Met192Leu mutant will undoubtedly aid in a better understanding of the observed changes in the kinetic parameters. Also, additional kinetic assays with other chiral alcohols (e.g., *R*- and *S*-2-hexanol or 3-hexanol) and their corresponding ketones as substrates for the Met192Leu mutant may prove useful.

With regard to the 2-KPC reduction catalyzed by *rR*-HPCDH1 Met192Leu mutant, the most interesting observation was the 30% increase in the apparent k_{cat} value exhibited by Met187Leu. It is speculated that in the ketone reduction catalyzed by *rR*-HPCDH1 steric factors associated with the differences in shape of leucine and methionine residues play an important role in positioning of the substrate for catalysis (Figure 4-9). These, together with the differences in geometry between the ketone and alcohol functional groups (trigonal planer vs. tetrahedral) and

the occupied volume might by a reason why the k_{cat} values for the ketones are less altered than those observed for the alcohols (Table 4-6).

Finally, since enantioselectivity of *rR*-HPCDH1 is largely controlled by k_{cat} (*6*), it is not surprising that differences in the apparent k_{cat} values for the Met187Leu and Met192Leu mutants relative to the wild-type enzyme had a direct effect on their enantioselectivity. For the Met187Leu mutant enantioselectivity increased by 53% ($E_{R\text{-HPCDH1}}$ = 1182 vs. $E_{R\text{-HPCDH1\_M187L}}$ = 1813), whereas for the Met192Leu mutant it decreased by almost three-fold ($E_{R\text{-HPCDH1\_M192L}}$ = 428). The latter change resulted from an increase in catalytic efficiency exhibited by the Met192Leu mutant in an oxidation of the opposite enantiomer (*S*-HPC), which was mostly dictated by a three-fold increase in the apparent k_{cat} value. Based on the presented herein data it is proposed that the methionines at position 187 and 192 are involved in modulating the enantioselectivity of the *rR*-HPCDH1 enzyme towards the HPC enantiomers. This hypothesis could be further tested through the additional kinetic analysis of the new site-directed mutants such as Met187Ile or Met192Ile.

Structural Analysis of Met153Ala and Met194Ala Mutants of rS-HPCDH3. As revealed by the homology model, a characteristic feature of *rS*-HPCDH3 active site is the presence of two methionine residues situated on both sides of the substrate binding pocket. These are Met153 and Met194. Both residues appear 41 residues apart in the amino acid sequence of *S*-HPCDH3 and are located on two separate loops dividing β sheets and α helixes (Figure 4-11). In the homology model however they are oriented in a similar way to the corresponding methionines in *R*-HPCDH1, namely flanking the substrate from both sides (Figure 4-6 and 4-12). By comparison, Met187 and Met192 in *R*-HPCDH1 are located on the same loop, separated by only four residues. To investigate the role of Met153 and Met194 in *S*-HPCDH3 in substrate binding and catalysis, both residues were mutated to alanines. The kinetic studies of the site-directed mutants of *S*-HPCDH3, supported by the structural analysis, complement those of *R*-HPCDH1 and thus provide an insight to the importance of the active site methionines in controlling the

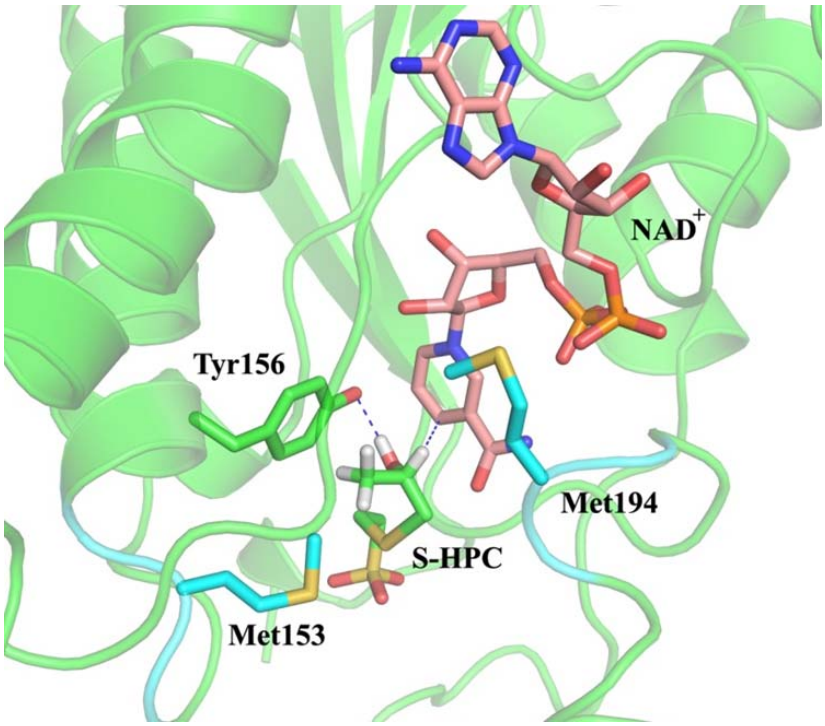

Figure 4-11. Structural representation of the active site of rS-HPCDH3 based on the homology model, with highlighted positions of Met153 and Met194 (cyan) located on the separate loops connecting β sheets and α helixes.

enantioselectivity of the HPCDH enzymes. The X-ray structure of *R*-HPCDH1 reveals that Met192 is involved in binding of the NAD^+ cofactor. As shown in Figure 4-12A possible interactions include: hydrogen bonding with the phosphate groups and hydrophobic interactions with the ribose ring of the cofactor. Superimposition of the homology model of *S*-HPCDH3 with the X-ray structure of *R*-HPCDH1 suggests a similar role of Met194 in *S*-HPCDH3 (Figure 4-12A). In contrast Met187 of *R*-HPCDH1 is positioned around the CoM moiety of the substrate. Similar orientation of Met153 with respect to the general base (Tyr156) and the CoM moiety of the substrate is predicted for *S*-HPCDH3 as indicated by the homology model (Figure 4-12B).

Similar to *R*-HPCDH1, Met153 and Met194 in *S*-HPCDH3 are situated at the entrance of a channel leading to the active site, suggesting that both methionines may play a role of "gate

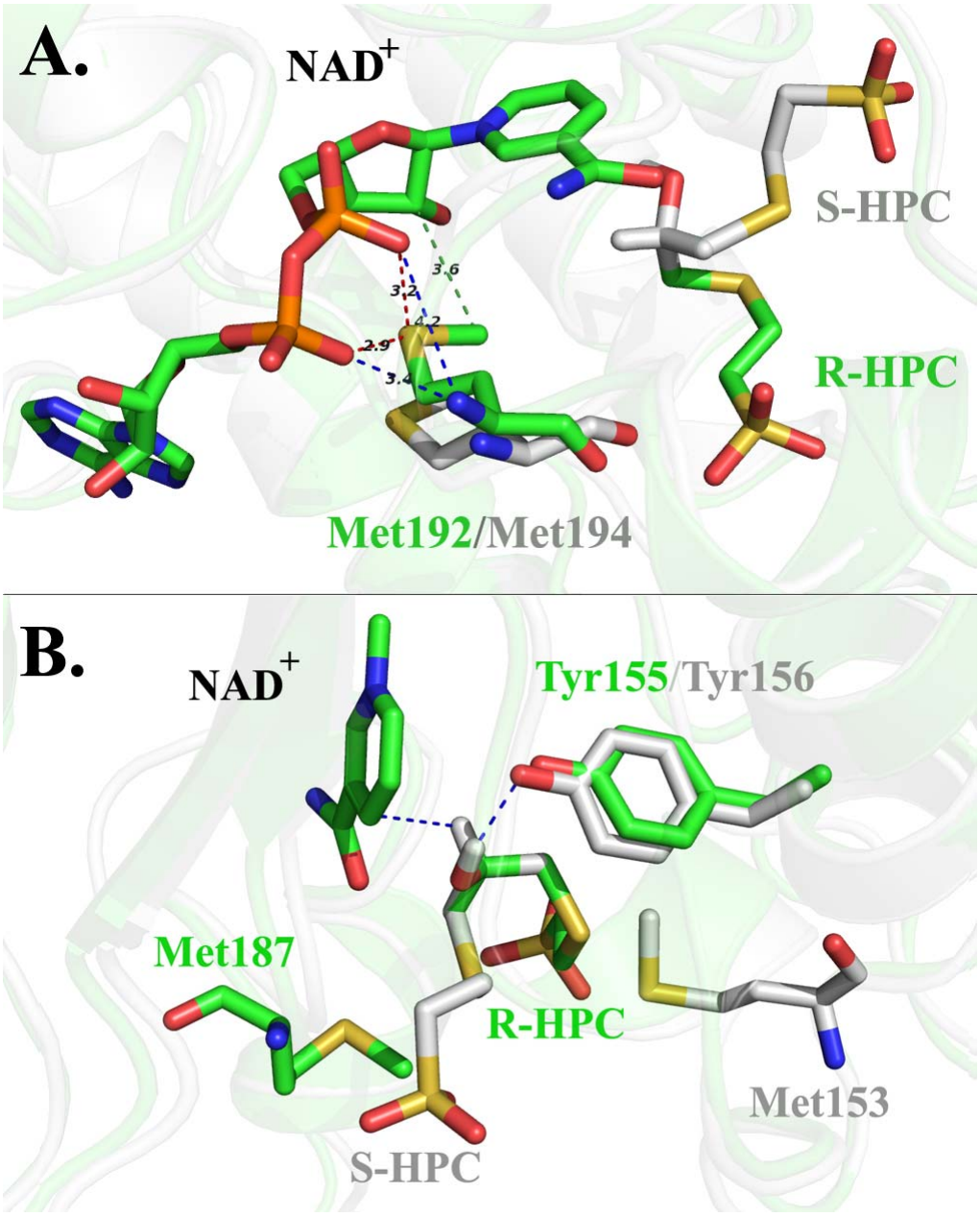

Figure 4-12. Superimposed structure of *rR*-HPCDH1 (green) and the homology model of *rS*-HPCDH3 (grey). (A) Superimposed are Met192 of *rR*-HPCDH1 (green) and Met194 of *rS*-HPCDH3 (grey) to show possible interactions with NAD^+ cofactor. Distances are shown in Å. (B) Superimposed are Met187 of *rR*-HPCDH1 (green) and Met153 of *rS*-HPCDH3 (grey) to show their orientation relative to each other and the respective substrates.

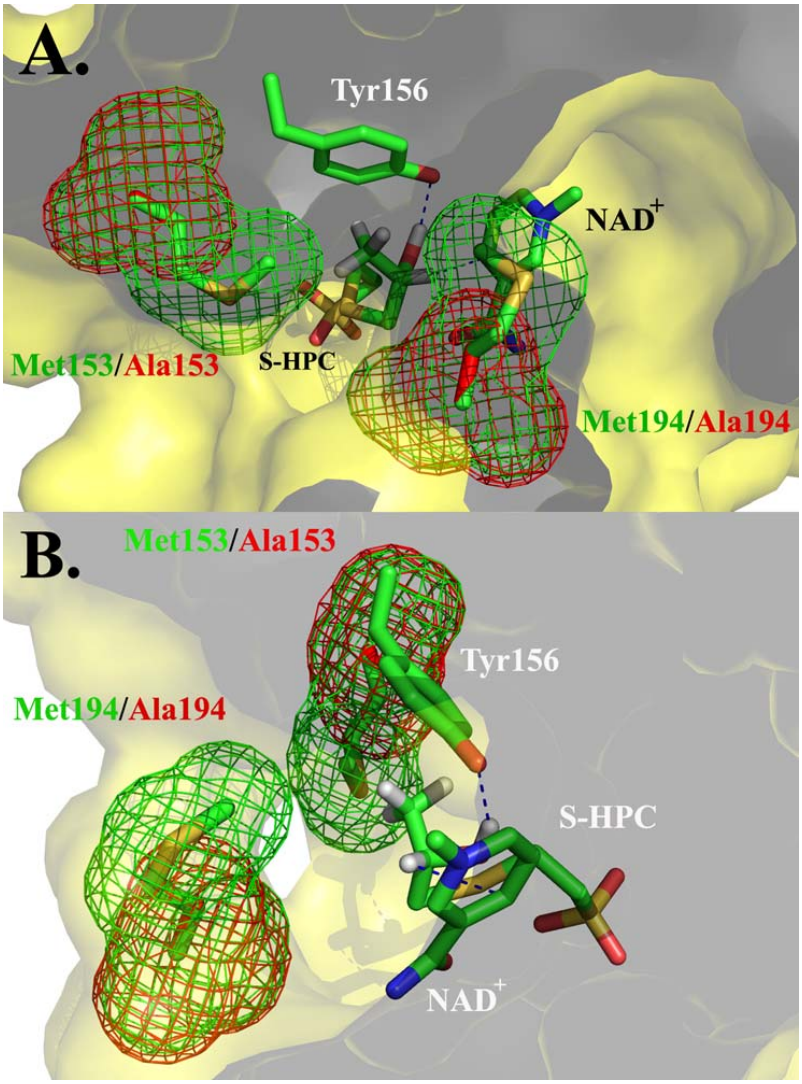

Figure 4-13. Homology model of *rS*-HPCDH3 with the substrate *S*-HPC and the cofactor NAD^+ bound. Superimposed are Met153 and Met194 residues (green) with Ala187 and Ala192 residues (red) shown with their predicted electron density to highlight differences in shape and occupied volume. (A) Position of Met153 and Met194 with respect to two channels leading to the active site cavity. (B): Alternative view on Met153 and Met194 in the active site highlighting strategic position of Met194 at the interface of two channels.

keepers" (Figure 4-13). Since no X-ray structures are available for Met153Ala and Met194Ala mutants, modeling studies were conducted using PyMol 1.2 to visualize possible structural changes introduced by the substitution. Superimposition of Met153 and Met194 on the

corresponding alanine residues (Ala153 and Ala194) reveals a large solvent accessible pocket created around the active site, which was previously well shielded from the surroundings (Figure 4-13). This could allow non-specific interactions of the critical active site residues with the solvent thus significantly altering binding and catalysis of the physiological substrates. It appears that Met194, at its bridging position between two channels, might be susceptible to minor changes which would likely affect the binding affinity of the substrate and the cofactor.

Kinetic Analysis of Met153Ala and Met194Ala Mutants of rS-HPCDH3. Table 4-7 summarizes the effect of methionine to alanine substitutions at positions 153 and 194 on the kinetic parameters of *rS*-HPCDH3, when *R*-HPC, *S*-HPC and 2-KPC were variable substrates and NAD^+/NADH was the fixed saturating substrate. The kinetic analyses of wild-type *rS*-HPCDH3 were also performed in identical conditions for side by side comparison with the mutated variants. The apparent k_{cat} and K_m values determined for *R*-HPC and *S*-HPC oxidation, and 2-KPC reduction, by *rS*-HPCDH3 were comparable to those reported previously (*6*). The most significant changes for *rS*-HPCDH3 methionine mutants were observed in the apparent K_m values (Table 4-7). Specifically, in *S*-HPC oxidation catalyzed by Met153Ala and Met194Ala mutants the apparent K_m values increased by about 100-fold, as compared to the wild-type enzyme. At the same time, the apparent K_m values for *R*-HPC oxidation and 2-KPC reduction by Met194Ala mutant increased by seven- and 24-fold, respectively. These results are analogous to the Met187Ala and Met192Ala mutants of *rR*-HPCDH1 and suggest a similar role for both methionine residues in protecting the active side from non-productive interactions with the solvent molecules. Structural analysis of the homology model of *rS*-HPCDH3 shows that Met153 and Met194 are lining a small channel leading to the active site cavity, and thus could serve a role of "gate keepers" (Figure 4-13). The corresponding kinetic parameters for Met153Ala mutant with *R*-HPC and 2-KPC could not be determined due to the lack of detectable activity. This is not surprising considering that in the reaction of *S*-HPC oxidation Met153Ala mutant showed minimal activity, exhibiting five-orders of magnitude decrease in catalytic efficiency (k_{cat}/K_m).

Table 4-7. Kinetic Parameters for *rS*-HPCDH3 WT and its Methionine Mutants at 30°C and pH 7.5[a]

Enzyme	K_m (μM)	Change in K_m (x-fold)	V_{max} (units•mg^{-1})	k_{cat} (s^{-1})	Change in k_{cat} (x-fold)	k_{cat}/K_m (M^{-1} s^{-1})
			Substrate: *S*-HPC			
WT	135.2 ± 9.7	1.00	57.1 ± 1.0	25.8	1.0	1.91×10^5
M153A	13990 ± 1100	103	0.188 ± 0.0048	0.0848	0.0033	6.06×10^0
M194A	13440 ± 850	99.4	93.2 ± 2.3	42.1	1.6	3.13×10^3
M194L	381 ± 54	2.82	12.3 ± 0.43	5.53	0.21	1.45×10^4
			Substrate: *R*-HPC			
WT	8217 ± 570	1.00	4.18 ± 0.10	1.89	1.0	2.29×10^2
M153A	ND[b]		ND[b]	ND[b]		ND[b]
M194A	57060 ± 4500	6.94	0.677 ± 0.025	0.310	0.16	5.35×10^0
M194L	15360 ± 2449	1.87	1.30 ± 0.091	0.585	0.31	3.81×10^1
			Substrate: 2-KPC			
WT	223.8 ± 17	1.00	24.3 ± 0.42	11.0	1.0	4.89×10^4
M153A	ND[b]		ND[b]	ND[b]		ND[b]
M194A	5367 ± 860	24.0	11.7 ± 0.71	5.30	0.48	9.87×10^2
M194L	2229 ± 423	9.96	6.16 ± 0.38	2.78	0.25	1.25×10^3

[a]Assay for *S*-HPC oxidation contained the following amounts of enzyme: 1.0 μg of *rS*-HPCDH3 WT and M194L, 118 μg of M153A and 1.5 μg of M194A. Assay for *R*-HPC oxidation contained the following amounts of enzyme: 5 μg of *rS*-HPCDH3 WT, 29 μg of M194L, 118 μg of M153A and 100 μg of M194A. Assay for 2-KPC reduction contained the following amounts of enzyme: 1.0 μg of *rS*-HPCDH3 WT, 2.0 μg of M194L, 118 μg of M153A and 1.5 μg of M194A. Apparent k_{cat} and K_m values are reported as means ± standard deviations. All assays were performed at 30 ˚C with fixed concentrations of NAD^+ (10 mM). Apparent kinetic constants were determined by fitting experimental data to the standard form of the Michaelis-Menten equation. [b]ND – no detectable activity at concentrations up to 34 mM.

Therefore by analogy to the wild-type enzyme the reaction of *R*-HPC and 2-KPC catalyzed by the Met153Ala mutant would be expected to proceed with even lower values of k_{cat}/K_m, possibly below detectable levels. The dramatic decrease in k_{cat}/K_m observed for

Met153Ala mutant is a result of over 100-fold higher K_m value and over 300-fold lower k_{cat} value, relative to wild-type *rS*-HPCDH3. Substitution of Met153 to Ala renders an enzyme practically inactive at the physiological concentrations of substrates and cofactors, thus suggesting that this residue is especially important in substrate binding and catalysis. The homology model of *rS*-HPCDH3 shows that Met153 is in a close proximity of the general acid/base (Tyr156). This suggests that it might participate in its positioning for catalysis and/or in protecting Tyr156 from the solvent. With respect to the apparent k_{cat} values, Met194Ala mutant revealed two- to six-fold decrease in its value for 2-KPC and *R*-HPC as substrates, respectively. Interestingly however, in *S*-HPC oxidation the apparent k_{cat} value increased by 63%, implying that similar to Met192Leu mutant of *rR*-HPCDH1 some steric restrictions imposed by Met194 could be involved in the improved substrate positioning for catalysis. It is speculated that substitution of Met194 to alanine (significantly smaller in volume) could enlarge the active site and provide the substrate with more conformational freedom to assume the most suitable position for catalysis. Despite the increased apparent k_{cat} value, the overall catalytic efficiency for the Met194Ala mutant decreased over 60-fold compared to wild-type *rS*-HPCDH3, due to the highly elevated apparent K_m value. Finally, an intriguing observation coming from the kinetic data is the disproportionately high increase in the apparent K_m values for *S*-HPC oxidation, as compared to the corresponding increase for 2-KPC and *R*-HPC displayed by the same mutants (Table 4-7).

Structural Analysis of Met153Leu and Met194Leu Mutant of rS-HPCDH3. To further investigate the role of the substrate flanking methionines in the active site of *rS*-HPCDH3, methionines 153 and 194 were substituted with leucines. This substitution was chosen based on the similarities of both the residues and was intended to preserve the compact and solvent inaccessible structure of the active site. Modeling studies (in PyMol) where Met153 and Met194 were converted to leucines and then superimposed on the homology model of the wild-type *rS*-HPCDH3, revealed noticeable differences in the shape of their electron density clouds. Specifically, the side chain of Met153 in its most favorable conformation is oriented towards the

opening of the channel thus determining its diameter. When shorter in length Leu153 was modeled at the same position, it became clear that this substitution will likely result in a wider opening of the channel (Figure 4-14). A similar effect is believed to apply in the case of Met194, which is bridging the two channels leading to the active site cavity. Together, the Met to Leu substitutions could grant an easier access of the surrounding solvent into an otherwise compact active site of *rS*-HPCDH3, thus permitting non-productive interactions with charged amino acids (e.g., Tyr156, Arg211 or Lys214). Therefore, as stated for methionine to alanine mutants and observed again here, one of the proposed functions for Met153 and Met194 is to serve a role of "gate keepers" in sealing the active site from the immediate solvent environment.

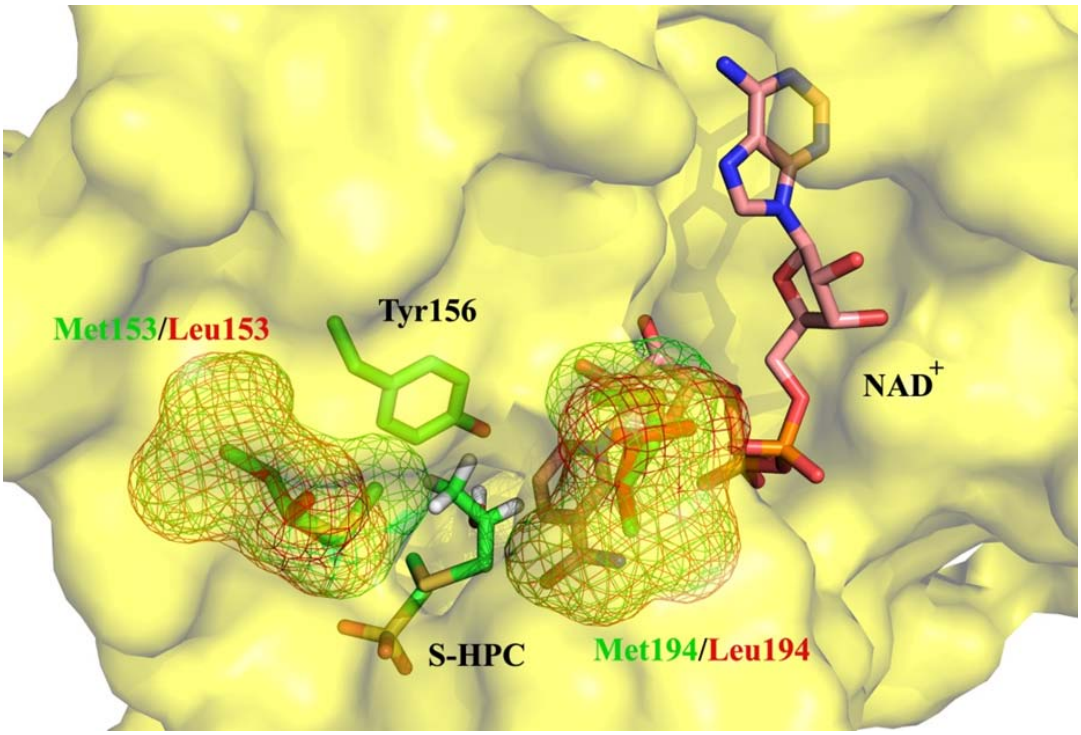

Figure 4-14. Homology model of *rS*-HPCDH3 showing the active site cavity with S-HPC and NAD+ bound. Superimposed are Met153 and Met194 residues (green) with Leu187 and Leu192 residues (red) shown with their predicted electron density to highlight differences in shape and occupied volume.

To shed more light on the possible involvement of both methionines in controlling enantioselectivity of *rS*-HPCDH3, two PyMol models were built with *R*-HPC and *S*-HPC bound in the active site. Both enantiomers were positioned in such a way that their hydroxyl groups were identically oriented with respect to the general base Tyr156. It has been proposed that the enantioselectivity of *rS*-HPCDH3 is largely dictated by changes in K_m values (over 60-fold difference in K_m for *S*- and *R*-enantiomers) as a result of steric clashes imposed by the presence of the methyl group on the chiral carbon of *R*-HPC (*6*). It was therefore intriguing to test the possiblilty of the substrate flanking methionines being involved in chiral discrimination. When *S*-HPC is bound in the active site with its hydroxyl group and the hydrogen atom in the proper orientation with respect to Tyr156 and the nicotinamide ring of NAD^+, the terminal methyl group points towards Met153 (Figure 4-17A). No steric clashes are observed for this enantiomer. However, when *R*-HPC is present in the active site (with the identical orientation of the hydroxyl group) its hydrogen atom becomes misaligned relative to the nicotinamide ring of NAD^+, while the terminal methyl group (now in the position of the hydrogen atom of *S*-HPC) clashes with the nicotinamide ring of NAD^+ (Figure 4-17B). Moreover, any rotation of the chiral center around C2 – C3 bond to lessen the observed steric hindrance would result in further clashes of the hydroxyl group with the nicotinamide ring plus, even greater misalignment of both: the hydroxyl group and the hydrogen atom of the substrate. Clearly only *S*-HPC can be effectively bound in the active site of *rS*-HPCDH3 to fulfill the required alignment for catalysis and avoid unfavorable steric clashes. As shown in Figure 4-17A, a compact structure of the active site imposes steric restrictions on *S*-HPC to bind in the specific manner.

Structural analysis of Met153 and Met194 substitution to leucines (in PyMol) suggests some minor changes to the active site environment directly involved in catalysis. Specifically, the shorter in length Leu153 residue is likely to remove extensive steric hindrance imposed on the terminal methyl group of *S*-HPC (Figure 4-15A and 4-17A). It is speculated that the ethyl group substituent at the chiral center could probably be accommodated as a result of the enlarged

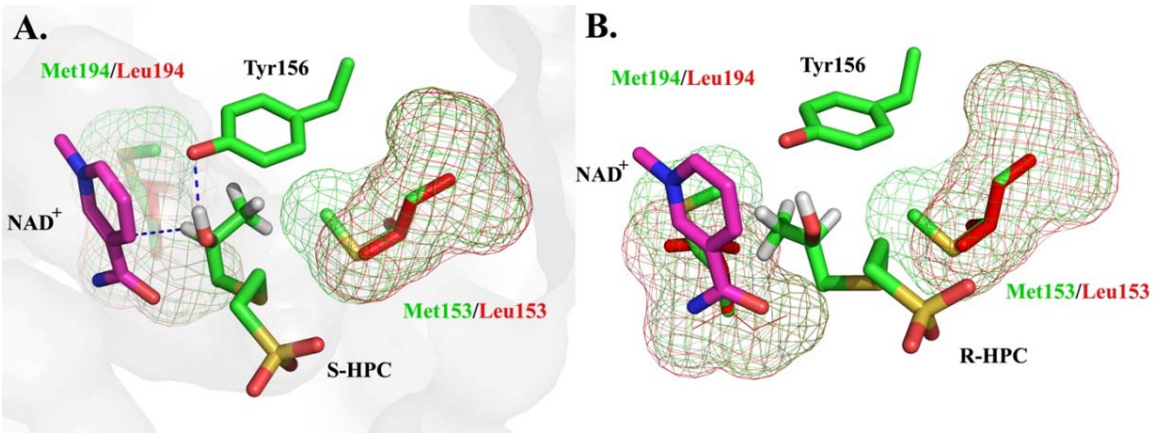

Figure 4-15. Active site of *rS*-HPCDH3 highlighting an orientation of the substrates with respect to Met153. Superimposed are Met153 (green) and Leu153 (red) to show differences in their electron density and possible interactions with substrates: *S*-HPC (Panel A) or *R*-HPC (Panel B). Alignment of the hydroxyl group and the hydrogen atom of the substrate with respect to Tyr156 and nicotinamide ring of NAD^+ are depicted in dashed lines.

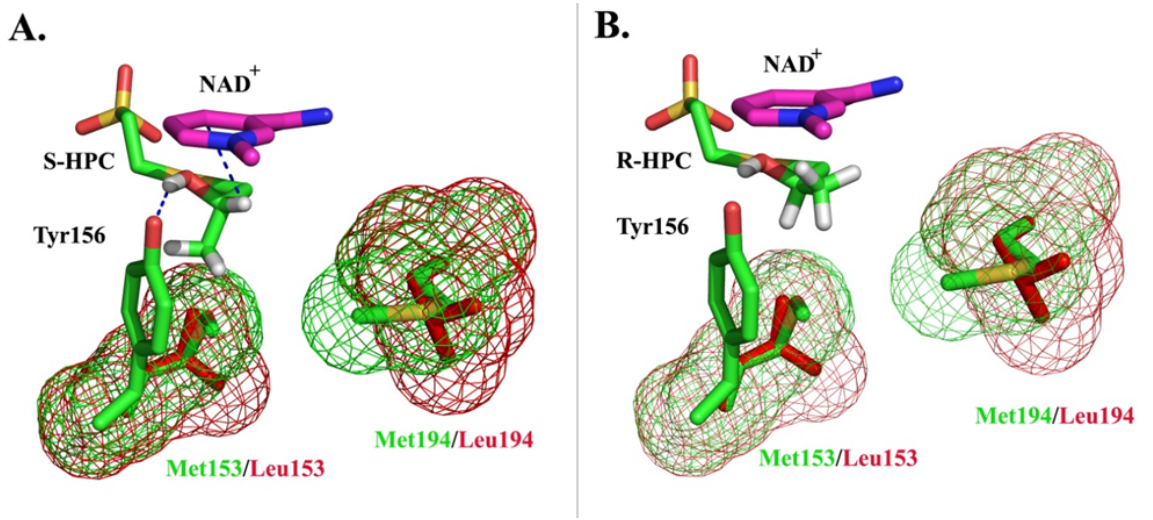

Figure 4-16. Active site of *rS*-HPCDH3 highlighting an orientation of the substrates with respect to Met194. Superimposed are Met194 (green) and Leu194 (red) to show differences in their electron density and possible interactions with substrates: *S*-HPC (Panel A) or *R*-HPC (Panel B). Alignment of the hydroxyl group and the hydrogen atom of the substrate with respect to Tyr156 and nicotinamide ring of NAD^+ are depicted in dashed lines.

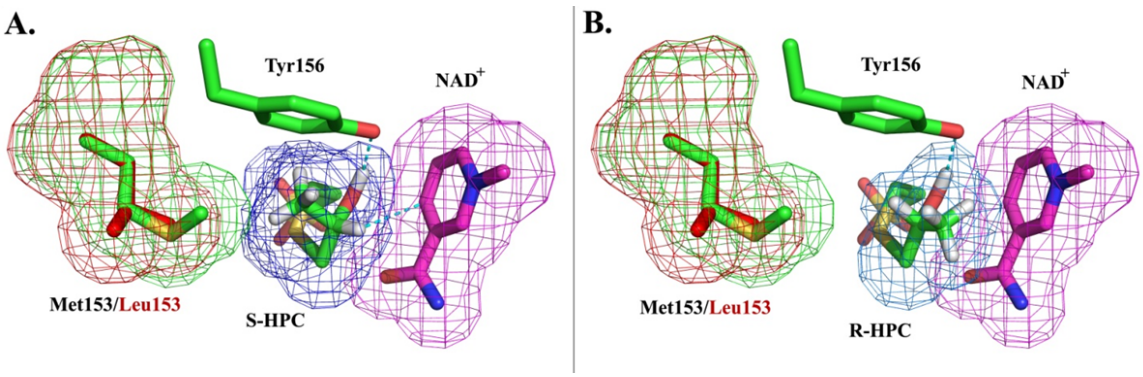

Figure 4-17. Active site of *rS*-HPCDH3 (homology model) highlighting steric effects of docking two enantiomeric forms of HPC alcohol. Superimposed are Met153 (green) and Leu153 (red) to show differences in their electron density and possible interactions with the substrates: *S*-HPC (Panel A) or *R*-HPC (Panel B). Alignment of the hydroxyl group and the hydrogen atom of the substrate with respect to Tyr156 and nicotinamide ring of NAD^+ are depicted in dashed lines.

"methyl binding pocket". The position of Met194 further away from the "business" end of the substrate does not seem to have any direct influence on the enantioselectivity of *rS*-HPCDH3 (Figure 4-16). Accordingly, Met194 to leucine substitution is not expected to significantly alter the enantioselectivity of *rS*-HPCDH3, which as noted before is controlled by means of K_m. On the other hand, the close proximity of Met194 to NAD^+ suggests its role in the cofactor binding through hydrophobic and hydrogen bond interactions. If this hypothesis holds true, one would expect noticable changes in binding affinity for NAD^+ exhibited by the Leu194 mutant. This however requires additional kinetic analysis and has not been further pursued in this study.

Kinetic Analysis of Met194Leu Mutant of rS-HPCDH3. The substrate flanking methionines (Met153 and Met194) in the active site of *rS*-HPCDH3 were substituted with leucines. Although Met194Leu mutant was cloned and expressed in a fully active form, numerous efforts to isolate Met153Leu were unsuccessful due to low expression level of the mutant protein. In general, the kinetic parameters for Met194Leu mutant of *rS*-HPCDH3 were fairly similar to the corresponding parameters exhibited by the wild-type *rS*-HPCDH3, however with some

interesting differences (Table 4-7). Specifically, the apparent k_{cat} values for all substrates used in the assay decreased by three- to five-fold. Simultaneously, the apparent K_m values for the oxidation of *S*-HPC and *R*-HPC increased by two- to three-fold, while the apparent K_m value for the reduction of 2-KPC increased by 10-fold. Differences in K_m values could suggest that the oxidation state (ketone vs. alcohol) and geometry (trigonal planar vs. tetrahedral) of the substrate might be important in determining its binding affinity. Analysis of the homology model of *rS*-HPCDH3 corraborate an important role of Met194 located on the surface between two channels leading to the active site (Figure 4-13). Based on this model Met194 is proposed to form part of a lining of the active site and contributes to NAD^+ binding (Figure 4-12A). Superimposition of the homology model of *rS*-HPCDH3 and the X-ray structure of *rR*-HPCDH1 suggests that Met194 of *rS*-HPCDH3 is positioned in the similar fashion to Met192 of *rR*-HPCDH1 and may form hydrogen bond interaction with the phosphate groups and hydrophobic interactions with the ribose ring of NAD^+.

Initial Velocity Studies with a Substrate Analogue. 2-(2-hydroxyethylthio) ethanesulfonate (HEC) is an achiral mimic of both *R*-HPC and *S*-HPC in which the terminal methyl group is replaced by hydrogen. HEC was previously shown to be a substrate for both the *R*- and *S*-HPCDH enzymes with identical K_m values, suggesting that for this substrate the CoM moiety and hydroxyl group have become equal determinants in binding affinity (assuming K_m approximates affinity). Structural and kinetic analysis of the methionine mutants presented above suggested that these residues might be involved in modulating enantioselectivity of the enzyme through steric interactions with the C2 methyl group of the substrate. To test this hypothesis HEC was used as a substrate for Met187Leu and Met192Leu mutants of *rR*-HPCDH1 along with Met194Leu mutant of *rS*-HPCDH3. Presented in Table 4-8 are kinetic parameters for HEC oxidation determined at a fixed saturating concentration of NAD^+ (10 mM) and a variable concentration of HEC at pH 7.5. For comparison purposes and to better visualize the effect of the terminal methyl group on the biding affinity of the analyzed substrates secondary tables were

assembled (Table 4-9 and 4-10). The first important observation coming out from the data presented here is a significantly higher K_m for HEC as compared to K_m values for the corresponding natural substrates of *R*- and *S*-HPCDH enzymes, thus highlighting the contribution of the C2 methyl group to substrate binding (Table 4-9 and 4-10). These differences range from two-fold for *rS*-HPCDH3 Met194Leu mutant to 16-fold for *rR*-HPCDH1 Met192Leu mutant. Similar comparison of k_{cat} values (Table 4-6 and 4-8) also suggests an important role of the methyl group in determining proper orientation of the substrate for catalysis. This was especially articulated for the *rR*-HPCDH1 enzyme where the apparent k_{cat} value for HEC oxidation decreased by 75-fold with respect to *R*-HPC oxidation, while the corresponding decrease of k_{cat} value in *rS*-HPCDH3 was only seven-fold. This corroborates well with the previous results showing that the enantioselectivity of *rR*-HPCDH1 is controlled by k_{cat}, while in *rS*-HPCDH3 it is dictated in terms of K_m (*6*). The oxidation of HEC by Met187Leu mutant and wild-type *rR*-HPCDH1 shows identical values of apparent k_{cat} and apparent K_m thus suggesting that Met187 plays an important role in the binding and catalysis of the physiological substrates (*R*- and *S*-HPC), but not substrates analogs lacking the terminal methyl group (e.g., HEC). Activity assays of Met187Leu mutant with *R*-HPC and *S*-HPC revealed 74% and 64% increase in the apparent K_m values, respectively, compared to wild-type *rR*-HPCDH1 (Table 4-6). Kinetic parameters for HEC oxidation by Met192Leu mutant were significantly different from those of the wild-type enzyme. In particular, the values of apparent K_m and apparent k_{cat} increased by seven- and 1.4-fold, respectively. Especially dramatic change in K_m value exhibited by Met192Leu mutant relative to the corresponding values of K_m exhibited by Met187Leu mutant and the wild-type enzyme are nicely visualized by the saturation curves of steady-state kinetics in Figure 4-18A. Interestingly also the oxidation of *R*- and *S*-HPC by the Met192Leu mutant was characterized by highly elevated K_m values and a concomitant increase in k_{cat} values (Table 4-6). Similar trends observed for substrates differing in a substitution at C2 carbon imply that the presence of the terminal methyl group on the substrate may not be responsible for the increased K_m values

exhibited by Met192Leu mutant. Accordingly, higher turnover may not be substrate dependent, but rather a result of some rearrangement of the active site architecture induced by Met192 substitution to leucine. This is an important observation suggesting a critical role of Met192 strategically positioned at the entrance to active site and in a close proximity of the general acid/base residue (Tyr155).

Table 4-8. Kinetic parameters for the oxidation of HEC by *R*-HPCDH, *S*-HPCDH and their methionine mutants at pH 7.5[a]

Enzyme	K_m (μM)	Change in K_m (x-fold)	V_{max} (units•mg^{-1})	k_{cat} (s^{-1})	Change in k_{cat} (x-fold)	k_{cat}/K_m (M^{-1} s^{-1})
			R-HPCDH1			
WT	958.7 ± 107	1.0	1.10 ± 0.03	0.55	1.00	5.70×10^2
M187L	1020 ± 81.7	1.1	1.09 ± 0.02	0.54	0.93	5.28×10^2
M192L	6841 ± 608	7.1	1.58 ± 0.05	0.78	1.4	1.15×10^2
			S-HPCDH3			
WT	974.7 ± 248	1.0	8.34 ± 0.6	3.8	1.00	3.86×10^3
M194L	674.1 ± 65.5	0.7	5.36 ± 0.1	2.4	0.93	3.59×10^3

[a]Assay for HEC oxidation by *rR*-HPCDH1 WT and Met mutants contained 20 μg and 34 μg of enzyme, respectively. Assay for HEC oxidation by *rS*-HPCDH3 WT and Met mutant contained 4.0 μg of enzyme. Apparent k_{cat} and K_m values are reported as means ± standard deviations. All assays were performed at 30 ˚C with fixed concentrations of NAD^+ (10 mM). Apparent kinetic constants were determined by fitting experimental data to the standard form of the Michaelis-Menten equation.

The kinetic parameters for HEC oxidation by Met194Leu mutant of *rS*-HPCDH3 revealed that although values of the apparent k_{cat} and the apparent K_m changed noticeably compared to the wild-type enzyme, the overall catalytic efficiency (k_{cat}/ K_m) remained the same. Specifically, a 31% increase in binding affinity (expressed in terms of K_m) was compensated by a similar decrease in value of the k_{cat} (37%). In contrast the k_{cat}/ K_m for oxidation of *S*-HPC and *R*-

HPC decreased dramatically (13- and six-fold, respectively) for the same mutant enzyme (Table 4-7). As mentioned before, *rS*-HPCDH3 is believed to discriminate between the two enantiomeric forms of HPC by means of steric effects that reflect on their K_m values. Accordingly, catalysis of the opposite enantiomer is characterized by over 60-times higher K_m value. Since the steric clashes with the terminal methyl group of the substrate are at the origin of the enantioselectivity of *rS*-HPCDH3, it is likely that removal of this methyl group from the chiral center of the substrate could alter its binding affinity for the enzyme. Indeed, when HEC (a substrate analogue in which the terminal methyl group is replaced by hydrogen) is a substrate for *rS*-HPCDH3, the apparent K_m value decreases by over eight-fold, as compared to *R*-HPC (Table 4-10). Although the same holds true for the Met194Leu mutant of *rS*-HPCDH3 this increase is much more dramatic (23-fold). A distinct trend can be observed in the data presented in Table 4-10, the K_m values displayed by both the wild-type and mutant *rS*-HPCDH3 increase in the following order: *S*-HPC, HEC and *R*-HPC. An important and somewhat surprising result is that the substitution of Met194 to leucine produces an enzyme with a greater binding affinity for HEC than that of the wild-type *rS*-HPCDH3. The homology model of *rS*-HPCDH3 indicates that Met194 is located further away from the "business end" of the substrate (6.2 Å from the C2 carbon) thereby making it less likely to clash with the methyl group of the substrate (Figure 4-16A). It remains unclear at this point why the Met194Leu mutation has a positive effect on the K_m for HEC oxidation. It can be speculated that the Met to Leu substitution could cause some small but sufficient rearrangements of the neighboring residues (due to differences in shape), thereby remodeling the active site cavity and introducing novel steric constrains on the substrate. Although the presented results suggest that Met194 is important in modulating binding affinity and possibly enantioselectivity of the physiological substrates in *rS*-HPCDH3, this hypothesis requires further investigation (e.g., solving of Met194Leu mutant X-ray structure).

Table 4-9. Comparison of the apparent K_m values for *R*-HPC, *S*-HPC and HEC oxidation by *rR*-HPCDH1 WT, Met187Leu and Met192Leu mutants of *rR*-HPCDH1

Substrate	WT K_m (μM)	Change (x-fold)	M187L K_m (μM)	Change (x-fold)	change (x-fold) relative to WT	M192L K_m (μM)	Change (x-fold)	change (x-fold) relative to WT
R-HPC	82.7 ± 6.8	1.0	144 ± 10	1.0	1.7	431± 14	1.0	5.2
S-HPC	265 ± 72	3.2	434 ± 69	3.0	1.6	881 ± 54	2.0	3.3
HEC	958 ± 110	11.6	1020 ± 82	7.1	1.1	6840 ± 610	15.9	7.1

Table 4-10. Comparison of the apparent K_m values for *S*-HPC, *R*-HPC and HEC oxidation by *rS*-HPCDH3 WT and Met194Leu mutant of *rS*-HPCDH3

Substrate	*rS*-HPCDH3 WT K_m (μM)	Change (x-fold)	M194L K_m (μM)	Change (x-fold)	change (x-fold) relative to WT
S-HPC	135 ± 9.7	1.0	381 ± 54	1.0	2.8
HEC	975 ± 250	7.2	674 ± 66	1.8	0.7
R-HPC	8220 ± 570	60.8	15400 ± 2400	40.3	1.9

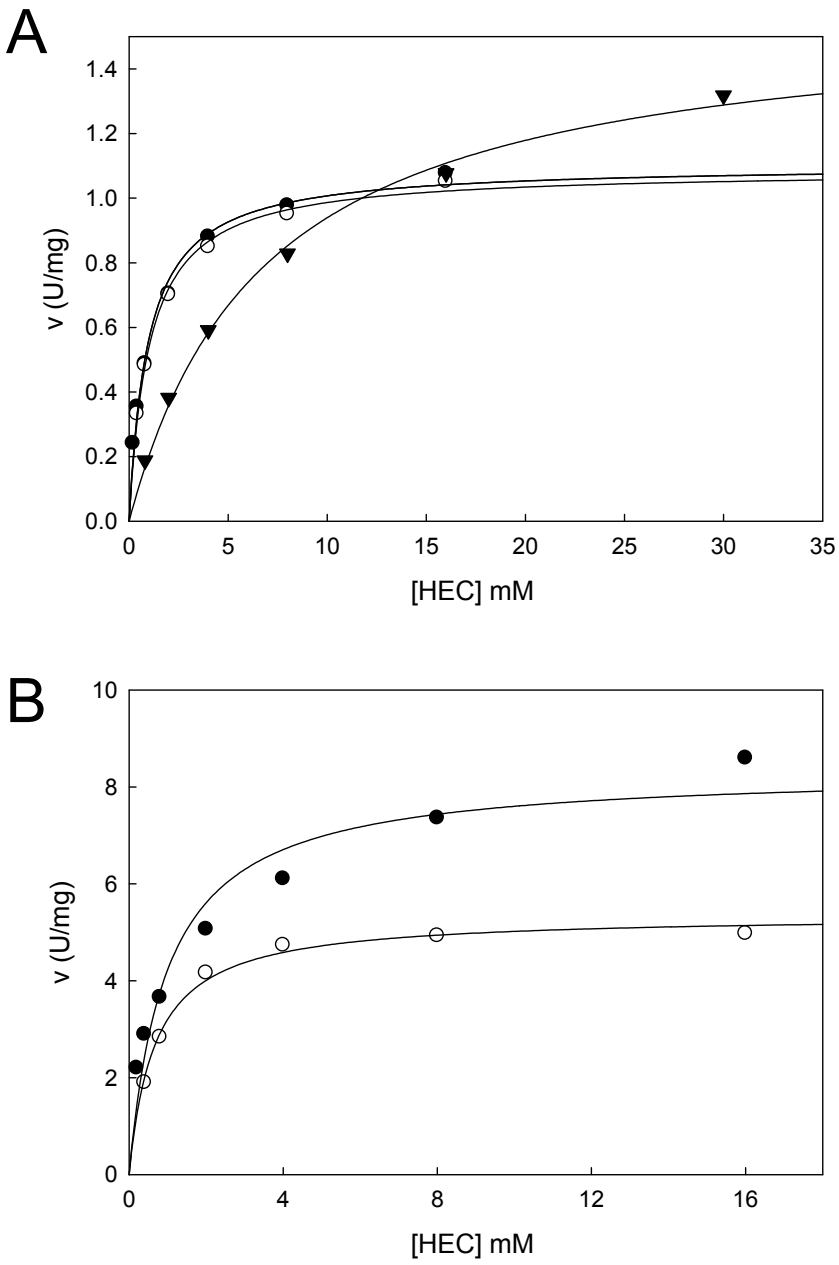

Figure 4-18. Catalytic activity of *rR*-HPCDH1 and *rS*-HPCDH3 enzymes in oxidation of 2-(2-hydroxyethylthio) ethanesulfonate (HEC), an achiral substrate homolog. Panel A: *v* vs. S plots for HEC oxidation by (●) wild-type *rR*-HPCDH1, (○) Met187Leu *rR*-HPCDH1 and (▼) Met192Leu *rR*-HPCDH1 at variable concentrations of HEC (0.2 mM – 30 mM). Panel B: *v* vs. S plots for HEC oxidation by (●) wild-type *rS*-HPCDH3 and (○) Met194Leu *rS*-HPCDH3 at variable concentrations of HEC (0.2 mM – 16 mM). The solid lines were generated by fitting data points from each assay to a rectangular hyperbola described by a standard form of the Michaelis-Menten equation using SigmaPlot 11.0. Data points represent the average of duplicate experiments.

Rapid Equilibrium Inhibition Studies with a Substrate Analogue. 2-(2-methyl-2-hydroxypropylthio) ethanesulfonate (M-HPC) is an achiral analog of both *R*-HPC and *S*-HPC where the hydrogen atoms of each alcohol are replaced by a methyl group. Thus, M-HPC is a tertiary alcohol that cannot be oxidized due to lack of an abstractable hydride. As shown in Table 4-5 and Table 4-7, the K_m values for *S*-HPC and *R*-HPC oxidation exhibited by *rR*-HPCDH1 are in the same range, whereas K_m values exhibited by *rS*-HPCDH3 for *R*-HPC were 60-times higher than for *S*-HPC. These results are similar to those reported previously (*6*) and suggest that enantioselectivity of *rS*-HPCDH3 is brought about by steric constraints with the misaligned methyl group of the opposite enantiomer. Subsequent inhibition studies revealed that M-HPC is a competitive inhibitor for *R*-HPC oxidation by *rR*-HPCDH1 but not for *S*-HPC oxidation by *rS*-HPCDH3, thereby confirming an important role of the terminal methyl group in modulating binding affinity of enantiomeric substrates for the *R*- and *S*-specific dehydrogenases. Inhibition studies with M-HPC were further extended to methionine mutants of HPCDH enzymes to shed light on a possible role of the substrate flanking methionines in controlling enantioselectivity. Kinetic analysis of *R*-HPC oxidation in the presence of variable concentrations of M-HPC revealed competitive inhibition for the Met187Leu and Met192Leu mutants of *rR*-HPCDH1 with K_{is} values comparable to the corresponding K_m values for *R*-HPC (Table 4-11). The K_{is} values for M-HPC were also similar to the K_m values for *S*-HPC, demonstrating that all three compounds bind to *R*-HPCDH1 with comparable affinities and substitution of the active site methionines to leucines has no significant effect on M-HPC binding. As shown in Figure 4-20, the double reciprocal plots showed a clear competitive inhibition pattern for both Met187Leu mutant and the wild-type enzyme. An ambiguous line pattern was observed for Met192Leu mutant. However, the theoretical data calculations using equations 1 – 3 confirmed the competitive model. In contrast, no detectable inhibition was observed for M-HPC vs. the natural substrate *S*-HPC with any of *rS*-HPCDH3 methionine mutants (Table 4-11). This is in agreement with the results of the kinetic assays presented in Table 4-7, showing that *R*-HPC binds to *rS*-HPCDH3 with a 60-fold lower

Table 4-11. Summary of the inhibition studies performed for the *rR*-HPCDH1 and *rS*-HPCDH3 enzymes and their methionine mutants in the oxidation of *R*- and *S*-HPC, respectively, in the presence of M-HPC at pH 7.5[a]

Enzyme	K_m (μM)	Change in K_m (x-fold)	K_{is} (μM)	Change in K_{is} (x-fold)	Inhibition
			R-HPCDH1		
WT	82.7 ± 6.8	1.0	290 ± 14	1.00	Competitive
M187L	144 ± 10	1.7	269 ± 12	0.93	Competitive
M192L	431 ± 14	5.2	714 ± 46	2.46	Competitive
			S-HPCDH3		
WT	135 ± 9.7	1.00	ND[b]		None
M153A	14000 ± 1100	103	ND[b]		None
M194A	13400 ± 850	99.4	ND[b]		None
M194L	381 ± 54	2.82	ND[b]		None

[a]Assay for *R*-HPC oxidation at different constant concentrations of M-HPC (0 – 1.6 mM) by *rR*-HPCDH1 WT and Met mutants contained 1.0 μg of enzyme. Assay for *S*-HPC oxidation contained: 1.0 μg of *rS*-HPCDH3 WT and M194L mutant, 1.5 μg of M194A and 118 μg of M153A mutant. Apparent K_m values were determined by fitting experimental data to the standard form of the Michaelis-Menten equation and are reported as means ± standard deviations. All assays were performed at 30 ˚C with fixed concentrations of NAD^+ (10 mM).
[b]ND – no detectable inhibition at concentrations up to 10 mM of M-HPC.

affinity than the native enantiomer *S*-HPC presumably due to the steric clashes of the misaligned methyl group on *R*-HPC with the nicotinamide ring of NAD^+. It is plausible that the addition of the methyl group on C2 carbon of the substrate could cause further steric constrains thereby enabling such a substrate to bind in the active site of *rS*-HPCDH3.

Lack of inhibition by M-HPC in oxidation of *S*-HPC exhibited by methionine mutants of *rS*-HPCDH3 confirms this prediction. Structural analysis of *rS*-HPCDH3 with M-HPC modeled in the active site suggests extensive steric clashes of the methyl groups with the nicotinamide ring of NAD^+ and to some extent with Tyr156 (Figure 4-19). The fact that none of the tested methionine mutants showed any inhibition in the presence of M-HPC suggests that Met153 and

Met194 are not involved in imposing those steric clashes. Moreover, expanding the active site cavity in the direct proximity of the "business end" of the substrate by substitution of either of the methionines with much smaller alanine residues does not release the steric restriction imposed upon binding of M-HPC. Together, these results further support the hypothesis that steric clashes of the terminal methyl group of the HPC substrates with the nicotinamide ring of NAD^+ are a major determinant of the enantioselectivity in *rS*-HPCDH3.

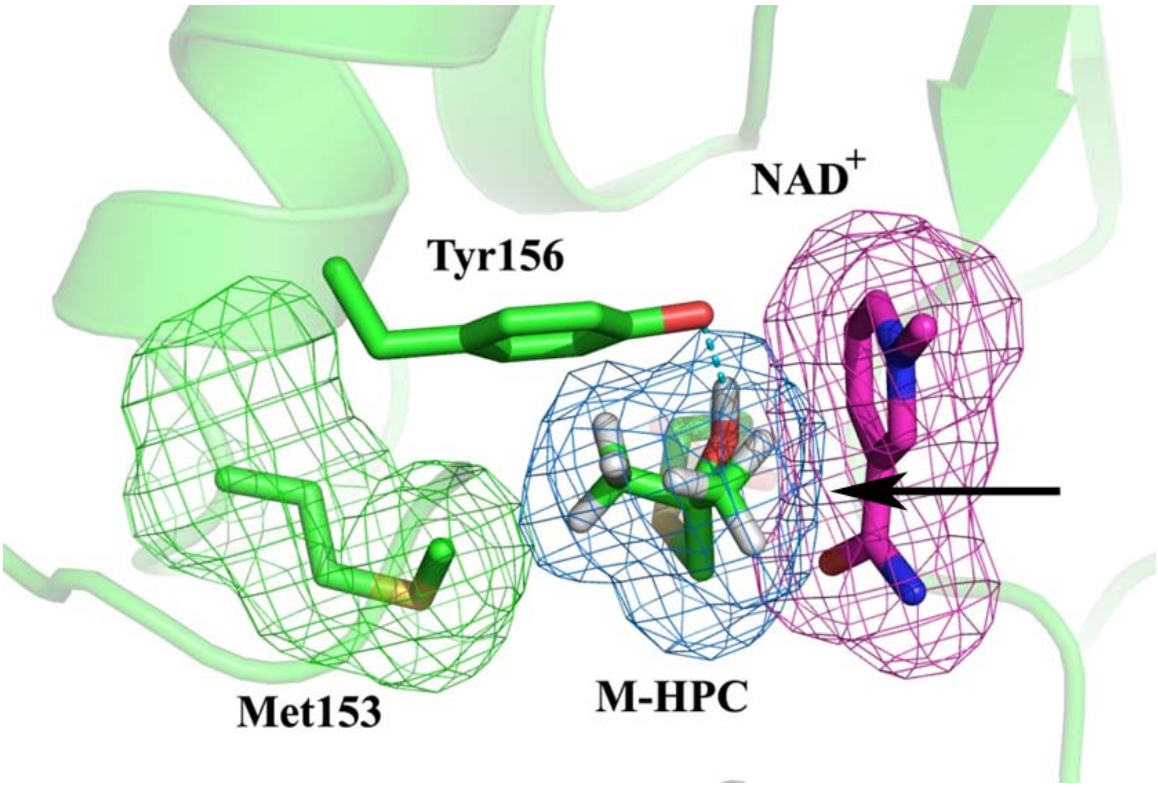

Figure 4-19. The active site of *rS*-HPCDH3 showing steric effects of the nicotinamide ring of NAD^+ with M-HPC inhibitor (modeled in PyMol).

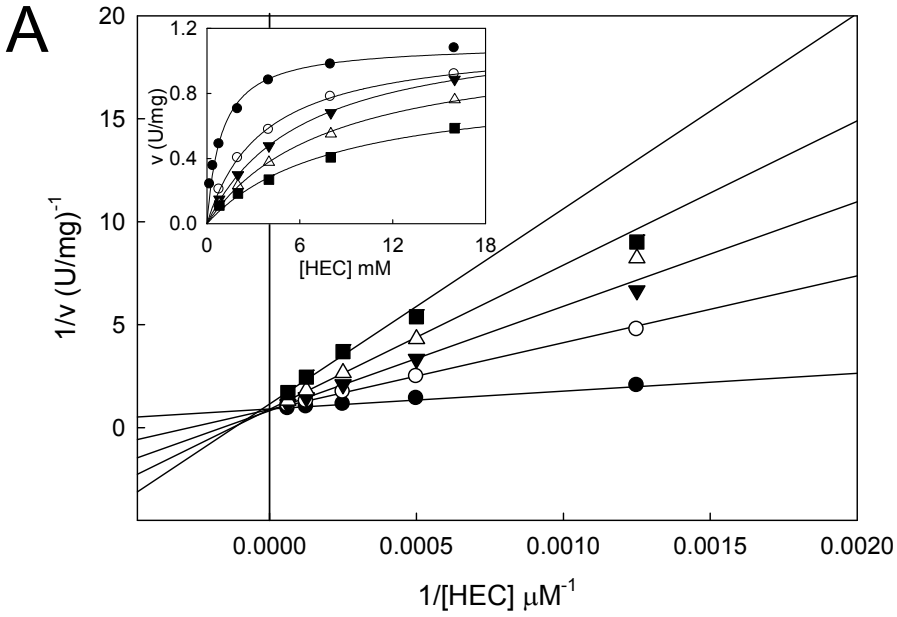
A
20
15
10
5
0
1/v (U/mg)$^{-1}$
0.0000
0.0005
0.0010
0.0015
0.0020
1/[HEC] μM^{-1}
1.2
0.8
0.4
0.0
v (U/mg)
0
6
12
18
[HEC] mM

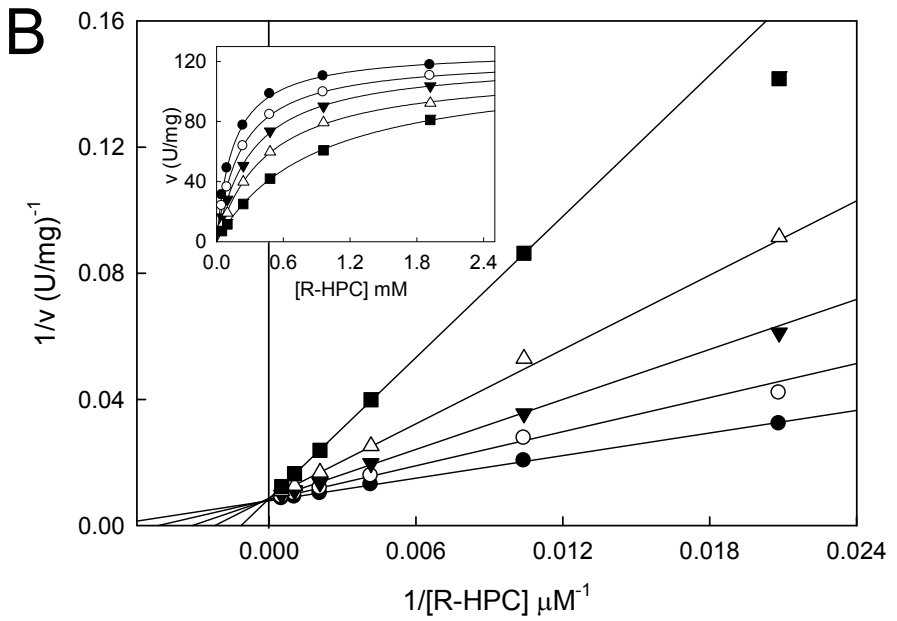
B
0.16
0.12
0.08
0.04
0.00
1/v (U/mg)$^{-1}$
0.000
0.006
0.012
0.018
0.024
1/[R-HPC] μM^{-1}
120
80
40
0
v (U/mg)
0.0
0.6
1.2
1.8
2.4
[R-HPC] mM

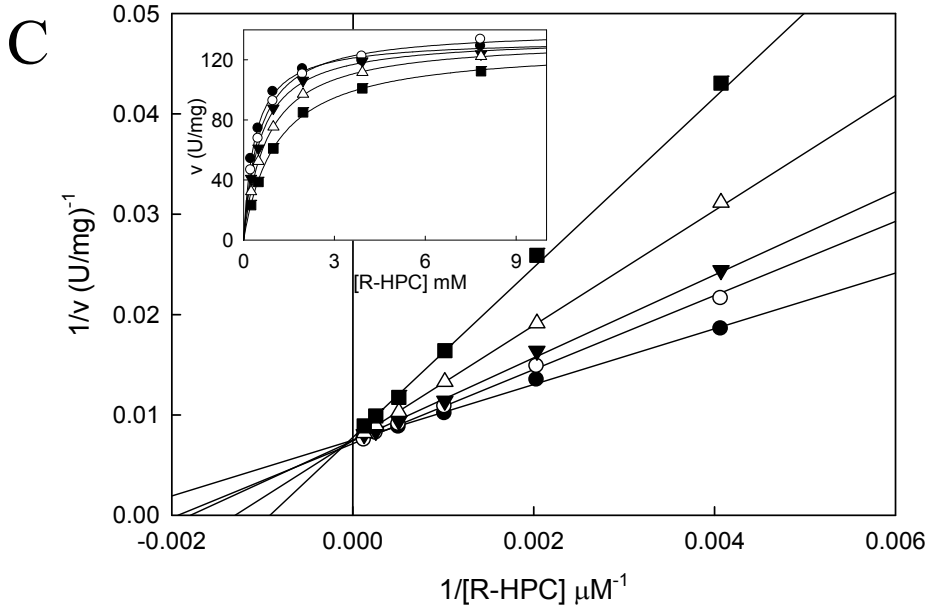

Figure 4-20. Effects of 2-(2-methyl-2-hydroxypropylthio)ethanesulfonate (M-HPC) on *R*- and *S*-HPC oxidation by wild-type *rR*-HPCDH1, and Met187Leu and Met192Leu mutants of *rR*-HPCDH1. Panel A: Competitive inhibition of wild-type *rR*-HPCDH1-catalyzed *R*-HPC oxidation by M-HPC. Panel B: Competitive inhibition of Met187Leu mutant-catalyzed *R*-HPC oxidation by M-HPC. Panel C: Competitive inhibition of Met192Leu mutant-catalyzed *R*-HPC oxidation by M-HPC. The double reciprocal plots for assays performed in the presence of different concentrations of M-HPC are shown in the main diagram. The solid lines were generated by nonlinear least-square fits of the *v* vs. S data, shown in the *inset*, to the equation for a rectangular hyperbola using SigmaPlot. M-HPC concentrations: (●) 0 mM, (○) 0.2 mM, (▼) 0.4 mM, (Δ) 0.8 mM, (■) 1.6 mM.

CONCLUSIONS

Structural analysis of the enzymes involved in the epoxide carboxylase pathway found in *X. autotrophicus* Py2 revealed striking similarities in their active site architecture. Highly conserved positively charged residues (Arg and/or Lys) lining the CoM binding pocket and two methionine residues flanking the substrate were common to three of the four enzymes of the pathway (*R*-HPCDH, *S*-HPCDH and 2-KPCC). This intriguing observation prompted the study aimed at elucidating a possible role of the substrate flanking methionines. The subject of investigation presented in this chapter is a pair of enantiocomplementary *R*- and *S*-HPC

dehydrogenases. A series of site-directed mutants were made to substitute specific methionines to alanine and subsequently to leucine. A total of nine mutants were obtained and subjected to kinetic analysis with various substrates. The most significant change in the kinetic parameters observed for the methionine to alanine mutants of *rR*-HPCDH1 and *rS*-HPCDH3 was a dramatic increase in the apparent K_m values for the physiological substrates. As a result the catalytic efficiency for these mutants was significantly impaired, especially for the double mutant of *rR*-HPCDH1. The X-ray structures for Met187Ala and Met192Ala of *rR*-HPCDH1 were determined in support of the kinetic and mechanistic studies. The Met187Ala mutant structure revealed a large solvent accessible pocket near the CoM binding site. The lack of the sulfonate moiety of the substrate in this region suggested non-productive interaction of the arginine residues (involved in the sulfonate binding) with the surrounding solvent molecules. Although, the sulfonate moiety was visible in the structure of the Met192Ala mutant, the kinetic analysis showed a dramatic increase in the apparent K_m values for this mutant (24-fold), also suggesting opening of the active site to the solvent. Based on these results the Met187 and Met192 residues are proposed to play an important role in shielding the active site from the surrounding solvent. Additionally, because Met192 is in close proximity to the chiral carbon of the substrate molecule where chemistry occurs, it is also speculated that Met192 might be shielding charges on both ends of the substrate during catalysis. When Met187 and Met192 residues were changed to leucine, the resulting mutants displayed kinetic parameters similar to the wild-type enzyme, which suggested a structural, rather than catalytic function of the methionines. Comparison of the leucine mutants of both dehydrogenases revealed some interesting and potentially important differences. Namely, the Met187Leu and Met192Leu mutants of *rR*-HPCDH1 showed a substrate dependent increase in the k_{cat} values, while the Met194Leu mutant of *rS*-HPCDH3 revealed a substrate dependent increase in the K_m values. This corroborates with the previous study (*6*) where *rR*-HPCDH1 and *rS*-HPCDH3 were demonstrated to control their enantioselectivity via changes in k_{cat} and K_m, respectively. Surprisingly, in the reaction of *R*-HPC oxidation catalyzed by Met187Leu and

Met192Leu mutants of *rR*-HPCDH1, the apparent k_{cat} values increased by 42% and 59%, respectively, as compared to the wild-type enzyme. In the reaction of *S*-HPC oxidation by *rR*-HPCDH1 this increase was almost three-fold. Interestingly however, this enhancement of activity was abolished for 2-KPC reduction and the apparent k_{cat} value remained fairly similar to the corresponding value of the wild-type enzyme. These results suggest that chirality and/or oxidation state of the substrate might be important determinants of the enzyme's activity. Based on the structural and kinetic analysis presented herein, it is proposed that the methionines at position 187 and 192 may be also involved in modulating the enantioselectivity of the *rR*-HPCDH1. With respect to the Met153 and Met194 residues in *S*-HPCDH3, their strategic position at the entrance of a channel leading to the active site suggests a role of "gate keepers", protecting the active site from non-productive interactions with the ambient solvent. The natural substrate analogue HEC (2-hydroxyethyl-CoM) was used as a substrate for the leucine mutants of *rR*-HPCDH1 and *rS*-HPCDH3. Similar values of K_m were obtained in all enzymes (except for Met192Leu of *rR*-HPCDH1). Interestingly, Met192Leu mutant showed 42% increase in k_{cat} value and over seven-fold increase in the K_m value. The apparent k_{cat} and apparent K_m values exhibited by Met187Leu mutant and wild-type *rR*-HPCDH1 were identical and suggested that Met187 plays an important role in binding and catalysis of the physiological substrates (*R*- and *S*-HPC), but not substrate analogs lacking the terminal methyl group. Inhibition studies show that the tertiary alcohol, 2-methyl-2-hydroxypropyl-CoM (M-HPC) is a competitive inhibitor of *R*-HPC oxidation by Met187Leu and Met192Leu of *rR*-HPCDH1, with a K_{is} similar to the K_m values for *R*-HPC. No inhibition of *S*-HPC oxidation by M-HPC was observed for any of Met mutants of *rS*-HPCDH3, thus suggesting that Met153 and Met194 are not directly involved in the steric clashes with the terminal methyl group of the substrate. As proposed in Chapter 2, these steric clashes are believed to prevent proper binding of *R*-HPC and M-HPC and result in a different mechanism for controlling substrate specificity and enantioselectivity. Structural and kinetic analysis of the *rS*-HPCDH3 mutants with M-HPC suggests that the steric clashes of the terminal methyl group of

the HPC substrates with the nicotinamide ring of NAD^+ are a major determinant of the enantioselectivity in *rS*-HPCDH3. Based on the structural data Met192 of *rR*-HPCDH1 is proposed to be involved in the NAD(H) cofactor binding. The homology model of *rS*-HPCDH3 suggests a similar role for the Met194 residue. An importance of the active site methionine in orienting the cofactor nicotinamide ring with respect to the substrate has been previously reported for 6-phosphogluconate dehydrogenase enzyme (*29*). As mentioned earlier, methionine is one of the most readily oxidized amino acid constituents of proteins. Considering the reversibility of Met oxidation followed by its functional changes, it is speculated that the presence of the substrate flanking methionines might crucial in protecting enzymes involved in the propylene and epoxide degradation pathway from the oxidative stress. However, this hypothesis requires more research and was not further explored in the current study.

Together, the presented results provide evidence for the importance of the substrate flanking methionines in the active site of the *R*- and *S*-HPCDH enzymes. Furthermore, it is proposed that the high enantioselectivity of *rS*-HPCDH3 is due to the steric clashes of the NAD^+ cofactor with the improperly aligned methyl group on the C2 carbon of the substrate.

Finally, a general architecture of the active site with the substrate flanking methionines and positively charged amino acids interacting with the sulfonate moiety observed in 2-KPCC, *R*-HPCDH and *S*-HPCDH may prove useful in identifying new CoM-dependent enzymes.

REFERENCES

1. Ensign, S. A., and Allen, J. R. (2003) Aliphatic epoxide carboxylation. *Annu. Rev. Biochem. 72*, 55-76.

2. Allen, J. R., and Ensign, S. A. (1998) Identification and characterization of epoxide carboxylase activity in cell extracts of *Nocardia corallina* B276. *J. Bacteriol. 180*, 2072-2078.

3. Allen, J. R., and Ensign, S. A. (1999) Two short-chain dehydrogenases confer stereoselectivity for enantiomers of epoxypropane in the multiprotein epoxide carboxylating systems of *Xanthobacter* strain Py2 and *Nocardia corallina* B276. *Biochemistry 38*, 247-256.

4. Small, F. J., and Ensign, S. A. (1997) Alkene monooxygenase from *Xanthobacter* strain Py2. *J. Biol. Chem. 272*, 24913.

5. Clark, D. D., and Ensign, S. A. (2002) Characterization of the 2-[(R)-2-hydroxypropylthio]ethanesulfonate dehydrogenase from *Xanthobacter* strain Py2: product inhibition, pH dependence of kinetic parameters, site-directed mutagenesis, rapid equilibrium inhibition, and chemical modification. *Biochemistry 41*, 2727-2740.

6. Sliwa, D. A., Krishnakumar, A. M., Peters, J. W., and Ensign, S. A. (2010) Molecular basis for enantioselectivity in the (R)- and (S)-hydroxypropylthioethanesulfonate dehydrogenases, a unique pair of stereoselective short-chain dehydrogenases/reductases involved in aliphatic epoxide carboxylation. *Biochemistry 49*, 3487-3498.

7. Krishnakumar, A. M., Nocek, B. P., Clark, D. D., Ensign, S. A., and Peters, J. W. (2006) Structural basis for stereoselectivity in the (R)- and (S)-hydroxypropyl thioethanesulfonate dehydrogenases. *Biochemistry 45*, 8831-8840.

8. Clark, D. D., Boyd, J. M., and Ensign, S. A. (2004) The stereoselectivity and catalytic properties of *Xanthobacter autotrophicus* 2-[(R)-2-Hydroxypropylthio]ethanesulfonate dehydrogenase are controlled by interactions between C-terminal arginine residues and the sulfonate of coenzyme M. *Biochemistry 43*, 6763-6771.

9. Nocek, B., Jang, S. B., Jeong, M. S., Clark, D. D., Ensign, S. A., and Peters, J. W. (2002) Structural basis for CO_2 fixation by a novel member of the disulfide oxidoreductase family of enzymes, 2-ketopropyl-coenzyme M oxidoreductase/carboxylase. *Biochemistry 41*, 12907-12913.

10. Vogt, W. (1995) Oxidation of methionyl residues in proteins: tools, targets, and reversal. *Free Radic. Biol. Med. 18*, 93-105.

11. Luo, S., and Levine, R. L. (2009) Methionine in proteins defends against oxidative stress. *The FASEB Journal 23*, 464.

12. Kachurin, A., Golubev, A., Geisow, M., Veselkina, O., Isaeva-Ivanova, L., and Neustroev, K. (1995) Role of methionine in the active site of alpha-galactosidase from Trichoderma reesei. *Biochem. J. 308*, 955.

13. O'Neil, K. T., and DeGrado, W. F. (1990) How calmodulin binds its targets: sequence independent recognition of amphiphilic [alpha]-helices. *Trends Biochem. Sci. 15*, 59-64.

14. Gellman, S. H. (1991) On the role of methionine residues in the sequence-independent recognition of nonpolar protein surfaces. *Biochemistry 30*, 6633-6636.

15. Janin, J., Wodak, S., Levitt, M., and Maigret, B. (1978) Conformation of amino acid side-chains in proteins. *J. Mol. Biol. 125*, 357-386.

16. Pal, D., and Chakrabarti, P. (2001) Non-hydrogen bond interactions involving the methionine sulfur atom. *J. Biomol. Struct. Dyn. 19*, 115-128.

17. Tatko, C. D., and Waters, M. L. (2004) Investigation of the nature of the methionine–interaction in -hairpin peptide model systems. *Protein Sci. 13*, 2515.

18. Ma, B., and Nussinov, R. (2007) Trp/Met/Phe hot spots in protein-protein interactions: potential targets in drug design. *Curr. Top. Med. Chem. 7*, 999-1005.

19. Sui, J., Hwang, W. C., Perez, S., Wei, G., Aird, D., Chen, L., Santelli, E., Stec, B., Cadwell, G., and Ali, M. (2009) Structural and functional bases for broad-spectrum neutralization of avian and human influenza A viruses. *Nat. Struct. Mol. Biol. 16*, 265-273.

20. Bone, R., Fujishige, A., Kettner, C. A., and Agard, D. A. (1991) Structural basis for broad specificity in. alpha.-lytic protease mutants. *Biochemistry 30*, 10388-10398.

21. Rosental, N., and Kanner, B. I. (2010) A conserved methionine residue controls the substrate selectivity of a neuronal glutamate transporter. *J. Biol. Chem.285*, 21241-21248.

22. Allen, J. R., Clark, D. D., Krum, J. G., and Ensign, S. A. (1999) A role for coenzyme M (2-mercaptoethanesulfonic acid) in a bacterial pathway of aliphatic epoxide carboxylation. *Proc. Natl. Acad. Sci. U.S.A. 96*, 8432-8437.

23. Laemmli, U. K. (1970) Cleavage of structural proteins during the assembly of the head of bacteriophage T4. *Nature 227*, 680-685.

24. Nocek, B., Clark, D. D., Ensign, S. A., and Peters, J. W. (2002) Crystallization and preliminary X-ray analysis of an R-2-hydroxypropyl-coenzyme M dehydrogenase. *Acta Crystallogr. D. Biol. Crystallogr. 58*, 1470-1473.

25. Krishnakumar, A. M. (2007) Structural studies of enzymes involved in propylene and acetone metabolism in *Xanthobacter autotrophicus*, Thesis, Montana State University, Bozeman.

26. Price, A. C., Zhang, Y. M., Rock, C. O., and White, S. W. (2004) Cofactor-induced conformational rearrangements establish a catalytically competent active site and a proton relay conduit in FabG. *Structure 12*, 417-428.

27. O.B. Ptitsyn, T. E. C. (1992) *Protein Folding*, W.H. Freeman, New York.

28. Lipscomb, L. A., Gassner, N. C., Snow, S. D., Eldridge, A. M., Baase, W. A., Drew, D. L., and Matthews, B. W. (1998) Context-dependent protein stabilization by methionine-to-leucine substitution shown in T4 lysozyme. *Protein Sci. 7*, 765-773.

29. Cervellati, C., Dallocchio, F., Bergamini, C. M., and Cook, P. F. (2005) Role of methionine-13 in the catalytic mechanism of 6-phosphogluconate dehydrogenase from sheep liver. *Biochemistry 44*, 2432-2440.

CHAPTER 5

SUMMARY

The SDR superfamily has very few enzymes that can be characterized by their unique ability to discriminate or produce enantiomeric alcohols. Even more unusual are enantiocomplementary dehydrogenases present in a common metabolic pathway that would catalyze the same reaction but with the opposite enantioselectivity. The *R*- and S-HPCDH possess these characteristics, and thus provide an excellent model for studying features controlling enantioselectivity among SDR enzymes. Although *R*-HPCDH has been extensively characterized, very little is known about *S*-HPCDH due to the solubility problems encountered in expressing its recombinant form. Herein, we report a heterologous expression of an active form of *rS*-HPCDH and its kinetic and mechanistic characterization (Chapter 2). Although both *R*- and *S*-HPCDH are highly homologous and highly enantioselective for their respective substrates, they reveal some significant differences. The most significant difference is observed in the inhibition studies and in the reaction with the non-physiological substrates (aliphatic alcohols and ketones lacking the CoM moiety). Most importantly, they employ different mechanisms of controlling their enantioselectivity. Although both enzymes are highly enantioselective and hold high potential for the biocatalytic production of optically pure alcohols, the *rS*-HPCDH3 makes an especially noteworthy candidate for a biocatalyst, considering its near absolute stereoselectivity for some aliphatic *(S)*-alcohols (Chapter 3). The results presented herein provide a further evidence for the importance of the positively charged residues (Arg and/or Lys) in the active site of *R*- and *S*-HPCDH. It was demonstrated that strong ionic interactions of these residues with the sulfonate moiety of the substrate are essential for the high binding affinity and proper orientation of the substrate.

In Chapter 4, a role of the active site methionines was investigated for the *R*- and *S*-HPCDH enzymes. Nine site-directed mutants were produced where specific methionines were

replaced with either alanine or leucine. Subsequently, all the mutants were subjected to kinetic and mechanistic analysis with various substrates. Analogous of the natural substrate HEC and M-HPC were used in the activity assay. No inhibition was observed for any of Met mutants of *rS*-HPCDH3 in the oxidation of *S*-HPC in the presence of M-HPC. This suggests that Met153 and Met194 are not directly involved in the steric clashes with the terminal methyl group of the substrate. As proposed in Chapter 2, these steric clashes in the active site of *rS*-HPCDH3 are believed to prevent proper binding of *R*-HPC and M-HPC and result in a different mechanism for controlling enantioselectivity. The substrate flanking methionines in *R*- and *S*-HPCDH enzymes were shown to play a role of "gate keepers" in shielding the active site from the non-productive interactions with the surrounding solvent. Additionally, they might be important in modulating enantioselectivity of both enzymes by imposing specific steric constrains in the direct vicinity of the substrate binding site, thus facilitating selection of the proper enantiomeric substrate. The Met192 of *rR*-HPCDH1 and by analogy Met194 of *rS*-HPCDH3 are also involved in the cofactor binding. It is proposed that the high enantioselectivity of *rS*-HPCDH3 is dictated by the steric clashes of the nicotinamide ring of NAD^+ with the improperly aligned methyl group on the C2 carbon of the substrate. To our knowledge, this dissertation provides the first side by side characterization of a pair of SDR enzymes expressed simultaneously to act on two enantiomers of the same alcohol produced in a metabolic pathway. These dehydrogenases are distinguished from all other known members of the SDR family in using the novel sulfonate functional group of coenzyme M as a handle for chiral discrimination. The differential control of enantioselectivity by means of k_{cat} vs. K_m is a surprising yet explainable result in the context of cellular metabolism. These results provide a standard for examining the molecular basis of stereoselectivity in other such enzyme pairs.

More work still has to be done in order to confirm the hypothesis proposed above. For example, the X-ray structure of *rS*-HPCDH3 will undoubtedly aid in better understanding of the

observed results and provide further insight into the mechanism of high degree of chiral discrimination exhibited by *R*- and *S*-HPCDH.

APPENDIX

PERMISSIONS

AMERICAN CHEMICAL SOCIETY LICENSE
TERMS AND CONDITIONS

Aug 23, 2010

This is a License Agreement between Dariusz A Sliwa ("You") and American Chemical Society ("American Chemical Society") provided by Copyright Clearance Center ("CCC"). The license consists of your order details, the terms and conditions provided by American Chemical Society, and the payment terms and conditions.

All payments must be made in full to CCC. For payment instructions, please see information listed at the bottom of this form.

License Number	2494850385053
License Date	Aug 23, 2010
Licensed content publisher	American Chemical Society
Licensed content publication	Biochemistry
Licensed content title	Molecular Basis for Enantioselectivity in the (R)- and (S)-Hydroxypropylthioethanesulfonate Dehydrogenases, a Unique Pair of Stereoselective Short-Chain Dehydrogenases/Reductases Involved in Aliphatic Epoxide Carboxylation
Licensed content author	Dariusz A. Sliwa et al.
Licensed content date	Apr 1, 2010
Volume number	49
Issue number	16
Type of Use	Thesis/Dissertation
Requestor type11	Not specified
Format	Print
Portion	Full article
Author of this ACS article	Yes
Order reference number	
Title of the thesis / dissertation	KINETIC, MECHANISTIC AND STRUCTURAL INVESTIGATION OF FEATURES CONTROLLING STEREOSELECTIVITY OF (R)- AND (S)-HYDROXYPROPYL COM DEHYDROGENASES FROM XANTHOBACTER AUTOTROPHICUS STRAIN PY2
Expected completion date	Aug 2010
Estimated size(pages)	220
Billing Type	Invoice
Billing Address	Chemistry and Biochemistry Department 0300 Old Main Hill Logan, UT 84322 United States
Customer reference info	
Total	0.00 USD
Terms and Conditions	

Thesis/Dissertation

ACS / RIGHTSLINK TERMS & CONDITIONS
THESIS/DISSERTATION

INTRODUCTION
The publisher for this copyrighted material is the American Chemical Society. By clicking "accept" in connection with completing this licensing transaction, you agree that the following terms and conditions apply to this transaction (along with the Billing and Payment terms and conditions established by Copyright Clearance Center, Inc. ("CCC"), at the time that you opened your Rightslink account and that are available at any time at <http://myaccount.copyright.com>).

LIMITED LICENSE
Publisher hereby grants to you a non-exclusive license to use this material. Licenses are for one-time use only with a maximum distribution equal to the number that you identified in the licensing process; any form of republication must be completed within 60 days from the date hereof (although copies prepared before then may be distributed thereafter).

GEOGRAPHIC RIGHTS: SCOPE
Licenses may be exercised anywhere in the world.

RESERVATION OF RIGHTS
Publisher reserves all rights not specifically granted in the combination of (i) the license details provided by you and accepted in the course of this licensing transaction, (ii) these terms and conditions and (iii) CCC's Billing and Payment terms and conditions.

PORTION RIGHTS STATEMENT: DISCLAIMER
If you seek to reuse a portion from an ACS publication, it is your responsibility to examine each portion as published to determine whether a credit to, or copyright notice of, a third party owner was published adjacent to the item. You may only obtain permission via Rightslink to use material owned by ACS. Permission to use any material published in an ACS publication, journal, or article which is reprinted with permission of a third party must

be obtained from the third party owner. ACS disclaims any responsibility for any use you make of items owned by third parties without their permission.

REVOCATION
The American Chemical Society reserves the right to revoke a license for any reason, including but not limited to advertising and promotional uses of ACS content, third party usage, and incorrect figure source attribution.

LICENSE CONTINGENT ON PAYMENT
While you may exercise the rights licensed immediately upon issuance of the license at the end of the licensing process for the transaction, provided that you have disclosed complete and accurate details of your proposed use, no license is finally effective unless and until full payment is received from you (by CCC) as provided in CCC's Billing and Payment terms and conditions. If full payment is not received on a timely basis, then any license preliminarily granted shall be deemed automatically revoked and shall be void as if never granted. Further, in the event that you breach any of these terms and conditions or any of CCC's Billing and Payment terms and conditions, the license is automatically revoked and shall be void as if never granted. Use of materials as described in a revoked license, as well as any use of the materials beyond the scope of an unrevoked license, may constitute copyright infringement and publisher reserves the right to take any and all action to protect its copyright in the materials.

COPYRIGHT NOTICE: DISCLAIMER
You must include the following copyright and permission notice in connection with any reproduction of the licensed material: "Reprinted (“Adapted” or “in part”) with permission from REFERENCE CITATION. Copyright YEAR American Chemical Society."

WARRANTIES: NONE
Publisher makes no representations or warranties with respect to the licensed material.

INDEMNITY
You hereby indemnify and agree to hold harmless publisher and CCC, and their respective officers, directors, employees and agents, from and against any and all claims arising out of your use of the licensed material other than as specifically authorized pursuant to this license.

NO TRANSFER OF LICENSE
This license is personal to you or your publisher and may not be sublicensed, assigned, or transferred by you to any other person without publisher's written permission.

NO AMENDMENT EXCEPT IN WRITING
This license may not be amended except in a writing signed by both parties (or, in the case of publisher, by CCC on publisher's behalf).

OBJECTION TO CONTRARY TERMS
Publisher hereby objects to any terms contained in any purchase order, acknowledgment, check endorsement or other writing prepared by you, which terms are inconsistent with these terms and conditions or CCC's Billing and Payment terms and conditions. These terms and conditions, together with CCC's Billing and Payment terms and conditions (which are incorporated herein), comprise the entire agreement between you and publisher (and CCC) concerning this licensing transaction. In the event of any conflict between your obligations established by these terms and conditions and those established by CCC's Billing and Payment terms and conditions, these terms and conditions shall control.

JURISDICTION
This license transaction shall be governed by and construed in accordance with the laws of the District of Columbia. You hereby agree to submit to the jurisdiction of the courts located in the District of Columbia for purposes of resolving any disputes that may arise in connection with this licensing transaction.

THESES/DISSERTATION TERMS
Publishing implications of electronic publication of theses and dissertation material
Students and their mentors should be aware that posting of theses and dissertation material on the Web prior to submission of material from that thesis or dissertation to an ACS journal may affect publication in that journal. Whether Web posting is considered prior publication may be evaluated on a case-by-case basis by the journal’s editor. If an ACS journal editor considers Web posting to be “prior publication”, the paper will not be accepted for publication in that journal. If you intend to submit your unpublished paper to ACS for publication, check with the appropriate editor prior to posting your manuscript electronically.

If your paper has already been published by ACS and you want to include the text or portions of the text in your thesis/dissertation in **print or microfilm formats**, please print the ACS copyright credit line on the first page of your article: “Reproduced (or 'Reproduced in part') with permission from [FULL REFERENCE CITATION.] Copyright [YEAR] American Chemical Society." Include appropriate information.

Submission to a Dissertation Distributor: If you plan to submit your thesis to UMI or to another dissertation distributor, you should not include the unpublished ACS paper in your thesis if the thesis will be disseminated electronically, until ACS has published your paper. After publication of the paper by ACS, you may release the entire thesis (**not the individual ACS article by itself**) for electronic dissemination through the distributor; ACS’s copyright credit line should be printed on the first page of the ACS paper.

Use on an Intranet: The inclusion of your ACS unpublished or published manuscript is permitted in your thesis in print and microfilm formats. If ACS has published your paper you may include the manuscript in your thesis on an intranet that is not publicly available. Your ACS article cannot be posted electronically on a publicly available medium (i.e. one that is

not password protected), such as but not limited to, electronic archives, Internet, library server, etc. The only material from your paper that can be posted on a public electronic medium is the article abstract, figures, and tables, and you may link to the article's DOI or post the article's author-directed URL link provided by ACS. This paragraph does not pertain to the dissertation distributor paragraph above.

Other conditions:

v1.1

Permission Letter

Arathi Krishnakumar, Ph.D.
Department of Physiology, University of Pennsylvania School of Medicine,

July 29, 2010

Dariusz A. Sliwa
Utah State University
Department of Chemistry and Biochemistry
Logan, UT 84322-0300

This letter grants my permission to Dariusz Adam Sliwa to use the following publication in part or in full for inclusion in his PhD dissertation:

Sliwa, D. A., Krishnakumar, A. M., Peters, J. W., and Ensign, S. A. (2010) Molecular Basis for Enantioselectivity in the (*R*)- and (*S*)-Hydroxypropylthioethanesulfonate Dehydrogenases, a Unique Pair of Stereoselective Short-Chain Dehydrogenases/Reductases Involved in Aliphatic Epoxide Carboxylation, *Biochemistry 49*, 3487-3498.

Sincerely,

Arathi Krishnakumar, Ph.D.

Permission Letter

Scott A. Ensign
Utah State University
Department of Chemistry and Biochemistry
Logan, UT 84322-0300

July 29, 2010

Dariusz A. Sliwa
Utah State University
Department of Chemistry and Biochemistry
Logan, UT 84322-0300

This letter grants my permission to Dariusz Adam Sliwa to use the following publication in part or in full for inclusion in his PhD dissertation:

Sliwa, D. A., Krishnakumar, A. M., Peters, J. W., and Ensign, S. A. (2010) Molecular Basis for Enantioselectivity in the (*R*)- and (*S*)-Hydroxypropylthioethanesulfonate Dehydrogenases, a Unique Pair of Stereoselective Short-Chain Dehydrogenases/Reductases Involved in Aliphatic Epoxide Carboxylation, *Biochemistry 49*, 3487-3498.

Sincerely,

Scott A. Ensign, Ph.D.

Permission Letter

John W. Peters
Montana State University
Department of Chemistry and Biochemistry
Bozeman, MT 59717

July 30, 2010

Dariusz A. Sliwa
Utah State University
Department of Chemistry and Biochemistry
Logan, UT 84322-0300

This letter grants my permission to Dariusz Adam Sliwa to use the following publication in part or in full for inclusion in his PhD dissertation:

Sliwa, D. A., Krishnakumar, A. M., Peters, J. W., and Ensign, S. A. (2010) Molecular Basis for Enantioselectivity in the (*R*)- and (*S*)-Hydroxypropylthioethanesulfonate Dehydrogenases, a Unique Pair of Stereoselective Short-Chain Dehydrogenases/Reductases Involved in Aliphatic Epoxide Carboxylation, *Biochemistry 49*, 3487-3498.

Sincerely,

John W. Peters, Ph.D.

CURRICULUM VITAE

Dariusz Adam Sliwa
(July 2010)

EDUCATION

PhD, Biochemistry 2004-2010
Department of Chemistry and Biochemistry,
Utah State University (USU), Logan, Utah, USA
Thesis: "Kinetic, Mechanistic and Structural Investigation of Features Controlling Stereoselectivity of *(R)*- and *(S)*-hydroxypropyl CoM Dehydrogenases from *Xanthobacter autotrophicus* strain Py2"
Advisor: Prof. Scott A. Ensign

MSc., Organic Chemistry December 2003
Department of Chemistry, Silesian Technical University (STU), Gliwice, Poland
Perstorp Specialty Chemicals AB, Perstorp, Sweden
Thesis title: "Low migrating initiators of photocuring systems"
Advisor: Prof. Stefan Baj (Poland), Prof. Nicola Rehnberg (Sweden)

RESEARCH EXPERIENCE

Graduate Student/Research Assistant 08/04 – 08/10
Department of Chemistry and Biochemistry, USU, Logan, Utah, USA

Research Assistant 01/03 - 06/03
Perstorp Specialty Chemicals AB, R&D Department, Perstorp, Sweden

Graduate Student/Research Assistant 10/98 - 12/03
Department of Chemistry, STU, Gliwice, Poland

Research Assistant 06/02 - 09/02
Cimpor, R&D Department, Loule, Portugal

TEACHING EXPERIENCE

Teaching Assistant, Utah State University, Logan, UT
Biochemistry Laboratory Spring 2010
General Chemistry Laboratory Fall 2009
Organic Chemistry Laboratory Fall 2004

PUBLICATIONS

Dariusz A. Sliwa, Arathi M. Krishnakumar, John W. Peters and Scott A. Ensign, *Molecular basis for enantioselectivity in the (R)- and (S)-hydroxypropylthioethanesulfonate dehydrogenases, a unique pair of stereoselective short-chain dehydrogenases/reductases involved in aliphatic epoxide carboxylation.* Biochemistry, 2010, published online.

Arathi M. Krishnakumar, Dariusz Sliwa, James A. Endrizzi, Eric S. Boyd, Scott A. Ensign, and John W. Peters, *Getting a Handle on the Role of Coenzyme M in Alkene Metabolism,* Microbiology and Molecular Biology Reviews, September 2008, p. 445-456, Vol. 72, No. 3

AWARDS AND HONORS

- Dissertation Fellowship, School of Graduate Studies, USU 2010
- Joseph Reuel Harris Scholarship, College of Science, USU 2010
- The best poster presentation in Chemistry and Biochemistry at the 13th Intermountain Graduate Research Symposium, USU 2010
- ACS Travel Award from the ACS Division of Biological Chemistry 2010
- USU Graduate Student Travel Award for 236th, 237th and 239th ACS meeting 2008 – 2010
- E.L. & Inez Waldron Endowment Fund Scholarship, USU 2008
- The AAAS/Science Program for Excellency in Science Award 2008
- Scholarship for Outstanding Chemistry Student at STU 2000 – 2002

SELECTED PRESENTATIONS AT SEMINARS AND PROFESSIONAL MEETINGS

- Poster. Dariusz A. Sliwa, Scott A. Ensign, *Understanding the mechanism of catalysis and stereoselectivity of R- and S-hydroxypropyl CoM dehydrogenases from* Xanthobacter autotrophicus *strain* Py2, 239th ACS National Meeting, San Francisco, CA, 2010
- Poster. Dariusz A. Sliwa, Scott A. Ensign, *Uneven twins: Molecular basis for enantioselectivity in the (R)- and (S)-hydroxypropyl-CoM dehydrogenases,* 13th Intermountain Graduate Research Symposium, Logan, UT, 2010
- Poster. Dariusz A. Sliwa, Arathi M. Krishnakumar, John W. Peters and Scott A. Ensign, *Interactions between positively charged residues (Arg, Lys) and the Sulfonate of Coenzyme M responsible for stereoselectivity of R- and S-hydroxypropyl CoM dehydrogenases,* 237th ACS National Meeting, Salt Lake City, UT, 2009
- Poster. Dariusz A. Sliwa, Arathi M. Krishnakumar, John W. Peters and Scott A. Ensign, *Structural basis for high degree of stereospecificity in S- and R-hydroxypropyl CoM dehydrogenase enzymes revealed,* 12th Intermountain Graduate Research Symposium, Logan, UT, 2009
- Poster. Dariusz A. Sliwa, Arathi M. Krishnakumar, John W. Peters and Scott A. Ensign, *Stereoselectivity and kinetics of R-and S-hydroxypropyl-CoM dehydrogenases from Xanthobacter autotrophicus Py2,* 236th ACS National Meeting, Philadelphia, PA, 2008
- Slide talk. Dariusz A. Sliwa, Scott A. Ensign, *Biochemical Characterization of the Acetone Carboxylase Protein from Helicobacter pylori,* 11th Annual Intermountain Graduate Research Symposium, Logan, UT, 2008

- Slide talk. Dariusz A. Sliwa, Scott A. Ensign, *Stereoselectivity and Kinetics of R- and S-hydroxypropyl CoM dehydrogenases from Xanthobacter autotrophicus,* 10th Annual Intermountain Graduate Research Symposium, Logan, UT, 2007
- Slide talk. Dariusz A. Sliwa, Nicola Rhenberg, *Low migrating initiators of photocuring systems,* Karolinska Institute in Stockholm, Sweden, 2003

PROFESSIONAL AFFILIATIONS

- American Chemical Society 2008 - present
  (Division of Biochemical Technology and Biological Chemistry)
- American Association for the Advancement of Science 2008 - present

FUNCTIONS AND POSITIONS HELD

- Graduate Student Senate Representative for 2008 – 2009
  Chemistry and Biochemistry Department, USU, Logan, UT
- Board Member*,* The International Association for The Exchange of 2001 – 2004
  Students for Technical Experience (IAESTE), *STU,* Gliwice, Poland